

**Automatic, script-based radiation therapy treatment planning for organs-at-risk sparing: Design,
feasibility, and validation**

A Dissertation Presented

by

Gurtej Gill

to

The Graduate School

in Partial Fulfillment of the

Requirements

for the Degree of

Doctor of Philosophy

in

Biomedical Engineering

Stony Brook University

August 2020

ProQuest Number:28090436

All rights reserved

INFORMATION TO ALL USERS

The quality of this reproduction is dependent on the quality of the copy submitted.

In the unlikely event that the author did not send a complete manuscript and there are missing pages, these will be noted. Also, if material had to be removed, a note will indicate the deletion.



ProQuest 28090436

Published by ProQuest LLC (2020). Copyright of the Dissertation is held by the Author.

All Rights Reserved.

This work is protected against unauthorized copying under Title 17, United States Code
Microform Edition © ProQuest LLC.

ProQuest LLC
789 East Eisenhower Parkway
P.O. Box 1346
Ann Arbor, MI 48106 - 1346

Stony Brook University

The Graduate School

Gurtej Gill

We, the dissertation committee for the above candidate for the

Doctor of Philosophy degree, hereby recommend

acceptance of this dissertation.

Terry Button, Ph.D. – Dissertation Advisor

**Associate Professor, Department of Radiology and Biomedical Engineering
Director of Medical Physics Track, Department of Biomedical Engineering**

Paul Vaska, Ph.D. - Chairperson of Defense

Professor, Department of Radiology and Biomedical Engineering

Wei Yin, Ph.D. – Inside Member

**Associate Professor, Department of Biomedical Engineering
Undergraduate Program Director, Department of Biomedical Engineering**

Jenghwa Chang, Ph.D. – Additional Outside Member and Co-advisor

**Associate Professor and Director of Therapeutic Medical Physics Residency Program
Department of Radiation Oncology, Hofstra Northwell Health**

This dissertation is accepted by the Graduate School

Eric Wertheimer

Dean of the Graduate School

Abstract of the Dissertation

Automatic, script-based radiation therapy treatment planning for organs-at-risk sparing:

Design, feasibility, and validation

by

Gurtej Gill

Doctor of Philosophy

in

Biomedical Engineering

Stony Brook University

2020

This dissertation develops a novel approach of designing automated script-based treatment plans for radiation therapy dose delivery in brain and breast sites. This coronal plane delivery technique includes dynamic couch motion at static gantry positions. This work is achieved using both application programming interface (API) scripting and MATLAB[®]. ESAPI is an integrated programming tool embedded in treatment planning system which facilitates the custom beam designing within same planning framework. This information is used to explore the strategies that reduces laborious work on designing manual plans. Dosimetric indices such as conformity index (CI), gradient measure (GM), mean dose, maximum dose, dose fall off, and dose volume histogram (DVH) are used to quantify the plan quality in comparison with standard treatment planning techniques. In addition, a novel method is designed to evaluate the accuracy of six degrees of freedom (6DoF) couch motion and its integration in treatment delivery. This information is used to predict the patient motion during beam ON and provides possible solutions for smooth couch start and stop positions exploring couch speed and dose rate. Potential patient immobilization methods are also discussed. The delivery of custom beams onto linear accelerator is achieved using eXtensible markup language (XML) based scripts under Varian developer mode application which facilitates a research tool to deliver and test custom treatment plans. This work, from design to validation, provides a thorough end to end test for custom treatment planning. The coronal plane delivery improves the plan quality and lowers dose to normal structures. The investigations in this experimental framework primarily focuses on developing a novel methodology to design custom treatment plans. Treatment sites with highly sensitive regions (i.e. brain, breast etc.) can potentially benefit most from such improvements. The developed methodology can be applied to other body sites and serves a reference for future treatment planning systems (TPS).

Dedication

This dissertation is dedicated in loving memory of my father, Amar Singh Gill to whom I shared special relationship. May his memories be for a blessing.

To my mother, Raghdish K Gill who continue to support me and believed in my abilities before I had the confidence to fulfil as only parents could.

To my sibling, Gurjeet K Chhina, thank you for your words of encouragement.

To my children, Harleen, Jasraj and Sukhraj who have graciously accompanied me on this sojourn. I hope that you will have the opportunity I have had to follow your dreams and accomplish great things.

And finally.

To my wife, Kamaldeep K Gill. I could not have achieved this milestone without you and for that I will forever be in-debted. You have stood by me with support over the last number of years, and I stand with you today, reflecting on all we have accomplished, anticipating a future of love, health and happiness. It is my hope that we continue to share in even greater successes as we embark on our “tomorrow” and bring much joy into the world throughout our lives.

List of Figures	ix
List of Tables	xiv
List of Abbreviations	xvi
Acknowledgments.....	xvii
Publications.....	xix
Peer-Reviewed Articles	xix
Selected Conference Proceedings.....	xix
Chapter 1: Background and Significance	1
1.1. What is Cancer?	2
1.2. Treatment Options ¹	3
1.3. Radiation Therapy.....	4
1.3.1. External Beam Radiation Therapy.....	4
1.3.2. Linear Accelerator and its Components.....	5
1.3.3. Basic Overview of Linear Accelerator	6
1.3.4. Truebeam LINAC configuration.....	7
1.3.5. Varian’s Developer Mode Application.....	7
1. 4. Radiation therapy treatment planning systems	7
1.5. Literature Review.....	8
1.5.1. Current approaches of doing VMAT treatment planning	8
1.5.1.1. Coplanar arcs (CP).....	8
1.5.1.2. Non-coplanar arcs (NCP).....	8
1.5.2. Trajectory based volumetric arc therapy (tVMAT)	9
1.5.3. Limitations of current VMAT treatment planning methodologies.....	9
1.6. Introduction of Gantry Static Couch Motion Optimization (GsCMO) technique	9
1.6.1. Limitations to this Research.....	9
1.6.2. Evaluation metrics.....	10
1.6.3. Dose delivery validation metrics.....	10
1.7 Scope of this Dissertation	11
Chapter 2: Gantry static couch motion optimization (GsCMO) technique	13
2.1. Introduction.....	14
2.2. Design	15
2.3. Application of GsCMO in brain	20
2.3.1. To evaluate the feasibility of gantry static couch motion (GsCM) technique for brain external beam radiation therapy.....	20

2.3.1.1. Significance.....	20
2.3.1.2. Methods.....	21
2.3.1.3. Results.....	23
2.3.1.4 Conclusion	24
2.4. Application of GsCMO in breast boost treatment (Single isocenter based technique)	24
2.4.1. Significance.....	24
2.4.2. Methods.....	25
2.4.3. Results.....	27
2.4.4. Summary and Conclusions	28
2.5. Single vs Dual Isocenter	29
Chapter 3: Design and evaluate the dosimetric advantages of volumetric modulated arc therapy based coronal arc delivery technique in brain stereotactic radiosurgery	31
3.1. Background and Introduction	32
3.2. Methods.....	32
3.2.1. Treatment planning study	32
3.2.2. Coplanar arcs (CP).....	34
3.2.3. Non-coplanar arcs (NCP).....	34
3.2.4. Coronal arc (cARC) delivery technique	35
3.2.5. SRS planning criteria	35
3.2.6. Dosimetric indices and their definitions	35
3.3. Results.....	36
3.4. Discussion	39
3.5. Conclusions.....	44
Chapter 4: Application of gantry-static couch-motion (GsCM) technique in breast radiation therapy: Reduced dose to organs-at-risk and improved dosimetric indices	45
4.1. Application in breast boost treatment	46
4.1.1. Overview.....	46
4.1.2. Materials and Methods.....	47
4.1.2.1. The gantry static couch motion (GsCM) technique.....	47
4.1.2.2. Patient selection, radiation dose prescription and treatment volume.....	48
4.1.2.3. Treatment planning, optimization goal and plan comparison.....	49
4.1.2.3.1. Gantry static couch motion (GsCM) technique	49
4.1.2.3.1.1. Design and feasibility test.....	49
4.1.2.3.2. 3D conformal external beam radiotherapy (3D-CRT).....	51

4.1.2.3.3. 3D planning using wedge-pair technique in supine (WPS) and in decubitus position (WPD).....	52
4.1.2.4. Plan comparison and dosimetric indices.....	52
4.1.2.5. Validation of GsCM technique.....	52
4.1.3. Results.....	53
4.1.3.1. Group A: Right breast patients.....	53
4.1.3.2. Group B: left breast patients.....	55
4.1.3.3. Dose delivery and validation.....	57
4.1.4. Discussion.....	58
4.1.5. Conclusions.....	60
4.2. Application in partial breast irradiation (PBI).....	60
4.2.1. Overview.....	60
4.2.2. Methods.....	61
4.2.3. Results.....	62
4.2.4. Discussion.....	65
4.2.5. Conclusion.....	66
Chapter 5: Couch motion integration and dose delivery validation techniques for GsCM technique.....	67
5.1. To verify the accuracy of 6DoF couch motion.....	68
5.1.1. Purpose.....	68
5.1.2. Methods.....	68
5.1.3. Results.....	70
5.1.4. Findings and discussion.....	71
5.1.5. Conclusion.....	71
5.2. Integration of couch travel and speed into GsCMO technique.....	72
5.2.1. Significance.....	72
5.2.2. Methods.....	72
5.2.3. Results.....	72
5.2.4. Summary and Conclusion.....	74
5.3. Effect of couch motion on patients with immobilization devices and without and including the dose rate variability integrated with couch motion.....	74
5.3.1. Significance.....	74
5.3.2. Methods.....	74
5.3.3. Results.....	75
5.3.4. Discussion.....	75

5.3.5. Summary and Conclusion	75
5.4. Validation of dose delivery	76
5.4.1. Purpose.....	76
5.4.2. Methods.....	76
5.4.3. Results.....	78
5.4.4. Discussion.....	81
5.4.5. Conclusion	82
Chapter 6: Automated script-based implementation of step & shoot, sliding window, continuous coronal arc and gantry static couch optimized radiation therapy	83
6.1. MATLAB based approach.....	84
6.1.1. Overview.....	84
6.1.2. Methods.....	84
6.1.3.1. Layout of design and its application in brain case.....	86
6.1.3.2. Simulation.....	87
6.1.3.3. Treatment Planning.....	87
6.1.3. Results.....	93
6.1.4. Conclusions.....	93
6.2. Automated workflow using C# scripting approach in Visual Studio platform	93
6.2.1. Purpose.....	93
6.2.2. Methods.....	94
6.2.2.1. Patients selection, imaging and target definition	94
6.2.2.2. Auto-planning workflow.....	95
6.2.2.3. Automatic script-based treatment planning	95
6.2.2.4. Delivery and validation of automated script-based planning	96
6.2.2.4.1. Design XML scripts to verify the beam parameters	96
6.2.2.4.2. Gamma analysis	99
6.2.2.4.3. Trajectory log file analysis.....	106
6.2.3. Results.....	106
6.2.4. Discussion.....	111
6.2.5. Conclusion	112
Chapter 7: Summary, conclusions, and future work.....	113
References.....	116
Appendix.....	122

List of Figures

- Figure 1. 1. Apoptosis is the programmed cell death which controls healthy tissues in the body. Cancer cells bypass the apoptosis process and continue to grow in number. 2*
- Figure 1. 2. The megavoltage linear accelerator (LINAC) and its components. 6*
- Figure 1. 3. Conceptual diagram of a typical medical linear accelerator 7*
- Figure 2. 1. Shown here is the location of targets and their description utilized for treatment planning 21*
- Figure 2. 2. Beam orientation for coplanar (CP), non-coplanar (NCP) and gantry static-couch motion optimization (GsCMO) techniques. 22*
- Figure 2. 3. Shows the description of GsCMO arc simulation process. It consisted of multiple static fields conformed around the PTV. The arc delivery is from 90 to 270 degrees which is considered as a single pi-plane dose delivery..... 23*
- Figure 2. 4. On the left panel the comparison of dose distribution between standard coplanar and GsCMO technique is shown here. It is evident to notice the sharp fall-off in the anterior-posterior direction. Similar trend is shown in the right-hand side panel showing dose distribution comparison of non-coplanar technique with GsCMO technique 23*
- Figure 2. 5. The DVH graph shows the PTV coverage and dose to the normal structures. Noticed here is the dose reduction to brain stem and optical chiasm while maintaining the same dose coverage to PTV..... 24*
- Figure 2. 6. Layout of GsCMO technique. Both medial and lateral arcs in this case deliver dose in a coronal plane. 25*
- Figure 2. 7. Single isocenter technique is mostly applicable for central and lateral targets..... 26*
- Figure 2. 8. Comparison of dose distribution between GsCMO with wedge 3-dimensional techniques (WPS, WPD) is shown here. It clearly shows no dose to ipsilateral lung due to the tangential nature of medial and lateral beams 26*
- Figure 2. 9. Comparison of Eclipse simulated plans with script plans were conducted on Truebeam LINAC. The plans were delivered onto 2D-ion chamber array. 27*
- Figure 2. 10. DVH comparison among all 3 techniques (GsCMO, WPS, WPD) clearly shows the reduction of dose to heart, ipsilateral lung, and contralateral lung while maintaining the dose coverage to the target 27*

<i>Figure 2. 11. Single isocenter technique cannot provide a wider lateral arc for medial targets. This can be mitigated by moving the patient laterally by approximately 20cm as shown in this figure.</i>	<i>29</i>
<i>Figure 2. 12. After applying the lateral shift for medial targets provides more clearance laterally. In order to encompass the PTV another anterior shift was applied as shown in this figure.</i>	<i>30</i>
<i>Figure 3. 1. Simulated planning target volumes with incremental margins near organs at risk. "Post PTVs" (Left Panel) is located posterior to the brainstem. "Ant PTVs" (Right Panel) is located in between the optic chiasm and the brainstem.</i>	<i>33</i>
<i>Figure 3. 2. Beam orientation for coplanar (CP), non-coplanar (NCP) and coronal arc (cARC) techniques.</i>	<i>33</i>
<i>Figure 3. 3. Axial and sagittal isodose distributions for "Ant PTV1" using coplanar (CP), non-coplanar (NCP) and coronal arc (cARC) techniques. By looking at the dose distribution, cARC shows superior dose fall-off in the anterior-posterior direction</i>	<i>36</i>
<i>Figure 3. 4. Axial and sagittal isodose distributions for "Post PTV1" using coplanar (CP), non-coplanar (NCP) and coronal arc (cARC) techniques. The cARC technique shows superior dose fall-off in anterior-posterior direction. NCP technique shows compact dose distribution around the PTV as compared to both CP and NCP.....</i>	<i>37</i>
<i>Figure 3. 5. Comparison of fractional volume vs dose to "Ant PTVs" and "Post PTVs", Chiasm and Brainstem for coplanar (CP), non-coplanar (NCP) and coronal arc (cARC) techniques. Graph "a-c" are for "Ant PTVs" and "d-h" for "Post PTVs". To represent a true comparison, all plans were normalized equally. It clearly shows an improvement of dose reduction to brainstem and optical chiasm</i>	<i>38</i>
<i>Figure 3. 6. Dose fall-off is shown here which was calculated by drawing a line profile at the center of "Ant PTVs" and anterior to center of "Post PTVs". For example, this figure shows dose fall-off for "Post PTVs" (as shown in graph "a-e") with its profile directional directionality is shown in graph "f" (for e.g. "Post PTV1). Similar way it is shown for "Ant PTVs" in graph "h-j" and their directionally (for e.g. "Ant PTV1) in graph "g")</i>	<i>40</i>
<i>Figure 4. 1. The location of lumpectomy cavity is shown for a right breast (a) and a left breast (b) patient included in this study. In both pictures, the lumpectomy cavities were contoured in pink color as the gross tumor volume.....</i>	<i>49</i>
<i>Figure 4. 2. The field arrangement of gantry static couch motion (GsCM) technique for the case in Figure 1(a). The GsCM field arrangement consists of two oblique arcs aiming at the isocenter as shown in an axial view (a), coronal view (b), sagittal view (c), and a 3D view (d). Each arc utilizes multiple static fields (e) conformed around the target volume (f). For each beam MLCs were conformed around the PTV as shown in the beams-eye-view (f) for right sided target with single isocenter approach.....</i>	<i>50</i>
<i>Figure 4. 3. Comparison of the field arrangement and their respective axial, coronal, sagittal, and 3-dimensional (3D) view of isodoses overlay for the right breast lumpectomy boost</i>	

treatment plan of the case in Figure 1A: (a) gantry static couch motion (GsCM), (b) 3-dimensional conformal radiation therapy (3D-CRT), (c) wedge pair in supine position (WPS), and (d) wedge pair in decubitus position (WPD) techniques..... 51

Figure 4. 4. Dose volume histogram (DVH) comparison for a left breast patient (a,b) and a right breast patient (c,d). The graph shows the dose reduction to 10%, 30% and 50% of the volume getting prescription dose to heart and ipsilateral lung using GsCM technique while maintaining same PTV coverage as compared to 3D-CRT, WPS, and WPD..... 55

Figure 4. 5. Delivery and validation of GsCM technique was conducted utilizing an ion chamber array (a) scanned in a vertical position to avoid any side beam entrance. Measured (b) and planned (c) dose were compared using a criteria (d) of 2mm distance-to-agreement (DTA), 2% dose difference (%DD), and 2D gamma (e) passing rate of more and equal to 95% and dose profile comparison from left to right (transverse) direction (f). 58

Figure 4. 6. The GsCMO (a) technique utilizing two coronal arcs was compared with VMAT (partial arcs), and VMATa (partial arcs with 90 degrees avoidance sector) shown here is for a right-sided test patient..... 63

Figure 4. 7. The DVH shows the dose to heart, ipsilateral breast and ipsilateral lung for outer and central targets (a), and for inner targets (b)..... 65

Figure 5. 1. In-house build phantom utilized to test the pitch, jaw and roll angles of 6DoF couch 69

Figure 5. 2. All the measurements shown above were conducted using an in-house built phantom under Varian's Truebeam. Evaluation is done based on pixel location of metal bb in X, Y and Z directions. Figure (a-d) shows the calculation method used to calculate pitch, yaw and roll of ± 3 degrees. 69

Figure 5. 3. All the measurements shown above were conducted using an in-house built phantom under Varian's Truebeam. Evaluation is done based on pixel location of metal bb in X, Y and Z directions. Figure (e-h) shows the calculation method used to calculate pitch, yaw and roll of ± 3 degrees. 70

Figure 5. 4. Figure (i-l) shows the comparison of calculated and measured pitch, yaw and roll angles. Figure (l) is an indication of mechanical shifting of KV and MV panels over time which could be easily addressed using our approach. 71

Figure 5. 5. Variation of couch speed is shown. Top view is without any couch speed limit. Middle view shows the variation when 1 degree per sec couch limit was applied. This shows a smooth couch transition from one position to another. Even though a constant couch motion was noticed for a couch speed limit of 2 degrees per sec, but the positioning error was larger than 1 degree per sec. 73

Figure 5. 6. Variation of dose rate impacts couch start and stop positioning 75

Figure 5. 7. Test plans as shown were simulated in treatment planning system including a variety of plans from simple (open field) to complex (with multiple control pois and dose

modulation).....	76
Figure 5. 8. Eclipse plans vs script-based plans were delivered and tested on Truebeam LINAC	77
Figure 5. 9. 2D ion chamber array was utilized for the validation of radiation dose delivery. This phantom was scanned under CT-simulation and brought into treatment planning system	77
Figure 5. 10. PTW Octavius phantom utilized to compare the treatment planning dose verses the measured dose was set up on the treatment couch as shown.	78
Figure 5. 11. Verification of dose delivery for Eclipse plan vs delivery for an open field defined by Jaws only.....	79
Figure 5. 12. Verification of dose delivery for Eclipse plan vs delivery for an open field defined by Jaws and MLCs	79
Figure 5. 13. Verification of dose delivery for Eclipse plan vs delivery for a shaped conformal field defined by MLCs	80
Figure 5. 14. Verification of dose delivery for Eclipse plan vs delivery for an optimized field modulated by MLCs utilizing the sliding window IMRT approach	80
Figure 5. 15. Verification of dose delivery for Eclipse plan vs XML plans for a conformal field defined by MLCs	81
Figure 5. 16. Verification of dose delivery for an XML plan vs delivery for a conformal field defined by MLCs	81
Figure 6. 1. Current workflow of planning, delivery and quality assurance check of 3D and an IMRT treatment plan.....	85
Figure 6. 2. Workflow (additional step is shown in the hashed box) of planning, delivery and quality assurance check of 3D and an IMRT treatment plan	85
Figure 6. 3. Five executed treatment plans with increasing complexity, starting from very simple open static field to complex IMRT fields with multiple control points. All these plans were run in Eclipse treatment planning system and exported to MATLAB. A single XML file was created by combining all the multiple fields.....	85
Figure 6. 4. Workflow of planning to validation testing using MATLAB script, an IMRT QA device (PTW Octavius 1500ion chamber array) and Truebeam trajectory log files.....	86
Figure 6. 5. PTW OCTAVIUS IMRT QA phantom setup for CT simulation (left) vs. setup on the couch for treatment delivery (right).....	86
Figure 6. 6. Shows the selection of fields and dose distribution for GsCMO technique	96
Figure 6. 7. Here is an example of dose verification onto a PTW ion chamber array comparing the XML file vs the measure dose. The XML measured dose for a continuous couch	

motion is shown in the top left and bottom left is the same plan designed in Eclipse. Overall, the passing rate satisfies our criteria of accepting the IMRT QA. As noticed the gamma fails at the top portion of the gamma plot which is due to the beam entrance at the side of the detector. The detector cannot process this low dose and causing the passing rate to degrade a little. This is just due to the construction of an ion chamber array and nature of beam entrance. 99

Figure 6. 8. Dose delivery comparison of continuous (upper left) versus the step and shoot (lower left) dose delivery. Both dose distribution satisfies the passing criteria of 2mm/2% with a passing rate of 100%..... 106

Figure 6. 9. Relationship of couch and gantry position is shown and correlated with the MU delivered. Based on the graphs for 5 test plans (step and shoot on the left column and continuous delivery on the right-hand side column), it is clear how dose was delivered at each planned gantry and couch positions. On X-axis, number of recorded events are shown which also correlates to total time took to deliver the plan. 108

Figure 6. 10. On left hand column, step and shoot delivery is shown. It is clear how the couch positions are represented in discrete lines also describes no beam ON while the couch is in transit. On the right-hand side column, the continuous couch motion is presented which clearly shows that couch was in motion during the beam in ON state. 109

Figure 6. 11. For each individual leaf position, root mean square error (mm) is shown for step and shoot delivery (left hand side column) and for continuous delivery (right hand side column) 110

List of Tables

Table 2. 1. Conversion from Eclipse to treatment machine developer mode application is shown here. The XML script helped to transfer the machine parameters from Eclipse to treatment machine correctly	16
Table 2. 2. An example if shown for 3 static fields. This XML file automated the delivery from one position to another position. We just need to mode up the beam and hit start once. Afterwards the system takes care of the rest and delivers the rest of the fields.....	16
Table 3. 1. SRS Planning Treatment Volumes (PTVs) with associated description of margins... 34	
Table 3. 2. Conformity Index (C.I.) and Gradient Measure (G.M.) comparison of coplanar (CP), non-coplanar (NCP) and coronal arc (cARC) planning techniques. Non-coplanar (NCP) technique has better C.I. and G.M. indices. Conformity Index (C.I.) for cARC is comparable to both NCP and CP. Gradient Measure (G.M.) for cARC resides in between NCP and CP but superior to CP.....	41
Table 3. 3. Comparison of brainstem and chiasm dose for CP, NCP and cARC techniques following PTV: D95=100% criteria. As per TG101, max point dose where “point” is defined as 0.035cc or less, for brainstem and chiasm it is limited to 15Gy and 10Gy. The V10Gy to brainstem and V8Gy to chiasm are the threshold doses. $D_{\leq 0.5cc}$ for brainstem and $D_{\leq 0.2cc}$ for chiasm are chosen as meaningful points for “max critical volume above threshold”	42
Table 3. 4. Comparison of D95 (cGy) and mean dose to “Ant PTVs” and “Post PTVs” for all techniques satisfying TG101 criteria of dose constraints to brainstem (0.5cc<10Gy, max point dose<15Gy) and optic chiasm (0.2cc<8Gy, max point dose<10Gy).....	43
Table 4. 1. Primary tumor laterality and patient characteristics.	48
Table 4. 2. Right breast dosimetric parameters show improvement in PTV coverage, ipsilateral lung and heart. GsCM is superior when compared to 3D-CRT, WPS and WPD. All results are shown as mean± standard deviation ($p \leq 0.05$ to consider statistically significant).	53
Table 4. 3. Left breast dosimetric parameters show improvement in PTV coverage, ipsilateral lung and heart. GsCM is superior when compared to 3D-CRT, WPS and WPD. All results are shown as mean± standard deviation ($p \leq 0.05$ to consider statistically significant).	56
Table 4. 4. The dose constraints used in this study to compare the dosimetry of GsCMO with VMAT and VMATa plans	62

<i>Table 4. 5. Dose constraints shown for outer and central targets, and for inner targets for GsCMO, VMAT, and VMATa techniques for right breast (n=20)</i>	<i>64</i>
<i>Table 6. 1. XML file for static conformal fields. All fields were combined to create a single deliverable arc</i>	<i>88</i>
<i>Table 6. 2. XML file for IMRT step & shoot fields. All fields were combined to create a single deliverable arc</i>	<i>90</i>
<i>Table 6. 3. The scaling convention “Varian IEC” tested for one to one translation of treatment planning parameters to machine delivery. It shows the difference in parameters in XML script and the planning system.....</i>	<i>97</i>
<i>Table 6. 4. Left column shows script designed by our C# program in Visual Studio and the right-hand side column is from the Truebeam system. Developer mode application has the capability to convert a DICOM plan into an XML but only for single field or a plan consists of single field</i>	<i>98</i>
<i>Table 6. 5. XML file for step and shoot delivery where beam remain on hold while couch moves from one position to next position. In this example, control points 3 and 5 are duplication of their following control points which just act as initialization positions for them</i>	<i>100</i>
<i>Table 6. 6. Example of continuous delivery. This XML file does not have any dummy/duplicate controls points which have been deleted by utilizing out custom script. As we see here, there is a smooth transition from control point 1 to 2 to 3, and so on.</i>	<i>103</i>

List of Abbreviations

cGy	Centi-gray
CRT	Conformal radiation therapy
CTV	Clinical target volume
DNA	Deoxyribonucleic acid
DTA	Distance to agreement
GsCMOT	Gantry static couch motion optimization technique
GTV	Gross tumor volume
IMRT	Intensity modulated radiation therapy
LINAC	Linear accelerator
MLC	Multi-leaf collimator
MU	Monitor units
QA	Quality assurance
RMSE	Root mean square error
RT	Radiation therapy
VMAT	Volumetric modulated arc therapy
XML	eXtensible markup language

Acknowledgments

I would like to thank my supervisors, Dr. Terry Button and Dr. Jenghwa Chang, for their support and guidance over the course of my academic career. I consider myself privileged to be mentored by these individuals and look forward to working with them in the future.

Dr. Button has overseen my progression from graduate student to independent researcher, providing valuable insight into my Doctoral research, contributing to the development of fundamental critical thinking skills which will only assist me in furthering my career objectives. Dr. Button runs the medical physics track of the graduate program in the department of Biomedical Engineering and supervises diagnostic physics residency, including teaching new residents from many different professions at Stony Brook University, where with sufficient motivation, a student can carry out novel, cutting edge bench to bedside research, and apply their knowledge to directly impact patient care. Further, Dr. Button's support in the advancement of my career as a clinical Medical Physicist and appreciation for family values, especially after completing MS degree in 2012 and returning back to Stony Brook University for PhD in 2016, is a testament to a certain quality of character not always evident in typical supervisor/student relationships. It has been an honor working with Dr. Button and I look forward to collaborating in the future.

Dr. Jenghwa Chang has served as my mentor over the last few years, serving as teacher, mentor, and finally colleague. Dr. Chang has always shown confidence in my abilities as I learned Medical Physics at Northwell Health. Dr. Chang also provided my first exposure to a research environment, which only served as motivation for further research pursuits. I have always admired Dr. Chang's passion for physics and consider myself privileged to have had the opportunity to interact with him.

I would like to thank Dr. Paul Vaska for serving as chairperson of my advisory committee. Dr. Vaska served as a guide, mentor, and advisor throughout my PhD. Your advice and input were much appreciated.

I would like to thank Dr. Wei Yin for serving as member of my advisory committee. Dr. Yin played a major role in the development of my research abilities early in my student life as a teaching assistant in Biomedical Engineering department and has served as a mentor and advisor over the last several years.

I would like to thank Dr. Jameson Baker, Dr. Raphael Jakubovic, and Mr. Salar Soury for their contributions to this work and for bringing their unique experience to the table.

Special thanks to Dr. Nand Relan for his support throughout this journey.

Finally, I would like to acknowledge and thank my peers at Northwell Health for your support and help over the last few years. Dr. Yijian Cao, Dr. Abolghassem Jamshidi, Dr. Luis Potters. I will always cherish these experiences.

Publications

Peer-Reviewed Articles

Gill, G. , Jakubovic, R. , Baker, J. , Button, T. and Chang, J. (2019), Dosimetric Advantages of Volumetric Modulated Arc Therapy Based Coronal Arc Delivery Technique in Brain Stereotactic Radiosurgery: A Feasibility Study. *International Journal of Medical Physics, Clinical Engineering and Radiation Oncology*, 2019; **8**, 80-94.

Gill, G.S., Jakubovic, R.Y., Baker, J., Button, T. and Chang, J. (2020), Dosimetric benefits of gantry-static couch-motion (GsCM) technique for breast boost radiation therapy: Reduced dose to organs-at-risk and improved dosimetric indices. *J Appl Clin Med Phys* 2020, doi:10.1002/acm2.12969

Gill, G.S., Jakubovic, R.Y., Baker, J., Button, T. and Chang, J. (2020), Automated script-based implementation of step & shoot, sliding window, continuous coronal arc and gantry static couch optimized radiation therapy. *J Appl Clin Med Phys* (Under preparation)

Selected Conference Proceedings

Gill, G. , Jakubovic, R. , Baker, J. , Button, T. and Chang, J. The Gantry-Static Couch-Motion Optimization (GsCMO) Technique for Partial Breast Irradiation Reduced Dose to Organs-At-Risk and Improved Plan Quality. AAPM annual meeting, *Med Phys.*, 2020. Abstract ID: 52956

Gill, G. , Jakubovic, R. , Martanez, J, Baker, J. , Button, T. and Chang, J. Automatic Generation of XML Files for Treatment Delivery. AAPM annual meeting, *Med Phys.*, 2019. Abstract ID: 45462

Gill, G. , Jakubovic, R. , and Chang, J. Trajectory-Based Dynamic Couch Motion Optimization Technique for Intracranial Stereotactic Radiosurgery: A Single π -Based Geometry Approach for Brain SRS Treatment Planning. AAPM annual meeting, *Med Phys.*, 2018. Abstract ID: 40237

Gill, G. , Jakubovic, R. , and Chang, J. Gantry Static Couch Motion Optimization Technique (GsCMOT) for Breast Boost Applications: Reduces Dose to Organs-At-Risk and Improves Dosimetric Indices. AAPM annual meeting, *Med Phys.*, 2018. Abstract ID: 40246

Jakubovic, R. , **Gill, G.** , and Chang, J. Simulation and Validation of a Gantry Static Couch Motion Optimization Technique (GsCMOT): A Feasibility Study. AAPM annual meeting, *Med Phys.*, 2018. Abstract ID: 40318

Gill, G. , and Chang, J. To Check the Accuracy of 6DoF (degrees-Of-Freedom) Couch Using a Novel Method. AAPM annual meeting, *Med Phys.*, 2017. Abstract ID: 36880

Chapter 1: Background and Significance

1.1. What is Cancer?

Cancer¹ is an abnormal growth of cells. Normal cells grow normally and go through a programmed cell death, or apoptosis, that maintains their abundance in the body. On the other hand, cancer cells do not respond to apoptotic signals, resulting in uncontrolled cell division and ultimately invasion into surrounding tissues (metastasize) as shown in Figure 1.1. This uncontrolled extra-cellular growth, which distinguishes cancerous cells from normal cells, is commonly referred to as cancer. Cancer can originate anywhere in the body. Benign and malignant are the two-common types of tumor. Benign tumors are localized and good candidates for surgery. Malignant tumors spread into nearby organs via the blood stream or the lymphatic system. In this case surgery and radiation may be considered for local control.

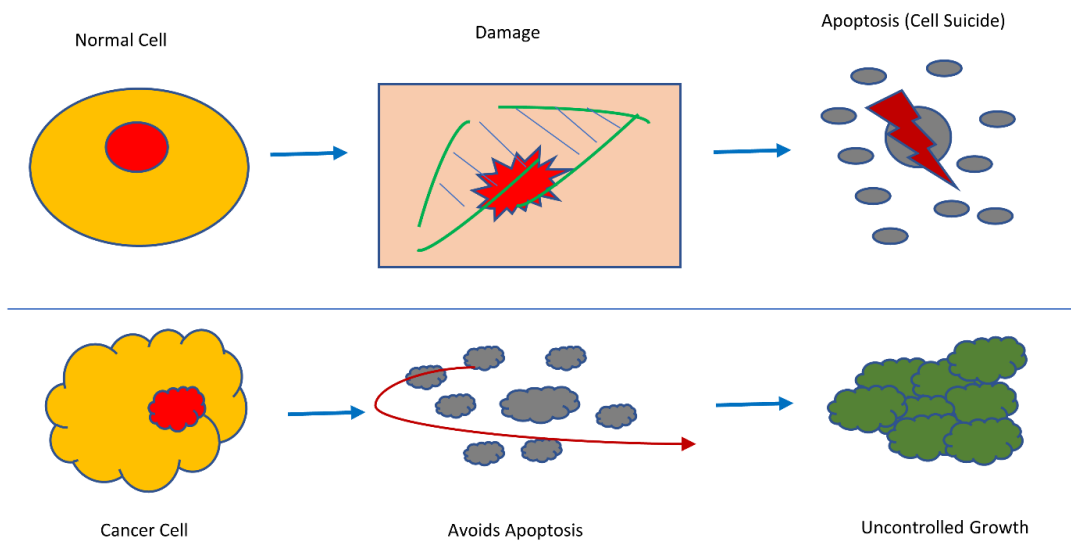


Figure 1. 1. Apoptosis is the programmed cell death which controls healthy tissues in the body. Cancer cells bypass the apoptosis process and continue grow in number.

In addition to apoptosis (programmed cell death), there are other factors which contribute to the development of cancer cells². There are various genes that control the cell division in general by keeping a balance between promoting cell growth and their suppression. Due to the accumulation of mutations in those genes which control the cell proliferation causes normal cell to become cancerous by accelerating cell division rates. The challenge is in determining which mutation is responsible for a particular cancer type. Growth promoting genes (growth factors-GFs), such as signaling protein kinase often mutate in tumors such as breast (ErbB-2/HER2) and, in brain cancer (EGFR)³. Conversely, tumor suppressor genes⁴ are de-activated for certain cancer types which lead to cancer cell growth. For example, cancer cells can inhibit P53, a common checkpoint for gene control.

There are various risk factors that may increase a person's chance of developing cancer such as smoking, diet, toxic chemicals, family history, inheritance, genetic disorders, environmental exposures, and radiation induced cancers.

1.2. Treatment Options ¹

The most common treatment for cancer is surgery, chemotherapy, immunotherapy, targeted therapy, hormone therapy, and radiation.

Surgery is one of the earlier options of removing the tumor before it spreads out to nearby tissues. The surgeon will either remove the entire tumor or achieve a partial resection. In the case of breast cancer, this would be manifested by performing a lumpectomy on early stage breast cancer or in the case of brain cancer, the removal of a malignant lesion. The decision to remove tumor is based on a multi-variable clinical workup and is not considered for all types of cancers.

Chemotherapy⁵⁻⁷, i.e. drug therapy, can be used to kill cancer cells. Chemotherapy is delivered intravenously (IV) (into a vein via a needle) or orally in the form of a pill. This drug is distributed throughout the body in short period of time. Chemotherapy is usually administered in conjunction with surgery, radiation therapy or hormone therapy. Chemotherapy after surgery, also known as adjuvant chemotherapy, can lower the risk of cancer recurring and kills any residual tumor cells. Adjuvant chemotherapy is commonly prescribed for early stage breast cancer. Chemotherapy before surgery, also known as neoadjuvant therapy, is beneficial to shrink large size tumors. This allows the surgeon to remove the tumor with known margins and helps to reduce the spread of tumor to nearby tissues. Neoadjuvant therapy is often used for inflammatory breast cancer, HER2-positive breast cancer, high grade and large size tumors, which are associated with higher risk of spread to nearby tissues. There are short-term (hair loss, fatigue, weakness, loss of appetite, loss of memory and concentration) and long-term (infertility, amenorrhea, osteopenia, osteoporosis, heart damage and leukemia) side effects associated with chemotherapy.

Immunotherapy⁸⁻¹¹, is a type of biological therapy, focused on fighting cancer through a strengthened immune response. The immune system consists of white blood cells which are found in the lymphatic system and aid the body in fighting infections. Immunotherapy utilizes natural or synthetic agents to train the body to reject cancerous cells. Immunotherapy can be used to treat some types of breast cancer cells. There are certain checkpoints in our immune cells (protein) which need to be turned on to start an immune response. For example, breast cancer cells use these checkpoints to avoid being attacked by the immune system. Therefore, to restore the immune system response against the cancer cells, drugs are used which target these checkpoints. In breast cancer cells, PD-L1 inhibitors inhibit the immune response. Atezolizumab and abraxane drugs target PD-L1, a protein in tumor cells, blocking it helps boost the immune response against cancer cells. Another popular immunotherapy is known as chimeric antigen receptor (CAR) T-cell therapy where T-cells from the blood stream are mixed with a special virus. The modified T-cells attach the cancer cells more effectively. There are some side effects associated with

immunotherapy such as fatigue, nausea, diarrhea, and loss of appetite. Immunotherapy drugs are mainly administered via intravenous (IV) system, for ex., atezolizumab drug for breast cancer.

Targeted therapy¹²⁻¹⁸ is comprised of small-molecule drugs or monoclonal antibodies which are designed to target the mechanisms of cancerous cells that drive cell growth, division and invasion to nearby cells or tissues. Similar to chemotherapy, these drugs enter the bloodstream and target tumor cells. In breast cancer, HER2 growth promoting protein is found in excess, also known as HER2-positive. Certain monoclonal antibodies such as Trastuzumab attach the HER2 protein found in breast cancer cells and control their growth. Pertuzumab drug is effective for advanced stage breast cancer. Both these monoclonal antibody drugs are given into a vein (IV). There are some monoclonal antibody drugs work in conjunction with chemotherapy, also known as antibody drug conjugate (ADC) which make the chemo more effective to target HER2 protein. Kadcyla (TDM-1) and Enhertu are two examples of ADC drugs. HER2 protein is a type of *kinase* which tells the cell to grow. Drugs that block the kinase are called *kinase inhibitors*. Lapatinib is an example of *kinase inhibitors* used to treat advanced stage breast cancer. Side effects associated with targeted therapy are heart failure, fatigue, liver problems, and weakness.

Hormonal therapy¹⁹⁻²¹ is primarily comprised of targeted cells that slow or completely stop the growth of tissues in an organism. For example, in breast cancer, hormonal therapy can reduce expression of the epidermal growth factor receptor (EGFR) that has been identified playing an important role in the development of certain aggressive types of breast cancer. For women who have hormone receptor-positive, like estrogen (ER-positive) and progesterone (PR-positive), tumor cells continue to grow. In order to control the cancer cells growth, there are several drugs that block estrogen receptors, for ex., Tamoxifen. This drug lowers the risk of developing breast cancer. Side effects associated with hormonal therapy are blood clots, fatigue, nausea, joint or muscle pain, and vaginal dryness.

Radiation¹⁶⁻¹⁸ is one of the most common non-invasive types of treatment, where radiation is delivered as external beam radiation therapy. Radiation is often combined with surgery or chemotherapy depending upon tumor pathology and histology. The linear accelerator is utilized to produce and deliver high energy x-rays with photons for deep seated tumors (4MV – 25MV) or electrons (4MeV – 22MeV) for superficial targets. Electron are limited to treat shallow targets due to their finite range.

1.3. Radiation Therapy

1.3.1. External Beam Radiation Therapy

Radiation therapy is a proven technique in cancer treatment. The fundamental approach is based on cells being most susceptible to radiation damage during mitosis. As a result, cells with the highest proliferation rate (in mitosis most often) are greatly impacted while normal cells with lower proliferation are less impacted. This difference in response can be enhanced by focusing the radiation onto the tumor and avoiding normal tissues.

The radiation dose is defined as amount of energy delivered per unit mass (J/kg) and is called radiation absorbed dose in units of Gy (Gray = J/kg). Smaller units are cGy (centi-gray, 1Gy=100cGy). Unfortunately, both healthy and cancer cells are irradiated during radiation therapy. The goal is to spare the healthy tissues as much as possible with less dose, which can be achieved utilizing various external radiation beam geometries.

External beam radiation therapy delivers radiation to the targeted volume from an external source, which is Linear Accelerator²² (LINAC). The schematic of LINAC is shown in Figure 1.2. During the radiation delivery, patient lies on the treatment couch and the LINAC delivers the radiation beam from different angles. Treatment planning is typically performed by Medical Dosimetrists who plan a uniform dose to the tumor, a low dose to surrounding normal tissue, and assure the plan is deliverable to the patient. The role of the Medical Physicist is to ensure the safe delivery of the treatment plan. As such, the physicist is responsible to ensure proper quality assurance of treatment plan is performed and to verify that treatment plan is executable on the LINAC. This includes pre-flight validation of the treatment plan and the performance of routine quality control to ensure that the treatment is delivered safely without collision of the treatment couch, gantry or patient. The treatment plan is executed by the Radiation Therapist once the plan is approved by the Radiation Oncologist.

1.3.2. Linear Accelerator and its Components

Linear accelerator (LINAC) is a symbol of advanced technology equipped with electronics, mechanics and engineering. The LINAC machine produces photons, also known as X-rays of energy 4-25MV, and electrons of energy 4-22MeV. Inside the waveguide, electrons are generated in an electron gun by heating the gun filament, a process called thermionic emission (also known as boiling off the electrons). These electrons are accelerated in the waveguide by applying a very high potential (4,000KV to 25,000KV) across the waveguide. 1 electron volt (eV) is the energy that an electron will gain after passing through a potential difference of 1 volt (1V). 1MV is called mega-voltage, energy gained under potential difference of 1000KV. After acceleration, electrons are steered to a point to hit a high atomic number target (high-Z) and produce photons. This phenomenon of stopping electrons and producing photons is called bremsstrahlung or breaking radiation. This photon beam is further flattened out using filters and finally modulated before it is delivered to the patient. These photons are highly penetrating radiation and mostly used for deep seated tumors. Another beam that gets generated inside the LINAC are electrons, where the electrons do not hit the target but rather a scatter foil and come out of the gantry as a uniform beam of electrons. Electrons have a very finite range and are ideal for superficial tumors. This research is focused on the use of the linear accelerator for photons and for treatment of cancer patients.

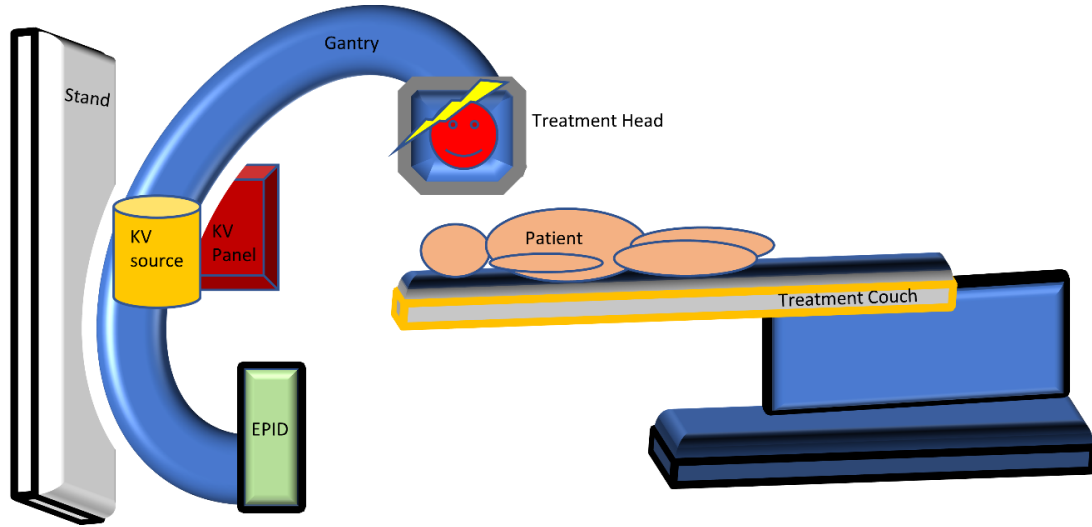


Figure 1. 2. The megavoltage linear accelerator (LINAC) and its components.

1.3.3. Basic Overview of Linear Accelerator

The initial component of energetic electron generation is the electron gun. After generation by thermionic emission electrons are accelerated toward the target material. The schematic shown (Figure 1.3.) is the view inside of the linear accelerator (LINAC) used at our institution. The modulator area is the main power supply. The microwaves from RF power source combine with electrons in the electron waveguide to accelerate the electrons to a 270-degree achromatic bending magnet which is used to select the proper electron energy and to focus the electrons back onto the target. The energy provided depends whether the full or partial waveguide is being used. For photon production, the accelerated electrons hit the target. This results in an intense pencil beam that is further flattened out using the flattening filter. For electrons the accelerated electrons are used as it is, but the intense peaked beam gets flattened out using a set of scattering foils.

Once the beam exits the exit window it passes through a set of fixed primary collimators which define the shape of the beam. Going down towards the patient, the beam passes through a flattening filter, and set of ion chambers which monitor the flatness and symmetry and measures the number of monitor units (MUs) needed to deliver the prescribed radiation dose in cGy. After passing through the ion chambers the beam passes through the secondary collimators. Secondary collimators are made from lead and tungsten alloy with Y jaws and X jaws, to further define the field shape. Y jaws (Y1 and Y2) are the upper jaws and X jaws (X1 and X2) are the lower jaws. X and Y jaws can provide only a square or rectangular field. In order to modulate the beam, multileaf collimators (MLCs) are utilized for this task. MLCs are ruler shaped leaves and made out of tungsten alloy. The resulting beam conforms to the tumor shape. After passing through the MLCs the beam gets delivered to the patient based on the prescribed dose determined by the Radiation Oncologist.

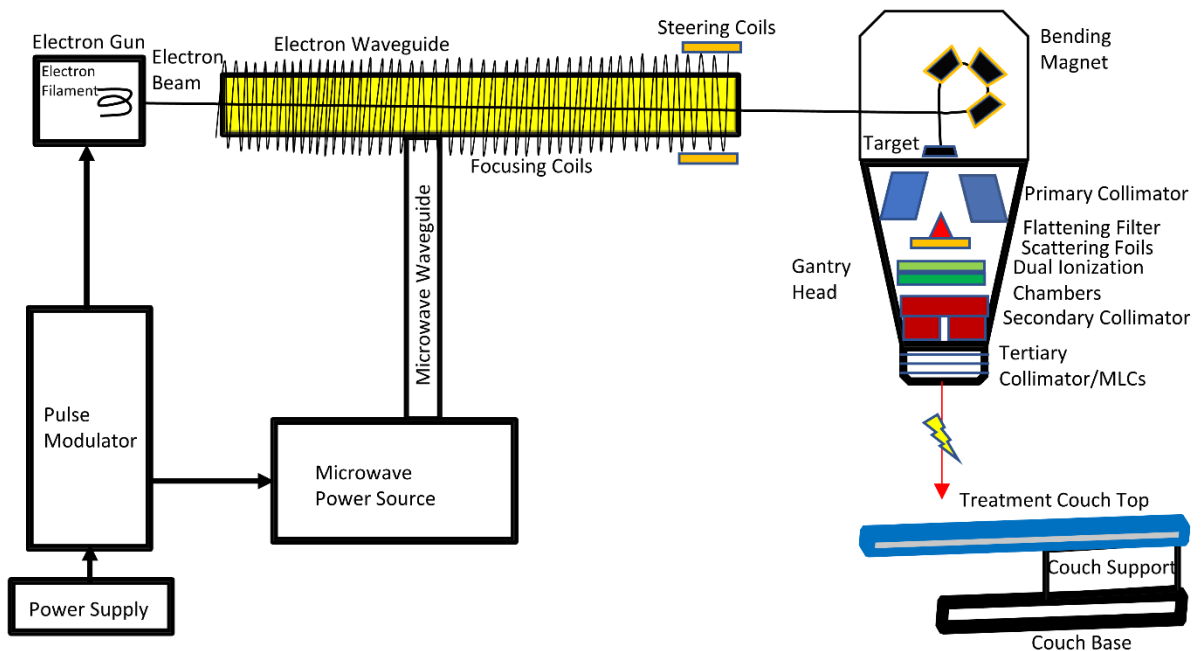


Figure 1. 3. Conceptual diagram of a typical medical linear accelerator

1.3.4. Truebeam LINAC configuration

The Truebeam LINAC was utilized for this study. It consists of six photon energies (4MV, 6MV, 6MV FFF, 10MV, 10MV FFF, and 15MV) and five electron energies (6MeV, 9MeV, 12MeV, 16MeV and 20MeV).

1.3.5. Varian's Developer Mode Application

Varian developer mode application is very powerful tool which allows users to control the LINAC, to design and deliver non-clinical beams for research. This platform allows users to manipulate the advanced features on the LINAC such as mechanical axes (gantry, collimator, couch), dose rate, and imaging capabilities (KV, MV) to design custom beams for research use. The gantry, collimator and couch positions can be optimized for superior treatment angles by keeping in mind the safety zone of all mechanical axes. The Varian developer mode application can be controlled using custom eXtensible markup language (XML) files which are created by expert users. The XML file control the full functionality of LINAC. For this research work, XML files were designed and customized using MATLAB and C# programming software. These deliverable files are fully supported in Varian developer mode platform.

1. 4. Radiation therapy treatment planning systems

The treatment planning system is a software provided by different vendors. The planning system contains all the LINAC related beam data. The data from the LINAC is configured into the panning system. The workflow of any patient getting the radiation treatment is as follows: 1. The

patient undergoes a computed tomography (CT) which is often called a CT-Simulation. 2. During simulation the patient is positioned and immobilized on the CT couch so that the same set up can be reproduced onto LINAC couch. 3. The resulting CT-Sim information is transferred to the treatment planning system. 4. The beam data is used to compute isodose distributions allowing for creation of an optimized plan. The Eclipse treatment planning system (Version 15.6, Varian Medical Systems, Palo Alto, CA) was utilized for this study.

There are various vendors which provide the platform for designing treatment planning for patient. Some of the major ones are Eclipse (Varian Medical Systems, Palo Alto, CA), Pinnacle (Philips Medical Systems, NV), Raystation (Ray Search Lab, Sweden). For this study Eclipse treatment planning was utilized and all the treatment plans were designed in this software. This planning system was commissioned for photons (4MV, 6MV, 6MV FFF, 10MV, 10MV FFF, 15MV) and electrons (6MeV, 9MeV, 12MeV, 16MeV, 20MeV) using the commissioning data from Truebeam LINAC.

1.5. Literature Review

1.5.1. Current approaches of doing VMAT treatment planning

Volumetric modulated arc therapy (VMAT)²³ is an extension to intensity modulated radiation therapy (IMRT) where dose is modulated with gantry speed, variable dose rate and jaw tracking to facilitate an arc fashioned dose delivery. VMAT utilizes 360-degree gantry rotation around the patient to provide more options of delivering and modulating the dose at set gantry intervals.

1.5.1.1. Coplanar arcs (CP)

The coplanar arc technique consists of multiple beams planned in a single plane to facilitate the delivery of higher doses in regions of beam intersection. This rapid arc approach consists of variable dose rate, variable gantry speed and dynamic MLCs. For example, in brain study (Chapter 3) two coplanar arcs rotating clockwise from 181-179⁰ and counterclockwise from 179 to 181⁰ were used. Couch angle remained stationary at 0⁰.

1.5.1.2. Non-coplanar arcs (NCP)

The non-coplanar arc technique utilizes multiple beam geometry strategically planned to use non-standard couch angles. This rapid arc approach consists of variable dose rate, variable gantry speed and dynamic MLCs. This technique is advantageous in the context of radiosurgery, where the goal of treatment is to deliver an ablative tumoricidal dose to the lesion while sparing the close by critical structures. This technique offers significant advantage over coplanar arcs when considering the dose delivered to the target by looking at the conformity of high isodose lines. Therefore, non-coplanar arc therapy has the ability to shift the distribution away from the critical structures because the dose distribution is shaped based on beam entrance. Use of non-standard couch angles can impose concerns of collision but with careful selection of couch and gantry angle, collisions can be avoided. For example, in brain study, four arcs were used (clockwise: gantry

angle 0-179⁰, couch angle 45⁰; anticlockwise: gantry angle 0-181⁰, couch angle 315⁰ along with two coplanar arcs mentioned earlier in section 1.5.1.1.

1.5.2. Trajectory based volumetric arc therapy (tVMAT)

Trajectory based volumetric arc modulated therapy (tVMAT) is an advancement to rapid arc planning where the dose is delivered by set of defined trajectories of gantry and couch motions knowing the collision model of gantry and couch motion²⁴⁻³¹. This technique is mainly used for stereotactic radiosurgery (SRS) applications employing extremely complex motions of gantry and couch (i.e., the trajectories) during the radiation beam delivery. The main idea is to achieve the highest-level dose conformity/gradient around the PTV so that the nearby organs-at-risk (OARs) can be spared³².

1.5.3. Limitations of current VMAT treatment planning methodologies

The VMAT planning technique is an emerging technology with significant potential to improve the dose conformity to PTV and promising gradient index (fall off of dose from PTV to surrounding normal tissues). This technique is mature, complex, faster, and has been improved over time. The delivery part of VMAT is limited in axial plane (coplanar). The sagittal plane dose delivery is possible but only for cranial cases. There are some areas of body where the coronal plane delivery can be appreciated but not possible due to the limitations in current treatment planning. This limitation was mitigated by introducing a gantry static couch motion optimization (GsCMO) technique. The GsCMO technique utilizes continuous couch motion at static gantry positions.

Although progress towards the integration of couch motion is underway, the current VMAT approach in modern treatment planning systems is still limited especially in regard to the integration of treatment couch motion during dose calculation.

1.6. Introduction of Gantry Static Couch Motion Optimization (GsCMO) technique

The gantry static couch motion optimization (GsCMO) technique utilizes an arc geometry consisting starting with conformal, IMRT fields, and a VMAT type dose delivery. This technique consists of multiple static fields as a starting point. Each static segment has its own dose rate, shape of MLCs and couch rotation. During the beam delivery, the collimator jaws are in motion and the dose delivered is controlled by changing the speed of leaves, the gaps between leaves and the dose rate. Design of the IMRT fields involve optimization of leaf positions and dose rate at every few (typically two) degrees of couch motion while maintaining static gantry angles. As such, the treatment couch rotates during radiation beam delivery with the gantry stays at a fixed positions (see Chapter 2).

1.6.1. Limitations to this Research

This research was applied to two potential body sites such as brain and breast. Many body sites were not included because of the nature of the treatment area and limitation of couch and gantry positioning, which could possibly cause collision due to the limited range of couch motion.

1.6.2. Evaluation metrics

The dose distribution for GsCMO technique was evaluated utilizing standard approaches of plan evaluation employed in clinic. When comparing GsCMOT with other techniques, all plans were normalized equally (D95=100%) as recommended by ICRU report 83³² to compare the doses to PTVs. Dosimetric distributions were evaluated using the homogeneity index (H.I.)³³, conformity index (C.I.)³⁴, and gradient measure (G.M.). Briefly:

$$H.I. = (D2\% - D98\%) / D50\% \quad (1)$$

where D98%, D2% and D50% are dose received by 98%, 2% and 50% of the volume. Homogeneity Index values approaching zero are considered as an ideal value for plan comparison.

$$C.I. = V_{95\%} / V_{PTV} \quad (2)$$

where $V_{95\%}$ is the volume enclosed by isodose surface of 95% prescription dose and V_{PTV} is the target volume. Conformity index approaching 1 is considered an optimal plan for comparison.

$$G.M. (cm) = R_p - R_{50} \quad (3)$$

where R_p and R_{50} are the equivalent sphere radius of the prescription and half prescription isodoses. Gradient measure describes dose fall off from the PTV for the central slice.

Mean gradient fall-off calculates the dose fall off in a central (single) slice of PTV in a 2-dimensional area. This measures the difference between the average dose to the 100% and 50% two-dimensional isodose surfaces ($IS_{100\%}$ and $IS_{50\%}$) in anterior and posterior directions with respect to PTV.

$$\text{Mean gradient fall-off} = \text{Average} [(IS_{ant50\%} - IS_{ant100\%}) - (IS_{post50\%} - IS_{post100\%})].$$

A plan that has lowest value of mean gradient fall-off is considered an acceptable plan for comparison.

The Eclipse planning system (Varian medical systems, Palo Alto, CA) calculates the above dosimetric indices after computation of final dose calculation.

1.6.3. Dose delivery validation metrics

The fields for the GsCMO technique were validated utilizing IMRT QA phantom (Octavius1500, PTW-Freiburg, Germany). The QA phantom was scanned under CT simulation

and imported into Eclipse planning system, and the planar dose was generated for each simulated arc. The simulated arcs were delivered onto this phantom under Truebeam® developer mode application using the converted machine control file in XML format as described earlier. The measured dose was compared with the calculated dose using the criteria of percentage dose difference (%DD), distance to agreement (DTA), and 2D gamma (γ) comparison. For our study we used 2%DD, 2mm DTA, and $\gamma \leq 1$ with passing criteria of $\geq 90\%$ which is standard of care in our institution for all IMRT patients.

1.7 Scope of this Dissertation

This Dissertation develops a novel radiation dose delivery technique which has potential applications in brain and breast cancer treatment. In the context of radiotherapy, there are various presentations where dose delivery is challenging, particularly when the planning target volume (PTV) is adjacent to the organs-at-risk (OARs). In such scenarios, a trade-off exists whereby the dose constraints to the OARs must be considered in tandem with the coverage requirements of PTV. Volumetric modulated arc therapy (VMAT), an extension of intensity modulated radiation therapy (IMRT), has the ability to outperform the conventional approaches of dose delivery such as static IMRT (step & shoot or sliding window), conformal arc (C-ARC), or 3-dimensional conformal radiation therapy (3D-CRT). VMAT in an axial plane can significantly improve the coverage to the planning target volume (PTV) and lower the dose to nearby organs-at-risk (OARs). The two primary approaches to VMAT are coplanar (single plane/axial plane, 0^0 couch) or non-coplanar (multiple planes/axial and sagittal, non-zero couch static positions) geometries. The non-coplanar approach tends to be more advantageous than coplanar geometries facilitating a more conformal dose distribution with sharper dose fall-off outside the target volume in close proximity to the organs at risk. However, to compensate for sharper fall-off near the OARs, additional dose is deposited along another plane.

The current VMAT approach in modern treatment planning systems is still limited especially with regards to the integration of treatment couch motion during dose calculation. Couch motion optimization would be particularly advantageous in highly sensitive regions where PTV coverage is limited by OAR constraints (i.e. brain, breast etc.). In such cases there is a trade-off between adequate PTV coverage and normal tissue sparing. This limitation can be mitigated by introducing a gantry static couch motion optimization (GsCMO) technique. The GsCMO technique utilizes continuous couch motion at static gantry positions.

This Dissertation is organized as follows. Chapter 2 reviews literature and theory relevant to the current VMAT treatment planning techniques. Chapter 3 describes the dosimetric advantages of volumetric modulated arc therapy based coronal arc delivery technique in brain stereotactic radiosurgery and evaluates the feasibility of a trajectory-based gantry static continuous couch motion optimization (GsCMO) technique for treating brain metastasis or a lesion in close proximity to brainstem and optical chiasm. This study is applicable to any patients who are candidates of stereotactic radiosurgery (SRS) or stereotactic radiotherapy (SRT) where delivery may be limited by the dose constraints of the organs at risk. This approach results in an adequate

dose reduction to organs-at-risk (OARs) as compared to standard techniques of treatment planning such as coplanar (CP) or non-coplanar (NCP) approaches of treatment planning. Chapter 4 evaluates the dosimetric benefits of GsCMO technique in breast boost radiation therapy and develops the capabilities of the gantry static continuous couch motion optimization (GsCMO) technique to treat photon breast boost treatment planning, thereby improving plan quality and reducing the dose to organs-at-risk. This isocentric based technique is suitable for deep seated lumpectomy cavities and it avoids uncomfortable decubitus position of patient which is the case for current approach of treating breast boost cavities. Next, this chapter discusses application of GsCMOT in partial breast irradiation (PBI) treatment. Chapter 5 studies the integration of couch motion with dose delivery, investigates the uncertainties of couch motion variations, and studies the optimal couch speed to implement the coronal arc delivery using GsCMO technique. In addition, this chapter describes the validation of GsCMOT based dose delivery onto Truebeam radiotherapy LINAC. Chapter 6 discuss the layout of automated script-based treatment planning approach. Chapter 7 summarizes key conclusions and briefly describes layout of future work.

Chapter 2: Gantry static couch motion optimization (GsCMO) technique

This chapter describes in detail the design, implementation, application, and validation of gantry static couch motion optimization technique.

2.1. Introduction

Radiation dose delivery techniques that include optimized couch motion are called gantry static couch motion optimization (GsCMO) planning. Inclusion of couch motion has the potential to outperform conventional delivery of dose in an axial plane, significantly improving the coverage of the planning target volume (PTV) while minimizing the dose to nearby organs-at-risk (OARs). There is a need to allow for the integration of couch motion-based delivery in prospective treatment planning systems. While progress towards this integrating including multiple mechanical axes (collimator, gantry, couch, MLCs) has been promising, there are currently no available commercial treatment planning systems with this capability. The inclusion of continuous couch motion during dose optimization is essential for certain areas in body that can take advantage of this new approach such as brain and breast irradiation in a coronal plane.

In the context of radiotherapy, there are various presentations where dose delivery is challenging, particularly when the planning treatment volume (PTV) is adjacent to the organs-at-risk (OARs). In such scenarios, a trade-off exists whereby the dose constraints of the OARs must be considered in tandem with the coverage requirements of the PTV³⁵⁻³⁷. This limitation can be mitigated by introducing a gantry-static continuous couch-motion optimization (GsCMO) technique (1-2° increments of couch motion). Introduction of multiple non-coplanar geometries via couch motion adds an additional level of complexity to treatment planning, specifically with regards to the risk of collision between gantry, couch, and patient. While this issue has been previously addressed by integrating 3-dimensional surface modeling of the machine and patient in order to create and validate patient specific collision prediction models, vendor support for clinical use of continuous couch motion is limited²⁷.

There have been many advancements in treatment planning techniques from 2-dimensional (AP/PA) and 3-dimensional (forward planning) to more advanced IMRT (Step & Shoot, sliding window, dynamic arc, conformal arc and RapidArc) techniques. RapidArc or VMAT planning where dose modulation includes gantry motion, collimator motion, jaws motion and MLCs are found to be a faster and highly conformal dose delivery technique as compared to IMRT alone (Step & Shoot, Sliding window). The current clinical paradigm of VMAT planning is either coplanar where one or more arcs can be utilized, and couch angle is at zero degrees or non-coplanar approach where more than one arc can be utilized at non-zero couch angles. Based on previous research, 4-pi geometry^{28,29,31} based multiple non-coplanar arcs at static couch positions (also known as trajectory based VMAT implemented by Varian as HyperArc® approach (new)) and others based on simultaneous movement of couch and gantry, are found to be more appealing for rapid dose fall off outside the PTV and better dose conformity inside the PTV. Currently, no planning system allows the dose optimization for dynamic couch motion.

We are introducing gantry-static couch-motion optimization (GsCMO) technique which is pi geometry-based approach where gantry is kept static and dose optimization happens at dynamic couch motion of an increment of every 1-2 degrees. The simulation work is based on designing a treatment plan in the current treatment planning system utilizing multiple beams and exporting and merging them into a single deliverable file in XML format in MATLAB® software. This file mirrors the simulated treatment plan which was tested and delivered onto the Varian Truebeam LINAC under the developer mode application.

Our technique addressed a crucial deficiency in the delivery of radiation to many hard to treat tumors. For example, a tumor situated between the optic chiasm and brainstem would typically be at risk of underdosage due to the proximity to the OARs using conventional co-planar techniques. However, implementation of continuous couch motion would provide sharp fall-off of dose to target anteriorly and posteriorly while minimizing dose to the OARs. Further, this approach is not limited to the brain and would be applicable to many other clinical scenarios including but not limited to breast where OARs are in close proximity to the PTV. Introduction of this technique clinically will ultimately result in improved PTV coverage and/or reduced dose to the OARs.

In this dissertation we developed an automated script-based implementation of 3D, step & shoot, sliding window, continuous coronal arc and gantry static couch optimized radiation therapy using Varian Truebeam developer mode. Implementation within the Varian developer mode is crucial as current clinical treatment delivery paradigms do not enable continuous couch motion.

2.2. Design

The layout of GsCMO technique started with simulating multiple static fields in the treatment planning system. Based on the dose distribution, we found out that a coronal plane delivery can be beneficial for patients where the need to minimize the dose to OARs arises.

The first part of design required to test the mechanical parameters conversion from treatment planning system to developer mode application via XML scripts. We used “VarianIEC” scale for our project since this was the same scale used clinically. This was completed utilizing the scripts as follows. Multiple fields were designed in the planning system to test this conversion. This was important to understand this conversion since all the work completed in this dissertation circles around choosing the correct mechanical axes for treatment plan design and delivery on the linear accelerator.


```
<A>0 0 0 0 0 0 0 0 0 0 0 0 0 0 0 0 0 0 0 0 0 0 0.18 0.975 1.218 1.372 1.439 1.483 1.578 1.548 1.35 0.675
0 0 0 0 0 0 0 0 0 0 0 0 0 0 0 0 0 0 0 0 0 0 </A>
</Mlc>
</Cp>
<Cp>*****2nd control point delivers 50.6 Mus at G90*****
<Energy>6x</Energy>
<Mu>50.6177866348435</Mu>
<DRate>600</DRate>
<GantryRtn>90</GantryRtn>
<CollRtn>180</CollRtn>
<CouchRtn>180</CouchRtn>
<Y1>1.1</Y1>
<Y2>1.1</Y2>
<X1>1.6</X1>
<X2>1.6</X2>
<Mlc>
<ID>1</ID>
<B>0 0 0 0 0 0 0 0 0 0 0 0 0 0 0 0 0 0 0 0 0 0 0.52 1.315 1.542 1.578 1.521 1.447 1.332 1.208 1.01 0.34 0
0 0 0 0 0 0 0 0 0 0 0 0 0 0 0 0 0 0 0 0 0 0 </B>
<A>0 0 0 0 0 0 0 0 0 0 0 0 0 0 0 0 0 0 0 0 0 0 0.18 0.975 1.218 1.372 1.439 1.483 1.578 1.548 1.35 0.675
0 0 0 0 0 0 0 0 0 0 0 0 0 0 0 0 0 0 0 0 0 0 </A>
</Mlc>
</Cp>
<Cp>*****mode up for the next control point*****
<Energy>6x</Energy>
<Mu>50.6177866348435</Mu>
<DRate>600</DRate>
<GantryRtn>90</GantryRtn>
<CollRtn>180</CollRtn>
<CouchRtn>270</CouchRtn>
<Y1>1.6</Y1>
<Y2>1.7</Y2>
<X1>1.6</X1>
<X2>1.6</X2>
<Mlc>
<ID>1</ID>
<B>0.0009999999 0.0009999999 0.0009999999 0.0009999999 0.0009999999 0.0009999999 0.0009999999
0.0009999999 0.0009999999 0.0009999999 0.0009999999 0.0009999999 0.0009999999 0.0009999999
0.0009999999 0.0009999999 0.0009999999 0.0009999999 0.0009999999 0.0009999999 0.0009999999
0.0009999999 0.0009999999 0.16 0.8149999 1.165 1.372 1.495 1.555 1.57 1.578 1.541 1.468 1.315 1.105
0.8349999 0.525 0.0009999999 0.0009999999 0.0009999999 0.0009999999 0.0009999999 0.0009999999
0.0009999999 0.0009999999 0.0009999999 0.0009999999 0.0009999999 0.0009999999 0.0009999999
0.0009999999 0.0009999999 0.0009999999 0.0009999999 0.0009999999 0.0009999999 0.0009999999
0.0009999999 0.0009999999 0.0009999999 </B>
<A>-0.0009999999 -0.0009999999 -0.0009999999 -0.0009999999 -0.0009999999 -0.0009999999 -
0.0009999999 -0.0009999999 -0.0009999999 -0.0009999999 -0.0009999999 -0.0009999999 -0.0009999999 -
0.0009999999 -0.0009999999 -0.0009999999 -0.0009999999 -0.0009999999 -0.0009999999 -0.0009999999 -
0.0009999999 -0.0009999999 -0.0009999999 0.51 0.875 1.185 1.375 1.502 1.564 1.576 1.571 1.512 1.415 1.242
1.045 0.775 0.445 -0.0009999999 -0.0009999999 -0.0009999999 -0.0009999999 -0.0009999999 -0.0009999999 -
0.0009999999 -0.0009999999 -0.0009999999 -0.0009999999 -0.0009999999 -0.0009999999 -0.0009999999 -
0.0009999999 -0.0009999999 -0.0009999999 -0.0009999999 -0.0009999999 -0.0009999999 -0.0009999999 -
0.0009999999 </A>
```

```

</Mlc>
</Cp>
<Cp>
*****delivers 107.9-50.6=57.3 Mus at G90 and couch 90 degrees*****
<Energy>6x</Energy>
<Mu>107.873004991063</Mu>
<DRate>600</DRate>
<GantryRtn>90</GantryRtn>
<CollRtn>180</CollRtn>
<CouchRtn>270</CouchRtn>
<Y1>1.6</Y1>
<Y2>1.7</Y2>
<X1>1.6</X1>
<X2>1.6</X2>
<Mlc>
<ID>1</ID>
<B>0.0009999999 0.0009999999 0.0009999999 0.0009999999 0.0009999999 0.0009999999 0.0009999999
0.0009999999 0.0009999999 0.0009999999 0.0009999999 0.0009999999 0.0009999999 0.0009999999
0.0009999999 0.0009999999 0.0009999999 0.0009999999 0.0009999999 0.0009999999 0.0009999999
0.0009999999 0.0009999999 0.16 0.8149999 1.165 1.372 1.495 1.555 1.57 1.578 1.541 1.468 1.315 1.105
0.8349999 0.525 0.0009999999 0.0009999999 0.0009999999 0.0009999999 0.0009999999 0.0009999999
0.0009999999 0.0009999999 0.0009999999 0.0009999999 0.0009999999 0.0009999999 0.0009999999
0.0009999999 0.0009999999 0.0009999999 0.0009999999 0.0009999999 0.0009999999 0.0009999999
0.0009999999 0.0009999999 0.0009999999 0.0009999999 0.0009999999 0.0009999999 0.0009999999
0.0009999999 0.0009999999 0.0009999999 </B>
<A>-0.0009999999 -0.0009999999 -0.0009999999 -0.0009999999 -0.0009999999 -0.0009999999 -
0.0009999999 -0.0009999999 -0.0009999999 -0.0009999999 -0.0009999999 -0.0009999999 -0.0009999999 -
0.0009999999 -0.0009999999 -0.0009999999 -0.0009999999 -0.0009999999 -0.0009999999 -0.0009999999 -
0.0009999999 -0.0009999999 -0.0009999999 0.51 0.875 1.185 1.375 1.502 1.564 1.576 1.571 1.512 1.415 1.242
1.045 0.775 0.445 -0.0009999999 -0.0009999999 -0.0009999999 -0.0009999999 -0.0009999999 -0.0009999999 -
-0.0009999999 -0.0009999999 -0.0009999999 -0.0009999999 -0.0009999999 -0.0009999999 -0.0009999999 -
0.0009999999 -0.0009999999 -0.0009999999 -0.0009999999 -0.0009999999 -0.0009999999 -0.0009999999 -
0.0009999999 -0.0009999999 -0.0009999999 </A>
</Mlc>
</Cp>
<Cp>
*****mode up the beam for next energy*****
<Energy>6x</Energy>
<Mu>107.873004991063</Mu>
<DRate>600</DRate>
<GantryRtn>270</GantryRtn>
<CollRtn>180</CollRtn>
<CouchRtn>180</CouchRtn>
<Y1>1.1</Y1>
<Y2>1.1</Y2>
<X1>1.6</X1>
<X2>1.6</X2>
<Mlc>
<ID>1</ID>
<B>-0.0009999999 -0.0009999999 -0.0009999999 -0.0009999999 -0.0009999999 -0.0009999999 -
0.0009999999 -0.0009999999 -0.0009999999 -0.0009999999 -0.0009999999 -0.0009999999 -0.0009999999 -
0.0009999999 -0.0009999999 -0.0009999999 -0.0009999999 -0.0009999999 -0.0009999999 -0.0009999999 -
0.0009999999 -0.0009999999 -0.0009999999 -0.0009999999 -0.0009999999 0.27 0.975 1.217 1.372 1.439 1.483

```

```

1.572 1.548 1.35 0.645 -0.0009999999 -0.0009999999 -0.0009999999 -0.0009999999 -0.0009999999 -
0.0009999999 -0.0009999999 -0.0009999999 -0.0009999999 -0.0009999999 -0.0009999999 -0.0009999999 -
0.0009999999 -0.0009999999 -0.0009999999 -0.0009999999 -0.0009999999 -0.0009999999 -0.0009999999 -
0.0009999999 -0.0009999999 -0.0009999999 -0.0009999999 -0.0009999999 -0.0009999999 </B>
<A>0.0009999999 0.0009999999 0.0009999999 0.0009999999 0.0009999999 0.0009999999 0.0009999999
0.0009999999 0.0009999999 0.0009999999 0.0009999999 0.0009999999 0.0009999999 0.0009999999
0.0009999999 0.0009999999 0.0009999999 0.0009999999 0.0009999999 0.0009999999 0.0009999999
0.0009999999 0.0009999999 0.0009999999 0.0009999999 0.61 1.315 1.542 1.573 1.521 1.448 1.332 1.208
0.9899999 0.34 0.0009999999 0.0009999999 0.0009999999 0.0009999999 0.0009999999 0.0009999999
0.0009999999 0.0009999999 0.0009999999 0.0009999999 0.0009999999 0.0009999999 0.0009999999
0.0009999999 0.0009999999 0.0009999999 0.0009999999 0.0009999999 0.0009999999 0.0009999999
0.0009999999 0.0009999999 0.0009999999 0.0009999999 0.0009999999 </A>
</Mlc>
</Cp>
<Cp>
****delivers 159.2-107.9=51.3Mus at G270 and couch 0 degree****
<Energy>6x</Energy>
<Mu>159.248587303439</Mu>
<DRate>600</DRate>
<GantryRtn>270</GantryRtn>
<CollRtn>180</CollRtn>
<CouchRtn>180</CouchRtn>
<Y1>1.1</Y1>
<Y2>1.1</Y2>
<X1>1.6</X1>
<X2>1.6</X2>
<Mlc>
<ID>1</ID>
<B>-0.0009999999 -0.0009999999 -0.0009999999 -0.0009999999 -0.0009999999 -0.0009999999 -
0.0009999999 -0.0009999999 -0.0009999999 -0.0009999999 -0.0009999999 -0.0009999999 -0.0009999999 -
0.0009999999 -0.0009999999 -0.0009999999 -0.0009999999 -0.0009999999 -0.0009999999 -0.0009999999 -
0.0009999999 -0.0009999999 -0.0009999999 -0.0009999999 -0.0009999999 0.27 0.975 1.217 1.372 1.439 1.483
1.572 1.548 1.35 0.645 -0.0009999999 -0.0009999999 -0.0009999999 -0.0009999999 -0.0009999999 -
0.0009999999 -0.0009999999 -0.0009999999 -0.0009999999 -0.0009999999 -0.0009999999 -0.0009999999 -
0.0009999999 -0.0009999999 -0.0009999999 -0.0009999999 -0.0009999999 -0.0009999999 -0.0009999999 -
0.0009999999 -0.0009999999 -0.0009999999 -0.0009999999 -0.0009999999 -0.0009999999 </B>
<A>0.0009999999 0.0009999999 0.0009999999 0.0009999999 0.0009999999 0.0009999999 0.0009999999
0.0009999999 0.0009999999 0.0009999999 0.0009999999 0.0009999999 0.0009999999 0.0009999999
0.0009999999 0.0009999999 0.0009999999 0.0009999999 0.0009999999 0.0009999999 0.0009999999
0.0009999999 0.0009999999 0.0009999999 0.0009999999 0.61 1.315 1.542 1.573 1.521 1.448 1.332 1.208
0.9899999 0.34 0.0009999999 0.0009999999 0.0009999999 0.0009999999 0.0009999999 0.0009999999
0.0009999999 0.0009999999 0.0009999999 0.0009999999 0.0009999999 0.0009999999 0.0009999999
0.0009999999 0.0009999999 0.0009999999 0.0009999999 0.0009999999 0.0009999999 0.0009999999
0.0009999999 0.0009999999 0.0009999999 0.0009999999 0.0009999999 </A>
</Mlc>
</Cp>
</ControlPoints>
</SetBeam>

```


Next part was to start creating the plans. This simulation process was conducted in Eclipse planning system. These simulated plans consisted of multiple static fields. Each field was conformed around the PTV. Once the plan was ready and dose distribution was adequate and acceptable then the plan was converted into an XML file. This file was loaded in the developer mode application and tested. The delivery of this dose was verified utilizing a 2D ion-chamber array detector. The following section describes the applications of our GsCMO technique in brain and breast. This was the feasibility study. Based on the results of this feasibility study in brain and breast, we applied our technique retrospectively for brain tumor patients who have lesion situated close to brainstem and optic chiasm and required saving these normal structures as much as possible, and secondly for breast tumor patients who are in their early stage of breast cancer and had undergone breast conserving surgery (BCS).

2.3. Application of GsCMO in brain

2.3.1. To evaluate the feasibility of gantry static couch motion (GsCM) technique for brain external beam radiation therapy

2.3.1.1. Significance

The evolution of treatment planning, particularly with regards to tailor-made, patient specific treatment design and delivery, has had a profound clinical impact, facilitating improved treatment outcomes while sparing the organs-at-risks (OARs).^{24-26,35,38} This development, with respect to brain pathologies, has enabled treatment of targets adjacent or near critical structures including the eyes, lenses, optic nerves, optic chiasm, brainstem and cochlea. These OARs pose significant challenges to the medical physicists/dosimetrists, who are responsible for safe and accurate treatment delivery.

Intensity modulated radiation therapy (IMRT) represents a major improvement over traditional forward planning technique. In the forward approach, treatment planning is an iterative manual process and the plan is designed to achieve the OAR dose constraints or planning target volume (PTV) coverage requirements. In contrast, IMRT utilizes computerized inverse planning by modulating the intensity of the radiation beam based on specific planning criteria (i.e. OAR dose constraints or PTV coverage goals). IMRT represents a more complex delivery paradigm, facilitating better OAR sparing and improved treatment accuracy when compared to traditional forward planning techniques. These advantages have become increasingly pronounced with the introduction of coplanar (CP) and non-coplanar (NCP) volumetric modulated arc therapy (VMAT), whereby dose modulation is performed by optimizing gantry, dynamic jaw, and dose rate, as well as, multileaf collimator (MLC) position, to achieve rapid dose fall-off outside the treatment volume.

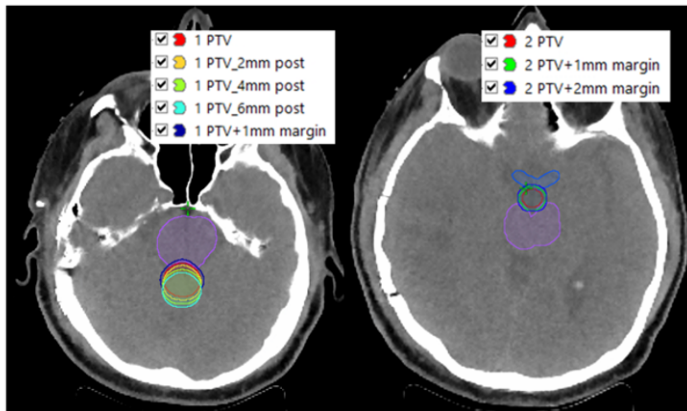
Previous attempts focused on coplanar and non-coplanar VMAT techniques resulted an integral dose spread to organ at risk structures. This dissertation describes the implementation of gantry static couch motion optimization technique where dose is optimized at dynamic couch

motion while gantry stays stationary. The results of which yielded sparing the organs at risk structures.

2.3.1.2. Methods

In this dissertation we evaluated the role of trajectory-based gantry-static couch motion optimization (GsCMO) technique by introducing dynamic couch rotation during arc delivery. This technique consists of multiple static IMRT fields, each field has multiple segments, combined to deliver them in an arc fashion. Dose was modulated at each two degrees couch angle rather than at gantry angle which is the current clinical paradigm of dose calculation in any commercially available treatment planning system. In the GsCMO application, the gantry remained stationary during radiation dose delivery. We presented a comparison of coplanar, non-coplanar and GsCMO techniques in the context of brain lesions, specifically in lesions situated in close proximity to the brainstem and/or optical chiasm.

Retrospective review of a brain study using two pre-selected planning target volumes (PTVs) was conducted as shown in Figure 2.1. PTVs were selected to simulate conditions where the GsCMO technique would be particularly advantageous. Varying margins and distance from the organs at risk (OARs, i.e. brainstem and/or optic chiasm) was used for each set of PTVs to assess the benefits of the GsCMO technique.



PTVs drawn for SRS planning	Description of margins
1 PTV	No margin
1 PTV+1mm margin	1 mm margin from 1PTV
1 PTV_2mm post	2 mm posterior from 1PTV
1PTV_4mm post	4 mm posterior from 1PTV
1PTV_6mm post	6mm posterior from 1PTV
2 PTV	No margin
2 PTV+1mm margin	1 mm margin from 2 PTV
2 PTV+2mm margin	2 mm margin from 2 PTV

Figure 2. 1. Shown here is the location of targets and their description utilized for treatment planning

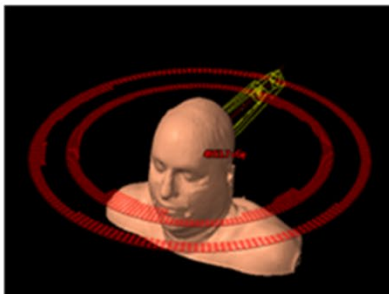

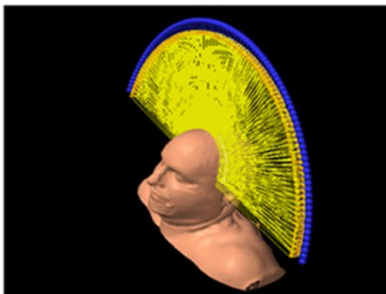
Coplaner ARC technique, 2 full ARCs	Non-coplaner ARC technique, 2 full ARCs and 2 half ARCs	Gantry static, couch motion optimization technique (GsCMOT)- π -geometry
		

Figure 2. 2. Beam orientation for coplanar (CP), non-coplanar (NCP) and gantry static-couch motion optimization (GsCMO) techniques.

Treatment planning was focused on stereotactic radiosurgery (SRS) approach delivering 21 Gy in a single fraction via 6 FFFMV photon beams. Treatment planning was performed using the Eclipse treatment planning system (Version # 13.6, Varian Medical Systems, Palo Alto, CA) with 1.5mm dose grid resolution. All treatment plans were created based on a high-definition millennium 120 multileaf collimator (HDMLC) system. The GsCMO was compared with two existing treatment design approaches – standard coplanar (CP) arcs and non-coplanar (NCP) as shown in Figure 2.2.

The simulation part of GsCMO was conducted in Eclipse. Two partial arcs were designed consisting of couch motion from 0 to 90 degrees while gantry stays at 90 degrees and couch rotation from 270-360 degrees at gantry 270 degrees as shown in Figure 2.3. The comparison of dose distribution of coplanar and no coplanar with GsCMO technique is shown in Figure 2.4. The dose volume histogram comparison is shown in Figure 2.5.

Simulation of GsCMO arc

- An ARC plan was created by simulating multiple intensity modulated radiation therapy (IMRT) fields
 - Gantry 90, 46 IMRT fields
 - Gantry 270, 46 IMRT fields
 - Combining them creates a 180 degree arc
 - It consists of π -geometry
 - Couch moves continuously at 2 degrees interval

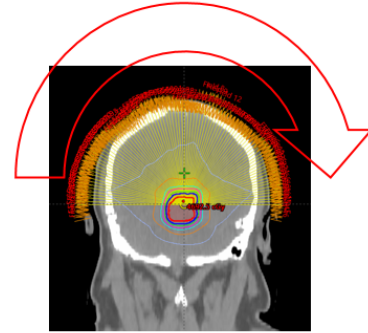


Figure 2. 3. Shows the description of GsCMO arc simulation process. It consisted of multiple static fields conformed around the PTV. The arc delivery is from 90 to 270 degrees which is considered as a single pi-plane dose delivery

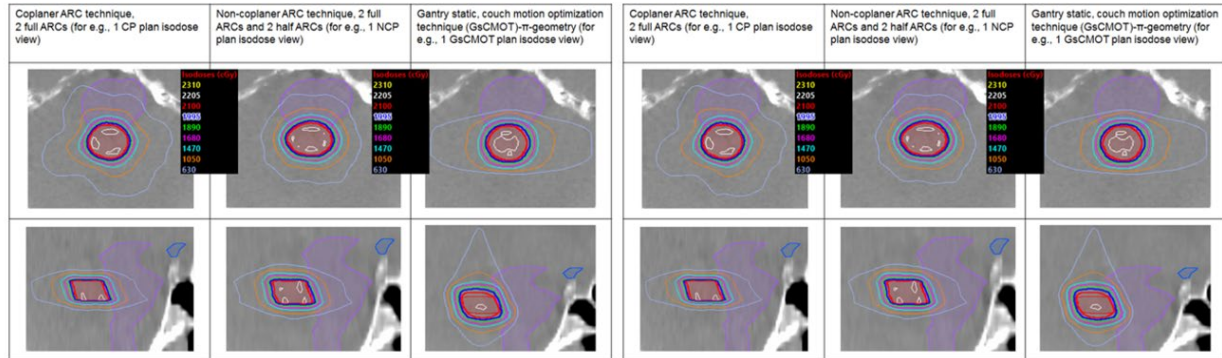


Figure 2. 4. On the left panel the comparison of dose distribution between standard coplanar and GsCMO technique is shown here. It is evident to notice the sharp fall-off in the anterior-posterior direction. Similar trend is shown in the right-hand side panel showing dose distribution comparison of non-coplanar technique with GsCMO technique

2.3.1.3. Results

Conformity index (C.I.), gradient measure (G.M.), and dose volume histograms (DVHs) were compared for coplanar (CP), non-coplanar (NCP) and GsCMO techniques. Timmerman's guidelines for organ-at-risks (OARs) and PTV coverage ($D_{95} = 100\%$) were used as meaningful endpoints. The D_{50} and D_{30} of brainstem were reduced by $48.9\% \pm 16.5\%$ and $65.9\% \pm 17.4\%$ for "1 PTVs", $8\% \pm 1\%$ and by $5.3\% \pm 2.9\%$ for "2 PTVs", and by $8.4\% \pm 3.1\%$ and $4.8\% \pm 1.6\%$ for chiasm using GsCMO as compared to CP. When comparing with the NCP technique, D_{50} and D_{30} of brainstem were reduced by $69.7\% \pm 9.2\%$ and $66\% \pm 17.4\%$ for planning target volume 1 (1 PTV), $70.4\% \pm 2.5\%$ and $50\% \pm 0.9\%$ for planning target volume 2 (2 PTVs), and $10.4\% \pm 1.9\%$ and $4.8\% \pm 2.1\%$ for chiasm using GsCMO technique. Conformity index (CI) was measured 1.37 ± 0.06 , 1.00 ± 0.06 , and 0.99 ± 0.03 for GsCMO, CP and NCP respectively. The overall gradient measure (in cm) was 0.86 ± 0.06 , 0.62 ± 0.05 , and 0.60 ± 0.04 for GsCMO, CP and NCP respectively. The mean distance gradient fall-off (in mm) was measured as 3.5 ± 0.03 (GsCMO), 6.0 ± 0.08 mm (CP), and $5.5 \text{ mm} \pm 0.09$ (NCP) in anterior-posterior direction of target volume.

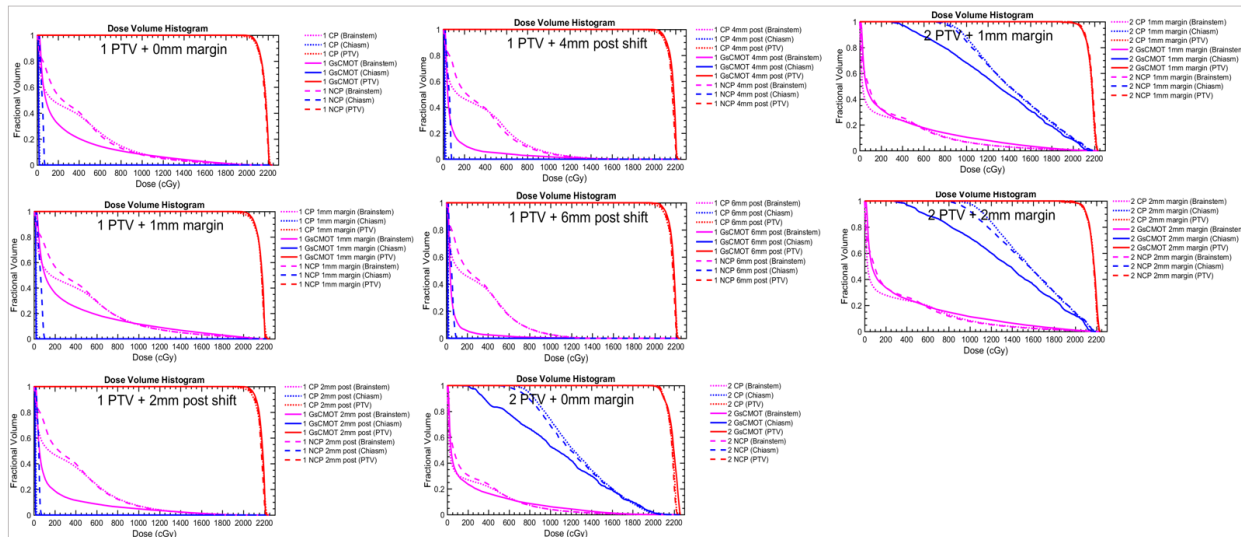


Figure 2. Comparison of fractional volume vs dose to PTV, Chiasm and Brainstem

Figure 2. 5. The DVH graph shows the PTV coverage and dose to the normal structures. Noticed here is the dose reduction to brain stem and optical chiasm while maintain the same dose coverage to PTV

2.3.1.4 Conclusion

In conclusion, implementation of the GsCMO technique enables integration of novel trajectory-based delivery technology, facilitating dose delivery during couch rotation unachievable using the current clinical paradigm (e.g., CP and NCP).

2.4. Application of GsCMO in breast boost treatment (Single isocenter based technique)

2.4.1. Significance

Patients who are in their early stage breast cancer and had undergone lumpectomy get partial breast irradiation as a sequential boost to lumpectomy cavity preceded by whole breast irradiation (WBI) as per the Radiation Therapy Oncology Group (RTOG) 1005³⁹. In modern era of radiation therapy, there are various external beam therapy techniques to deliver partial breast irradiation to lumpectomy cavity such as conventional 3-dimensional external beam radiation therapy (3D-CRT)⁴⁰, intensity modulated radiation therapy (IMRT)⁴¹ and its extension to more advanced volumetric modulated arc therapy (VMAT)²³. The latter are limited bound to positioning of mechanical axis such as gantry and couch. While all techniques aim for conformal irradiation of the target while minimizing the dose to OARs, selection of technique is carefully considered to avoid toxicity⁴².

This study developed and evaluated the clinical feasibility of gantry static couch motion (GsCM) technique for treating deep seated breast boost cavities as compared to conventional wedge pair techniques (WPS, WPD) techniques.

2.4.2. Methods

The gantry static couch motion (GsCM) technique utilized a simulated arc geometry consisting of multiple static fields as shown in Figure 2.6. The design of these fields involved dose calculation at every two degrees couch angle while maintaining static gantry positions at medial and lateral side of the beam entry. As such, the treatment couch rotated continuously while the beam is delivered in two-degree increments as shown in Figure 2.7.

GsCM technique was implemented for the boost treatments of 20 breast patients. This retrospective study consisted of 20 patients previously treated with external beam irradiation. All these patients previously received 50 Gy in 25 fractions to whole right/left breast irradiation with a photon boost of 10 Gy in 4 fractions to the partial breast. The dose distribution comparison of GsCMO with 3D-CRT and conventional wedge pair techniques (WPS, WPD) techniques is shown in Figure 2.8. The dosimetric accuracy of the plan delivery was evaluated by ion chamber array measurements in phantom as shown in Figure 2.9. The dose volume histograms (DVH) for lungs, normal breast tissue, and heart was calculated and compared with that of 3D-CRT and conventional wedge pair techniques (WPS, WPD) techniques as shown in Figure 2.10. The comparison with electrons was excluded in this study because of their finite range and anatomical location of lumpectomy cavity ($\geq 5\text{cm}$).

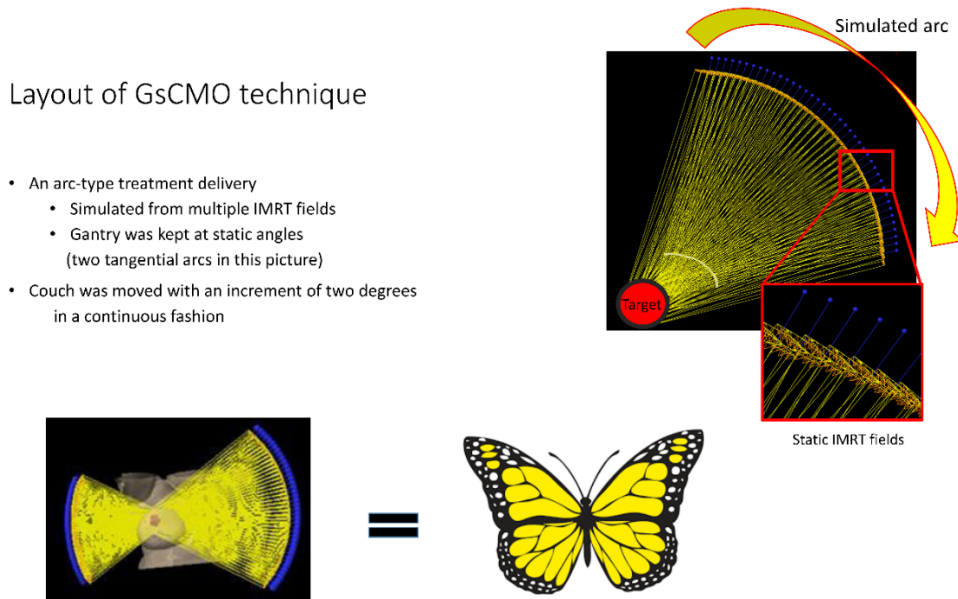


Figure 2. 6. Layout of GsCMO technique. Both medial and lateral arcs in this case deliver dose in a coronal plane.

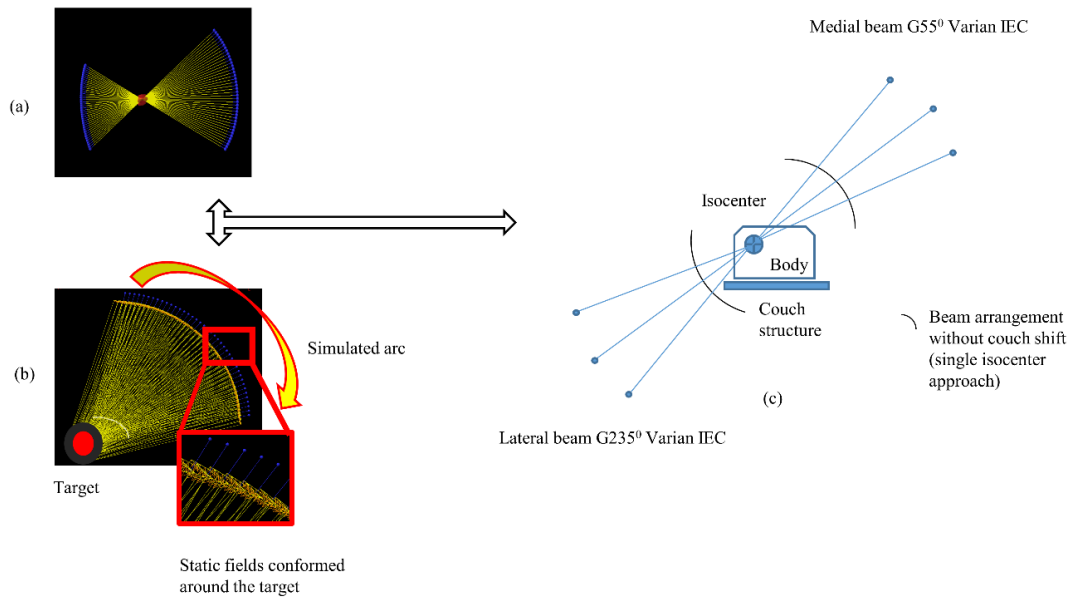


Figure 2. 7. Single isocenter technique is mostly applicable for central and lateral targets

Layout and comparison of GsCMO with wedge pair techniques

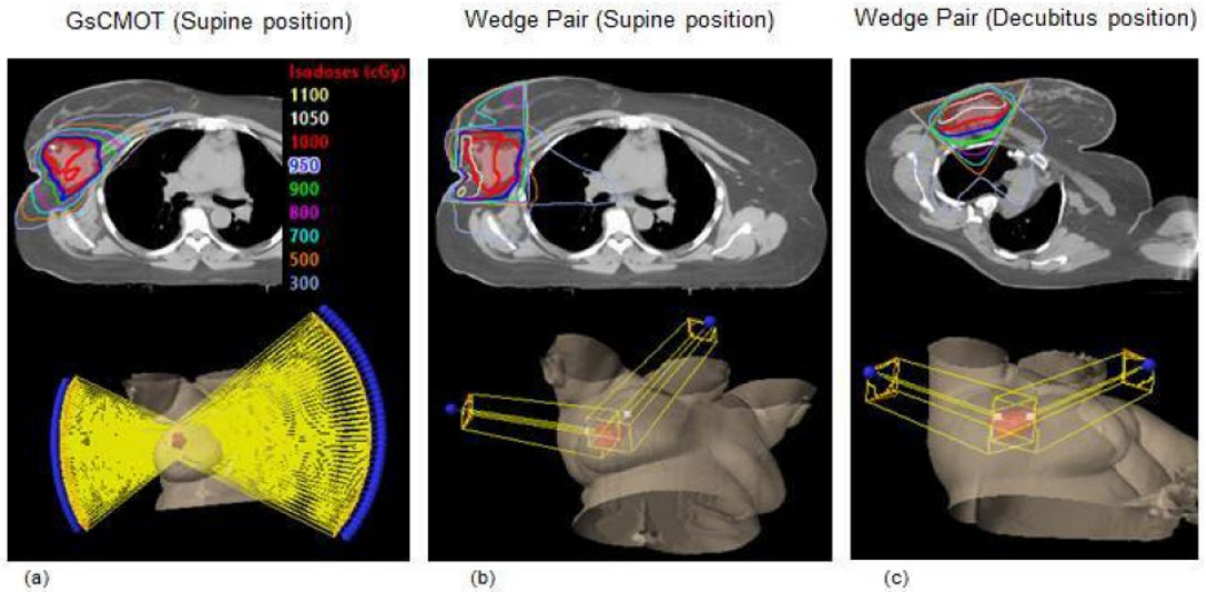


Figure 2. 8. Comparison of dose distribution between GsCMO with wedge 3-dimensional techniques (WPS, WPD) is shown here. It clearly shows no exist dose to ipsilateral lung due to the tangential nature of medial and lateral beams

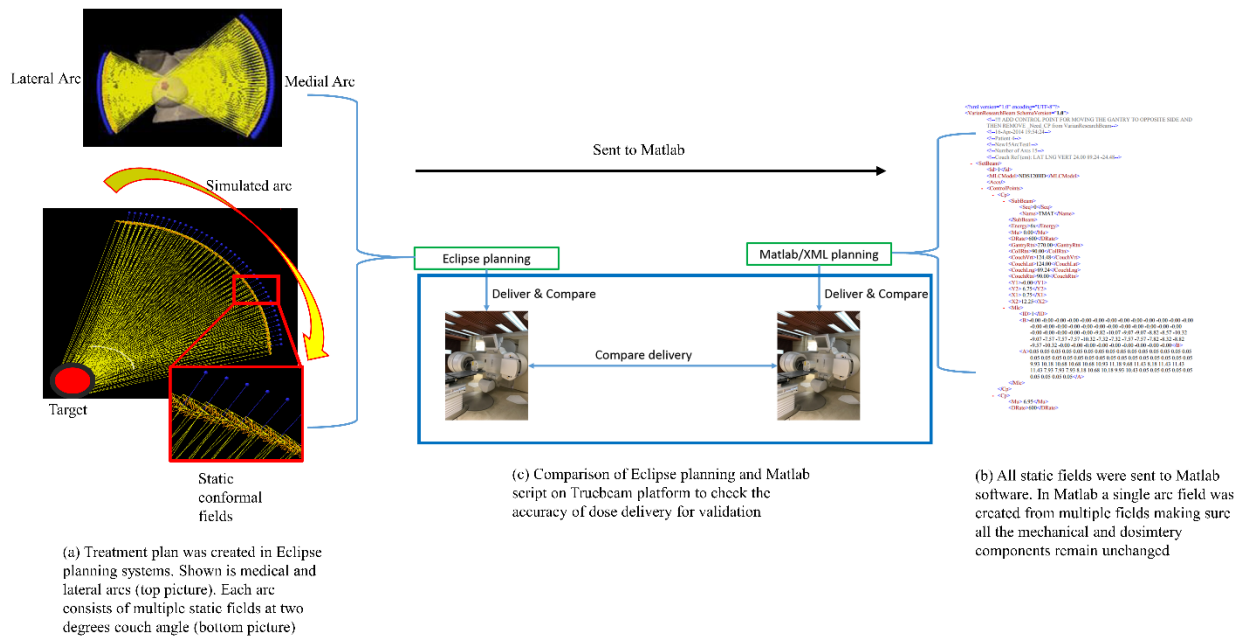


Figure 2. 9. Comparison of Eclipse simulated plans with script plans were conducted on Truebeam LINAC. The plans were delivered onto 2D-ion chamber array.

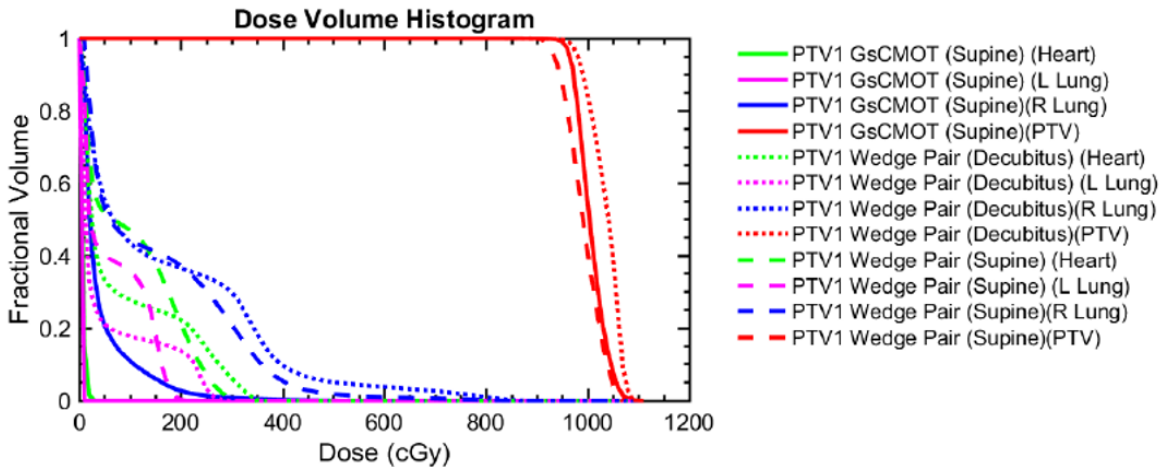


Figure 2. 10. DVH comparison among all 3 techniques (GsCMO, WPS, WPD) clearly shows the reduction of dose to heart, ipsilateral lung, and contralateral lung while maintaining the dose coverage to the target

2.4.3. Results

For both right and left breast boost, compared with GsCMO, 3D-CRT, WPS and WPD all provided an adequate coverage to PTV. GsCMO significantly reduced the ipsilateral lung V30% for right side (mean, 80%) and left side (mean, 70%). Heart V5% reduced by 90% (mean) for right and 80% (mean) for left side. Ipsilateral breast V50% and mean dose were comparable for all

techniques but for GsCMO, V100% reduced by 50% (mean) for right and left side. Maximum dose to contralateral breast showed significant improvement (95% for right and left side, mean) using GsCMO technique. The automated delivery of both arcs was under 2 minutes as compared to delivering individual fields (30±5 minutes). The gamma analysis using 2mm distance to agreement (DTA) and 2% dose difference (DD) was 98±1.5% for all 20 plans.

2.4.4. Summary and Conclusions

The reduction of high dose to normal breast tissue, spread of low dose to ipsilateral lung and heart, and significant dose conformity around the target volume makes GsCMO technique suitable for breast boost applications as described in detail in Chapter 3. We foresee the consideration of this study in future treatment planning systems which will require modification of their current dose calculation algorithms to consider the couch motion. Our approach is unique and opens the door for future advancement to existing treatment planning techniques. The GsCM technique also provides an opportunity to take advantage of capability of LINAC and treatment planning system for other body sites where the conformity and spread of low dose to organs-at-risk is highly appreciated. For our study, patient is a moving target on the treatment table. Therefore, it was important to study the patient motion during the GsCM delivery. Our study which raises the concern of mobility and immobilization issues related to patient during couch motion, is discussed in detail in Chapter 6.

One of the limitations we found with single isocenter technique was the short couch angular span on the lateral side of the beam for both right and left breast for medially located targets which was mitigated by introducing the lateral couch shift as shown in Figure 2.11. In order to encompass the whole PTV within the treatment field of view, the couch was moved up (anteriorly) in addition to the lateral shift. Hence, there is lateral and anterior shift for lateral side of the beam which was totally automated within our GsCM technique framework. This approach was based on two different isocenters for each arc using source-to-axis (SAD) approach. For the medical beam there is enough clearance for large angular span. This approach is equally applicable for left breast cases.

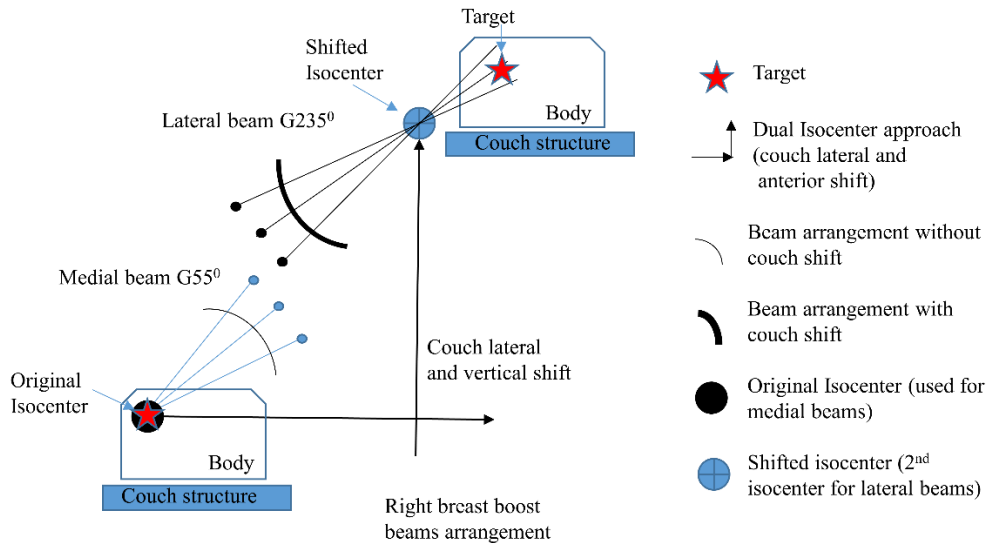


Figure 2. 11. Single isocenter technique cannot provide a wider lateral arc for medial targets. This can be mitigated by moving the patient laterally by approximately 20cm as shown in this figure.

2.5. Single vs Dual Isocenter

The single isocenter technique as shown in Figure 2.12 (a, b, and c) could be limited in regard to the couch span for the lateral arcs for both right and left breast for medial targets. In order to overcome this, we also introduced an option of dual isocenter technique where the medial arc remains the same, but the lateral arc can be widened by moving the couch laterally (away from the lateral gantry position) and in anterior (moving the couch upwards) direction. The dual isocenter option which provided more patient clearance was also automated to account the gantry switching from medial to lateral side, couch shift laterally and anteriorly, and dynamic couch motion.

The limitation of narrower lateral couch angular span for medial targets can be mitigated by utilizing the couch lateral shift of up to 20cm giving more room for a wider angular span (d) otherwise angular span is limited due to the close proximity of couch to gantry (e). This way a wider lateral angular span can be achieved (f) which helps enhance dose conformity around the target providing less spread of low dose to the ipsilateral breast. This technique was achieved by two isocenters. In order to keep the target volume encompassed within the MLC aperture, an anterior couch shift was applied (range of 2-5 cm) in addition to a lateral shift (e). In this way the target was always covered by MLCs. This approach is equally applicable to left breast if wider angular span is needed for the lateral arc. The concept of couch shift can be applied to get more clearance for both medial and lateral beams during the time of treatment planning. The design of

treatment fields can vary from patient to patient based on the location of the target volume and patient set up on the couch.

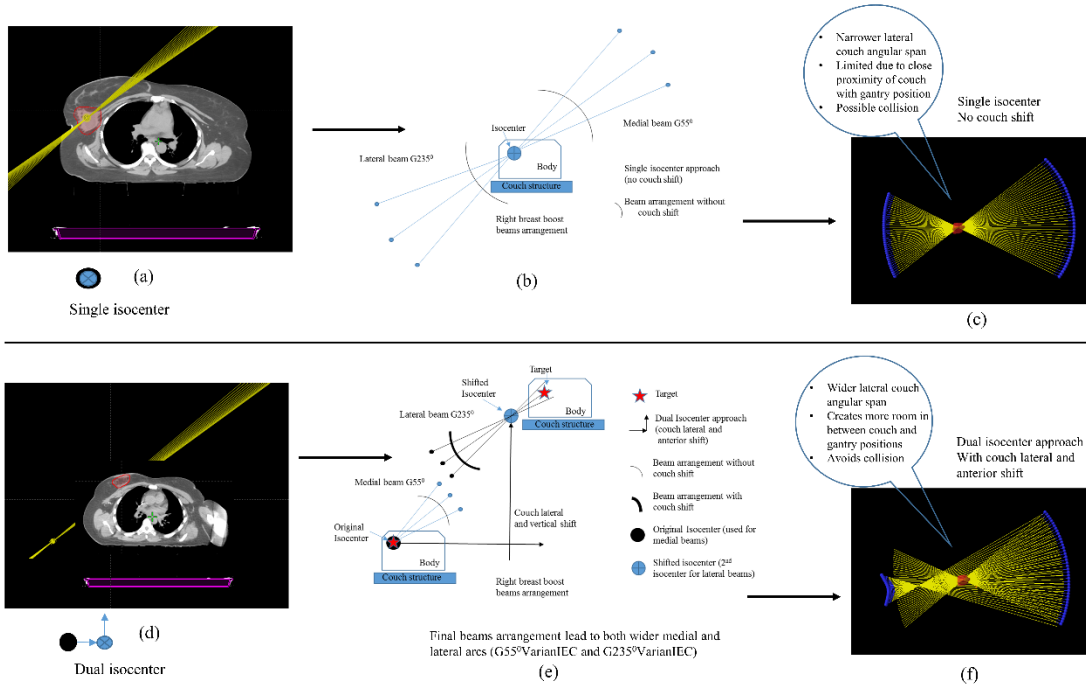


Figure 2. 12. After applying the lateral shift for medial targets provides more clearance laterally. In order to encompass the PTV another anterior shift was applied as shown in this figure.

Chapter 3: Design and evaluate the dosimetric advantages of volumetric modulated arc therapy based coronal arc delivery technique in brain stereotactic radiosurgery

Publication:
IJMPCERO. 2019; 8, 80-94

This chapter describes the feasibility of couch-based optimization technique based on a phantom study. The preliminary results presented in this study are the baseline for its applications in brain and breast cases.

3.1. Background and Introduction

The evolution of treatment planning, specific to patient treatment design and delivery has had a profound clinical impact, facilitating improved treatment outcomes while sparing the organs-at-risk (OARs).^{24-26,35,38} This development, with respect to brain pathologies, has enabled treatment of targets adjacent or near critical structures including the eyes, lenses, optic nerves, optic chiasm, brainstem and cochlea. These OARs pose significant challenges to the medical physicists/dosimetrists, responsible for safe and accurate treatment delivery. Intensity modulated radiation therapy (IMRT)⁴³ represents a major improvement over traditional forward planning techniques by utilizing computerized inverse planning and modulating the intensity of the radiation beam based on specific planning criteria including OARs dose constraints or PTV coverage goals. These advantages have become increasingly pronounced with the introduction of coplanar (CP) and non-coplanar (NCP) volumetric modulated arc therapy (VMAT)⁴⁴. In these applications dose modulation is performed by optimizing gantry rotation, dynamic jaw/ multileaf collimator (MLC) motion, and dose rate to achieve efficient dose delivery and superior OAR sparing.

Coronal arc (cARC) treatment planning consists of VMAT delivery in a coronal plane of the brain CT and differs from the axial plane delivery specifically with regard to beam orientation and delivery. In this study we evaluated the potential of VMAT based cARC technique. Since currently available treatment planning systems do not allow for patient rotation during beam delivery, the cARC technique was simulated using a vertically scanned anthropomorphic head and neck phantom. Each simulated cARC plan consisted of two multi-segmented partial (270° to 0° and 0° to 90° gantry angles) VMAT arcs, with dose modulation delivered along the coronal plane of phantom. Here we compare dosimetry results for the cARC to conventional coplanar and non-coplanar treatment of lesions of the brainstem or optic chiasm. Ongoing advancements in VMAT planning have the potential to provide crucial dose sparing of intracranial OARs, especially during hypo fractionated stereotactic radiosurgery (SRS) regimens.

3.2. Methods

3.2.1. Treatment planning study

The head and neck Alderson Rando anthropomorphic phantom (Model#ART 210: RSD Alderson Phantoms, Long Beach, California) was scanned axially using our in-house CT-SIM (Siemens Medical Solutions USA, Inc.) both horizontally and vertically (120KVp, 200mAs, 515x515 matrix size, 50cm field of view, and 2mm slice thickness) and exported to the Eclipse Treatment Planning system (Version #15.6, Varian Medical Systems, Palo Alto, CA) for treatment planning. PTVs were selected to simulate conditions where the cARC technique might be particularly advantageous as indicated in Figure 3.1. The PTVs were contoured posterior to the brainstem (Post PTVs) and centrally between the brainstem and optic chiasm (Ant PTVs). The set

of “Ant PTVs” and “Post PTVs” were drawn to evaluate the effectiveness of cARC delivery. Varying distances from OARs (i.e. brainstem and/or optic chiasm) were used for each set of PTVs to assess the potential benefits of the cARC technique. The naming convention and descriptions for all PTVs are provided in Table 3.1.

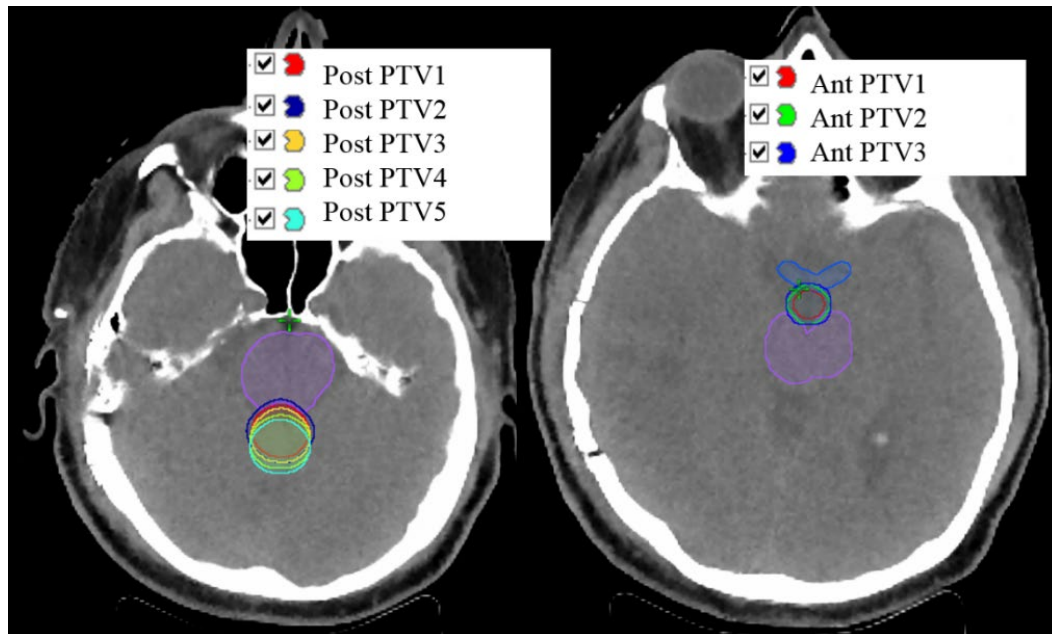


Figure 3. 1. Simulated planning target volumes with incremental margins near organs at risk. “Post PTVs” (Left Panel) is located posterior to the brainstem. “Ant PTVs” (Right Panel) is located in between the optic chiasm and the brainstem.

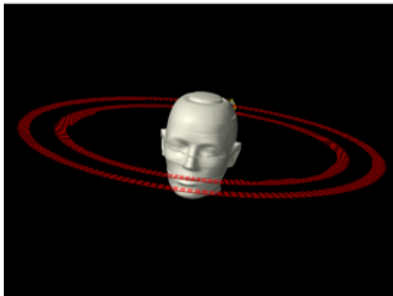
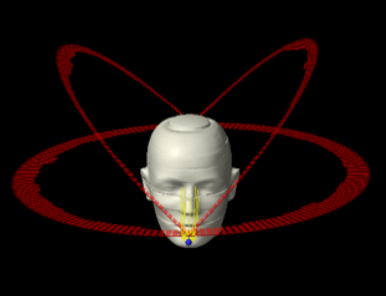
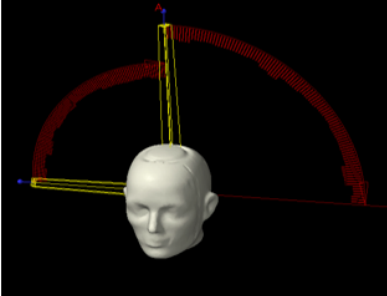
Coplanar ARC technique, 2 full ARCs	Non-coplanar ARC technique, 1 full ARC and 2 half ARCs	Coronal ARC technique, 2 half ARCs (combination of both ARCs represents a π -geometry)
		

Figure 3. 2. Beam orientation for coplanar (CP), non-coplanar (NCP) and coronal arc (cARC) techniques.

Table 3. 1. SRS Planning Treatment Volumes (PTVs) with associated description of margins

SRS Planning Treatment Volumes (PTVs)	Description of margins
Ant PTV1	PTV itself
Ant PTV2	1 mm margin from “antPTV1”
Ant PTV3	2 mm margin from “antPTV1”
Post PTV1	PTV itself
Post PTV2	1 mm margin from “postPTV1”
Post PTV3	2mm posterior from “brainstem”
Post PTV4	4mm posterior from “brainstem”
Post PTV5	6mm posterior from “brainstem”

Treatment planning consisted of a stereotactic radiosurgery (SRS) approach delivering 21 Gy in a single fraction using 6MV flattening free filter (FFF) photon beams. Treatment planning was performed using a high-definition multileaf collimator (HD-MLC) system consisting of 120 total leave (32 central 2.5mm width pairs + 28 peripheral 5mm width pairs) and 1.5mm dose grid resolution for all treatment plans. In the current study we consider two conventional treatment design approaches – standard coplanar (CP) arcs and non-coplanar (NCP) arcs were compared to the novel cARC approach as shown in Figure 3.2.

3.2.2. Coplanar arcs (CP)

The coplanar VMAT technique consists of multiple arcs planned in a single axial plane to facilitate the delivery of higher doses in regions of beam intersection. The Varian RapidArc®⁴⁵ approach consists of variable dose rate, variable gantry speed and dynamic MLCs. For the purpose of the study two coplanar arcs rotating clockwise from 181-179° and counterclockwise from 179 to 181° were utilized with a stationary couch angle of 0°.

3.2.3. Non-coplanar arcs (NCP)

The non-coplanar arc technique utilizes multiple beam geometries strategically planned to use non-standard couch angles. This technique is advantageous in the context of radiosurgery, where the goal of treatment is to deliver an ablative tumoricidal dose to the lesion while sparing the adjacent critical structures. It offers significant advantage over coplanar arcs when considering the dose delivered to the target by looking at the conformity of high isodose lines such as 80-95%. Therefore, non-coplanar arc therapy has the ability to shift the distribution away from the critical structures because the dose distribution follows the beam entrance. Use of non-standard couch angles can impose concerns of collision but with careful selection of couch and gantry angle collisions can be avoided. For this study three arcs were utilized clockwise: gantry angle 0-179° at couch angle 45°; anticlockwise: gantry angle 0-181° at couch angle 315° along with one coplanar arc mentioned earlier in the “coplanar arcs” section.

3.2.4. Coronal arc (cARC) delivery technique

The cARC technique utilizes two partial arcs delivered in a coronal plane. The main difference of cARC from standard VMAT delivery is delivering dose in a coronal plane by rotating the couch while the gantry is fixed at 90° or 270°. Since our treatment planning system doesn't allow couch rotation during the beam delivery, we simulated the cARC technique in this study by scanning the head and neck anthropomorphic phantom in a vertical position. The cARC beams were simulated with two VMAT beam at gantry angles of 0-90° and 270-0° respectively, with couch angle 0°. These partial arcs represent a π -geometry. The treatment planning design for this approach is demonstrated in Figure 3.2.

3.2.5. SRS planning criteria

Dosimetric indices for CP and NCP techniques were compared with the cARC technique. During the optimization process, the dose constraints to PTVs and OARs were kept constant for all plans. In addition, all plans were normalized to the same prescription dose coverage i.e. D95=100% (95% of PTV receives at least 100% of the prescription dose). Two different SRS planning approaches were used to compare CP, NCP, cARC techniques. The first approach evaluated dose to the brainstem and optic chiasm without compromising on PTV coverage (i.e. D95=100%). This simulates tumor invasion into nearby critical organs where adequate coverage to PTV is prioritized. The second approach followed the guidelines proposed by Timmerman et al⁴⁶, which have now incorporated into AAPM task group (TG) 101⁴⁷ for normal structures. In this case rigid dose constraints were made to the nearby critical structures. This simulates cases where the tumor has no invasion into nearby critical structures and sparing of OARs is highly prioritized.

3.2.6. Dosimetric indices and their definitions

The Eclipse planning system (Varian medical systems, Palo Alto, CA) calculated the following indices after computation of final dose calculation.

Conformity Index (C.I.) evaluates the dose conformity inside the PTV and is calculated as follows: $CI = V_{95\%}/V_{PTV}$, where $V_{95\%}$ is the volume enclosed by prescription isodose surface (95%) and V_{PTV} is the target volume. C.I. close to 1 is considered as an adequate plan for comparison.

Gradient Measure (G.M.) is the difference between the prescription and half of the prescription isodose spheres. G.M. accounts the spread of 50% isodose away from PTV and is calculated as follows: $G.M. = R_{50} - R_p$, where R_p and R_{50} are the equivalent sphere radius of the prescription and half prescription isodoses. A plan that has lowest value of G.M. is considered an adequate plan for comparison.

Mean gradient fall-off calculates the dose fall off in a central (single) slice of PTV in a 2-dimensional area. This measures the difference between the average dose to the 100% and 50%

two-dimensional isodose surfaces (IS_{100%} and IS_{50%}) in anterior and posterior directions with respect to PTV.

$$\text{Mean gradient fall-off} = \text{Average} [(IS_{\text{ant}50\%} - IS_{\text{ant}100\%}) - (IS_{\text{post}50\%} - IS_{\text{post}100\%})].$$

A plan that has lowest value of mean gradient fall-off is considered an adequate plan for comparison.

3.3. Results

Dosimetric indices of standard rapid arc techniques using coplanar (CP) and non-coplanar (NCP) beam arrangements were compared to the proposed cARC technique. Axial (top row) and sagittal (bottom row) isodose distributions are presented for “antPTVs” in Figure 3.3 and for “postPTVs” in Figure 3.4 respectively. Sharp dose fall-off in the anterior-posterior direction with respect to the PTV are seen for both “Ant PTVs” and “Post PTVs” using cARC technique (Figure 3.3 and Figure 3.4).

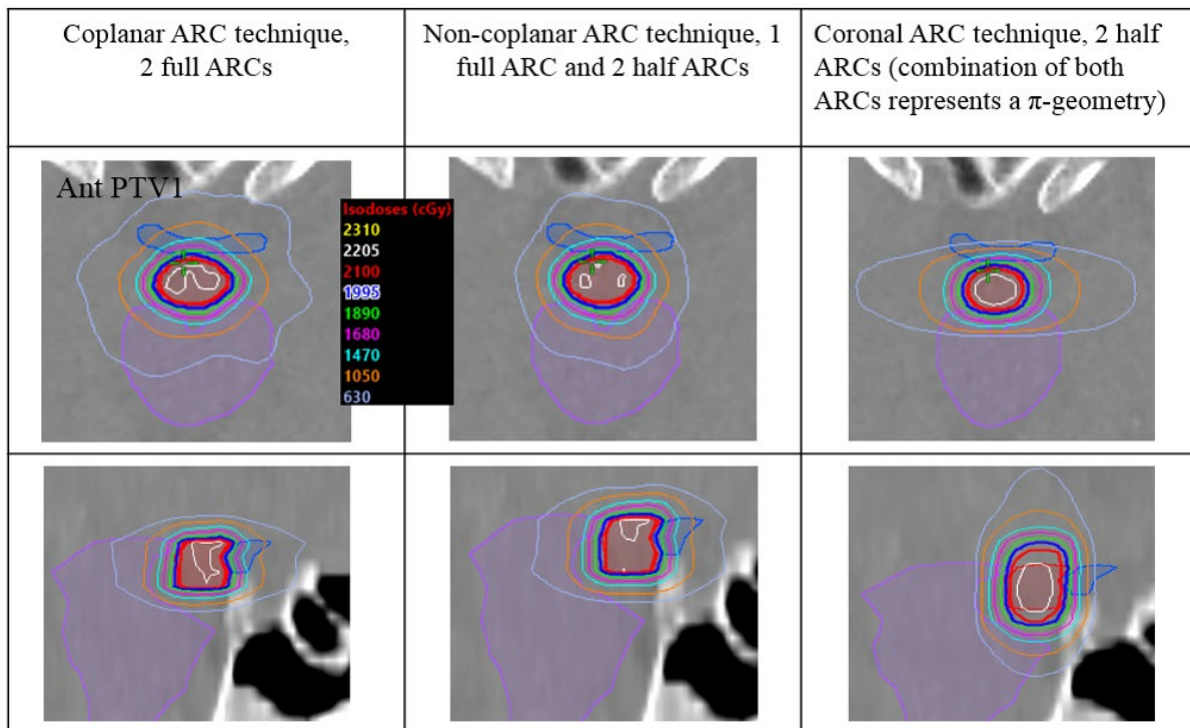


Figure 3. 3. Axial and sagittal isodose distributions for “Ant PTV1” using coplanar (CP), non-coplanar (NCP) and coronal arc (cARC) techniques. By looking at the dose distribution, cARC shows superior dose fall-off in the anterior-posterior direction

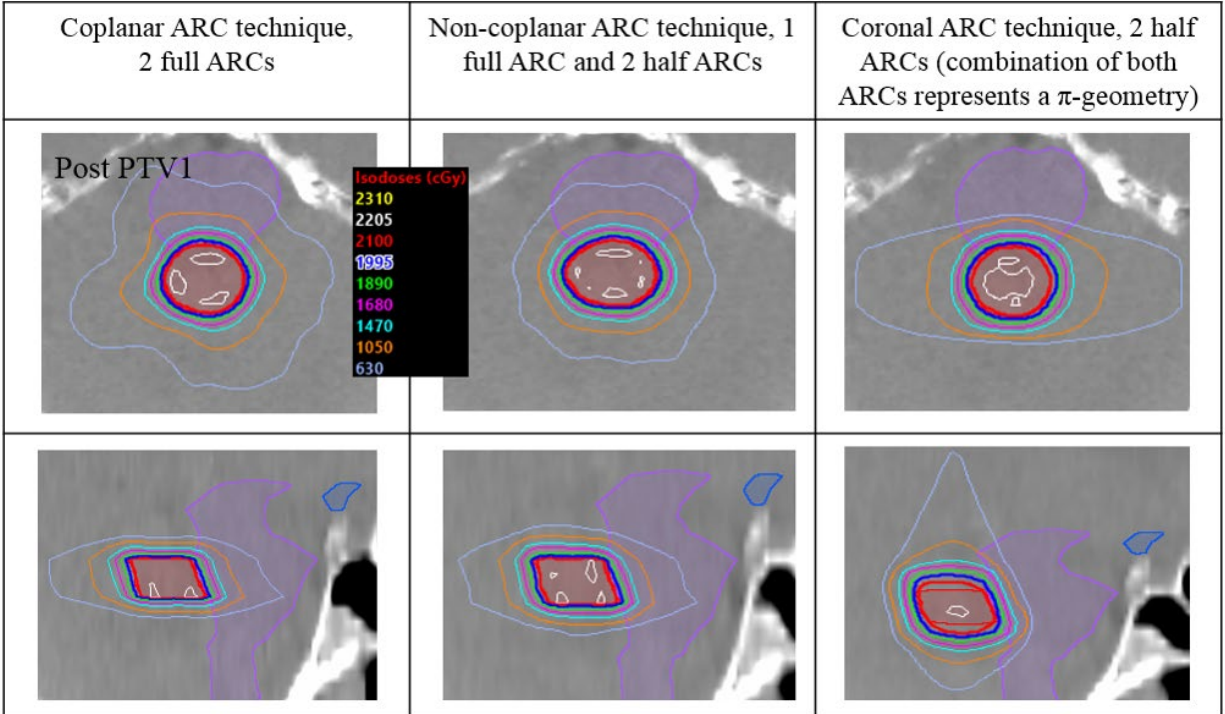


Figure 3. 4. Axial and sagittal isodose distributions for “Post PTV1” using coplanar (CP), non-coplanar (NCP) and coronal arc (cARC) techniques. The cARC technique shows superior dose fall-off in anterior-posterior direction. NCP technique shows compact dose distribution around the PTV as compared to both CP and NCP

Dose volume histograms (DVHs) comparing all three approaches are shown in Figure 3.5. Comparing cARC with CP, the D50 and D30 of brainstem was reduced by $85.1\% \pm 3.9\%$ and $87.6\% \pm 3.2\%$ for “Post PTVs”, by $51.1\% \pm 17.8\%$ and by $85.6\% \pm 6.0\%$ for “Ant PTVs”. For chiasm, the reductions were $61.7\% \pm 3.2\%$ and $44.2\% \pm 8.9\%$ for “Ant PTVs”, and $69.3\% \pm 8.0\%$ and $74.3\% \pm 8.2\%$ for “Post PTVs”. When comparing cARC with the NCP technique, D50 and D30 of brainstem was reduced by $80.9\% \pm 3.3\%$ and $84.6\% \pm 4.8\%$ for “Post PTVs”, by $74.4\% \pm 4.8\%$ and $79.6\% \pm 6.6\%$ for “Ant PTVs”. In addition, for chiasm reductions were $49.9\% \pm 2.6\%$ and $34.8\% \pm 8.2\%$ for “Ant PTVs” and by $84.8\% \pm 2.9\%$ and $86.7\% \pm 2.5\%$ for “Post PTVs”. Profiles of the dose fall-offs for all 3 techniques which were drawn at the center of “Ant PTVs” and anterior to “Post PTVs” are shown in Figure 3.6.

Comparison of brainstem and chiasm dose for CP, NCP and cARC techniques that followed the PTV: D95=100% criteria are shown in Table 3.3. As defined by TG101⁴⁷, the maximum point dose where a “point” is defined as 0.035cc or less, for brainstem and chiasm was limited to 15Gy and 10Gy respectively. Significant OAR dose reduction was observed for the cARC technique relative to CP and NCP techniques, particularly to brainstem and chiasm as shown in Figure 3.5.

With regards to the constraints outlined by Timmerman et al.⁴⁶, and now part of TG101⁴⁷ treatment plan quality was assessed by comparing D95 (dose received by 95% of the volume) and

the mean dose to the PTV while satisfying the aforementioned criteria. This allows fulfillment of the study goal of evaluating which technique can better maintain high mean dose and good coverage to PTV after meeting the dose constraints to critical structures. Sparing normal tissues and/or good coverage of the PTV is a foundation of the clinical decision making by radiation oncologist. The cARC technique resulted an overall increase in D95 and max dose to PTV as compared to CP and NCP as shown in Table 3.4.

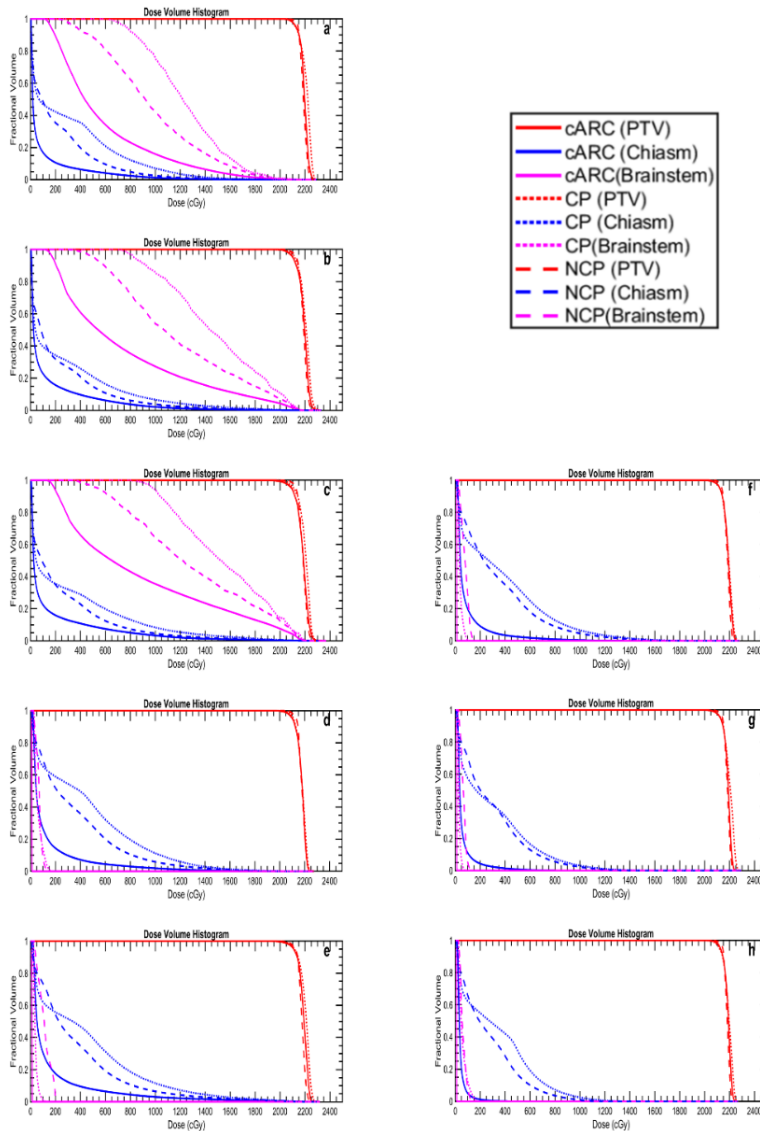


Figure 3. 5. Comparison of fractional volume vs dose to “Ant PTVs” and “Post PTVs”, Chiasm and Brainstem for coplanar (CP), non-coplanar (NCP) and coronal arc (cARC) techniques. Graph “a-c” are for “Ant PTVs” and “d-h” for “Post PTVs”. To represent a true comparison, all plans were normalized equally. It clearly shows an improvement of dose reduction to brainstem and optical chiasm

Conformity index (C.I.) analysis is shown in Table 3.2 demonstrating distinct differences between the cARC technique and standard CP and NCP techniques. The conformity index (C.I., mean±SD) was measured 1.101±0.038, 1.088±0.054, and 1.060±0.040 for cARC, CP and NCP respectively.

The overall gradient measure (G.M. in cm, mean±SD) was 0.581±0.097, 0.708±0.064, and 0.476±0.050 for cARC, CP and NCP respectively. Even though the gradient measure value of cARC was found inferior to NCP and superior to CP. This parameter is measured spherically. From the dose distribution of cARC, we are mainly focused on saving the OARs anteriorly and posteriorly. Thus, in addition to G.M., a parameter called mean distance gradient fall off was calculated. This provides a clear indication of dose fall off in a plane (2 dimensional) rather than 3 dimensional.

The mean distance gradient fall-off (in cm, mean±SD) was measured as 0.249±0.038 (cARC), 0.749±0.107 (CP), and 0.621±0.068 (NCP) at the center slice in anterior-posterior direction of PTV, clearly demonstrating a sharper gradient in the anterior-posterior direction.

3.4. Discussion

This work demonstrates that cARC applied to specific clinical applications can be a significant advancement over existing treatment planning techniques. This approach is particularly advantageous in brain when the treatment target is in close proximity to the brainstem and/or optic chiasm. Several investigators have studied the potential of trajectory-based treatment with integration of couch motion during dose delivery^{24-31,35,37,38,48-50}. We have focused on a single- π geometry rather than more complex treatment designs which are difficult to deliver and are more likely to result in collision with the patient or gantry. Further, single- π geometry has been shown to deliver comparable integral dose to the irradiated volume, sharp dose fall off in the anterior-posterior direction and less dose spread to brainstem and optic chiasm relative to highly complex 4 π -geometry treatment plans.^{28-31,49}

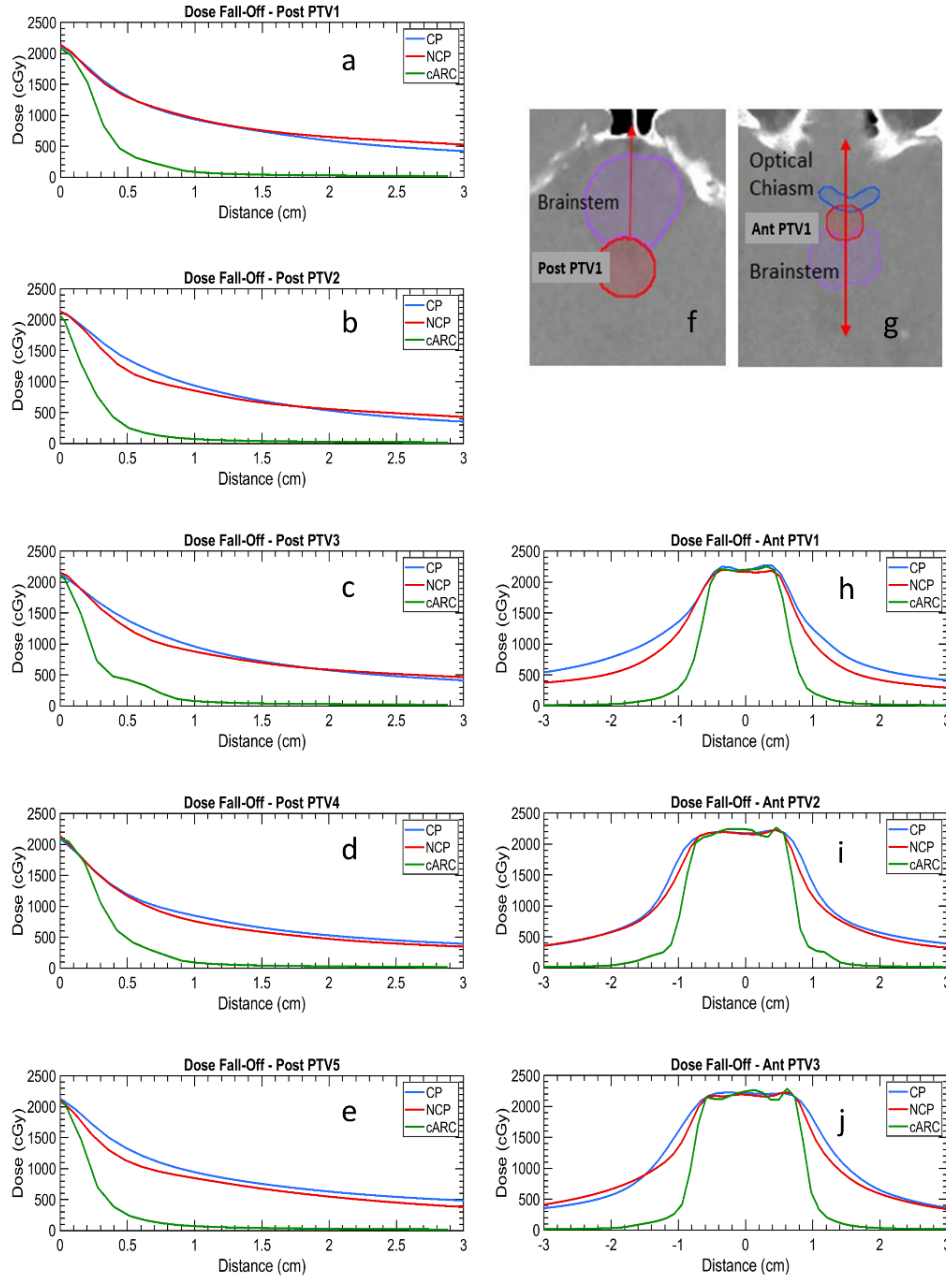


Figure 3. 6. Dose fall-off is shown here which was calculated by drawing a line profile at the center of “Ant PTVs” and anterior to center of “Post PTVs”. For example, this figure shows dose fall-off for “Post PTVs” (as shown in graph “a-e”) with its profile direct directionality is shown in graph “f” (for e.g. “Post PTV1). Similar way it is shown for “Ant PTVs” in graph “h-j” and their directionally (for e.g. “Ant PTV1) in graph “g”)

Our results demonstrate that the cARC beam arrangement provides better normal tissue sparing and comparable dose coverage to the target as compared to existing planning techniques of CP & NCP^{24-27,35,37}. This is evidenced by the various dose metrics sampled including reduced

dose to normal structures in terms of mean dose and max dose, comparable conformity index, and high dose fall-off obtained using the cARC technique relative to CP and NCP. Conformity Index (C.I.) for cARC is comparable to CP and NCP techniques. This suggests that the cARC technique can potentially be implemented for intracranial applications.

Table 3. 2. Conformity Index (C.I.) and Gradient Measure (G.M.) comparison of coplanar (CP), non-coplanar (NCP) and coronal arc (cARC) planning techniques. Non-coplanar (NCP) technique has better C.I. and G.M. indices. Conformity Index (C.I.) for cARC is comparable to both NCP and CP. Gradient Measure (G.M.) for cARC resides in between NCP and CP but superior to CP

PTVs	Conformity Index (C.I.)			Gradient Measure (G.M.)		
	Coplanar Arcs (CP)	Non-Coplanar Arcs (NCP)	CoronalArc (cARC)	Coplanar Arcs (CP)	Non-Coplanar Arcs (NCP)	CoronalArc (cARC)
Ant PTV1	1.21	1.15	1.16	0.73	0.42	0.44
Ant PTV2	1.08	1.06	1.12	0.61	0.41	0.46
Ant PTV3	1.08	1.03	1.04	0.63	0.42	0.50
Post PTV1	1.02	1.03	1.06	0.79	0.51	0.65
Post PTV2	1.08	1.03	1.09	0.78	0.51	0.66
Post PTV3	1.09	1.05	1.10	0.70	0.50	0.63
Post PTV4	1.08	1.06	1.11	0.70	0.52	0.64
Post PTV5	1.06	1.07	1.13	0.72	0.52	0.67
Mean±SD	1.088±0.054	1.060±0.040	1.101±0.038	0.708±0.064	0.476±0.050	0.581±0.097

Further justification of this approach is validated by our results with regards to G.M. and mean gradient fall off. Although G.M. for cARC was reduced relative to CP and comparable to NCP, the parameter is not necessarily appropriate for our analysis since G.M. is evaluated isotropically without any consideration of laterality. An appropriate analogy to describe the advantage of cARC technique is to compare dose distribution to the deformation of a balloon. Dose distribution can be likened to a balloon; if squeezed in two dimensions it will deform into the third dimension. For cARC, dose spillage into the lateral and superior-inferior direction into the normal brain is accepted, but the critical clinical advantage gained is dose fall-off in the anterior-posterior direction. This is in recognition that for lesions proximal to the brainstem and optic chiasm the greater concern is with the dose fall-off anteriorly and posteriorly. Based on this, mean dose gradient fall-off is a more meaningful parameter than gradient measure because the later applies spherically and degrades the advantage of cARC as compared to CP and NCP.

Table 3. 3. Comparison of brainstem and chiasm dose for CP, NCP and cARC techniques following PTV: D95=100% criteria. As per TG101, max point dose where “point” is defined as 0.035cc or less, for brainstem and chiasm it is limited to 15Gy and 10Gy. The V10Gy to brainstem and V8Gy to chiasm are the threshold doses. $D_{\leq 0.5cc}$ for brainstem and $D_{\leq 0.2cc}$ for chiasm are chosen as meaningful points for “max critical volume above threshold”

PTV	Planning Technique	Brainstem			Chiasm		
		$D_{\leq 0.5cc}$ (cGy)	$V_{\geq 10Gy}$ (cc)	$D_{0.035cc}$ (cGy)*	$D_{\leq 0.2cc}$ (cGy)	$V_{\geq 8Gy}$ (cc)	$D_{0.035cc}$ (cGy)*
Ant PTV1	CP	1375	2.21	1811	1477	0.83	1818
	NCP	1112	0.75	1731	1280	0.56	1743
	cARC	917	0.36	1591	809	0.21	1552
Ant PTV2	CP	1609	2.07	2074	1827	0.87	2087
	NCP	1362	1.16	2064	1605	0.66	2073
	cARC	1095	0.66	1989	1134	1133	2013
Ant PTV3	CP	1772	2.59	2146	1917	0.89	2155
	NCP	1514	1.44	2176	1780	0.72	2128
	cARC	1307	1.03	2133	1421	0.38	2104
Post PTV1	CP	1545	3.54	1936	82	--	132
	NCP	1462	1.85	1914	80	--	113
	cARC	1071	0.59	1752	12	--	13
Post PTV2	CP	1795	3.63	2154	47	--	79
	NCP	1666	2.03	2144	45	--	75
	cARC	1394	0.94	2113	14	--	14
Post PTV3	CP	1399	2.08	1762	48	--	80
	NCP	1309	1.46	1707	47	--	79
	cARC	656	0.14	1253	12	--	13
Post PTV4	CP	1138	0.98	1436	36	--	57
	NCP	1074	0.72	1361	35	--	55
	cARC	375	--	738	12	--	11
Post PTV5	CP	1063	0.76	1288	78	--	137
	NCP	926	0.27	1151	75	--	111
	cARC	173	--	376	11	--	12

*Volume receiving max point dose where “point” is defined as 0.035cc or less

This work presents two dosimetric approaches representing alternative treatment objectives. For the first approach of assuring D95=100% in our comparison of cARC relative to CP and NCP, an overall lower dose to the optic chiasm and brainstem results (D50 and D30 are significantly reduced). Unfortunately, $D_{0.035cc}$ is increased relative to TG101 targets of 15Gy to brainstem and 10Gy to optic chiasm. This is caused by the proximity and assumed invasion of “Ant PTV2”, “Ant PTV3”, “Post PTV1” and “Post PTV2” into OARs.

For the second approach, dose constraints to the brainstem (0.5cc<10Gy, maximum point dose <15Gy) and chiasm (0.2cc<8Gy, maximum point dose<10Gy) were met. Comparison of the dose to PTV in terms of D95 and mean dose shows that for acceptable plans cARC provides

dosimetric improvement relative to CP and NCP for “Ant PTV1”, “Ant PTV2”, “Ant PTV3”, “Post PTV1”, and “Post PTV2”. When PTV moves away from OARs such as for “Post PTV3”, “Post PTV4”, and “Post PTV5” the advantage of cARC becomes small and, in terms of dosimetry it is comparable to CP and NCP.

Constraining doses to OARs allowed for study of the usefulness of cARC for PTVs which had invaded OARs or have margins within OARs. To have clinically acceptable plan two options must be provided; either save OARs or to provide coverage to the PTV within the OARs. Clearly, a suitable clinically treatment plan must meet the patient condition which may include spread of disease into the nearby OARs. The ability to control dose to OARs or provide adequate coverage to PTV is a hallmark of cARC.

Table 3. 4. Comparison of D95 (cGy) and mean dose to “Ant PTVs” and “Post PTVs” for all techniques satisfying TG101 criteria of dose constraints to brainstem (0.5cc<10Gy, max point dose<15Gy) and optic chiasm (0.2cc<8Gy, max point dose<10Gy)

PTV	Technique	PTV D95(cGy)	Mean dose to PTV (cGy)
Ant PTV1	CP	1273	1523
	NCP	1508	1907
	cARC	1684	2045
Ant PTV2	CP	1031	1335
	NCP	1068	1702
	cARC	1658	2050
Ant PTV3	CP	978	1282
	NCP	1051	1698
	cARC	1445	2070
Post PTV1	CP	1802	2096
	NCP	2106	2176
	cARC	2120	2170
Post PTV2	CP	1598	2045
	NCP	1638	2103
	cARC	1850	2150
Post PTV3	CP	2082	2182
	NCP	2138	2176
	cARC	2140	2178
Post PTV4	CP	2118	2177
	NCP	2144	2178
	cARC	2145	2180
Post PTV5	CP	2120	2179
	NCP	2145	2180
	cARC	2150	2185

Implementation of this technique is particularly useful in instances where the lesion is in close proximity or invading the OARs. This is further compounded by the addition of a PTV margin accounting for set-up error. Maintaining coverage of the PTV while respecting the dose constraints of the critical structures is therefore a crucial component of the clinical decision-making process. However, in the current clinical paradigm, lesions in close proximity to the brainstem or chiasm must compromise PTV coverage to respect the dose constraints of the OARs.

The cARC technique introduces an alternative approach by shifting the dose distribution away from the OARs while maintaining PTV coverage not previously attainable using the CP and NCP techniques.

While the proposed cARC technique confers significant benefit over the current clinical alternatives, implementation of this technique is limited by the capabilities of the treatment planning and delivery systems. It is therefore necessary to not only develop the framework for coronal arc optimization planning and translate it such a way that it can be delivered in supine position but to also specify quality assurance measures to ensure safe treatment delivery. One possible approach to achieve this goal is to deliver cARC during treatment couch motion by keeping the gantry static. Further, while the utility of this technique is particularly advantageous in brain, opportunities exist for application in various extracranial sites including breast and extremities. Work is currently underway to recognize these goals.

3.5. Conclusions

In conclusion, this chapter described the simulation of an innovative cARC technique based on a phantom study that provides sharp fall-off of dose anteriorly and posteriorly from PTV in brain while minimizing dose to OARs. We proposed the benefits of this technique in treatment of SRS and SRT cases for those patients who are candidates of hypo-fractionation regimen. The couch-based optimization delivery technique (cARC) was compared with standard VMAT techniques such as coplanar and non-coplanar. The results presented here are the baseline for the generation of gantry static couch motion optimization (GsCMO) technique and its applications for external beam radiation therapy treatments in brain and breast cases in the following chapters.

Chapter 4: Application of gantry-static couch-motion (GsCM) technique in breast radiation therapy: Reduced dose to organs-at-risk and improved dosimetric indices

Publication:

JACMP:2020; DOI: 10.1002/acm2.12969

Med Phys., 2020. Abstract ID: 52956

This chapter describes in details the application of gantry static couch motion optimization technique (GsCMOT) in breast treatment. The first half of the chapter discusses the potential applications in breast boost radiation therapy. The second half provides a potential solution for partial breast irradiation (PBI) treatment. Patients who are diagnosed with early stage breast cancer undergo breast conserving surgery (BCS) and followed by radiation therapy. This chapter discusses in detail on how radiation therapy plays an integral role in treatment of lumpectomy cavity after surgery to avoid the spread of cancer to the normal breast tissue.

4.1. Application in breast boost treatment

4.1.1. Overview

Radiation therapy plays an important role for patients who undergo breast conservation therapy (BCT) which includes both breast conserving surgery (BCS) and radiotherapy. Breast conservation therapy (BCT) preserves the breast normal tissue as much as possible without compromising survival. Breast conservation surgery (BCS) as known as lumpectomy, quadrantectomy, partial mastectomy, or segmental mastectomy depending on how the tissue has been removed is important which includes resection of the primary tumor with or without axillary nodes followed by radiotherapy to eradicate the residual microscopic disease of the breast tissue^{51,52}. According to cancer statistics⁵³ in 2020 there were about 276,480 (30% of estimated new cases for all sites in female) new cases of breast cancer. In women, breast cancer has high incidence rate as compared to other types of cancer. Depending on the patient staging^{39,54}, for early-stage breast cancer with stage I and II, the conservative surgery and radiation therapy are standard alternatives to mastectomy. Radiation therapy after lumpectomy has been known for long term local control equivalent to mastectomy^{39,55} on the order of 85-95% with similar survival outcomes. Further, post lumpectomy radiation therapy is associated with reduction in local recurrence and improved overall survival rate as compared to surgery alone⁵⁶. Therefore, radiation therapy is considered a better approach for post lumpectomy treatment as compared to lumpectomy alone.

Patients who have early stage breast cancer and received a lumpectomy can get sequential boost (10-18 Gy) to post lumpectomy preceded by whole breast radiation therapy (46-50.4 Gy with 1.8 to 2Gy daily fractions) as per the Radiation Therapy Oncology Group (RTOG) 1005³⁹. Current clinical practice is to treat the whole breast followed by a coned down boost to the lumpectomy cavity using electrons for superficial cavities and photons for deep seated cavities. While both photons and electrons aim for conformal irradiation to the target while minimizing the dose to organs-at-risk (OARs), selection of one versus the other should be carefully considered to avoid toxicity⁴².

In a previous publication⁵⁷ we have developed the clinical feasibility of gantry static couch motion (GsCM) technique for treating deep seated brain tumors. This technique was found beneficial for brainstem tumors or targets in the middle of optic chiasm and brainstem. The main advantageous of this approach in brain tumors was a sharp dose fall-off anteriorly and posteriorly

to the target which spared normal tissues such as optical track and brainstem. In the current study, two partial arcs were simulated by adding multiple conformal static fields for each side. The GsCM technique is conceptually similar to volumetric modulated arc therapy (VMAT), because it includes dose modulation. Although, the modulation is achieved without inverse optimization. For GsCM the couch is dynamic with a static gantry (i.e. GsCM utilizes a fixed gantry and rotating couch).

In this study we investigated the potential dosimetric advantages of the GsCM technique for sequential/concurrent boost of post lumpectomy cavities as compared to existing 3-dimensional conformal radiation therapy (3D-CRT), conventional wedge pair in supine position (WPS) , and wedge pair in decubitus position (WPD) techniques. The dose volume histogram (DVH) for lungs, normal breast tissue, and heart were calculated and compared with that of 3D-CRT and conventional wedge pair techniques (WPS, WPD) techniques. The dosimetric accuracy of the plan delivery was evaluated by ion chamber array measurements in phantom.

4.1.2. Materials and Methods

In this study, the GsCM technique was implemented for the boost treatments of (n=20) breast patients. This retrospective study has received an institutional review board (IRB#19-1025) approval to conduct the comparison of different treatment planning techniques for breast boost treatments. This study is focused on women who have large breast size resulting in a post lumpectomy cavity that is greater than 5cm deep. Use of electrons in this case is inferior due to greater skin dose and inadequate coverage distally to the lumpectomy cavity. Therefore, comparison with electrons were excluded from this study.

4.1.2.1. The gantry static couch motion (GsCM) technique

In this study the GsCM technique was implemented by first selecting the medial and lateral beams arranged with 2° delta couch angles. The GsCM concept begins somewhat similar to dynamic conformal arc, in the sense that each beam initially conforms to the planning target volume (PTV) plus margin at every segment, which is actually a fixed static beam. However, the MLCs were conformed with a static gantry and a variable couch. After, the dose calculation, the beam weighting was adjusted to achieve good conformity around the target. Next, a fluence editing option was used to make the dose distribution homogenous as possible within the PTV. The MLCs were then generated with a limit of 1 segment per field. The groups of static beams then became like VMAT with both dose rate and aperture modulation. The main differences between standard VMAT and our GsCM technique are the moving couch instead of gantry, use of non-traditional inverse optimization, and the dose delivery at 2° increments rather than continuous.

The simulated fields for GsCM technique were then transferred to MATLAB[®] for in-house custom-made script to combine all the modulated fields. This provides a single deliverable file in XML format. This XML file mirrors all the beam characteristics as compared to the planned treatment fields. Implementation was performed within the Truebeam[®] (Varian Medical Systems,

Palo Alto, CA) developer mode application utilizing 6MV energy. Varian developer mode application in the research environment allows for custom XML scripting by controlling all the mechanical axes of the LINAC including gantry, couch, collimator, jaws, and MLC control points for safe delivery on the LINAC.

4.1.2.2. Patient selection, radiation dose prescription and treatment volume

This retrospective study consisted of 20 patients previously treated with external beam photon radiation therapy. All patients previously received 50 Gy in 25 fractions to whole right or left breast. In each case a photon boost of 10 Gy in 4 fractions was also delivered to the lumpectomy cavity. These 20 patients [(left breast (n=10) and right breast (n=10)] were re-planned for 3D-CRT, WPS, WPD, and for GsCM techniques for dosimetric comparison. This study focused on the “ARM I” criteria of RTOG 1005 protocol as a reference for inclusion of early stage breast cancer patients with stage I and II eligible for receiving radiation therapy. Random selection of these patients (treated from July 2019-December 2019) with tumors located in the central, upper-inner, upper-outer, lower-inner and lower-outer quadrants were included for this study. The number of patients, diagnosis, location of tumor, and their respective volumes are shown in Table 4.1.

Table 4. 1. Primary tumor laterality and patient characteristics.

Total Patients	Side of lesion	Stage	Quadrant	Excision cavity volume (cm ³), mean±SD	PTV volume (cm ³), mean±SD	Whole breast volume (cm ³), mean±SD
10	Right Breast	I and II	Lower inner, Upper outer, Central, Upper outer, Upper inner	8.10±1.80	100.29±18.85	1594.65±553.95
10	Left Breast	I and II	Lower inner, Central, Upper inner, Lower outer, Upper outer	14.01±3.32	105.15±9.29	1489.32±393.22

All patients were scanned under CT simulation (Philips medical systems, Netherlands) in house (2 mm slice thickness) in a supine position for the primary whole breast and in the decubitus position for the coned-down lumpectomy boost. The CT scan in the decubitus position was acquired for all patients under study since the cavity is deep seated and not easy to target in the

supine position. The gross tumor volume (GTV) was contoured by the radiation oncologist on both supine and decubitus CT studies which is the standard of practice at our center. The lumpectomy cavity plus a 1.0 cm expansion was applied to generate the clinical target volume (CTV) on both supine CT and decubitus CT. The planning target volume (PTV) was generated by adding 0.5 cm margin to CTV (a total of 1.5cm margin around the GTV) to account for set up uncertainty. Fig.1 shows the location of lumpectomy cavity (contoured in pink color as the gross tumor volume) for a right breast (a) and a left breast (b) patient included in this study. Bolus was not required due to the deep-seated nature of the lumpectomy cavities, as shown in Figure 4.1. The contralateral breast, ipsilateral lung, and heart structures were used as meaningful OARs for plan comparison.

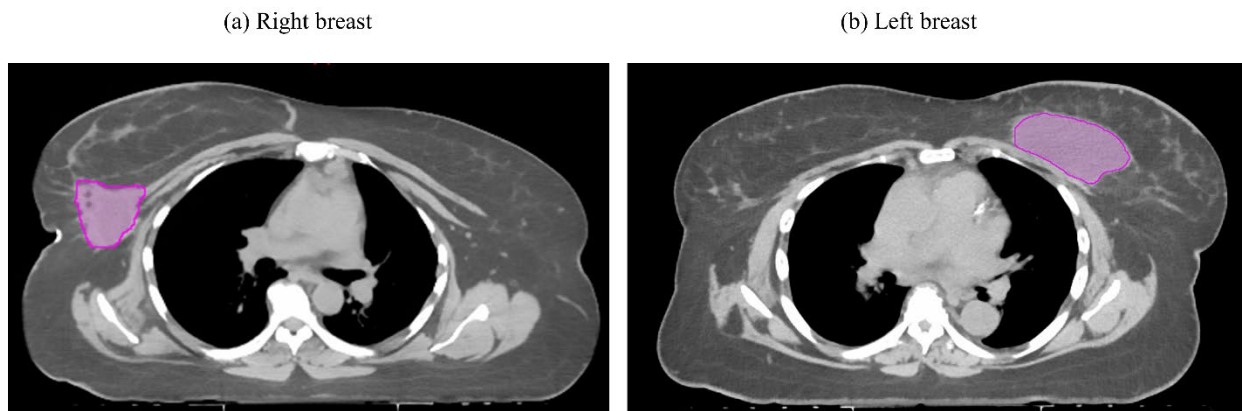


Figure 4. 1. The location of lumpectomy cavity is shown for a right breast (a) and a left breast (b) patient included in this study. In both pictures, the lumpectomy cavities were contoured in pink color as the gross tumor volume.

The dose constraints to the OARs were chosen based on the NASBP B-39/RTOG 0413⁵⁸ in addition to those listed in RTOG 1005 study to compare standard treatments to the GsCM technique. These dose constraints were supported by the study conducted by Popescu *et.al.*⁵⁹ on simultaneous couch and gantry dynamic arc rotation (CG-Darc) for APBI and Baglan *et.al.*⁴⁰ on accelerated partial breast irradiation using 3D-CRT approach. Both studies found these constraints meaningful for assessing normal tissue toxicity, tumor control, and better cosmetic results.

4.1.2.3. Treatment planning, optimization goal and plan comparison

Eclipse treatment planning system (Varian® medical systems, Palo Alto, CA) was utilized to create treatment plans based on CT simulation study (Anisotropic analytical algorithm (AAA) version 15.6; 0.2 mm dose grid resolution). All treatment plans utilizing 6MV photon beam were delivered on a Varian Truebeam® linear accelerator equipped with a high definition 120 MLC system.

4.1.2.3.1. Gantry static couch motion (GsCM) technique

4.1.2.3.1.1. Design and feasibility test

Twenty cases were re-planned utilizing the GsCM technique. As an example, Figure 4.2 shows the field arrangement of GsCM technique for the case in Fig.1(a). The selection of the couch positions for each arc was done visually in conjunction with the 3-dimensional (3D) rendering model in the planning system which was utilized to avoid any collision of gantry with patient and couch. The start and stop couch positions were different for each patient based on their anatomy and positioning on the breast board but within ± 10 degrees of the total couch span on each side as an average for all 20 patients.

In the current clinical context, implementation of this technique is not feasible since commercially available treatment planning systems (TPS) are unable to calculate dose while the treatment couch is set in motion. Also, Truebeam® does not allow the beam ON in clinical mode during couch motion. Therefore, for the purpose of this study, simulated arcs consisting of multiple static fields were designed. Specifically, two simulated arcs were generated for the right breast case as shown in Figure 4.2: 1) Medial beams with couch rotation from 40° - 320° and a fixed gantry angle at 55° , and 2) Lateral beams with couch rotation from 336° - 22° and a fixed gantry angle at 235° . Similarly, for the left breast: 1) Medial beams with couch rotation from 320° - 40° and a fixed gantry angle at 325° , and 2) Lateral beams with couch rotation from 22° - 336° and a fixed gantry angle at 145° . After creating the plan in Eclipse by simulating multiple fields for each medial and lateral arc, the treatment plan was exported to Matlab® and a machine control file in XML format was generated, combining the fields into deliverable arcs. The isodose distribution for this technique is shown in Figure 4.3(a).

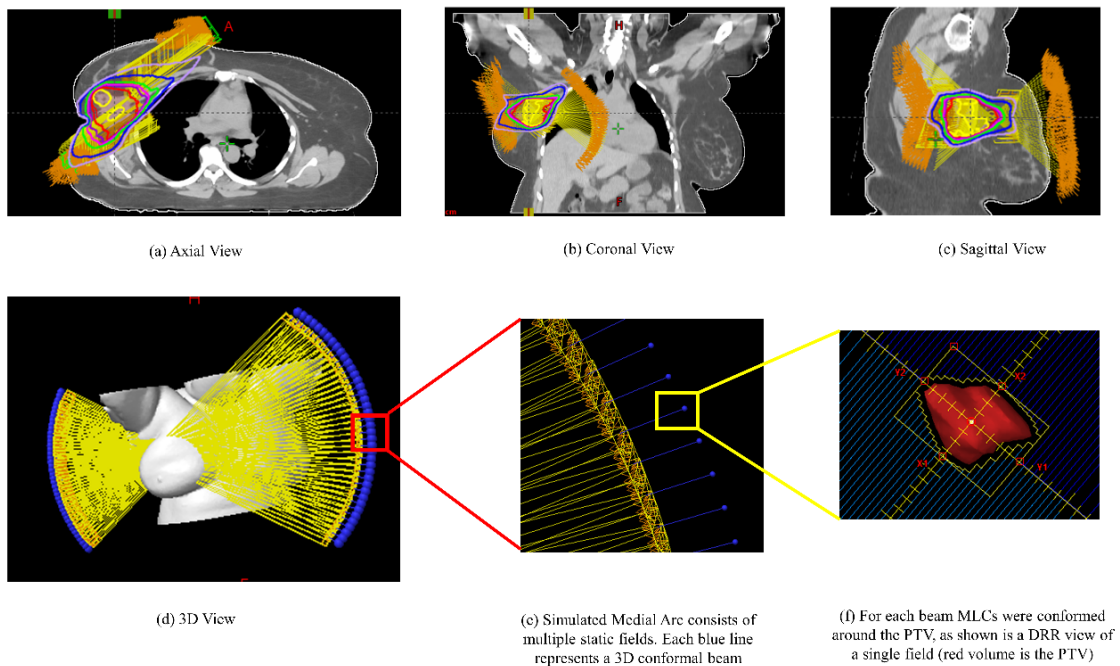


Figure 4. 2. The field arrangement of gantry static couch motion (GsCM) technique for the case in Figure 1(a). The GsCM field arrangement consists of two oblique arcs aiming at the isocenter as shown in an axial view (a), coronal view (b), sagittal view (c), and a 3D view (d). Each arc utilizes multiple static fields (e) conformed around the target volume (f). For each beam MLCs

were conformed around the PTV as shown in the beams-eye-view (f) for right sided target with single isocenter approach.

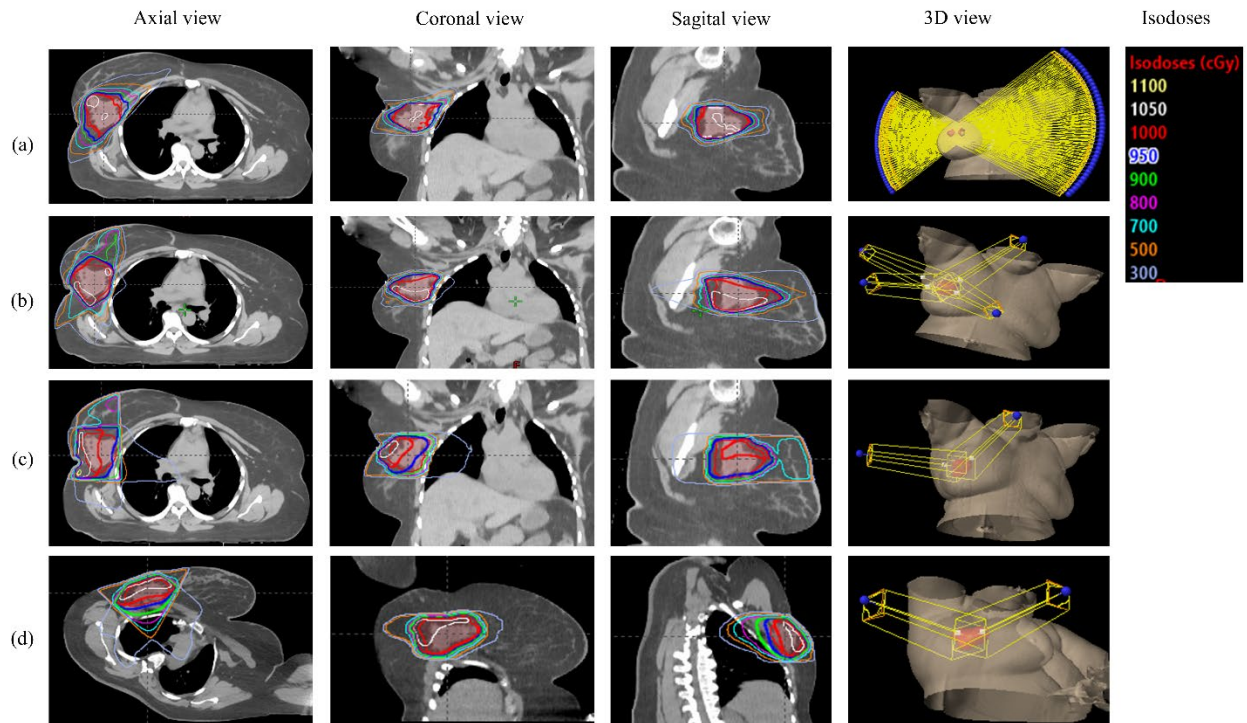


Figure 4. 3. Comparison of the field arrangement and their respective axial, coronal, sagittal, and 3-dimensional (3D) view of isodoses overlay for the right breast lumpectomy boost treatment plan of the case in Figure 1A: (a) gantry static couch motion (GsCM), (b) 3-dimensional conformal radiation therapy (3D-CRT), (c) wedge pair in supine position (WPS), and (d) wedge pair in decubitus position (WPD) techniques.

4.1.2.3.2. 3D conformal external beam radiotherapy (3D-CRT)

This technique follows the NSABP B-39/RTOG 0413⁵⁸ approach of choosing 3-5 non-coplanar fields using 6MV photons. Our 4-fields technique consists of a left anterior superior-to-inferior oblique (Lt ASIO), left anterior inferior-to-superior oblique (Lt AISO), right anterior inferior-to-superior oblique (Rt AISO), and right posterior superior-to-inferior oblique (Rt PSIO) for right breast lesions. For left breast lesions a 4-fields technique consisting of right anterior superior-to-inferior oblique (Rt ASIO), right anterior inferior-to-superior oblique (Rt AISO), left posterior superior-to-inferior oblique (Lt PSIO), and left posterior inferior-to-superior oblique (Lt PISO) was used. The combination of gantry and couch positions were chosen to avoid the beam entrance and exit dose to heart and contralateral breast and minimized the exit dose to contralateral lung. The gantry angles for medial beams were deliberately steep to minimize the dose to normal breast tissue. Couch angles (20° - 40°) were selected to spread out the fields and avoid collision of the gantry head and treatment couch. Each field included a 60 degrees wedge angle and the heel of wedge was kept anteriorly for all the fields. A 5 mm margin which defines the MLC aperture

around the PTV was used to account for beam penumbra. The field arrangement for this technique is shown in Figure 4.3(b).

4.1.2.3.3. 3D planning using wedge-pair technique in supine (WPS) and in decubitus position (WPD)

The wedge pair technique was applied to the static fields to make the dose more homogeneous within the PTV. The dose homogeneity was achieved by selecting combination of different wedge angles and hinge angles. Based on the location and depth of target a wedge angle of 45° - 60° was considered adequate for dose coverage. The fields arrangement utilizing this technique is shown in Figure 4.3(c) for WPS and Figure 4.3(d) for WPD.

4.1.2.4. Plan comparison and dosimetric indices

The dose distribution for GsCM, 3D-CRT, WPS, and WPD were compared by overlaying the isodoses on axial, coronal and sagittal slices as shown in Figure 4.3. A two-sided paired t-test statistical analysis was performed with $p \leq 0.05$ considered significant. All plans were normalized equally ($D_{95}=100\%$) as recommended by ICRU report 83³² to compare the mean doses to PTVs. Dosimetric distributions were evaluated using the homogeneity index (H.I.)³³, conformity index (C.I.)³⁴, and gradient measure (G.M.). Briefly:

$$H.I. = (D_{2\%} - D_{98\%}) / D_{50\%} \quad (1)$$

where $D_{98\%}$, $D_{2\%}$ and $D_{50\%}$ are dose received by 98%, 2% and 50% of the volume. Homogeneity Index values approaching zero are considered as an ideal value for plan comparison.

$$C.I. = V_{95\%} / V_{PTV} \quad (2)$$

where $V_{95\%}$ is the volume enclosed by isodose surface of 95% prescription dose and V_{PTV} is the target volume. Conformity index approaching 1 is considered an adequate plan for comparison.

$$G.M. (cm) = R_p - R_{50} \quad (3)$$

where R_p and R_{50} are the equivalent sphere radius of the prescription and half prescription isodoses. Gradient measure describes dose fall off from the PTV for the central slice.

4.1.2.5. Validation of GsCM technique

The fields for the GsCM technique were validated utilizing IMRT QA phantom (Octavius1500, PTW-Freiburg, Germany) as shown in Figure 4.5. The QA phantom was scanned under CT simulation and imported into Eclipse planning system and the planar dose was generated for each simulated arc. The simulated arcs were delivered onto this phantom under Truebeam® developer mode application using the converted machine control file in XML format as described earlier. The measured dose was compared with the calculated dose using the criteria of percentage

dose difference (%DD), distance to agreement (DTA), and 2D gamma (γ) comparison. For our study we used 2%DD, 2mm DTA, and $\gamma \leq 1$ with passing criteria of $\geq 95\%$ which is standard of care in our institution for all IMRT patients.

4.1.3. Results

4.1.3.1. Group A: Right breast patients

For the 10 right breast patients planned for lumpectomy boost, the mean PTV volume was 100.3cc (range of 75.8-130.5cc) as shown in Table 4.1. The mean whole breast volume was 1594.6cc (range of 998.9-2705.3cc). The lumpectomy boosts were located in the lower inner, central, upper inner, lower outer, lower inner, and upper outer quadrant of breast. The physical depth of all these cavities was greater than 5cm. An example is shown in Fig.1(a). The fields arrangement for GsCM, 3D-CRT, WPS and WPD are shown in Figure 4.3(a), 3(b), 3(c), and 3(d) respectively. The dose (mean \pm SD) to the normal structures has shown in Table 4.2 for all four techniques (GsCM, 3D-CRT, WPS, and WPD).

Table 4. 2. Right breast dosimetric parameters show improvement in PTV coverage, ipsilateral lung and heart. GsCM is superior when compared to 3D-CRT, WPS and WPD. All results are shown as mean \pm standard deviation ($p \leq 0.05$ to consider statistically significant).

Parameter (Objective)	GsCM	3D-CRT	WPS	WPD	p-value GsCM vs 3D-CRT	p-value GsCM vs WPS	p-value GsCM vs WPD	p-value 3D-CRT vs WPS	p-value 3D-CRT vs WPD
<i>PTV</i>									
CI	1.1 \pm 0.4	1.2 \pm 0.1	1.5 \pm 0.2	1.3 \pm 0.1	0.451	0.001	<0.001	<0.001	0.038
GM (cm)	2.6 \pm 0.3	1.5 \pm 0.1	2.0 \pm 0.2	1.6 \pm 0.1	<0.001	0.001	<0.001	<0.001	0.038
HI	0.08 \pm 0.0	0.10 \pm 0.02	0.15 \pm 0.02	0.11 \pm 0.02	0.096	<0.001	0.017	<0.001	0.278
V95% (>95%)	3	98.0 \pm 1.2	93.7 \pm 2.5	94.5 \pm 2.5	0.411	<0.001	0.003	0.001	0.006
Max. Dose (%)	97.3 \pm 0.8	105 \pm 2.3	106 \pm 3.1	106 \pm 2.1	1.00	0.403	0.289	0.423	0.323
<i>Ipsilateral Breast</i>									
V50% (<60%)*	21.3 \pm 5.1	19.1 \pm 2.3	17.9 \pm 1.7	17.7 \pm 3.2	0.229	0.061	0.075	0.139	0.216
V100% (<35%)*	2.3 \pm 0.5	4.2 \pm 0.5	4.9 \pm 1.2	8.9 \pm 2.3	<0.001	<0.001	<0.001	0.106	<0.001
Mean Dose (cGy)	263.6 \pm 2	240.2 \pm 23.	184.9 \pm 19.	211.3 \pm 40.	0.059	<0.001	0.004	<0.001	0.068
<i>Ipsilateral Lung</i>									
V30% (<15%)*	1.3 \pm 0.5	8.1 \pm 5.3	24.6 \pm 7.9	44.6 \pm 11.5	<0.001	<0.001	<0.001	<0.001	<0.001
D50% (cGy)	17.3 \pm 5.0	90 \pm 56.3	66.7 \pm 56	220.3 \pm 11	<0.001	0.022	<0.001	0.366	0.005
D30% (cGy)	29.8 \pm 9.6	169 \pm 32.6	230 \pm 91.6	359.8 \pm 54.	<0.001	<0.001	<0.001	0.063	<0.001
Mean Dose (cGy)	37.9 \pm 8.7	128 \pm 43.3	152.1 \pm 36.	251.4 \pm 59.	<0.001	<0.001	<0.001	0.197	<0.001

<i>Heart</i>									
V5% (<5%)*, %	0.1±0.05	1.1±1.0	42.8±18.8	61.2±21.1 142.7±10	6	0.005	<0.001	<0.001	<0.001
D50% (cGy)	3.6±0.7	6.2±2.4	57.5±56.4	231.9±77.	7	0.004	0.014	0.002	0.010
D30% (cGy)	6.2±1.0	10.4±3.4	150.8±69.	5	5	0.002	<0.001	<0.001	<0.001
Mean Dose (cGy)	5.2±1.0	10.9±4.4	98.6±33.2	159.3±55.	5	<0.001	<0.001	<0.001	<0.001
Max. Dose (cGy)	1	9	365.4±27	380.2±25.	5	<0.001	<0.001	<0.001	<0.001
<i>Contralateral Breast</i>									
Max. Dose (cGy)	8.52±2.5	115.79±2 5.6	225.53±6 5.3	350.5±55. 5		<0.001	<0.001	<0.001	<0.001

Abbreviations: GsCM = gantry static couch motion, 3D-CRT = three-dimensional conformal radiotherapy, WPS = wedge pair supine, WPD = wedge pair decubitus

*Constraints from NASBP B-39/RTOG 0413 are considered as meaningful endpoints including the additional constraints

The mean conformity index (CI) and homogeneity index (HI) of 1.1±0.4, 0.08±0.03 for GsCM is comparable to 3D-CRT (1.2±0.1, 0.1±0.02) and superior to WPS (1.5±0.2, 0.15±0.02) and WPD (1.3±0.1, 0.11±0.02) with $p < 0.01$. The overall dose coverage to PTV, the volume getting 95% of the dose (V95%) is comparable for GsCM and 3D-CRT (97.5%, mean) and superior to WPS and WPD (94%, mean). The gradient measure (cm) was measured to be 2.6±0.3, 1.5±0.1, 2.0±0.2, and 1.6±0.1 for the GsCM, 3D-CRT, WPS and WPD respectively.

For GsCM, the ipsilateral breast volume getting 50% of the dose (V50%) was 8-10% higher and the mean dose was 10-15% higher as compared to 3D-CRT, WPS and WPD. But the volume getting 100% of the dose (V100%) reduced by 40%, 53% and 75% for GsCM compared to 3D-CRT, WPS and WPD respectively.

Overall, an average dose to 30%, 50% (D30%, D50%) of the ipsilateral lung volume reduced using GsCM as compared to 3D-CRT, WPS and WPD by 82% (range: 65%-90%), 80% (range: 74%-85%), 70% (range: 56%-80%) respectively. For GsCM, volume getting 30% of the dose (V30%) reduced by 84%, 95% and 97% (mean) as compared to 3D-CRT, WPS and WPD respectively.

For heart, the volume getting 5% of the dose (V5%) reduced by 90%, 97% and 99% (mean) for GsCM compared to 3D-CRT, WPS and WPD respectively. A similar trend of reduction was noticed for dose getting to 30% and 50% of the volume (D30%, D50%) and maximum dose.

Regardless of the location of lumpectomy cavity, the GsCM significantly lowered the contralateral breast maximum dose to under 10cGy (8.5±2.5 cGy, mean ± SD, $p \leq 0.001$) as compared to 3D-CRT (115.8±25.6 cGy, $p \leq 0.001$), WPS (225.5±65.3 cGy, $p \leq 0.001$), and WPD (350.5±55.5 cGy, $p \leq 0.001$) respectively while maintaining the coverage to PTV ($p \leq 0.001$). The DVH comparison of a single patient with all four techniques are shown for heart, ipsilateral lung

and PTV in Figure 4.4(c) and Figure 4.4(d). Significant improvement in dose reduction to the ipsilateral lung and heart is noted for GsCM in terms of the dose to 30% and 50% of the volume (D30%, D50%).

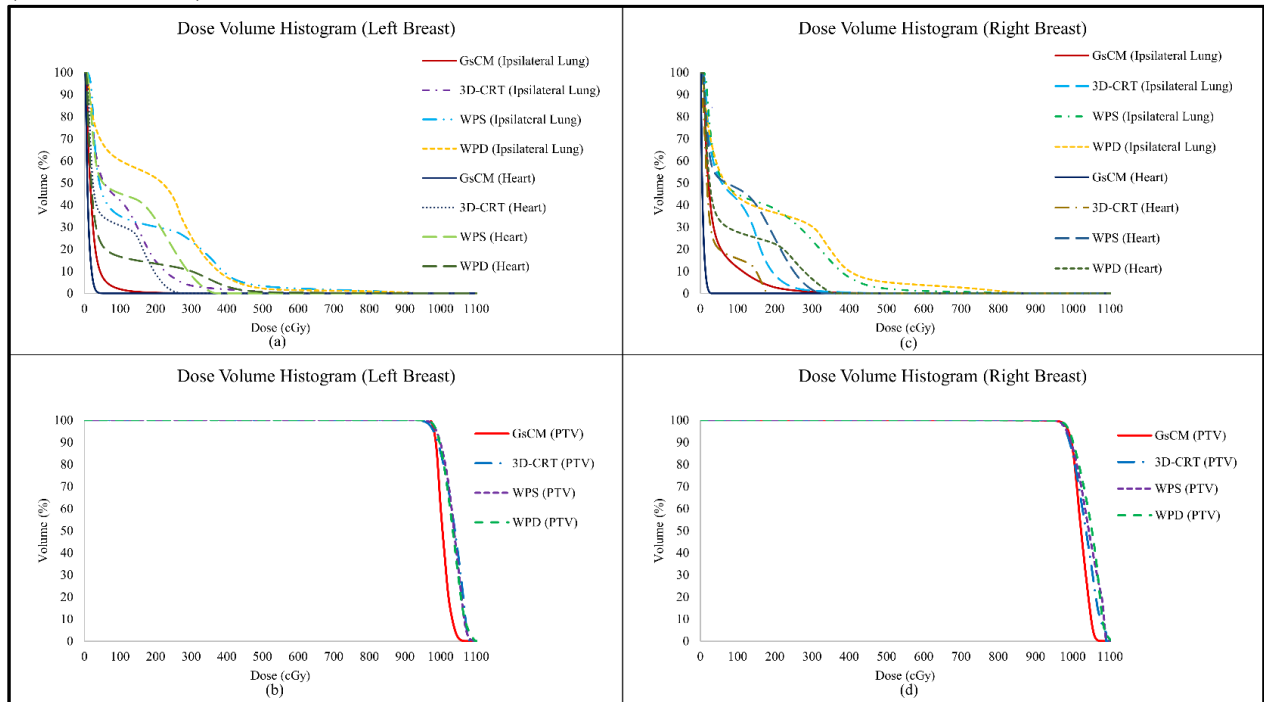


Figure 4. 4. Dose volume histogram (DVH) comparison for a left breast patient (a,b) and a right breast patient (c,d). The graph shows the dose reduction to 10%, 30% and 50% of the volume getting prescription dose to heart and ipsilateral lung using GsCM technique while maintaining same PTV coverage as compared to 3D-CRT, WPS, and WPD.

The monitor units (MU) reported for GsCM, 3D-CRT, WPS and WPD are 390, 490, 416, and 380 respectively for a prescription of 250cGy per fraction for four fractions, or a total dose of 1000 cGy.

4.1.3.2. Group B: left breast patients

For the 10 left breast patients planned for lumpectomy boost, the mean PTV volume was 105.1cc (range of 86.1-116.9cc) as shown in Table 4.1. The mean whole breast volume was 1489.3cc (range of 854.5-1854.3cc). The lumpectomy boost located in the lower inner, central, upper inner, lower outer, lower inner, and upper outer quadrant of breast. The physical depth of these cavities was greater than 5cm. A sample is shown in Figure 4.1(b) for a single patient. The mean DVH comparison between all four techniques for Heart, Ipsilateral Lung and PTV is shown in Figure 4.4(a) and Figure 4.4(b). The GsCM technique is considered dosimetrically superior to 3D-CRT, WPS and WPD as shown in Table 4.3.

Table 4. 3. Left breast dosimetric parameters show improvement in PTV coverage, ipsilateral lung and heart. GsCM is superior when compared to 3D-CRT, WPS and WPD. All results are shown as mean± standard deviation ($p \leq 0.05$ to consider statistically significant).

Parameter (Objective)	GsCM	3D-CRT	WPS	WPD	p-value GsCM vs 3D-CRT	p-value GsCM vs WPS	p-value GsCM vs WPD	p-value 3D-CRT vs WPS	p-value 3D-CRT vs WPD
<i>PTV</i>									
CI	1.0±0.2	1.43±0.2	2.1±0.2	1.6±0.2	<0.001	<0.001	<0.001	<0.001	0.074
GM (cm)	2.8±0.6	2.15±0.3	2.1±0.1	2.0±0.2	0.004	0.002	0.004	0.623	0.205
HI	0.08±0.0	0.11±0.0	0.12±0.01	0.11±0.01	<0.001	<0.001	<0.001	0.174	1
V95% (>95%)	1	2	95.4±0.4	95.0±0.9	<0.001	<0.001	<0.001	<0.001	<0.001
Max. Dose (%)	98.1±0.3 105±2.1	98±0.25 105±2.3	105.2±2.8	105.4±2.5	<0.001	<0.001	<0.001	0.863	0.714
<i>Ipsilateral Breast</i>									
V50% (<60%)*	14.8±4.5	12.1±1.9	17.5±2.2	20.1±4	0.097	0.106	0.012	<0.001	<0.001
V100% (<35%)*	1.9±0.3	2.8±0.6	5.1±0.7	4.6±0.7	<0.001	<0.001	<0.001	<0.001	<0.001
Mean Dose (cGy)	171.3±36.6	162.3±23.9	177.2±21.1	219.2±28.9	0.523	0.664	0.005	0.157	<0.001
<i>Ipsilateral Lung</i>									
V30% (<15%)*	1.0±0.8	11±4.9 89.7±12.2	29.1±7.4 82.3±68.4	14.2±8.8 97.2±76	<0.001	<0.001	<0.001	<0.001	0.328
D50% (cGy)	15.5±2.8	2	243.2±11	194.3±10	<0.001	0.012	0.008	0.742	0.762
D30% (cGy)	25.8±5.1	163±14.5	7.9	2.9	<0.001	<0.001	0.001	0.047	0.354
Mean Dose (cGy)	31.9±9.4	5 126±15.2	177.7±37.8	137.1±44.9	<0.001	<0.001	<0.001	0.528	0.469
<i>Heart</i>									
V5% (<40%)*, %	0.5±0.3	20.7±7	51.9±21.4	30.5±20.4 60.7±35.5	<0.001	<0.001	<0.001	<0.001	0.168
D50% (cGy)	6.9±0.5	57±5.0	99.5±50	127.7±10	<0.001	0.021	0.041	0.016	0.748
D30% (cGy)	10.9±0.8	163±7.5	185±102	0	<0.001	<0.001	0.021	0.505	0.280
Mean Dose (cGy)	9.7±0.5	55.1±5.0	143±51.9	96.7±61	<0.001	<0.001	0.001	<0.001	0.046
Max. Dose (cGy)	100.1±53.7	503.3±15.6	647.6±24.1.2	597±184.4	<0.001	<0.001	<0.001	0.075	0.127
<i>Contralateral Breast</i>									
Max. Dose (cGy)	3.1±1.1	129.7±22.3	215.5±68.3	310.6±47.8	<0.001	<0.001	<0.001	0.001	<0.001

Abbreviations: GsCM = gantry static couch motion, 3D-CRT = three-dimensional conformal radiotherapy, WPS = wedge pair supine, WPD = wedge pair decubitus

*Constraints from NASBP B-39/RTOG 0413 are considered as meaningful endpoints including the additional constraints

The mean conformity index (CI) and homogeneity index (HI) of 1.0±0.2, 0.08±0.01 for GsCM is comparable to 3D-CRT (1.43±0.2, 0.11±0.02) but superior to WPS (2.1±0.2, 0.11±0.01) and WPD (1.6±0.2, 0.11±0.01) with $p < 0.01$. The overall dose coverage to PTV, the volume getting

95% of the dose (V95%) for GsCM is comparable to 3D-CRT (98%, mean) but superior to WPS and WPD (95%, mean). The gradient measure (cm) was measured to be 2.8 ± 0.6 , 2.2 ± 0.3 , 2.1 ± 0.1 , and 2.0 ± 0.2 for the GsCM, 3D-CRT, WPS and WPD respectively.

For GsCM, the ipsilateral breast volume getting 50% of the dose (V50%) was 15-20% higher and the mean dose was 5-10% higher in comparison to 3D-CRT, WPS and WPD. But the volume getting 100% of the dose (V100%) was reduced by 32%, 63% and 59% for GsCM compared to 3D-CRT, WPS and WPD respectively.

Overall, the average dose to 30%, 50% (D30%, D50%) of the ipsilateral lung volume using GsCM was reduced by 83% (range: 79%-90%), 82% (range: 75%-85%), 75% (range: 70%-82%) when compared to 3D-CRT, WPS and WPD respectively. For GsCM, volume getting 30% of the prescription dose (V30%) was reduced by 90%, 98% and 93% (mean) as compared to 3D-CRT, WPS and WPD respectively.

For heart, the volume getting 5% of the dose (V5%) was reduced by 97%, 99% and 98% (mean) for GsCM compared to 3D-CRT, WPS and WPD respectively. Same trend of reduction was noted for dose getting to 30% and 50% of the heart volume (D30%, D50%) and the maximum dose.

Regardless of the location of lumpectomy cavity, the GsCM significantly decreased the contralateral breast maximum dose to be under 5cGy (3.1 ± 1.1 , mean \pm SD, $\rho\leq 0.001$) as compared to 3D-CRT (129.7 ± 22.3 , $\rho\leq 0.001$), WPS (215.5 ± 68.3 , $\rho\leq 0.001$), and WPD (310.6 ± 47.8 , $\rho\leq 0.001$) respectively while maintaining the coverage to PTV ($\rho\leq 0.001$).

The total monitor units (MU) reported for GsCM, 3D-CRT, WPS and WPD were 400, 480, 410, and 385 respectively for a prescription of 250cGy per fraction for four fractions, corresponding to a total dose of 1000cGy.

4.1.3.3. Dose delivery and validation

All GsCM plans were successfully converted to a single deliverable arc utilizing the in-house MATLAB[®] software that combines multiple static fields into one deliverable arc in an XML format consisting of multiple segments of MLC apertures, monitor units, couch and gantry positions. These XML files were delivered onto PTW Octavius ion chamber array to assess the accuracy of delivery. Comparison of simulated arcs and measured dose distributions utilizing GsCM yielded $98\pm 1.5\%$ (range of 96.5-100%) easily satisfying our institutional criteria. The median 2-dimensional gamma index was of 0.35 and absolute median dose difference was of 0.0256Gy. The delivery time for simulated arcs was significantly shorter (<2min) as compared to 3D-CRT and comparable to wedge pair techniques (~1.5min) at the dose rate of 600MU/min. This includes the time to prepare each field for each technique.

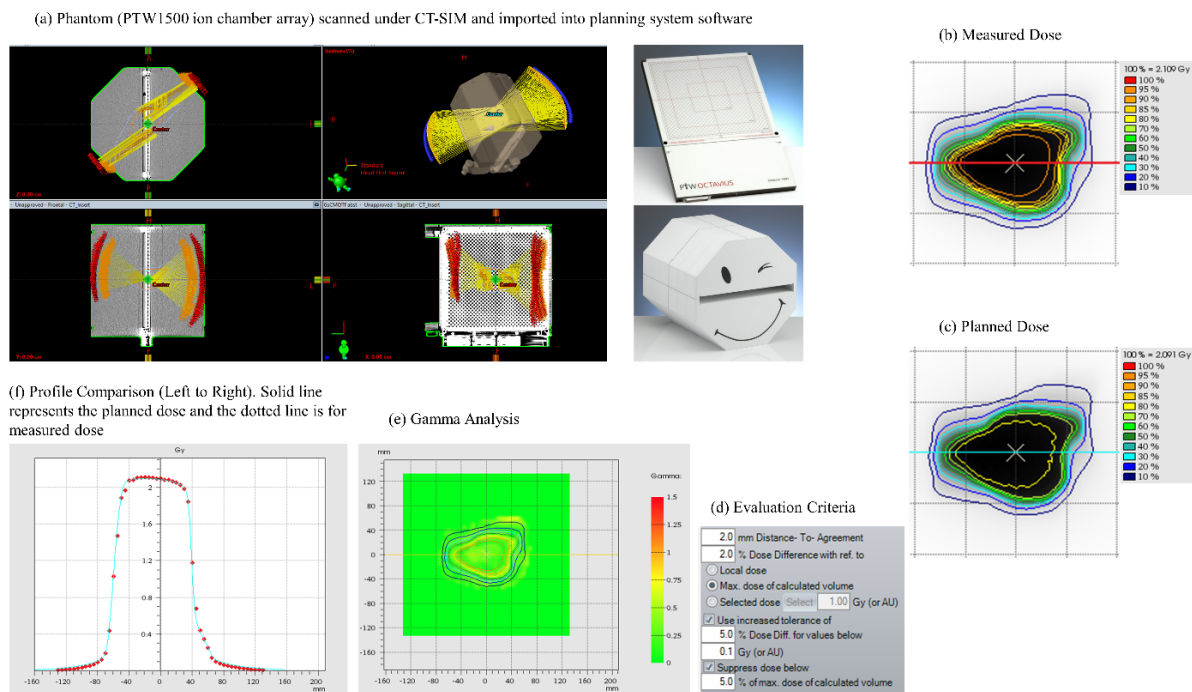


Figure 4. 5. Delivery and validation of GsCM technique was conducted utilizing an ion chamber array (a) scanned in a vertical position to avoid any side beam entrance. Measured (b) and planned (c) dose were compared using a criteria (d) of 2mm distance-to-agreement (DTA), 2% dose difference (%DD), and 2D gamma (e) passing rate of more and equal to 95% and dose profile comparison from left to right (transverse) direction (f).

4.1.4. Discussion

In this study, the GsCM technique was dosimetrically compared with 3D-CRT, WPS and WPD techniques for breast boost treatments. All patients selected for this study had undergone combined whole breast radiation therapy and photon boost to deeply seated lumpectomy cavities. Instead, 3D-CRT and WPS are typically used for treating these patients in supine position. Sometimes, decubitus position is utilized for patients who have lumpectomy cavity sitting under the breast fold to achieve adequate coverage and avoid any skin reaction from dose build up under the breast fold. The GsCM technique was considered because it provides a very comfortable alternative position (supine) to the decubitus position. Our technique is more like a VMAT type of dose delivery but no traditional inverse optimization. This is due do the inability to limit the fields to a single segment. We limited to a single segment to best mimic VMAT.

In this study, comparison of dose distribution (Conformity Index), dose fall off (Gradient Index) and dose volume histograms (V95%) of each technique, revealed similarities between GsCM and 3D-CRT and superiority of GsCM over WPS and WPD. For ipsilateral breast volume, V50% and mean dose were higher using GsCM because unlike other techniques, the tangent beams for GsCM are parallel to chest wall and do not exit through ipsilateral lung and/or heart. On the other hand, for all cases (right and left breast), the beam arrangement of GsCM significantly

reduced dose to 30% and 50% of heart and ipsilateral lung volume getting prescription dose (D30% and D50%), and mean and maximum dose to heart volume ($p \leq 0.01$). This indicates that although GsCM confers additional conformality and OAR sparing, there is still a trade-off with regards to low dose spillage to normal breast tissue. Overall, GsCM resulted in significantly ($p \leq 0.01$) lower dose to ipsilateral lung (V30%, D50%, D30% and mean dose), heart volume getting V5%, D50%, D30% and max dose, contralateral breast max dose, and resulted in better conformity and homogeneity index. The monitor units prescribed for GsCM were relatively lower than 3D-CRT and comparable to wedge pair techniques.

Our results supported the study conducted by Shaitelman *et al.*⁶⁰, where 3D-CRT significantly reduced ipsilateral breast V50% by the amount of 15-40% (mean). Fahimian *et al.*⁶¹ used LINAC based approach for trajectory modulated prone breast irradiation, a non-isocentric approach, showed significant improvement in conformity, less spread of dose to normal breast (V50%, V100%), parameters related to toxicity, negligible dose to ipsilateral lung and heart structure. Our GsCM approach is focused on single-isocenter approach for patients scanned in supine position, a position more appealing for faster dose delivery and patient comfort.

The delivery of multiple static fields at different couch positions is very time consuming and led us to merge all static fields to create a single deliverable arc. This was easily accomplished using MATLAB[®] scripting by creating XML files. The implementation and delivery of GsCM was conducted in the Truebeam[®] developer mode application because simultaneous dose delivery and couch motion is not available in clinical mode. The developer mode application allowed GsCM technique to be automated and faster as compared to delivering all the fields individually. We found that using these features, GsCM can be easily implemented in clinic, once dose delivery and couch motion are allowed in clinical mode.

Implementation of the GsCM technique is limited by characterization of patient motion and mitigation of potential collision during dose delivery as well as couch and gantry motion. In order to address this risk, 3D modelling of the planning system can be utilized for gantry and couch angles selection to avoid potential collision. Further, utilization of laser guard interlocks during treatment delivery can be considered. With regards to patient motion, a wireless bra /custom mesh type overlay on the patient can be used to minimize motion and ensure setup repeatability between fractions. To study the couch motion, patient motion, and couch speed integration during beam delivery are not part of this study and will be discussed in a future study.

One of the limitations uncovered in this study was the short couch angular span on the lateral side of the beam for both right and left breast patients who have lumpectomy cavity located more medially. This can be mitigated, using two separate isocenters, one for each arc so that wider angular span can be achieved for both arcs. For the medial arc, the isocenter is usually positioned at the geometric center of the boost volume since there is enough clearance for large angular spans no matter where the boost volume is located. For the lateral arc, collision can be a major concern if the boost volume is located close to the medial side of patient. For cases like this, in order to encompass the whole PTV within the treatment field of view, the couch needs to be moved

anteriorly and laterally from the isocenter of the medial arc, both shifts can be performed automatically within our GsCM technique framework. The data presented in this study is for single isocenter technique only.

The reduction of high dose to normal breast tissue, spread of low dose to ipsilateral lung and heart, and significant dose conformity around the target volume makes GsCM technique suitable for breast boost applications. This approach is unique and opens the possibility for future advancement for existing treatment planning techniques where the current dose calculation and dose optimization algorithms can be modified to perform GsCM type of treatment planning. The GsCM technique also provides an opportunity to take advantage of the capabilities of LINAC and treatment planning systems for other body sites where the conformity and spread of low dose to organs-at-risk are highly appreciated.

4.1.5. Conclusions

In conclusion, we presented in this study a novel GsCM treatment technique for breast boost radiation therapy. This technique utilized medial and lateral arcs created by automatic couch motion at larger angular span with a fixed gantry position. The dosimetric properties and novelty of the GsCM technique with patient in the supine position were compared with standard 3D-conformal breast boost treatment planning techniques. We demonstrated that the GsCM technique provides a compact and conformal dose distribution to deep seated breast surgical cavities where electrons would not be applicable. Good agreement was observed between the measured and calculated dose distribution. Due to the use of tangential fields placement, the GsCM technique produced no exit dose to contralateral/ipsilateral lung and heart and therefore lead to a significant dose reduction to surrounding critical organs in comparison to other photon boost techniques. Single and/or dual isocentric based oblique arcs with large medial and lateral angular span are adequate for breast boost applications with a shorter delivery time of ~2 minutes in a more convenient treatment position for the patient. Based on the results presented in this study, we applied the GsCMO technique in partial breast irradiation (PBI) as described in detail in next section of this chapter.

4.2. Application in partial breast irradiation (PBI)

4.2.1. Overview

The partial breast irradiation (PBI) in general has been very well known as adjuvant radiation therapy technique to prevent breast cancer recurrence after breast conserving surgery (BCS). Among the various radiation treatment options available to target early stage breast cancer, we explored the benefits of gantry-static couch-motion optimization (GsCMO) technique for partial breast irradiation therapy.

Accelerated partial breast irradiation (APBI) technique was initially introduced in 2003 presenting a novel three-dimensional conformal radiation therapy (3D-CRT)¹ technique to treat

lumpectomy cavity. The 3D-CRT feasibility technique for early stage breast cancer was found beneficial in terms of patient tolerance to radiation and less toxicity. Even though this technique is currently in effect in treatment for lumpectomy cavity for patients with early stage breast cancer but the need to improve this technique in terms of dose conformity and less exit dose to ipsilateral lung and heart still arises. Other investigators²⁻⁴ have worked on establishing the IMRT and more advanced VMAT technique and compared it with 3D-CRT. The VMAT dose delivery whether it was coplanar or non-coplanar superseded 3D-CRT in terms of more target conformity and sharp dose gradient. In the same line of improvement, we came up with a novel technique which not only provides an adequate dose conformity to target but also minimizes the exit dose to ipsilateral lung and heart.

The purpose of this study was to compare the dosimetry of a novel external beam planning based GsCMO technique with standard VMAT technique in treatment of early stage breast cancer.

4.2.2. Methods

The GsCMO technique is an arc-type treatment delivery where gantry was kept static while couch moved in an increment of one degree (both arcs look like butterfly wings). Two tangential arcs (coronal plane) with 6MV beams were utilized to re-plan 20 patients retrospectively for a total dose of 3850cGy in 10 fractions based on NSABP B-39/RTOG 0413 protocol and RAPID trial (strict constraints), and compared with standard gantry based VMAT planning utilizing partial arc (VMAT) and partial arc with an avoidance sector (VMATa) as shown in Figure 4.6. The dose constraints are shown in Table 4.4. Both medial and lateral arcs were simulated at two static (fixed) gantry angles and couch moved in an increment of one degree. The definition of PTV is similar in both NSABP B-39 and RAPID trial. Seroma is evident on CT study based on postoperative bed (gross tumor volume: GTV) which includes any surgical clips margin and excludes 5mm from skin and excludes the pectoralis muscle or chest wall. Clinical target volume (CTV) includes seroma plus 1cm margin, excluding chest wall and 5mm from skin. The planning target volume (PTV) includes CTV plus 1cm margin. The dose evaluation volume (PTV_eval) used for planning includes portion of PTV within the ipsilateral breast. In terms of dosimetric analysis, the volume histogram (DVH) comparison was conducted. Dosimetric indices such as conformity index (CI) and gradient measure (GM) were used to compare all three planning techniques.

The GsCMO technique is a VMAT type of dose delivery where couch moves in a continuous fashion at static gantry positions. The development of GsCMO technique was conducted in Eclipse treatment planning system (Version 15.6, Varian Medical Systems, Palo Alto, CA). The GsCMO technique consists of multiple static fields at the beginning conformed around the PTV, later modulated each field using intensity modulated approach to make the target dose more conformal and limit the spread of low dose outside the target as much as possible. All the modulated fields were carefully merged using C# scripting in Visual Studio application, and a single deliverable file in an extensible markup language (XML) format was created. The XML file kept the integrity of all mechanical axes involved in dose delivery and tested on Varian developer mode application. The dose delivery was tested using an ion chamber array.

Table 4. 4. The dose constraints used in this study to compare the dosimetry of GsCMO with VMAT and VMATa plans

Volume	NSABP B-39/RTOG 0413 constraints	RAPID trial constraints
Ipsilateral Breast	V50%≤60% V100≤35%	V50%≤50% (acceptable up to 65%) V95%≤25% (acceptable up to 35%)
Contralateral Breast	D _{max} ≤3%	D _{max} <3%
Ipsilateral Lung	V30%≤15%	V30%≤10% (acceptable up to 13%) V10%≤20% (acceptable up to 25%)
Contralateral Lung	V5%<15%	---
Heart (right-sided tumors) Heart (left-sided tumors)	V5%<5% V5%<40%	V5%<5% V10%<5% excluding lower inner quadrants V15%<5% lower inner quadrants
Target	D _{max} ≤120% V90%≥90%	V95%≥95%

4.2.3. Results

All techniques (GsCMO, VMAT, and VMATa) provided an adequate coverage to PTV (V95≥99%). As shown in Table 4.5, GsCMO significantly reduced the ipsilateral lung V30% by 44.5% (mean, 48.3%) and by 12.5% (mean, 9.2%) for outer and central targets, by 66.4% (mean, 62.4%) and by 70.8% (mean, 64.4%) for inner targets when compared with VMAT and VMATa respectively. Heart V5% reduced by 97.8% (mean, 51.5) and 99.3% (mean, 54.5) for outer and central tumors, and by 100% (mean, 65.4) and 100% (mean, 21.2) for inner tumors as compared to VMAT and VMATa. This is due to the tangential nature of GsCMO coronal arcs. Therefore, there is no exit dose to the ipsilateral lung and heart volume. On the other hand, ipsilateral breast V50% and mean dose were found higher for GsCMO, but V95% were comparable for all techniques. The maximum dose to the target for all techniques was less than 110%. The automated delivery of all techniques was found same (under 2 minutes).

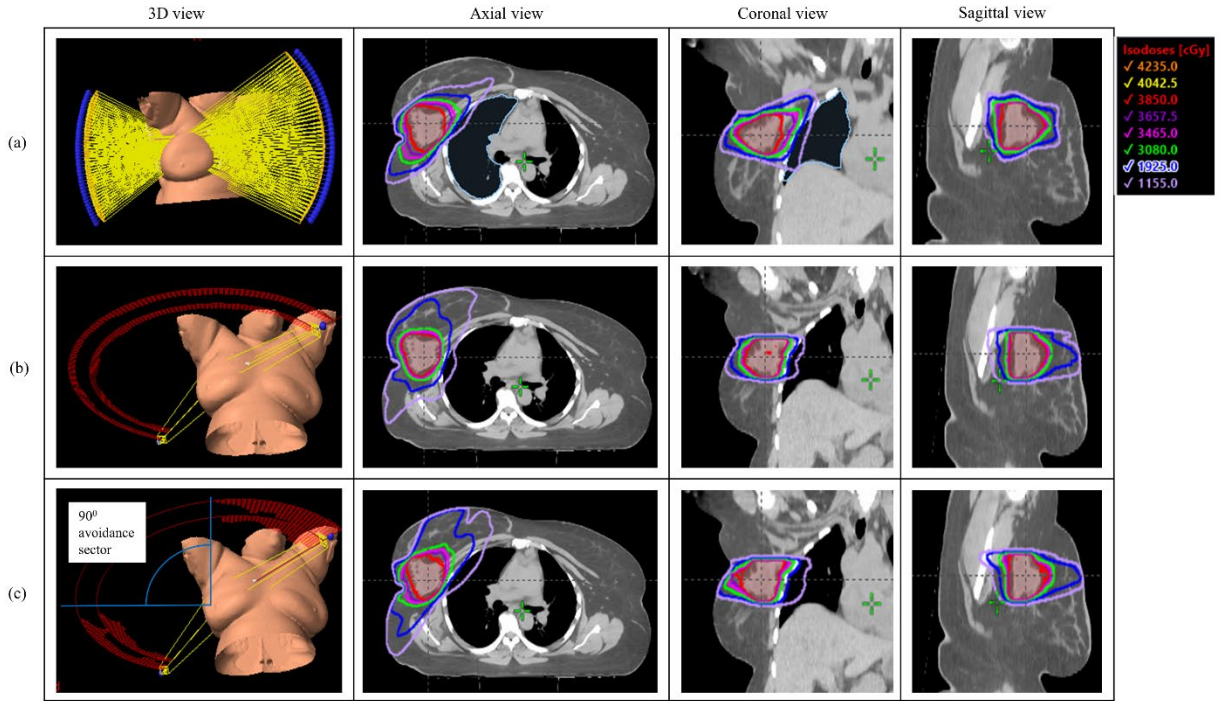


Figure 4. 6. The GsCMO (a) technique utilizing two coronal arcs was compared with VMAT (partial arcs), and VMATa (partial arcs with 90 degrees avoidance sector) shown here is for a right-sided test patient

The dose distribution is shown in Figure 4.6. It is clear from the picture, the tangential nature of GsCMO arcs minimize the exit dose to the ipsilateral lung but at the expense of increase in V50% to ipsilateral breast. Overall, GsCMO technique provides compact and conformal dose distribution comparable to VMAT technique with $CI=1.1\pm 0.1$ regardless of the location of lumpectomy cavity. The GM parameter which defines the difference of 50% isoline from prescription isoline for GSCMO was found comparable to VMATa and was higher as compared to VMAT.

Table 4. 5. Dose constraints shown for outer and central targets, and for inner targets for GsCMO, VMAT, and VMATa techniques for right breast (n=20)

Outer and central targets	PTV				Heart			Contralateral Lung			Ipsilateral Lung				Contralateral breast	Ipsilateral normal breast (whole breast-PTV_eval)	
	V95 (%)	Mean dose (cGy)	CI	GM (cm)	Mean Dose (cGy)	Max dose (cGy)	V5 (%)	Mean Dose (cGy)	Max dose (cGy)	V5 (%)	Mean Dose (cGy)	Max dose (cGy)	V10 (%)	V30 (%)	Dmax <3%	V50%	V95%
VMAT	99.4	3970.7	1.1	1.8	47.9	300.6	1.5	55.3	378.3	4.2	381.4	3237.0	37.9	4.9	3.3	10.8	0.9
SD	0.3	7.0	0.0	0.2	19.4	62.6	0.9	6.4	158.5	4.9	29.1	915.1	2.1	2.5	2.1	0.9	0.1
VMATa																	
Mean	99.3	3937.8	1.1	2.8	51.1	299.9	4.5	13.4	193.9	0.0	217.4	3263.6	16.5	2.4	8.2	19.2	1.8
SD	0.1	19.6	0.2	0.2	15.2	11.0	3.0	7.1	52.5	0.1	24.5	984.0	0.4	1.4	1.2	1.0	0.3
GsCMO																	
Mean	99.6	3951.3	1.0	2.9	23.2	197.0	0.0	4.1	17.5	0.0	197.3	2595.0	13.6	2.7	3.5	21.7	1.4
SD	0.3	15.1	0.1	0.2	2.8	71.4	0.1	1.1	2.6	0.0	30.3	384.6	3.3	1.2	0.9	4.1	0.2
Inner targets	PTV				Heart			Contralateral Lung			Ipsilateral Lung				Contralateral breast	Ipsilateral normal breast (whole breast-PTV_eval)	
	V95 (%)	Mean dose (cGy)	CI	GM (cm)	Mean Dose (cGy)	Max dose (cGy)	V5 (%)	Mean Dose (cGy)	Max dose (cGy)	V5 (%)	Mean Dose (cGy)	Max dose (cGy)	V10 (%)	V30 (%)	Dmax <3%	V50%	V95%
VMAT	99.2	3967.2	1.0	1.8	53.7	465.6	5.3	69.0	557.9	12.8	506.8	3640.8	49.6	10.6	1.4	7.9	0.7
SD	0.1	3.5	0.0	0.0	1.2	67.5	0.8	2.3	40.5	1.0	7.1	218.9	2.9	0.1	0.3	1.1	0.1
VMATa																	
Mean	99.4	3969.6	1.1	2.2	23.6	312.5	0.3	7.2	83.8	0.0	535.2	3672.3	50.0	12.2	6.1	10.6	1.0
SD	0.1	2.5	0.0	0.0	3.0	51.4	0.2	1.4	45.0	0.0	12.4	167.7	3.0	0.5	0.4	1.1	0.1
GsCMO																	
Mean	99.8	3975.9	1.1	2.4	18.6	128.1	0.0	2.3	13.9	0.0	190.7	3135.6	12.2	3.6	3.0	13.3	1.4
SD	0.2	5.1	0.0	0.2	0.6	0.7	0.0	0.1	0.6	0.0	17.8	126.9	1.6	1.2	0.1	4.4	0.3

Almost all treatment plans met the RAPID trial constraints which was stricter than NSABP B-39/RTOG 0413 protocol. VMAT plans for outer, central and inner targets did not meet the V10% for ipsilateral lung as shown in Table 4.5. VMATa plans for inner targets did not meet V10% for ipsilateral lung, and max point dose to contralateral breast.

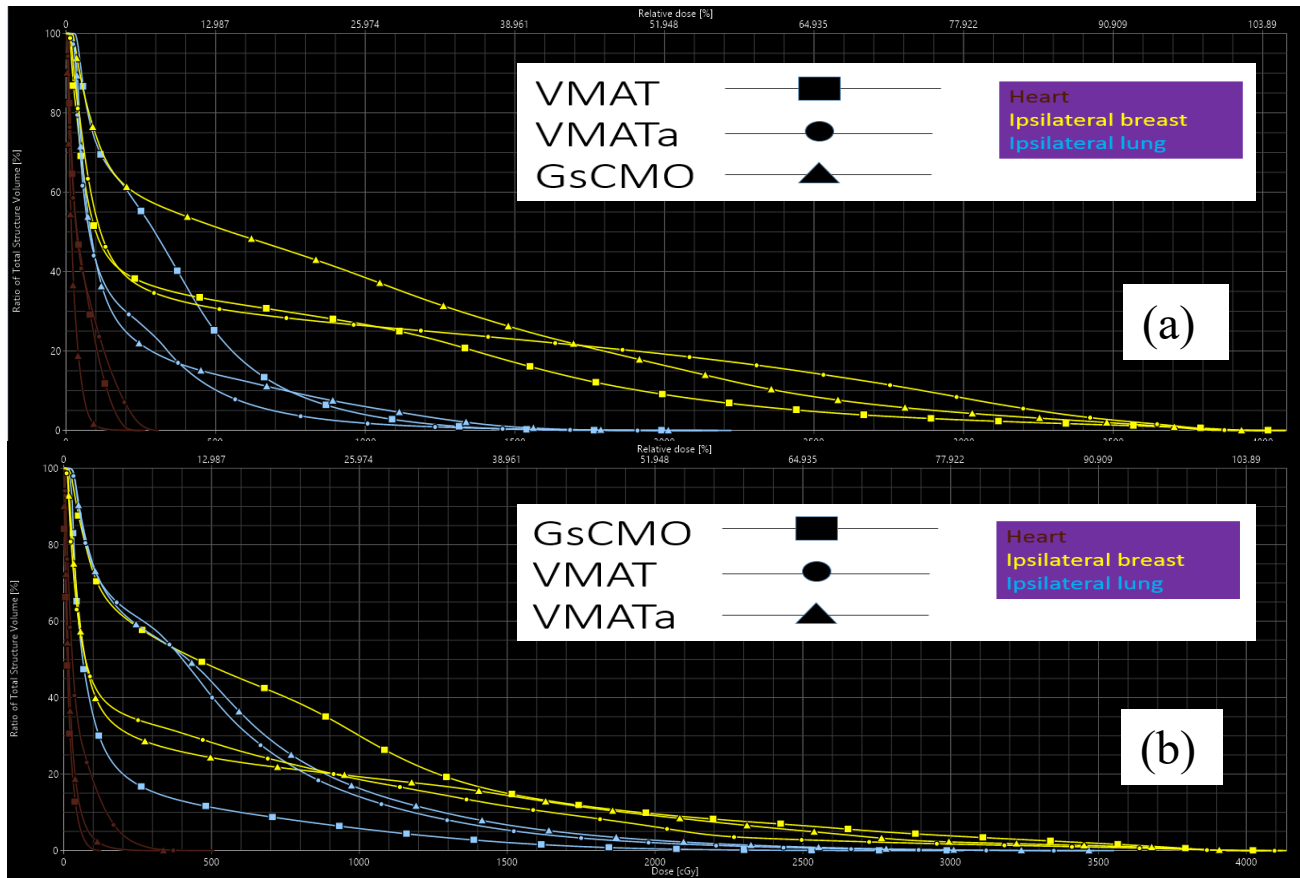


Figure 4. 7. The DVH shows the dose to heart, ipsilateral breast and ipsilateral lung for outer and central targets (a), and for inner targets (b).

The DVH comparison between all 3 techniques for a single patient is shown in Figure 4.7 for outer and central targets (a), and for inner targets (b). It is clear from both pictures, there is an adequate dose reduction to ipsilateral lung and heart volume.

All treatment plans were found satisfactory and passed the 2D gamma analysis with 2% dose difference and 2mm distance to agreement with a passing rate of $\geq 93\%$.

4.2.4. Discussion

Even though the PBI is an effective approach to prevent breast cancer recurrence after breast conserving surgery (BCS), but the previous data has shown some unacceptable level of toxicity and found non-inferior to whole breast irradiation (WBI)^{5,6}. Therefore, an adjuvant radiation therapy technique is needed which would be less invasive and less toxic.

Based on the previous studies on hypofractionation regimen, in which higher doses in few fractions are delivered was found safe and effective for partial breast irradiation⁷. Giving enough time to the normal tissue to heal which otherwise would not be sufficient if the treatment is given twice a day (BID). This makes hypofractionation technique more appealing for PBI. MD Anderson and team of RAPID trials are looking into the possibilities of utilizing hypofractionation scheme for patients with early stage breast cancer and require PBI. Our technique can be used and advanced further in this line.

4.2.5. Conclusion

The GsCMO technique is a novel itself and can be easily implemented for partial breast irradiation treatment planning improving the plan quality and lowering the dose to organs-at-risk in a least toxic way. This isocentric based coronal arc technique is suitable for any size and location of breast lumpectomy cavities.

The GsCMO technique provides an opportunity to take advantage of capability of both advanced functionality of LINAC and treatment planning system for certain body sites where an adequate conformity and less spread of low dose to organs-at-risk is highly appreciated. Our approach creates an opportunity to work on the advancement of existing treatment planning techniques.

Further improvement of this feasibility technique, in the line of hypofractionation scheme with one fraction a day, can provide dose escalation to lumpectomy cavity while satisfying the normal tissue constraints.

Our next chapter describes the importance of couch motion integration during dose delivery, and also discuss on how to account for patient motion during treatment.

Chapter 5: Couch motion integration and dose delivery validation techniques for GsCM technique

Publication
Med Phys., 2017. Abstract ID: 36880

This chapter describes in details the importance of inclusion of treatment couch during the radiation dose delivery. The first half of the chapter describes a methodology to check the accuracy of 6DoF couch and second half discusses the potential methods for validation of GsCMOT on the linear accelerator.

5.1. To verify the accuracy of 6DoF couch motion

5.1.1. Purpose

To check the accuracy of 6 DoF (degree-of-freedom) couch using Varian's developer mode application. In modern era of complex radiotherapy, it is very important to test the accuracy of various LINAC components including couch, collimator, gantry and on-board imaging devices. One of the crucial parts is to check the accuracy of couch that has 6 DoF (degrees of freedom) motion. The accuracy of whole radiation treatment delivery depends on couch positioning. Couch accuracy needs to be verified routinely. It has direct impact on patient treatment. Treatment couch plays an integral role in radiation therapy.

5.1.2. Methods

Existing methods to monitor the accuracy of couch are EPID or KV imager but both can sag over time. The challenging part is to test the pitch, yaw and roll along with translational motions of couch. Varian developer mode application was utilized for this task which controlled all mechanical motion axes and imaging using XML scripts. Evaluation of geometric accuracy of 6DoF couch was performed using an in-house built phantom consisting of set of bb's and a ruler placed at different plane as shown in Figure 5.1. Custom XML scripts were written to program the movement of 6DoF couch for various pitch, yaw and roll angles along with the acquisition of KV/MV images for each angle. Preliminary tests were performed first to assure the translational axis accuracy and leveling of the couch with the standard machine calibration equipment. The phantom was then placed on the couch and aligned with lasers. Varian's developer mode application was activated to move the 6DoF couch to the programmed positions; KV/MV beams delivered and images of the phantom were acquired following the commands in the XML file automatically and sequentially. Mathematical algorithm was developed to calculate the actual pitch, yaw and roll angles from the KV/MV images of the phantom, and the results were compared with the programmed angles as shown in Figure 5.2 and 5.3.

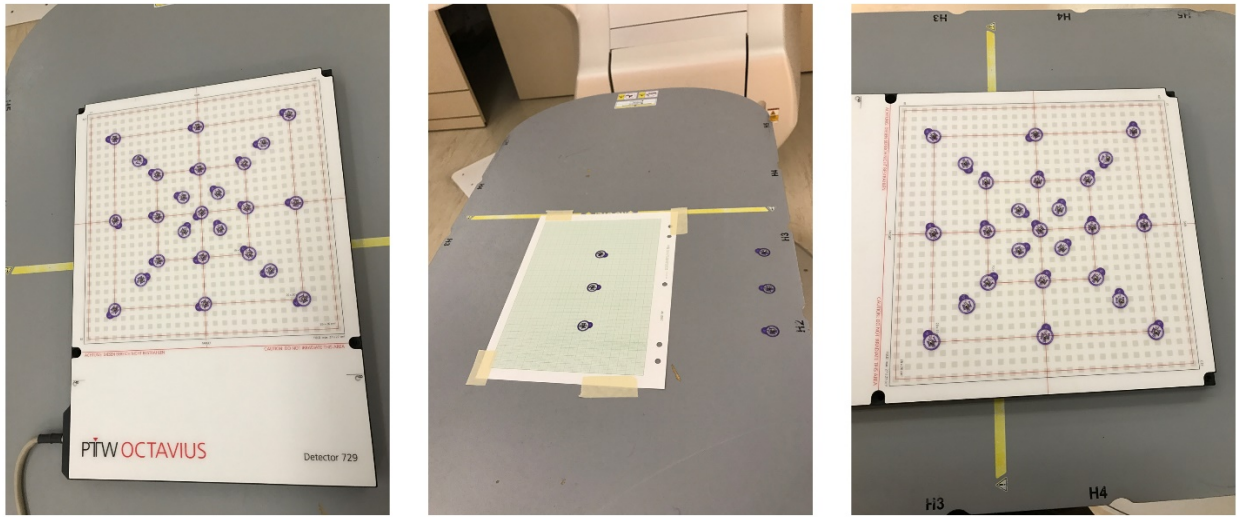


Figure 5. 1. In-house build phantom utilized to test the pitch, jaw and roll angles of 6DoF couch

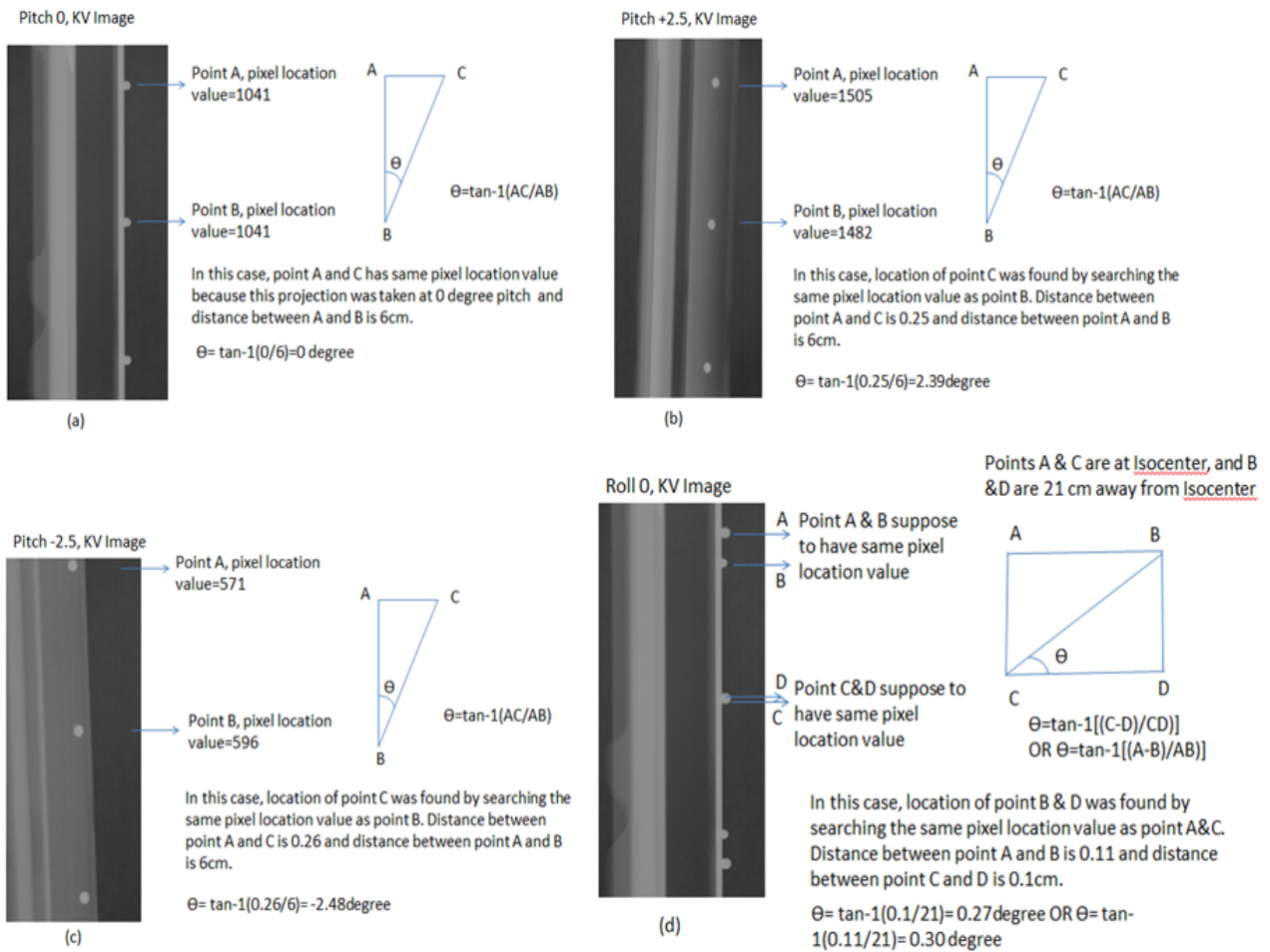


Figure 5. 2. All the measurements shown above were conducted using an in-house built phantom under Varian's Truebeam. Evaluation is done based on pixel location of metal bb in X, Y and Z

directions. Figure (a-d) shows the calculation method used to calculate pitch, yaw and roll of ± 3 degrees.

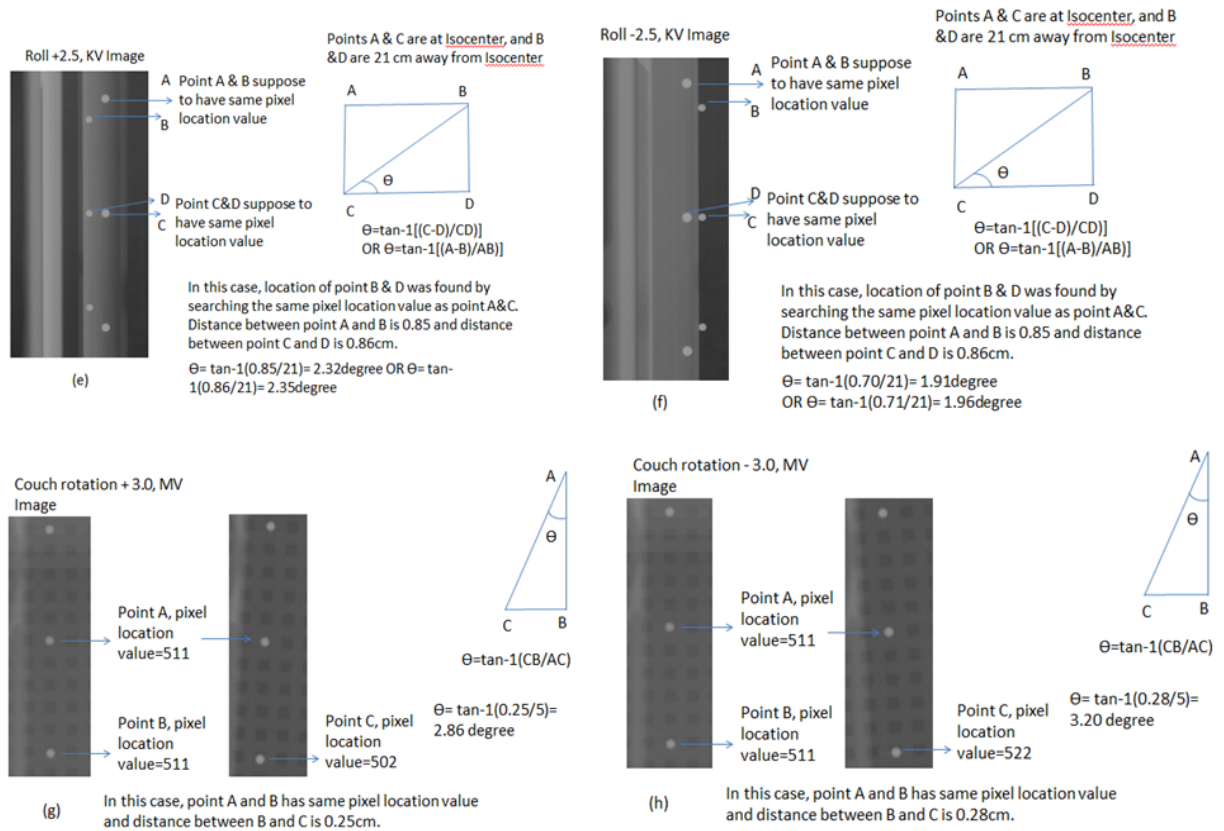


Figure 5. 3. All the measurements shown above were conducted using an in-house built phantom under Varian's Truebeam. Evaluation is done based on pixel location of metal bb in X, Y and Z directions. Figure (e-h) shows the calculation method used to calculate pitch, yaw and roll of ± 3 degrees.

5.1.3. Results

The accuracy of pitch, yaw and roll was tested for ± 3 degree of rotational angle with a 0.5-degree increment as shown in Figure 5.4. Linear regression of the measured (y) and planned (x) angles for pitch was $y=0.972x-0.0353$ with $R^2=0.9988$ and a maximal discrepancy of ± 0.16 degrees. For roll, it is $y=0.8873x+0.2$ with $R^2=0.9984$ and a maximal discrepancy of ± 0.56 degrees. For yaw the result is $y=0.9904x-0.1323$ with $R^2=0.9977$ and a maximal discrepancy of ± 0.31 degrees. While performing all the relevant tests, we have noticed that MV detector and KV detector were displaced off mechanically from isocenter axis position.

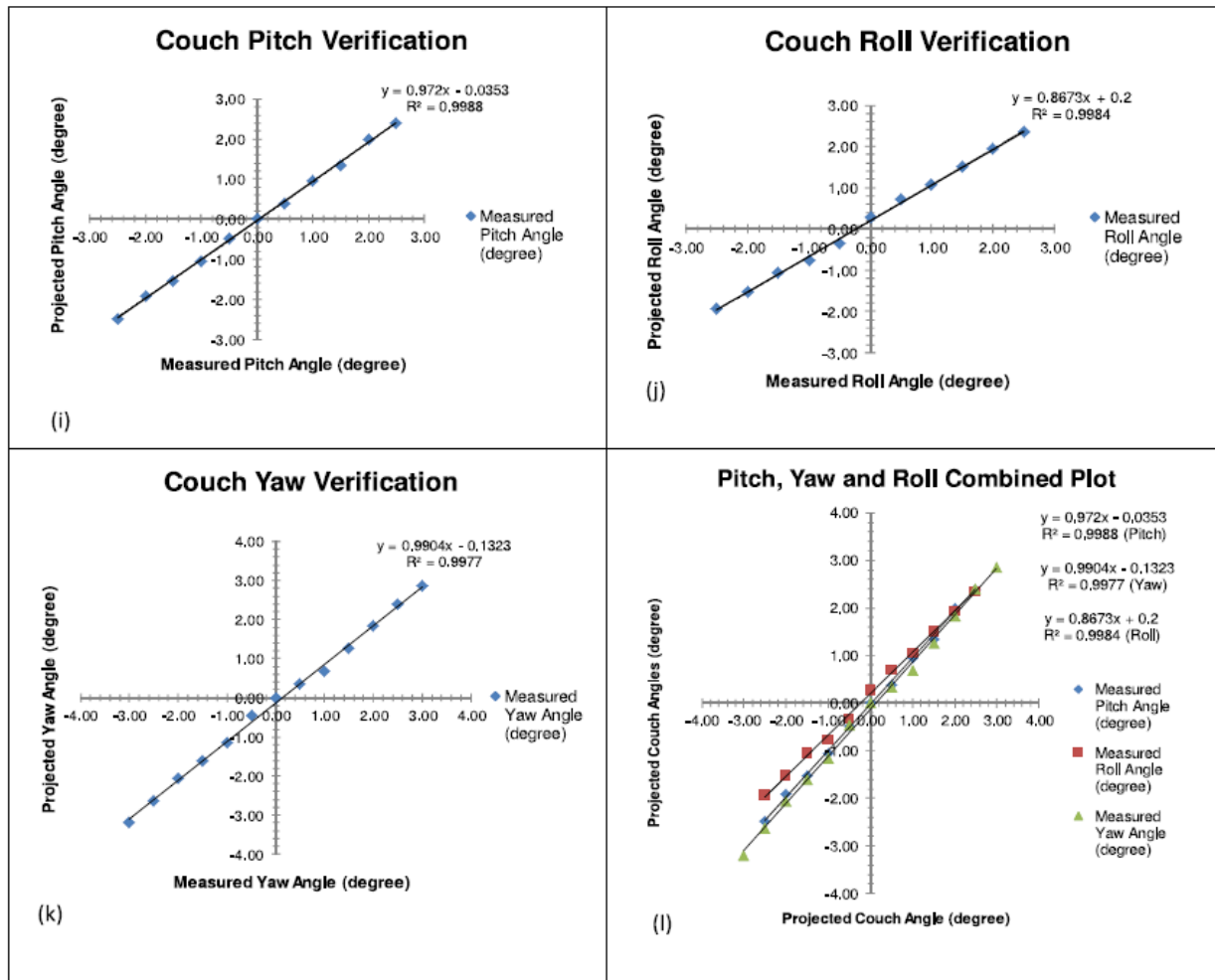


Figure 5. 4. Figure (i-l) shows the comparison of calculated and measured pitch, yaw and roll angles. Figure (l) is an indication of mechanical shifting of KV and MV panels over time which could be easily addressed using our approach.

5.1.4. Findings and discussion

KV imager panel was shifted over the time due to mechanical sag. A consistent shift of 0.5 degrees has seen for couch “roll” test for positive and negative angles. At small couch jaw angles of ± 2 degrees, the variation between the projected and measured couch angle was large. All the measurements were done at zero level of couch without any additional load applied. The maximum size of slabs in our phantom was 20x20cm with 1 cm thickness. One of the limitations was the size of our phantom which needed to be brought under 10x10cm to avoid the BBs positioning outside the imaging field of view.

5.1.5. Conclusion

Our written algorithm was able to find the location of BBs placed on different layers of phantom. Each layer in our phantom is unique for all translational and rotational positions.

Trigonometric formulas were used to calculate the location of BBs. Magnification factor of 1.5 was used for KV and MV images. Isocentric technique was used for this study to avoid any additional translational errors at different pitch, yaw and roll angles. All rotational angles errors are small but cannot be ignored especially for cases like stereotactic radiosurgery LINAC based treatments where the size and location of target volume can yield extra dose to organ at risks. The preliminary model of our phantom was able to detect the small couch rotational shifts. The developed test can be used to automate the annual quality assurance or commissioning of 6 DoF couch.

This phantom with future modification will look into the couch variations on daily bases and mechanical alignment of KV (Kilo-voltage X ray tube and panel) imager and MV (Mega-voltage) panel with respect to mechanical and radiation isocenter of LINAC. This unique study provided an invaluable tool to verify the accuracy of 6DoF couch and found useful for routine quality assurance.

5.2. Integration of couch travel and speed into GsCMO technique

5.2.1. Significance

The variations in the couch speed play an integral role for delivery of GsCMO technique. The implementation of couch parameters needed to be studied before implementing GsCMO technique fully in clinical application.

5.2.2. Methods

This dissertation constructed an experiment setup to perform couch motion measurements step-by-step using various test plans. The measurements were completed as function of couch speed in relationship to dose delivery. The important component was the variation of dose rate dependence on the couch motion. The couch starts and stop angle play a key role during the dose delivery. The gantry position remained static and delivered radiation at fixed position. The measurements were completed as function of, gantry position, dose rate change, and continuous couch motion. These measurements were used as a benchmark for GsCMO to achieve ‘successful’ couch motion speed and steps, as this is expected to result in comparable dose delivery to current gantry motion-based arc therapy but much smoother couch motion.

5.2.3. Results

Based on the graphs shown in Figure 5.5. the variation in couch position error is more pronounced for free couch motion (no limit added during delivery) with a minimum value of 0.05 degrees and maximum of 0.15 degrees. The speed of couch is automatically adjusted by the LINAC based on the MLC speed and dose rate. When we changed the couch speed manually to 1 degree per second, much smaller error was noticed with a minimum of 0.02 and maximum of 0.044 degrees. Also, based on the graph the couch moved in a constant fashion without being held at certain positions due to the dose rate variability. Lastly, when we changed the couch speed to 2-

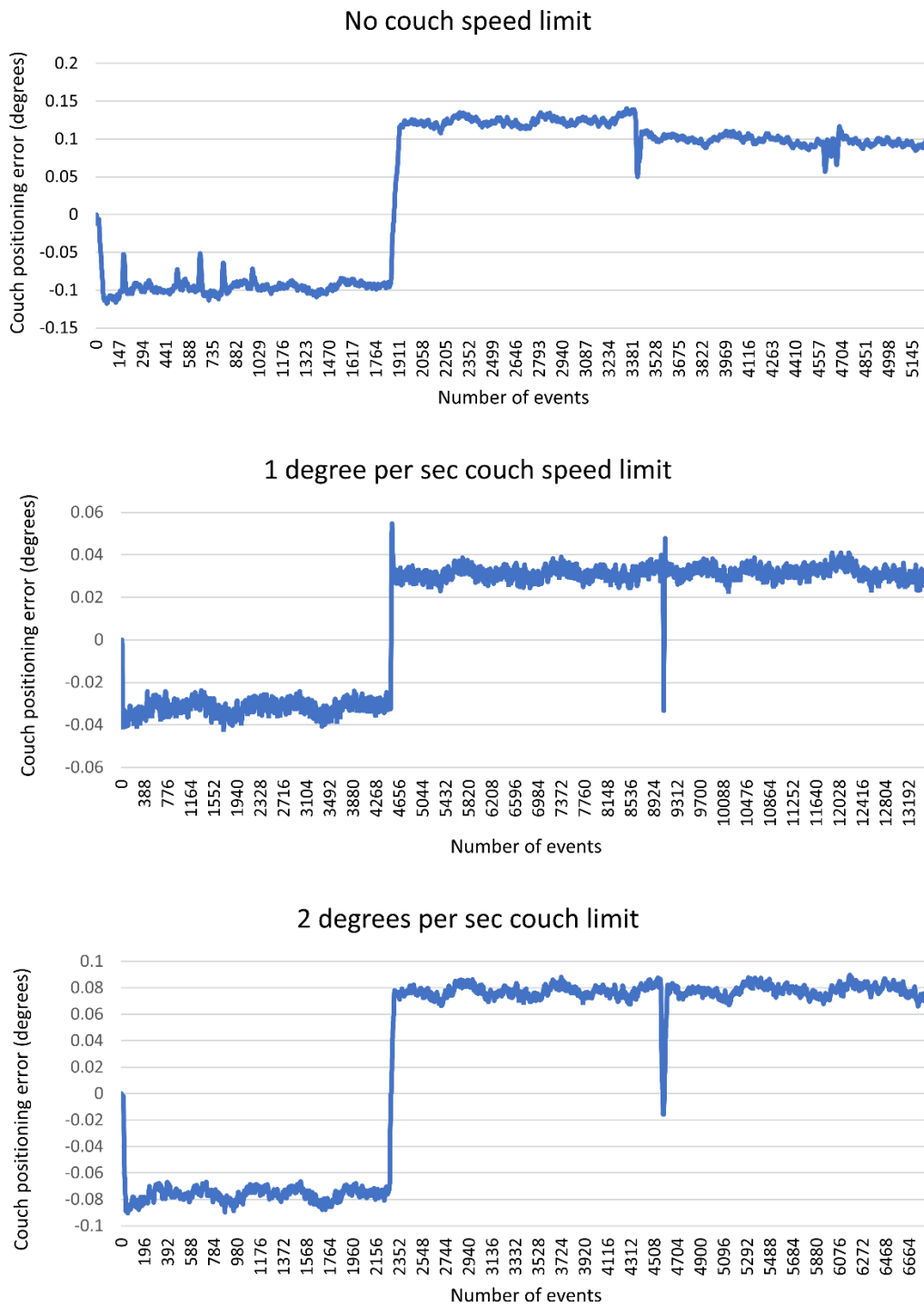


Figure 5. 5. Variation of couch speed is shown. Top view is without any couch speed limit. Middle view shows the variation when 1 degree per sec couch limit was applied. This shows a smooth couch transition from one position to another. Even though a constant couch motion was noticed for a couch speed limit of 2 degrees per sec, but the positioning error was larger than 1 degree per sec.

degrees per second, we noticed a constant couch speed, but the error was larger than 1 degree per sec with a minimum value of 0.065 and maximum value of 0.09 degrees.

5.2.4. Summary and Conclusion

The couch motion plays an integral role in our technique. Therefore, it was important to learn the behavior of its motion during the treatment. Based on the methods we utilized to study the rotational motion of couch and variation, we found that it has been well studied in this dissertation and ready to use clinically. This study also provides a guideline on how to implement couch motion for such treatments. And not to mention this also serves as a reference for medical physics community. The following chapter take this study as a precursor and works on how to automate GsCMOT to make it faster in terms of planning and delivery.

5.3. Effect of couch motion on patients with immobilization devices and without and including the dose rate variability integrated with couch motion

5.3.1. Significance

The objective of this study was evaluating couch motion dependence of the patient inclusive of patient weight variability, and presence of immobilization devices such as masks or body casts. During couch motion and especially at the initial point of motion, it is possible that the patient will experience exaggerated motion out of sync with the couch motion. This will result in a disparity between the treatment isocenter and patient isocenter. This disparity required further study and an investigation of the patient motion at the beginning, during, and at the end of couch motion were performed.

5.3.2. Methods

This study utilized C# programming software to adjust the dose rate in the treatment plan right before the creation of an XML file. This approach investigated the effect of different couch rotation and speed at static gantry positions. For brain treatments, a mask is placed over the head which keeps them immobilized during the treatment. For breast cases, patients are usually laying down on the body cast which is placed right over the breast board. For breast treatments, patient is a moving target. It is important to have some sort of immobilization to keep them intact on the treatment couch. Especially, our technique requires patient to motion during the dose delivery. Therefore, a body mesh type overlay is required on top of patient which keeps them immobilized on the treatment table. In addition to that, it was important to work on how to make couch starting and ending position smooth to get rid of any pulling or couch jerk feeling. We designed test plans in Eclipse treatment planning system. The plans were run using the same approach we had in earlier chapters 3 and 4. We trained our C# model to adjust the dose rate and couch speed. The main goal was to achieve smooth starting and ending of treatment couch. If we were to keep the free couch motion as it is, there is a little push at the beginning and end of treatment which will cause the patient to move or experience some pulling force. The results of these measurements,

coupled directly with couch position and speed, provided useful insight to couch motion dependent on patient weight and positioning. These measurements also provided estimations of the uncertainty levels for couch position and its effect on the treatment planning delivery.

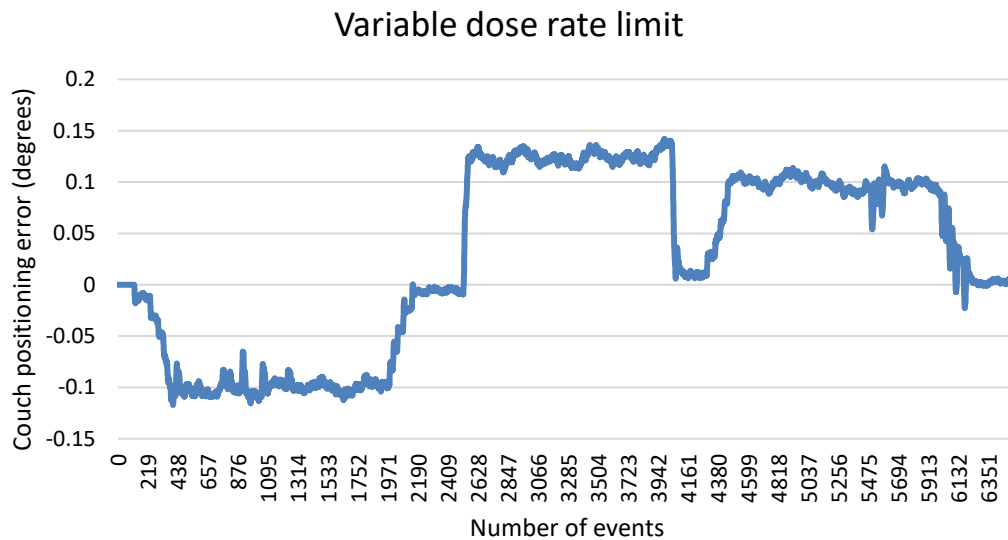


Figure 5. 6. Variation of dose rate impacts couch start and stop positioning

5.3.3. Results

Among all variables (couch speed, MLC speed and dose rate), adjustment of dose rate provided a slow start and stop positioning as shown in Figure 5.6. This is very important when the patient is on the table. Dose rate was adjusted in such a way that at the start position it couch ramps up slowly starting with 100MU/min to 600MU/min at the middle of the arc. Similarly, the dose rate decreases gradually when arc is about to finish. This adjustment of dose rate provided a better solution to control the couch speed. Maximum couch positioning error was under 0.12mm.

5.3.4. Discussion

This dissertation developed a platform to integrate continuous couch motion to the existing treatment planning systems and evaluated the delivered dose distributions with existing conventional treatment planning techniques. These methods were extended to evaluate the feasibility of dose delivery within the Truebeam radiotherapy platform. Further, this technique worked on making the couch start and stop positioning smoother to avoid any sudden couch pulling at those positions.

5.3.5. Summary and Conclusion

This study aimed to evaluate the accuracy of treatment couch motion and synchronization of couch motion while accounting for patient motion during delivery. This study is the first end-to-end validation of the couch motion. In next chapters, scripting for creating XML files were integrated into an automatic workflow for delivery onto Truebeam radiotherapy systems.

5.4. Validation of dose delivery

5.4.1. Purpose

Once all the treatment plans were ready, next part was to verify the radiation dose delivery onto Varian Truebeam linear accelerator.

5.4.2. Methods

We designed a combination of different plans with open fields, shaped fields, modulated fields with control points as shown in Figure 5.7. All plans were designed in Eclipse treatment planning system and XML script were created.

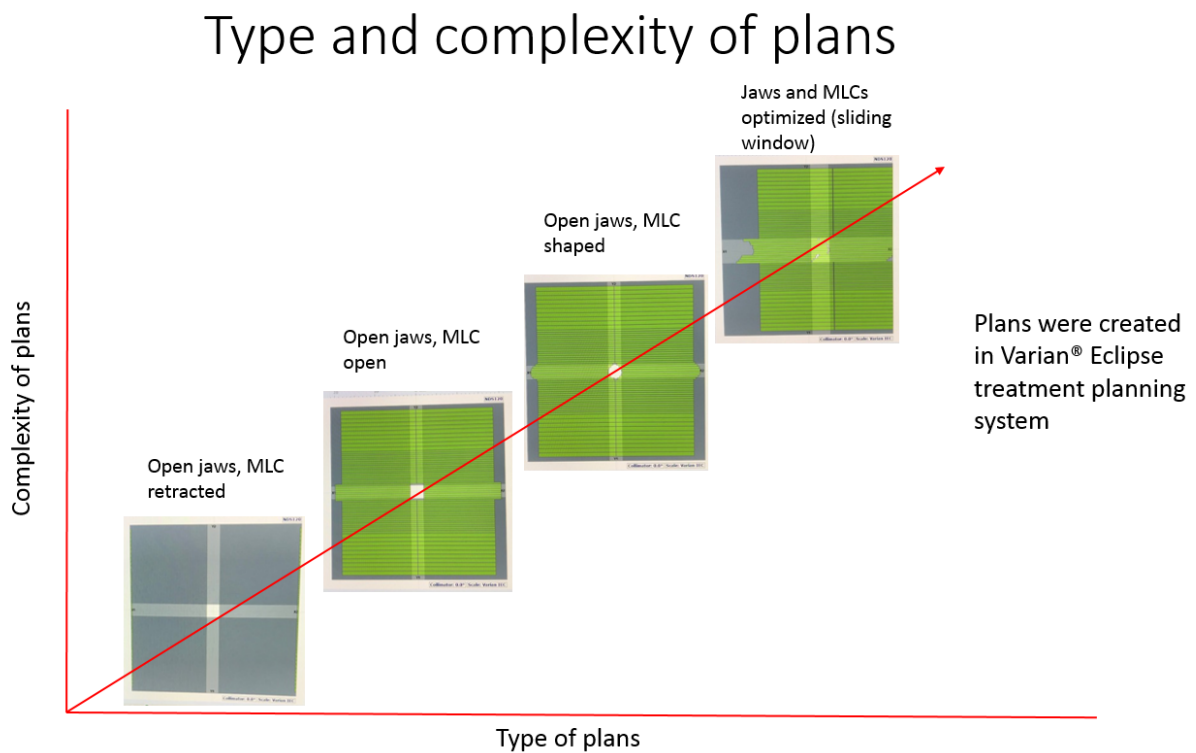


Figure 5. 7. Test plans as shown were simulated in treatment planning system including a variety of plans from simple (open field) to complex (with multiple control points and dose modulation)

Both simulated plans in Eclipse and script-based plans were tested onto Varian Truebeam LINAC as shown in Figure 5.8.

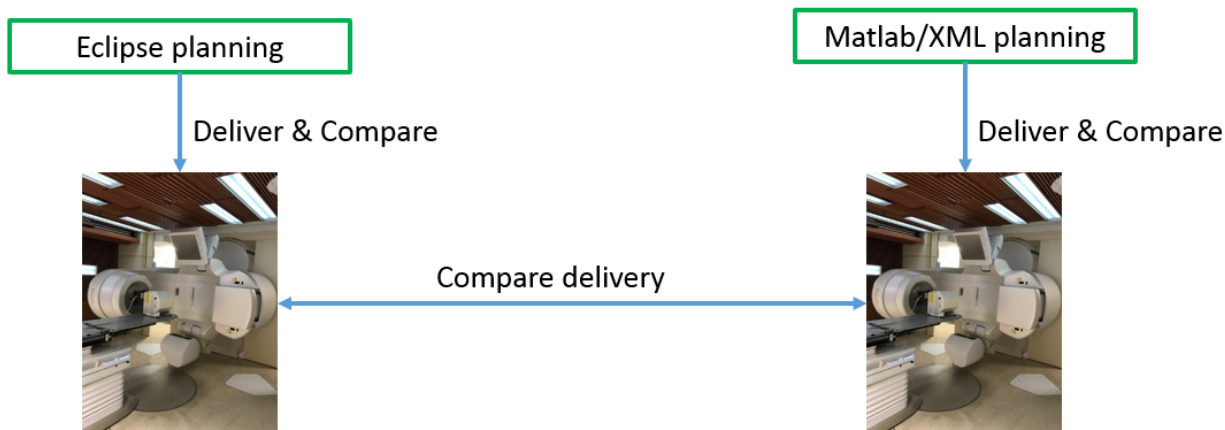


Figure 5. 8. Eclipse plans vs script-based plans were delivered and tested on Truebeam LINAC

All the treatment fields were delivered onto PTW Octavius 1500 ion chamber array. This array was first scanned in a vertical direction under the CT-Simulation and brought into the treatment planning system. The reason of scanning it vertically was to avoid any beam entrance at the edge of the array which otherwise would have degraded the accuracy of measurement.

IMRT QA setup (PTW 1500 array)

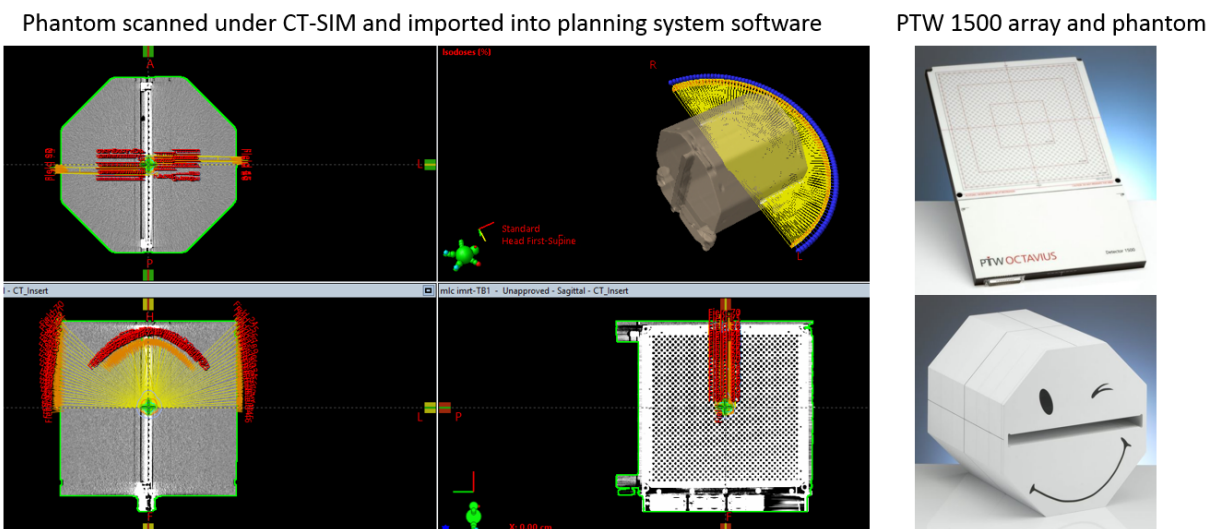


Figure 5. 9. 2D ion chamber array was utilized for the validation of radiation dose delivery. This phantom was scanned under CT-simulation and brought into treatment planning system

Next, part was to compare all the measured plans vs the script plans. We compared the delivery of eclipse simulated plans with script-based plans and delivery of both with respect to each other. After, calculating the plan in Eclipse, we transferred that plan onto the QA phantom (see Figure 5.9), and calculated the expected dose delivery which would be further compared with the beam delivery onto the Truebeam LINAC.

This IMRT QA phantom was set up on the couch and aligned it with the lasers such that the center of ion chamber array was at the isocenter of the LINAC (100cm). First part was to calibrate the array with the energy of interest which was utilized for designing the treatment plan. Based on the commissioning data available in the Eclipse, 163MUs give 100cGy at the isocenter which is 16cm depth from the surface of the Octavius phantom as shown in Figure 5.10.



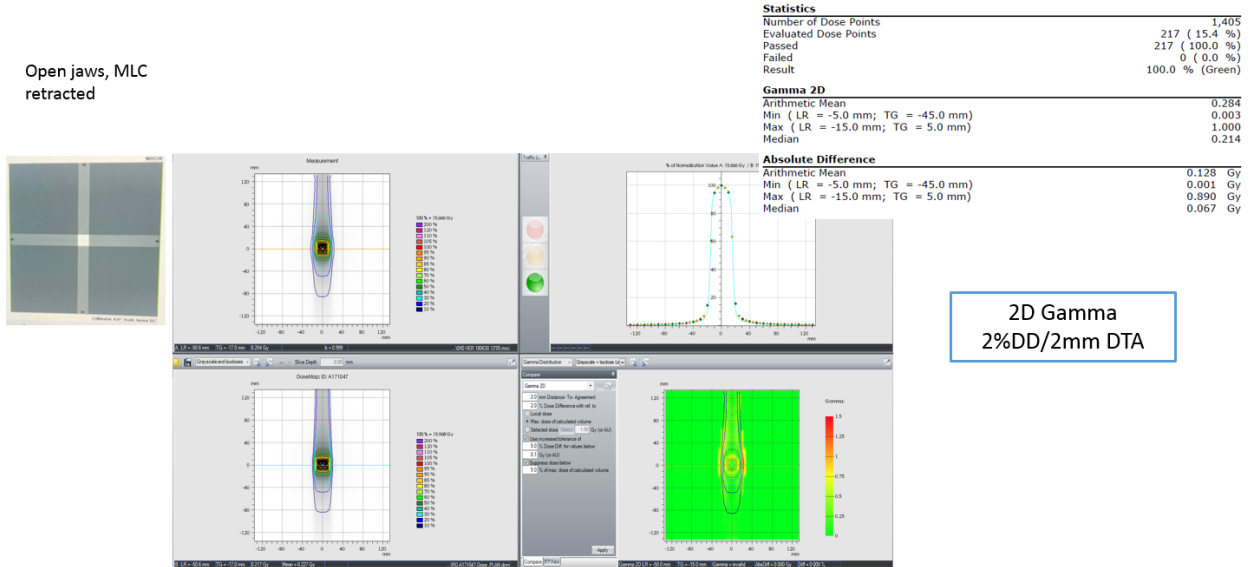
Figure 5. 10. PTW Octavius phantom utilized to compare the treatment planning dose verses the measured dose was set up on the treatment couch as shown.

5.4.3. Results

Once both the eclipse plans and script plans were delivered, the comparison among the both delivered plans was conducted utilizing the 2% dose difference (dd), 2mm distance-to-agreement (DTA), and 2D gamma of passing rate $\geq 95\%$ as a baseline. All plans passed the above criteria as shown in the following figures (5.11 to 5.16).

Eclipse vs. Delivery: Open Jaw, MLC retracted

Open jaws, MLC retracted

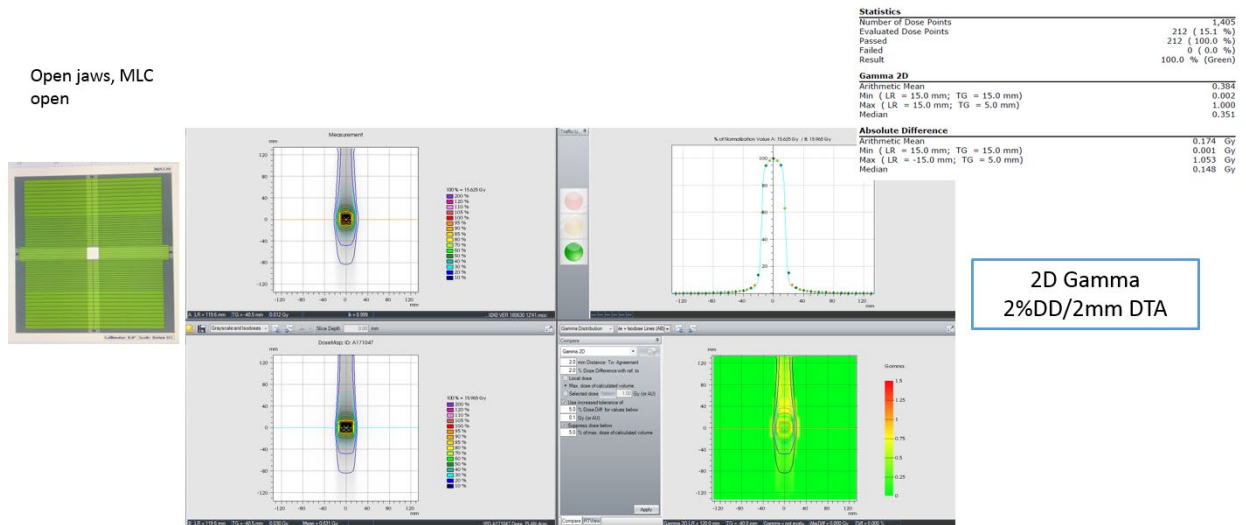


2D Gamma
2%DD/2mm DTA

Figure 5. 11. Verification of dose delivery for Eclipse plan vs delivery for an open field defined by Jaws only

Eclipse vs. Delivery: Open Jaw, Open MLC

Open jaws, MLC open

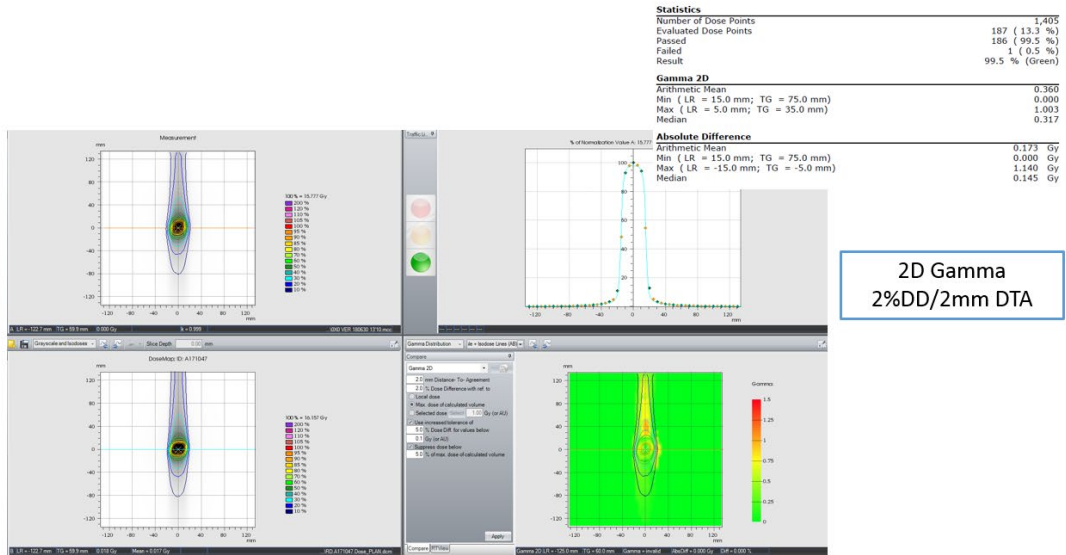
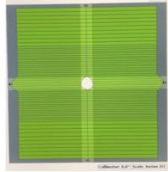


2D Gamma
2%DD/2mm DTA

Figure 5. 12. Verification of dose delivery for Eclipse plan vs delivery for an open field defined by Jaws and MLCs

Eclipse vs. Delivery: Open Jaw, MLC Shaped

Open jaws, MLC shaped

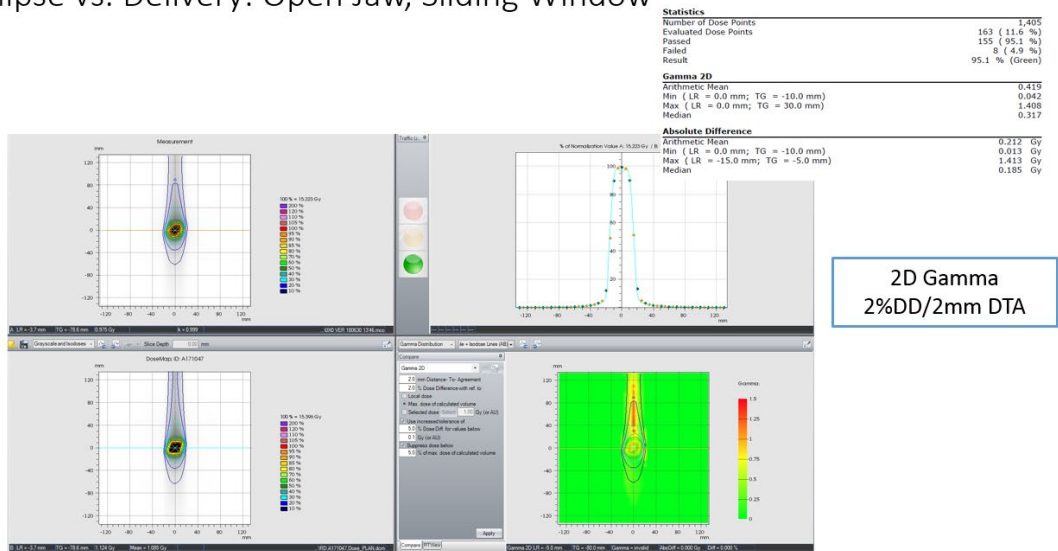
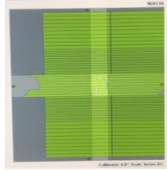


2D Gamma
2%DD/2mm DTA

Figure 5. 13. Verification of dose delivery for Eclipse plan vs delivery for a shaped conformal field defined by MLCs

Eclipse vs. Delivery: Open Jaw, Sliding Window

Jaws and MLCs optimized



2D Gamma
2%DD/2mm DTA

Figure 5. 14. Verification of dose delivery for Eclipse plan vs delivery for an optimized field modulated by MLCs utilizing the sliding window IMRT approach

Eclipse vs. XML: Open Jaw, MLC Shaped

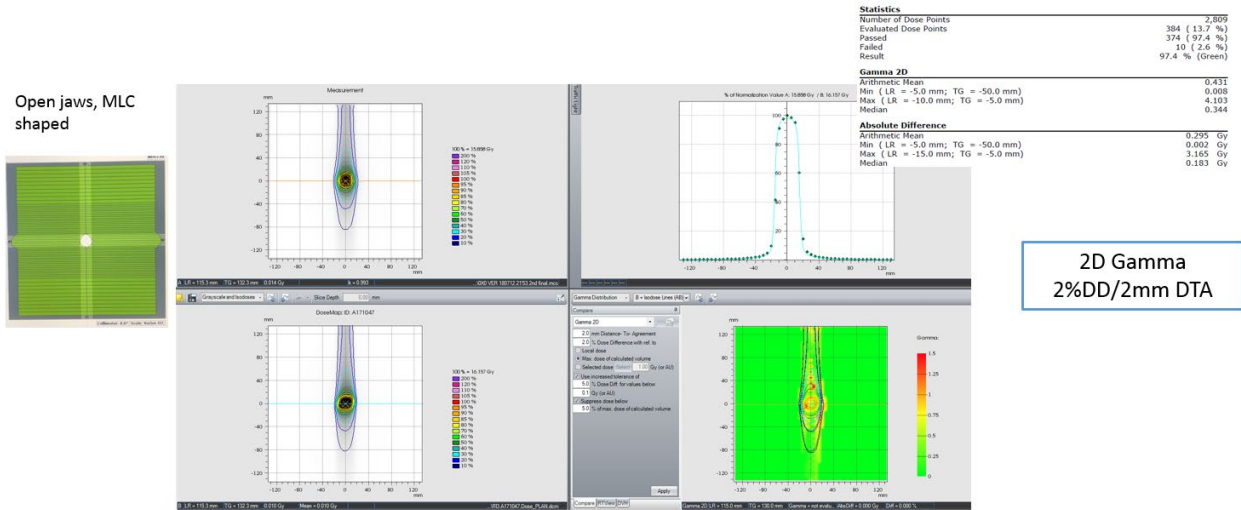


Figure 5. 15. Verification of dose delivery for Eclipse plan vs XML plans for a conformal field defined by MLCs

Delivery vs. XML: Open Jaw, MLC Shaped

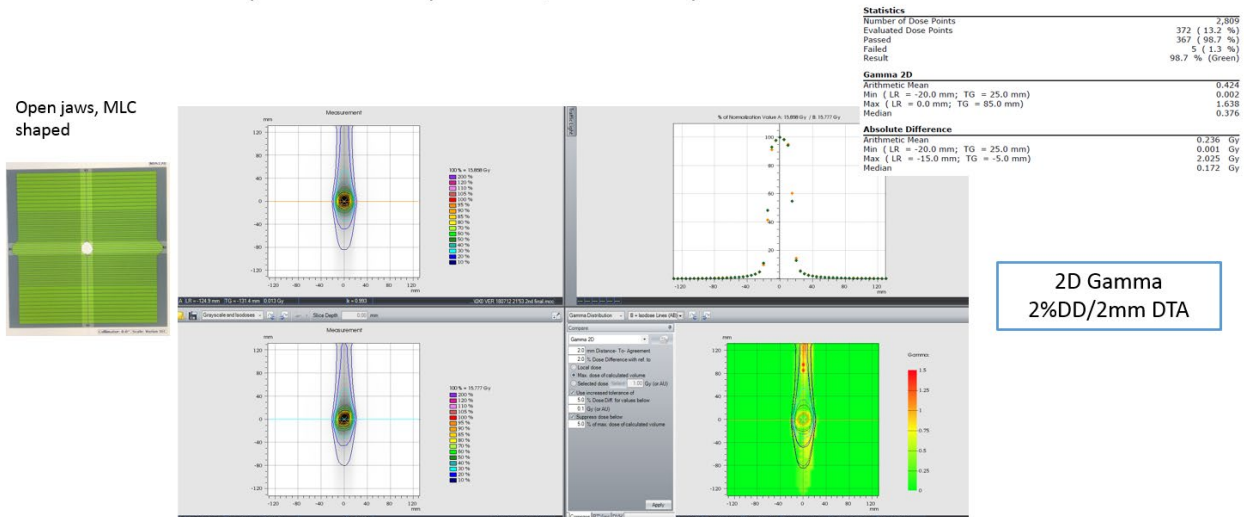


Figure 5. 16. Verification of dose delivery for an XML plan vs delivery for a conformal field defined by MLCs

5.4.4. Discussion

The comparison of treatment planning plans versus script plans passed the criteria of acceptance. Therefore, based on the results, our technique can be implemented in clinic. 2D-ion chamber array was utilized to analyze the QA of plans using 2D-gamma analysis. There are other solid phantoms and gel-phantoms available to perform the 3D-gamma analysis which would

provide the overall dose distribution comparison volumetrically in 3D space. Based on our experience, if we had used those expensive phantoms to analyze the custom plans, the results would not be very different in comparison of what we received with 2D-ion chamber array. Hence, there is no question in the accuracy and performance of 2D-ion chamber array and results we received are very well clinically acceptable.

5.4.5. Conclusion

Gantry static continuous motion treatment planning is feasible using Eclipse using multiple subfields and comparable to individually delivered subfields. Implementation and delivery of gantry static continuous motion technique is feasible within the framework of the TrueBeam® Radiotherapy System developer mode.

Chapter 6: Automated script-based implementation of step & shoot, sliding window, continuous coronal arc and gantry static couch optimized radiation therapy

Publication

Med Phys., 2019. Abstract ID: 45462

This chapter describes in detail on designing robust and automated treatments plans in treatment planning systems utilizing dynamic couch motion. The developed methodology to automate the process is discussed in detail. The potential role of eclipse scripting application programming interface (ESAPI) script is discussed in detail.

6.1. MATLAB based approach

6.1.1. Overview

Recent advances in clinically available treatment planning systems has facilitated ongoing innovation in tackling many of the challenges that have been previously limited technologically. In that context, we were faced with a clinically challenging scenario whereby it would be particularly advantageous to deliver dose in a coronal plane while keeping the gantry in a static position during continuous couch motion. However, implementation of this technique is not currently feasible since current treatment planning systems are not able to calculate or optimize the dose during couch motion. Further, while continuous couch motion can be integrated into a multiple static or IMRT fields, treatment delivery is a particularly time-consuming, clinically inefficient procedure. This particular challenge serves as the motivation for the development of a software to automatically convert an exported DICOM RT file utilizing couch-motion optimization into a single XML file and to verify the accuracy of delivery with treatment planning system.

6.1.2. Methods

Our in-house developed MATLAB® software reads the exported DICOM RT files of a treatment plan and combines all fields in the plan into a single XML file, considering the positioning accuracy of all mechanical axes. This software was tested using five treatment plans of increasing complexity for treating a planning target volume (PTV), (1) three-dimensional (3D) X and Y jaws, (2) 3D X and Y jaws with open field multileaf collimators (MLCs), (3) 3D X and Y jaw with single control point, (4) step-and-shoot intensity-modulated radiotherapy (IMRT) with 5 control points, and (5) step-and-shoot IMRT with 10 control points. All plans were generated with 92 individual fields and compiled into a single XML file using the developed MATLAB® software. Each plan was delivered onto an IMRT QA phantom. Planned dose was compared to measured dose using 2-dimensional (2D) gamma analysis with passing criteria of 2% dose difference (DD) and 2 mm distance to agreement (DTA). As a secondary QA check, the LINAC trajectory log files of beam delivery were used to verify the leaf position accuracy of MLC per control point for multiple fields.

Current workflow of planning and delivering static fields or IMRT fields is shown in Figure 6.1. We added an additional layer as shown in Figure 6.2 which merged all the fields together and created a single automated deliverable file. A set of simple to complex treatment plans as shown in Figure 6.3 were used to access the feasibility of using our MATLAB® XML file approach. All

the plans were delivered onto Varian's Truebeam® under developer mode application and validated using an IMRT QA device as shown in Figure 6.4 and 6.5.

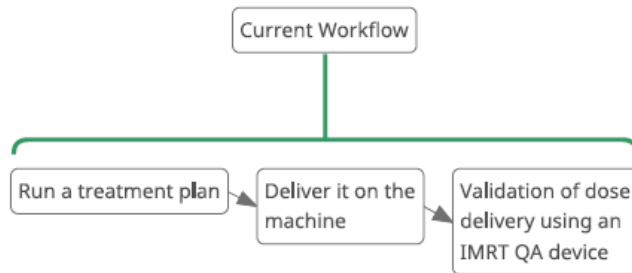


Figure 6. 1. Current workflow of planning, delivery and quality assurance check of 3D and an IMRT treatment plan

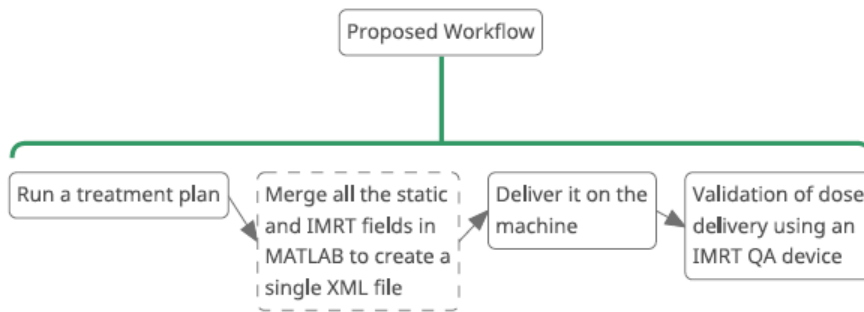


Figure 6. 2. Workflow (additional step is shown in the hashed box) of planning, delivery and quality assurance check of 3D and an IMRT treatment plan

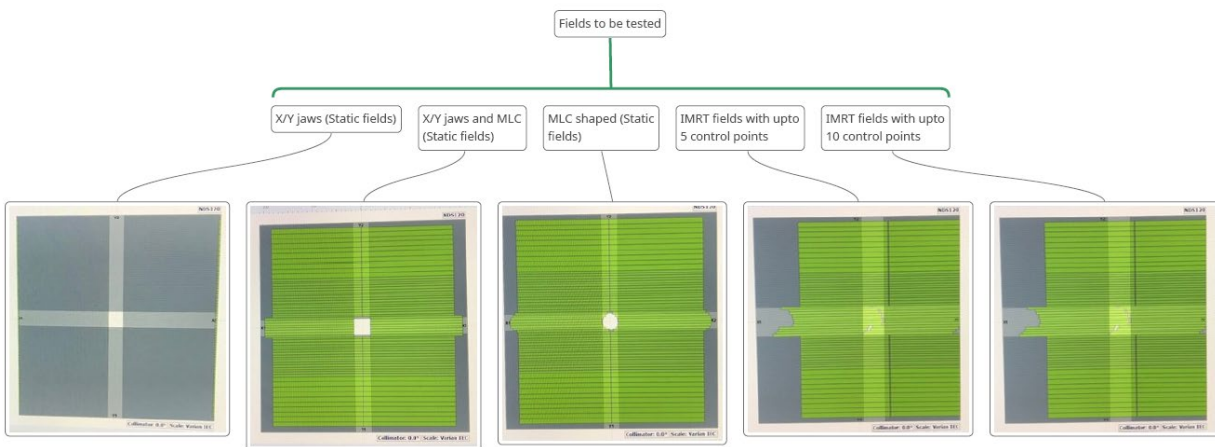


Figure 6. 3. Five executed treatment plans with increasing complexity, starting from very simple open static field to complex IMRT fields with multiple control points. All these plans were run in

Eclipse treatment planning system and exported to MATLAB. A single XML file was created by combining all the multiple fields

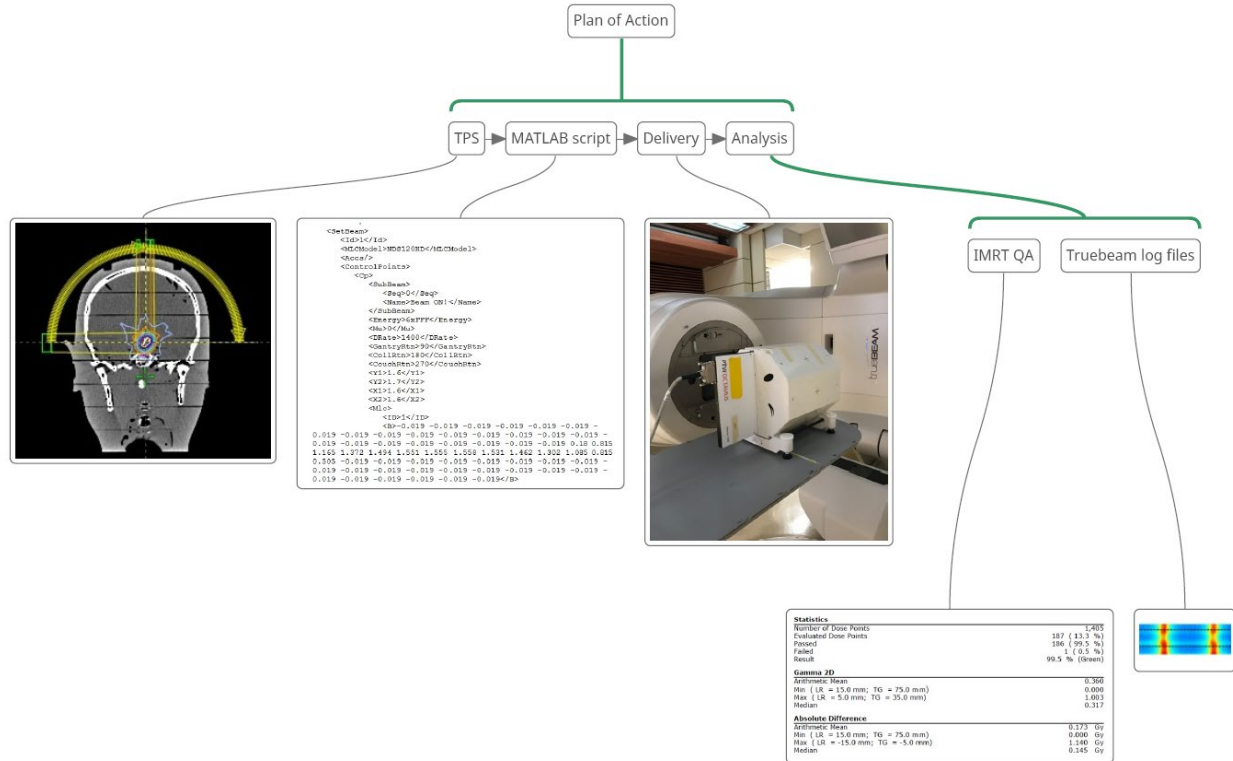


Figure 6. 4. Workflow of planning to validation testing using MATLAB script, an IMRT QA device (PTW Octavius 1500ion chamber array) and Truebeam trajectory log files

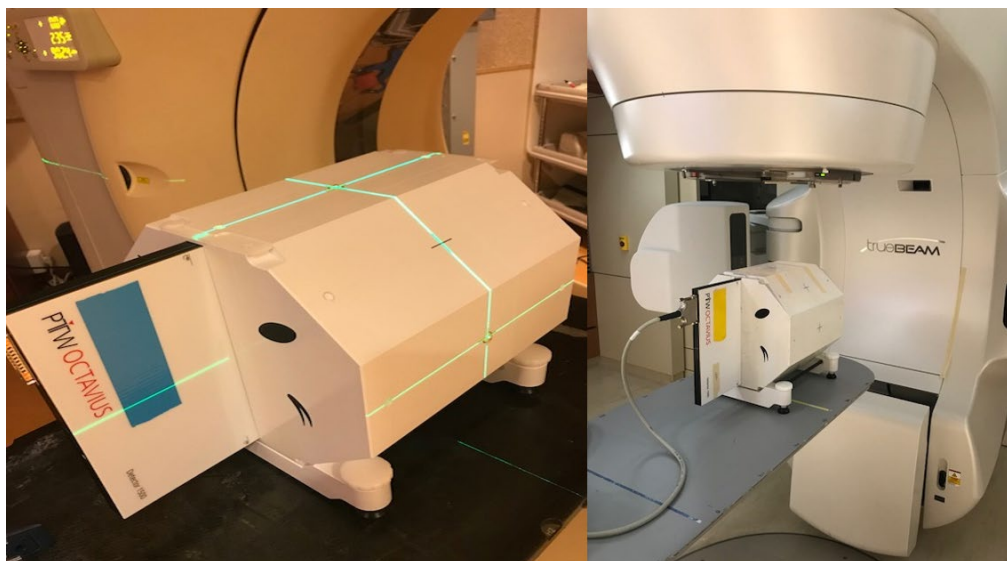


Figure 6. 5. PTW OCTAVIUS IMRT QA phantom setup for CT simulation (left) vs. setup on the couch for treatment delivery (right).

6.1.3.1. Layout of design and its application in brain case

Simulated treatment plans utilizing multiple static fields and sliding window intensity modulated radiotherapy (IMRT) gantry static couch motion was applied in brain for a tumor situated between the optical chiasm and brainstem. Fields were automatically merged using in house developed MATLAB® scripts, producing a single XML file facilitating continuous delivery of the treatment plan within the TrueBeam® Radiotherapy System developer mode. Treatment was delivered to an IMRT quality assurance phantom, scanned vertically to avoid beam entry at the edge of the phantom. Comparison of the simulated radiation dose vs measured dose distributions was performed based on various metrics including 3% dose difference, 3mm distance to agreement and 2-dimensional gamma analysis.

All treatment fields were exported from the Eclipse planning system in a Digital Imaging and Communications in Medicine (DICOM) standard format. For scenario #1, #2, and #3 static fields were automatically merged using an in house developed MATLAB® script, producing a single XML file facilitating continuous delivery of the treatment plan within the TrueBeam® Radiotherapy System developer mode. For scenario #4 and #5 IMRT fields were automatically merged using an in house developed MATLAB® script, producing a single XML file facilitating automated delivery of the treatment plan within the TrueBeam® Radiotherapy System developer mode. Treatment was delivered to an IMRT quality assurance phantom, scanned vertically to avoid beam entry at the edge of the phantom (Figure 6.5).

6.1.3.2. Simulation

Patients were scanned axially using our in-house CT-SIM (Siemens Medical Solutions USA, Inc.) both horizontally and vertically (120 KVp, 200 mAs, 515 × 515 matrix size, 50 cm field of view, and 2 mm slice thickness) and exported to the Eclipse Treatment Planning system (Version #15.6, Varian Medical Systems, Palo Alto, CA) for treatment planning.

6.1.3.3. Treatment Planning

Treatment planning consisted of an external beam planning approach delivering 20 Gy in 1 fraction via 6MVFFF photon beams. Treatment planning was performed using the Eclipse treatment planning system with 1.5mm dose grid resolution. All treatment plans were created based on a high-definition 120 multileaf collimator (MLC) system with 2.5mm width x 32 pairs at the center and 5mm width x 28 pairs at the periphery.

For the current study, 4 treatment plans of increasing complexity were generated in order to simulate various likely clinical scenarios in brain where gantry static couch motion optimization would be particularly beneficial. Specifically, treatment planning was performed for a PTV located in the brain for a tumor situated between the optical chiasm and brainstem.

Scenario #1 integrated MLC shaping with couch motion with a static gantry to delivery conformal arc. Delivery of dose was integrated in 2° couch increments for two partial couch arcs (270° to 0° and 0° to 90°) while the gantry as positioned contralaterally with respect to the target to avoid collisions. MLC shaping was only permitted while the couch was stationary. A single

control point was used for each couch angle as shown in Table 6.1. The script 2.0 is attached under Appendix.

Table 6. 1. XML file for static conformal fields. All fields were combined to create a single deliverable arc

```
<?xml version="1.0" encoding="utf-8"?>
<VarianResearchBeam SchemaVersion="1.0"
  <SetBeam>
    <Id>1</Id>
    <MLCModel>NDS120</MLCModel>
    <Accs/>
    <ControlPoints>
      <Cp>
        <SubBeam>
          <Seq>0</Seq>
          <Name>Beam ON!</Name>
        </SubBeam>
        <Energy>6x</Energy>
        <Mu>0</Mu>
        <DRate>600</DRate>
        <GantryRtn>270</GantryRtn>
        <CollRtn>180</CollRtn>
        <CouchRtn>90</CouchRtn>
        <Y1>1.6</Y1>
        <Y2>1.7</Y2>
        <X1>1.6</X1>
        <X2>1.6</X2>
        <Mlc>
          <ID>1</ID>
          <B>0.019 0.019 0.019 0.019 0.019 0.019 0.019 0.019 0.019 0.019 0.019 0.019 0.019 0.019 0.019 0.019
0.019 0.019 0.019 0.019 0.019 0.019 0.019 0.18 0.815 1.165 1.372 1.494 1.551 1.555 1.558 1.531 1.462 1.302
1.085 0.815 0.505 0.019 0.019 0.019 0.019 0.019 0.019 0.019 0.019 0.019 0.019 0.019 0.019 0.019 0.019 0.019
0.019 0.019 0.019 0.019 0.019 0.019 0.019 0.019</B>
          <A>0.019 0.019 0.019 0.019 0.019 0.019 0.019 0.019 0.019 0.019 0.019 0.019 0.019 0.019 0.019 0.019
0.019 0.019 0.019 0.019 0.019 0.019 0.019 0.55 0.895 1.205 1.393 1.514 1.574 1.597 1.591 1.518 1.417 1.242
1.045 0.775 0.425 0.019 0.019 0.019 0.019 0.019 0.019 0.019 0.019 0.019 0.019 0.019 0.019 0.019 0.019 0.019
0.019 0.019 0.019 0.019 0.019 0.019 0.019 0.019</A>
        </Mlc>
      </Cp>
      <Cp>
        <Mu>0</Mu>
        <GantryRtn>270</GantryRtn>
        <CouchRtn>90</CouchRtn>
        <Y1>1.6</Y1>
        <Y2>1.7</Y2>
        <X1>1.6</X1>
        <X2>1.6</X2>
        <Mlc>
          <ID>1</ID>
          <B>0.019 0.019 0.019 0.019 0.019 0.019 0.019 0.019 0.019 0.019 0.019 0.019 0.019 0.019 0.019 0.019
0.019 0.019 0.019 0.019 0.019 0.019 0.019 0.16 0.85 1.165 1.375 1.495 1.551 1.555 1.558 1.526 1.455 1.295 1.077
```

```

0.81 0.515 0.019 0.019 0.019 0.019 0.019 0.019 0.019 0.019 0.019 0.019 0.019 0.019 0.019 0.019 0.019 0.019 0.019 0.019 0.019
0.019 0.019 0.019 0.019 0.019 0.019 0.019 0.019 0.019 0.019 0.019 0.019 0.019 0.019 0.019 0.019 0.019 0.019 0.019 0.019 0.019
0.019 0.019 0.019 0.019 0.019 0.019 0.019 0.019 0.019 0.019 0.019 0.019 0.019 0.16 0.85 1.165 1.375 1.495 1.551 1.555
1.558 1.526 1.455 1.295 1.077 0.81 0.515 0.019 0.019 0.019 0.019 0.019 0.019 0.019 0.019 0.019 0.019 0.019 0.019 0.019
0.019 0.019 0.019 0.019 0.019 0.019 0.019 0.019 0.019 0.019 0.019 0.019 0.019 0.019</B>
  <A>0.019 0.019 0.019 0.019 0.019 0.019 0.019 0.019 0.019 0.019 0.019 0.019 0.019 0.019 0.019 0.019 0.019 0.019 0.019 0.019
0.019 0.019 0.019 0.019 0.019 0.019 0.019 0.019 0.16 0.85 1.165 1.375 1.495 1.551 1.555 1.558 1.526 1.455 1.295 1.077
0.81 0.515 0.019 0.019 0.019 0.019 0.019 0.019 0.019 0.019 0.019 0.019 0.019 0.019 0.019 0.019 0.019 0.019 0.019 0.019
0.019 0.019 0.019 0.019 0.019 0.019 0.019 0.019 0.019 0.019 0.019 0.019 0.019 0.019 0.019 0.019 0.019 0.019 0.019 0.019
0.019 0.019 0.019 0.019 0.019 0.019 0.019 0.019 0.019 0.019 0.16 0.85 1.165 1.375 1.495 1.551 1.555
1.558 1.526 1.455 1.295 1.077 0.81 0.515 0.019 0.019 0.019 0.019 0.019 0.019 0.019 0.019 0.019 0.019 0.019 0.019 0.019
0.019 0.019 0.019 0.019 0.019 0.019 0.019 0.019 0.019 0.019 0.019 0.019 0.019 0.019</A>
  </Mlc>
</Cp>
<Cp>
  <Mu>44.3769</Mu>
</Cp>
<Cp>
  <Mu>44.3769</Mu>
  <GantryRtn>270</GantryRtn>
  <CouchRtn>92</CouchRtn>
  <Y1>1.6</Y1>
  <Y2>1.6</Y2>
  <X1>1.6</X1>
  <X2>1.6</X2>
  <Mlc>
  <ID>1</ID>
  <B>0.02 0.02 0.02 0.02 0.02 0.02 0.02 0.02 0.02 0.02 0.02 0.02 0.02 0.02 0.02 0.02 0.02 0.02 0.02 0.02 0.02 0.02
0.02 0.02 0.02 0.55 0.89 1.205 1.395 1.508 1.552 1.555 1.559 1.521 1.445 1.272 1.067 0.79 0.455 0.02 0.02 0.02
0.02 0.02 0.02 0.02 0.02 0.02 0.02 0.02 0.02 0.02 0.02 0.02 0.02 0.02 0.02 0.02 0.02 0.02 0.02 0.02 0.02 0.02
0.02 0.02 0.02 0.02 0.02 0.02 0.02 0.02 0.02 0.02 0.02 0.02 0.02 0.02 0.02 0.02 0.02 0.02 0.02 0.02 0.55 0.89 1.205
1.395 1.508 1.552 1.555 1.559 1.521 1.445 1.272 1.067 0.79 0.455 0.02 0.02 0.02 0.02 0.02 0.02 0.02 0.02 0.02 0.02
0.02 0.02 0.02 0.02 0.02 0.02 0.02 0.02 0.02 0.02 0.02 0.02 0.02 0.02 0.02 0.02 0.02 0.02 0.02 0.02 0.02</B>
  <A>0.02 0.02 0.02 0.02 0.02 0.02 0.02 0.02 0.02 0.02 0.02 0.02 0.02 0.02 0.02 0.02 0.02 0.02 0.02 0.02 0.02 0.02
0.02 0.02 0.02 0.55 0.89 1.205 1.395 1.508 1.552 1.555 1.559 1.521 1.445 1.272 1.067 0.79 0.455 0.02 0.02 0.02
0.02 0.02 0.02 0.02 0.02 0.02 0.02 0.02 0.02 0.02 0.02 0.02 0.02 0.02 0.02 0.02 0.02 0.02 0.02 0.02 0.02 0.02
0.02 0.02 0.02 0.02 0.02 0.02 0.02 0.02 0.02 0.02 0.02 0.02 0.02 0.02 0.02 0.02 0.02 0.02 0.02 0.02 0.55 0.89 1.205
1.395 1.508 1.552 1.555 1.559 1.521 1.445 1.272 1.067 0.79 0.455 0.02 0.02 0.02 0.02 0.02 0.02 0.02 0.02 0.02 0.02
0.02 0.02 0.02 0.02 0.02 0.02 0.02 0.02 0.02 0.02 0.02 0.02 0.02 0.02 0.02 0.02 0.02 0.02 0.02 0.02 0.02</A>
  </Mlc>
</Cp>
-----continue for next control points and ends with the last control point-----
</Mlc>
</Cp>
<Cp>
  <Mu>3770.6251</Mu>
</Cp>
<Cp>
  <Mu>3770.6251</Mu>
  <GantryRtn>90</GantryRtn>

```



```

0.742 2.275 2.275 2.275 2.275 2.275 2.275 2.275 2.275 2.275 2.275 2.275 2.275 2.275 2.275 2.275 2.275 2.275
2.275 2.275 2.275 2.275 2.275 2.275 2.275 2.275</B>
  <A>-2.225 -2.225 -2.225 -2.225 -2.225 -2.225 -2.225 -2.225 -2.225 -2.225 -2.225 -2.225 -2.225 -2.225 -2.225 -
2.225 -2.225 -2.225 -2.225 -2.225 -2.225 -2.225 -2.225 -2.225 -2.225 -2.225 0.992 1.242 1.742 1.742 1.742 1.742
1.742 1.492 1.492 0.742 -2.225 -2.225 -2.225 -2.225 -2.225 -2.225 -2.225 -2.225 -2.225 -2.225 -2.225 -2.225 -2.225
-2.225 -2.225 -2.225 -2.225 -2.225 -2.225 -2.225 -2.225 -2.225 -2.225 -2.225 -2.225</A>
  </Mlc>
</Cp>

-----continue with the next control pins and end with the following last control point-----

</Mlc>
</Cp>
<Cp>
  <Mu>3929.4249</Mu>
  <GantryRtn>270</GantryRtn>
  <CollRtn>180</CollRtn>
  <CouchRtn>180</CouchRtn>
  <Y1>1.25</Y1>
  <Y2>1.25</Y2>
  <X1>1.75</X1>
  <X2>1.75</X2>
  <Mlc>
  <ID>92</ID>
  <B>2.275 2.275 2.275 2.275 2.275 2.275 2.275 2.275 2.275 2.275 2.275 2.275 2.275 2.275 2.275 2.275 2.275
2.275 2.275 2.275 2.275 2.275 2.275 2.275 2.275 2.275 2.275 2.275 -0.508 -0.508 -0.508 -0.758 -1.008 1.242 2.275 2.275
2.275 2.275 2.275 2.275 2.275 2.275 2.275 2.275 2.275 2.275 2.275 2.275 2.275 2.275 2.275 2.275 2.275 2.275
2.275 2.275 2.275 2.275 2.275 2.275 2.275 2.275</B>
  <A>-2.225 -2.225 -2.225 -2.225 -2.225 -2.225 -2.225 -2.225 -2.225 -2.225 -2.225 -2.225 -2.225 -2.225 -2.225 -
2.225 -2.225 -2.225 -2.225 -2.225 -2.225 -2.225 -2.225 -2.225 -2.225 -2.225 -2.225 -2.225 0.992 1.242 1.742 0.992 1.492
-0.758 -2.225 -2.225 -2.225 -2.225 -2.225 -2.225 -2.225 -2.225 -2.225 -2.225 -2.225 -2.225 -2.225 -2.225 -2.225 -
2.225 -2.225 -2.225 -2.225 -2.225 -2.225 -2.225 -2.225 -2.225 -2.225 -2.225 -2.225</A>
  </Mlc>
</Cp>
<Cp>
  <Mu>95.1079</Mu>
</Cp>
</ControlPoints>
</SetBeam>
</VarianResearchBeam>

```

Scenario #3 consisted of the delivery of two coronal half-arcs with the gantry rotating from 270° to 0° and 0° to 90°. This scenario consisted of a step&shoot technique whereby the MLC shaping was integrated with the delivery of radiation and the rotation of the gantry. Couch motion was not implemented in this scenario as shown in Table 6.2 based on script 3.0 shown in Appendix.

Scenario #4 built on the previous scenario by converting the two coronal half-arcs into a gantry-static couch optimized sliding window technique. This objective was achieved by substituting the continuous gantry motion with couch motion while keeping the gantry at a single

location. This approach was chosen due to the limitations of the treatment planning system precluding couch motion optimization.

Scenario#5 converts the gantry arc into a couch arc.

6.1.3. Results

All XML-based plans were delivered with passing 2D gamma criteria (3mm/3%) of $98 \pm 1.2\%$. The root mean square of log files was calculated as $0.0181 \pm 0.0012\text{mm}$ for 3D and $0.0256 \pm 0.0041\text{mm}$ for IMRT cases. Average delivery time was ~ 2 minutes for automated delivery as compared to ~ 30 minutes if delivered individually. We have developed a software that can convert the multiple fields of a treatment plan into a single XML file. Preliminary test of file-based delivery using this software demonstrated significant improvements in treatment delivery efficiency without compromising accuracy.

6.1.4. Conclusions

In the context of radiotherapy, there are various presentations where dose delivery is challenging, particularly when the planning treatment volume (PTV) is adjacent to the organ at risk (OAR). In such scenarios, a trade-off exists whereby the dose constraints of the OARs must be considered in tandem with the coverage requirements of the PTV. This limitation was addressed by introducing our gantry static couch motion optimization technique ($1-2^\circ$ increments). In this work, we evaluated the feasibility of executing both step & shoot and continuous couch motion sliding window implementations of this approach.

Delivery of gantry static couch motion optimization technique to introduce dose modulation in brain and ensure coverage of the PTV while respecting the dose constraints of the OARs in brain using is achievable within the TrueBeam® Radiotherapy System developer mode. Based on the results, we further advanced our technique to make it fully automated as discussed in next section of this chapter. This work will enable implementation of GsCMO technique into clinical practice.

6.2. Automated workflow using C# scripting approach in Visual Studio platform

6.2.1. Purpose

Modern treatment planning systems have the capability to design variety of deliverable plans from very simple to complex but the need to extend their ability to design custom beams for research or even clinically still exists. The need of custom beam designing arises due to deficiencies of current treatment planning systems or based on users' experience to add new features to the existing system which can be useful for certain body sites. The desire of improvement also

motivates the users to investigate the other programming applications which can be easily integrated to the planning system and work under the same planning platform so that the information between two applications can be easily exchanged among themselves. Most of the treatment planning system provides an open source tool for customers for beam modeling or plan designing to fit their clinical needs.

There are various programming language tools that fulfil the need such as MATLAB®, Python, or C#. These programs can work independently or can be integrated within the same treatment planning system platform. For custom plan designing, the output of planning system can be sent to the programming language software. The output of which can be easily brought back into planning system and run a final dose calculation or optimization to get a final deliverable plan. Eclipse scripting application programming interface⁶² (ESAPI: plug-in or standalone executable scripts) can be utilized for developing new ideas such as evaluating treatment plans⁶³ based on patient CT-simulation related parameters, treatment machine parameters for safety purpose, or a tool for physics 2nd check.

Based on the previous studies, for e.g., in brain⁶⁴, head and neck^{65,66}, breast⁶⁷⁻⁶⁹, prostate⁷⁰, the automated planning not only reduced the planning time but also generated deliverable plans with comparable or improved plan quality. We have chosen a brain site where the need of custom planning arises. Based on our previous publication⁷¹, the dose delivery utilizing dynamic couch motion at static gantry positions outperformed the standard delivery techniques at static couch positions. This motivated us to investigate it further and designed automated treatment plans for brain site utilizing continuous couch motion.

The aim of this study was to design automated script-based plans utilizing dynamic couch motion. We also introduced the gantry static couch motion (GsCM) technique that utilizes static gantry positions and dynamic couch motion. The dose calculation was performed while gantry remained static and couch moved in a continuous fashion. Currently, all the commercial treatment planning systems cannot generate dynamic couch motion-based treatment plans. This limitation was addressed by our GsCM technique. The plans were simulated in Eclipse (Varian Medical Systems, Palo, Alto, CA) treatment planning system. After simulation, all multiple static conformal fields were merged into a single deliverable file utilizing C#.NET as a programming tool in visual studio application. These plans were delivered and validated on Varian developer mode application. The focus of this study was to design automated plans which can minimize the time and effort put into designing treatment beams manually and explored the option of dose delivery including dynamic couch and static gantry positions for brain treatment site.

6.2.2. Methods

6.2.2.1. Patients selection, imaging and target definition

This retrospective study received institutional review board (IRB) approval to conduct the study for patients who had received radiation therapy to brainstem tumors. All patients received CT-Simulation on SOMATOM (Siemens Medical Solutions, USA) with 512 x 512 pixels at 1.0

mm slice thickness. All beams were placed using a 7mm isotropic margin around the planning target volume (PTV). The organ-at-risks (OAR) included normal brain excluding PTV, brainstem, optic chiasm, and optic nerves.

6.2.2.2. Auto-planning workflow

Multiple plans were created in Eclipse to test the scripting. Current scripting can create multiple fields for any static gantry position. In the past we created all the multiple fields manually which were very cumbersome and took almost 2-8 hours per plan. The treatment plans were designed using 6MV photon in Eclipse treatment planning system (Varian medical systems, Palo Alto, CA), and delivered on Truebeam Linear accelerator using Developer mode application.

6.2.2.3. Automatic script-based treatment planning

The next part of this study was to design automated plans using Eclipse treatment planning system. These simulated plans were delivered on the Varian developer mode application. The Varian developer mode application provides a platform for custom beam delivery also known as research beam platform. The design of GsCM technique was created using two approaches. The first approach was to create a set of treatment plans manually. Each beam was conformed around the PTV (planning target volume). We applied this approach in brain cases. The output of all multiple static fields was converted into a single deliverable type arc. This was a sort of conformal arc type delivery which involved no dose modulation as shown in Figure 6.6. The custom script tested variety of plans designed starting with 3 fields and all the way up to 180 fields. Adding more fields helped to conform the dose around the PTV and spread out the low dose evenly around the PTV area.

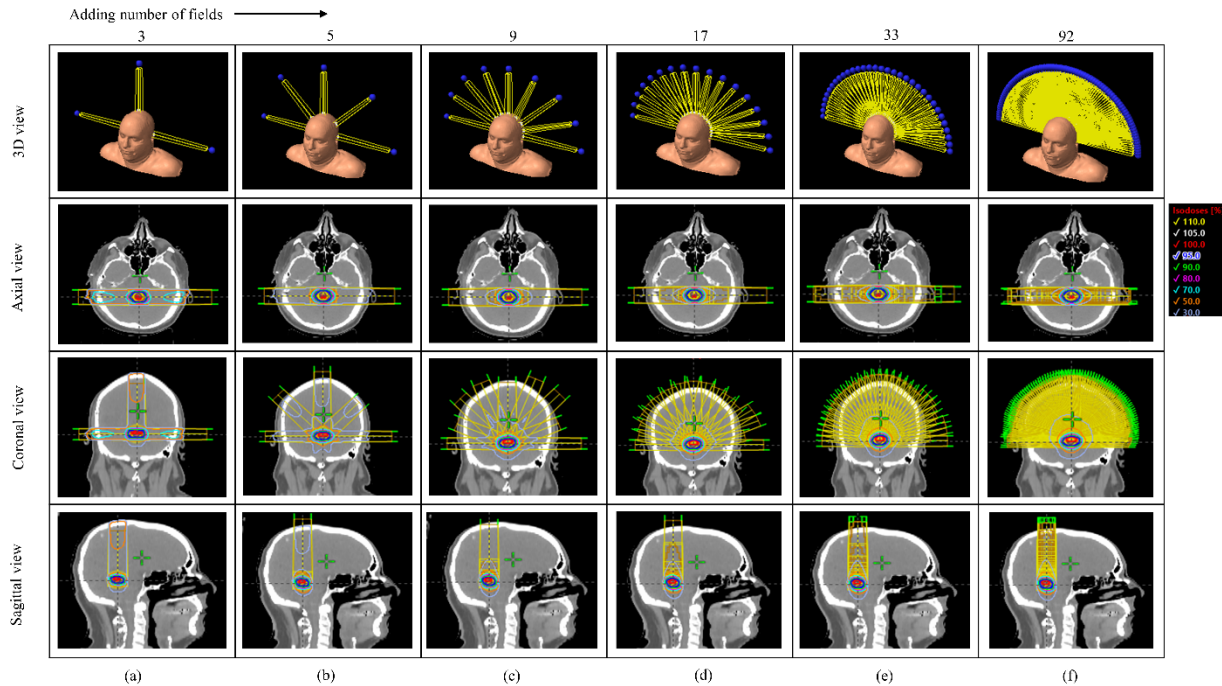


Figure 6. 6. Shows the selection of fields and dose distribution for GsCMO technique

Next, in Eclipse planning system we automated in such a way that it requires a dummy field as a starting point and MLCs. The MLC aperture was shaped using 0.7cm margin around the PTV. For this study we kept the collimator angle zero for all fields. The final script which can add 180 fields in less than 10 seconds is shown in Appendix (4.0). This whole script consists of; (a) an option to select the target (PTV), (b) an option to select the margin around the target, (c) number of beams at two static gantry positions G90 and G270, (d) calculate the final dose, and (e) create an XML to test on the Varian developer mode application.

The final XML file designed based on the script described in Appendix 4.0 is shown in Table 6.5 and 6.6. This provides a continuous couch motion during the dose delivery from couch angle 0 to 90 at G90 and 360-270 at G270 at an interval of one-degree couch angle.

6.2.2.4. Delivery and validation of automated script-based planning

6.2.2.4.1. Design XML scripts to verify the beam parameters

The first part of the validation was to test the ability of scripting to translate the beam parameters adequately from planning system to beam delivery system. This was a precursor of our study that allowed us to understand the scaling scheme used in clinic. Our treatment planning system utilizes “Varian IEC” convention. There are total three different conventions primarily used in the treatment planning and delivery system such as Varian IEC, IEC 61217, and Varian Standard. The scaling convention on delivery console always matches with the convention used in the treatment planning system. In order to test this nomenclature scheme, we designed various treatment plans from a single static field to multiple static fields.

The convention of mechanical parameters is very different in XML what comes out of the treatment plan. We tested both the correct translation of mechanical parameters and ability of scripting to merge multiple static fields into a single deliverable arc. The output of single deliverable arc was in XML format. The Varian developer mode application can easily read these XML files. We calculated mathematically the assigned values of gantry, couch and collimator angles in XML script in order to keep the same values of these mechanical axes on the machine utilizing “Varian IEC” scale. The Table 6.3 describes the relationship of gantry, couch and collimator position in Eclipse, XML script, and on the Truebeam® developer mode application.

Table 6. 3. The scaling convention “Varian IEC” tested for one to one translation of treatment planning parameters to machine delivery. It shows the difference in parameters in XML script and the planning system

Couch position*			Gantry position [‡]			Collimator position [‡]		
Eclipse	XML	LINAC	Eclipse	XML	LINAC	Eclipse	XML	LINAC
0	180	0	0	180	0	0	180	0
20	200	20	20	160	20	20	160	20
45	225	45	45	135	45	45	135	45
70	250	70	70	110	70	70	110	70
90	270	90	90	90	90	90	90	90
-	-	-	120	60	120	120	60	120
-	-	-	150	30	150	150	30	150
-	-	-	175	5	175	175	5	175
-	-	-	180	0	180	-	-	-
-	-	-	185	355	185	185	355	185
-	-	-	210	330	210	210	330	210
-	-	-	240	300	240	240	300	240
270	90	270	270	270	270	270	270	270
300	120	300	300	240	300	300	240	300
330	150	330	330	210	330	330	210	330
359.9	179.9	359.9	359.9	180.1	359.9	359.9	180.1	359.9
0.1	180.1	0.1	0.1	179.9	0.1	0.1	179.9	0.1

* Testing range of gantry angles from 180.1 to 179.9 degrees (In Eclipse, must be $\geq 0.0^0$ and $\leq 359.9^0$), [‡] Testing range of collimator angles from 185 to 175 degrees (In Eclipse, must be $\geq 0.0^0$ and $\leq 175.0^0$ or $\geq 185.0^0$ and $\leq 359.9^0$), [‡] Testing range of couch angles from 270 to 90 degrees (In Eclipse, must be $\geq 0.0^0$ and $\leq 95.0^0$ or $\geq 265.0^0$ and $\leq 359.9^0$).

Once the plan was designed in Eclipse planning system, it was processed through our custom-made C# script which created an XML file. Currently, Varian developer mode has an option too to convert a DICOM plan into an XML file. It works for a single field only. Hence, for multiple static fields, in our case, we created an XML using our own scripting. For an example Table 6.4 shows side by side comparison of our custom script to test all the machine parameters with what we get from the developer mode application.

Table 6. 4. Left column shows script designed by our C# program in Visual Studio and the right-hand side column is from the Truebeam system. Developer mode application has the capability to convert a DICOM plan into an XML but only for single field or a plan consists of single field

<pre><?xml version="1.0" encoding="UTF-8"?> <SetBeam> <Id>1</Id> <MLCModel>NDS120HD</MLCModel> <Accs /> <ControlPoints> <Cp> <Energy>6x</Energy> <Mu>0</Mu> <DRate>600</DRate> <GantryRtn>180</GantryRtn> <CollRtn>180</CollRtn> <CouchRtn>180</CouchRtn> <Y1>5</Y1> <Y2>5</Y2> <X1>5</X1> <X2>5</X2> <Mlc> <ID>1</ID> 10 0 0 0 0 0 0 0 0 0 0 0 10 10 10 5 0 0 0 0 0 0 0 0 0 0 0 0 <A>0 0 0 0 0 0 0 0 0 0 0 0 5 0 0 0 0 0 0 0 0 0 0 0 </Mlc> </Cp> </ControlPoints> </SetBeam></pre>	<pre><?xml version="1.0" encoding="utf-8"?> <SetBeam> <Id>2055609974</Id> <TreatmentMode><![CDATA[FTM]]></TreatmentMod e> <MLCModel><![CDATA[NDS120HD]]></MLCModel> <Accs /> <ControlPoints> <Cp> <TreatProgressEvent /> <SubBeam> <Seq>0</Seq> <SubbeamGUID><![CDATA[<BeamIdentifier><PlanInst anceUID>1.2.246.352.71.5.895657984438.355035.202 00202153238</PlanInstanceUID><BeamNumber>1</B eamNumber></BeamIdentifier>]]></SubbeamGUID> <Name><![CDATA[Field 1]]></Name> </SubBeam> <Energy>6x</Energy> <Mu>0</Mu> <DRate>600</DRate> <GantryRtn>180</GantryRtn> <CollRtn>180</CollRtn> <CouchRtn>180</CouchRtn> <CouchPit>0</CouchPit> <CouchRol>0</CouchRol> <Y1>5</Y1> <Y2>5</Y2> <X1>5</X1> <X2>5</X2> <Mlc> <ID>1</ID> 0 0 0 0 0 0 0 0 0 0 0 0 5 0 0 0 0 0 0 0 0 0 0 <A>0 0 0 0 0 0 0 0 0 0 0 0 5 0 0 0 0 0 0 0 0 0 0 0 </Mlc> </Cp> <Cp> <TreatProgressEvent /> <Mu>100</Mu> </Cp> </ControlPoints> </SetBeam></pre>
---	---

6.2.2.4.2. Gamma analysis

The validation of couch-based dose delivery was conducted using the ion chamber array scanned in the vertical direction to avoid any side beam entrance. The 2D gamma analysis was conducted using the 3% dose difference (dd%), 3mm distance-to-agreement (DTA), and 2D $\gamma \leq 1$. This was to verify the dose delivery accuracy as shown in Figure 6.7 for a single patient plans as an example.

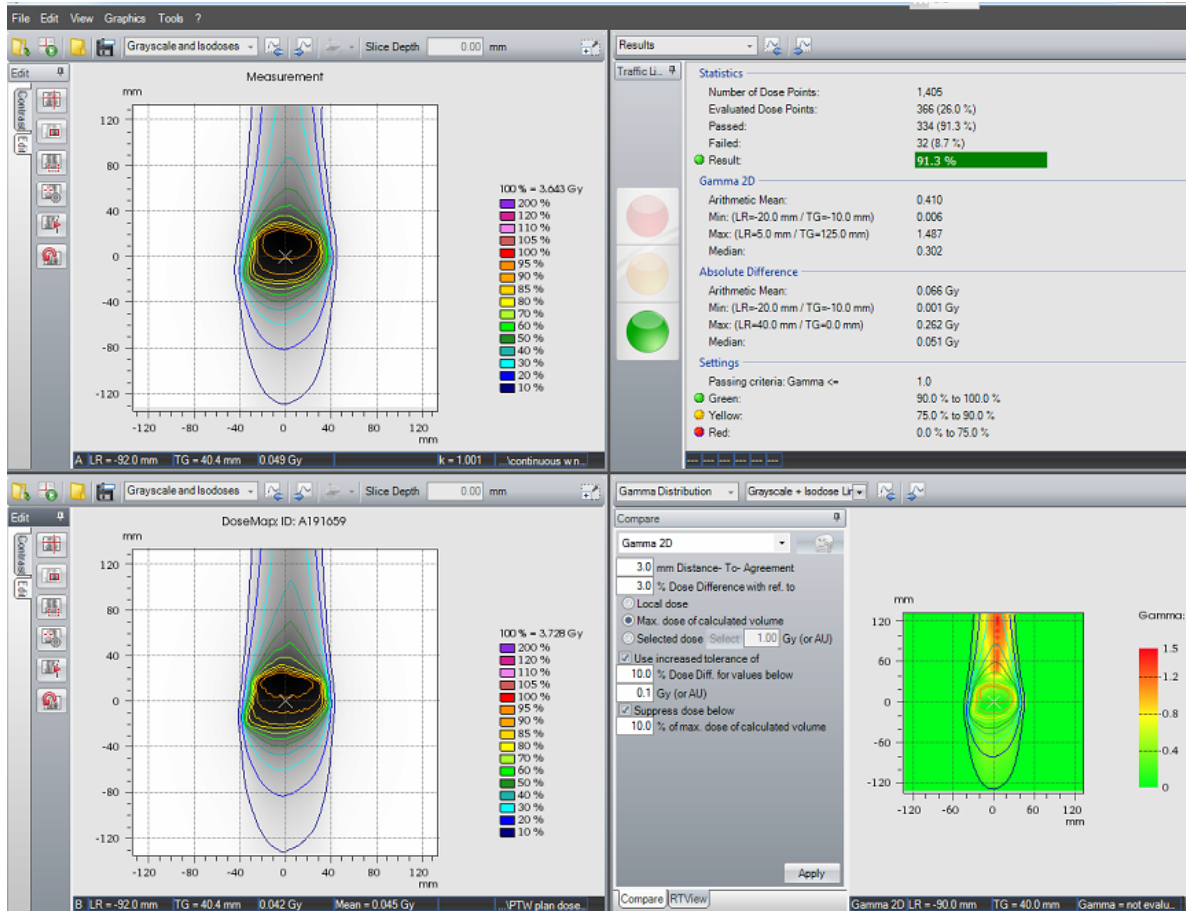


Figure 6. 7. Here is an example of dose verification onto a PTW ion chamber array comparing the XML file vs the measure dose. The XML measured dose for a continuous couch motion is shown in the top left and bottom left is the same plan designed in Eclipse. Overall, the passing rate satisfies our criteria of accepting the IMRT QA. As noticed the gamma fails at the top portion of the gamma plot which is due to the beam entrance at the side of the detector. The detector cannot process this low dose and causing the passing rate to degrade a little. This is just due to the construction of an ion chamber array and nature of beam entrance.

Before converting the multiple fields in a continuous arc, we merged all the static conformal fields. The delivery was more like a step and shoot nature because the beam was on hold in between the couch position as shown in Table 6.5. Even though the couch motion was automated, but it was not continuous. The dose delivery for this step and shoot was close to 5

0.002 0.002 0.002 0.002 1.76 1.94 1.996 2.05 2.18 2.298 2.372 2.36 2.375 2.56 2.664 2.595 2.41 2.18 1.49
0.9399999 0.8099999 0.5 -0.2 0.002 0.002 0.002 0.002 0.002 0.002 0.002 0.002 0.002 0.002 0.002 0.002 0.002 0.002
0.002 0.002 0.002 0.002 0.002 0.002 0.002
<A>-0.002 -0.002 -0.002 -0.002 -0.002 -0.002 -0.002 -0.002 -0.002 -0.002 -0.002 -0.002 -0.002 -0.002 -0.002 -0.002
-0.002 -0.002 -0.002 -0.002 -0.002 -0.002 0.78 1.03 1.235 1.39 1.72 2.02 2.32 2.5 2.53 2.395 2.34 2.51 2.66 2.653
2.527 2.5 2.39 2.08 1.2 -0.002 -0.002 -0.002 -0.002 -0.002 -0.002 -0.002 -0.002 -0.002 -0.002 -0.002 -0.002
-0.002 -0.002 -0.002 -0.002 -0.002 -0.002 -0.002
</Mlc>
</Cp>
<Cp>
<Energy>6x</Energy>
<Mu>3.83212117955808</Mu>
<DRate>600</DRate>
<GantryRtn>90</GantryRtn>
<CollRtn>180</CollRtn>
<CouchRtn>181</CouchRtn>
<Y1>2.5</Y1>
<Y2>2.4</Y2>
<X1>2.7</X1>
<X2>2.7</X2>
<Mlc>
<ID>1</ID>
0.003 0.003 0.003 0.003 0.003 0.003 0.003 0.003 0.003 0.003 0.003 0.003 0.003 0.003 0.003 0.003 0.003 0.003
0.003 0.003 0.003 0.003 1.76 1.94 1.997 2.06 2.205 2.306 2.38 2.36 2.4 2.59 2.666 2.565 2.39 2.14 1.37 0.9399999
0.8099999 0.48 -0.44 0.003 0.003 0.003 0.003 0.003 0.003 0.003 0.003 0.003 0.003 0.003 0.003 0.003 0.003 0.003
0.003 0.003 0.003 0.003 0.003
<A>-0.003 -0.003 -0.003 -0.003 -0.003 -0.003 -0.003 -0.003 -0.003 -0.003 -0.003 -0.003 -0.003 -0.003 -0.003 -0.003
-0.003 -0.003 -0.003 -0.003 -0.003 -0.003 0.78 1.03 1.235 1.39 1.72 2.03 2.32 2.5 2.53 2.395 2.34 2.51 2.66 2.653
2.527 2.5 2.39 2.08 1.16 -0.003 -0.003 -0.003 -0.003 -0.003 -0.003 -0.003 -0.003 -0.003 -0.003 -0.003 -0.003
-0.003 -0.003 -0.003 -0.003 -0.003 -0.003 -0.003
</Mlc>
</Cp>
<Cp>
<Energy>6x</Energy>
<Mu>7.66873393922665</Mu>
<DRate>600</DRate>
<GantryRtn>90</GantryRtn>
<CollRtn>180</CollRtn>
<CouchRtn>181</CouchRtn>
<Y1>2.5</Y1>
<Y2>2.4</Y2>
<X1>2.7</X1>
<X2>2.7</X2>
<Mlc>
<ID>1</ID>
0.003 0.003 0.003 0.003 0.003 0.003 0.003 0.003 0.003 0.003 0.003 0.003 0.003 0.003 0.003 0.003 0.003 0.003
0.003 0.003 0.003 0.003 1.76 1.94 1.997 2.06 2.205 2.306 2.38 2.36 2.4 2.59 2.666 2.565 2.39 2.14 1.37 0.9399999
0.8099999 0.48 -0.44 0.003 0.003 0.003 0.003 0.003 0.003 0.003 0.003 0.003 0.003 0.003 0.003 0.003 0.003 0.003
0.003 0.003 0.003 0.003 0.003
<A>-0.003 -0.003 -0.003 -0.003 -0.003 -0.003 -0.003 -0.003 -0.003 -0.003 -0.003 -0.003 -0.003 -0.003 -0.003 -0.003
-0.003 -0.003 -0.003 -0.003 -0.003 -0.003 0.78 1.03 1.235 1.39 1.72 2.03 2.32 2.5 2.53 2.395 2.34 2.51 2.66 2.653
2.527 2.5 2.39 2.08 1.16 -0.003 -0.003 -0.003 -0.003 -0.003 -0.003 -0.003 -0.003 -0.003 -0.003 -0.003 -0.003
-0.003 -0.003 -0.003 -0.003 -0.003 -0.003 -0.003


```
</SetBeam>
```

Table 6. 6. Example of continuous delivery. This XML file does not have any dummy/duplicate controls points which have been deleted by utilizing out custom script. As we see here, there is a smooth transition from control point 1 to 2 to 3, and so on.

```
<?xml version="1.0" encoding="UTF-8"?>
<SetBeam>
  <Id>1</Id>
  <MLCModel>NDS120HD</MLCModel>
  <Accs />
  <ControlPoints>
    <Cp>
      <Energy>6x</Energy>
      <Mu>0</Mu>
      <DRate>600</DRate>
      <GantryRtn>90</GantryRtn>
      <CollRtn>180</CollRtn>
      <CouchRtn>180</CouchRtn>
      <Y1>2.5</Y1>
      <Y2>2.4</Y2>
      <X1>2.7</X1>
      <X2>2.7</X2>
    <Mlc>
      <ID>1</ID>
      <B>0 0 0 0 0 0 0 0 0 0 0 0 0 0 0 0 0 0 0 0 0 0 0 0 0 0 0 0 0 0 0 0 1.75999999046326 1.939999993801117 1.99599993228912
2.04999995231628 2.17999982833862 2.2979998588562 2.37199997901917 2.3600001335144 2.375
2.55999994277954 2.66400003433228 2.59499979019165 2.41000008583069 2.179999982833862
1.49000000953674 0.939999938011169 0.809999942779541 0.5 -0.200000002980232 0 0 0 0 0 0 0 0 0 0 0 0 0 0 0
0 0 0 0 0 0 /<B>
      <A>0 0 0 0 0 0 0 0 0 0 0 0 0 0 0 0 0 0 0 0 0 0 0 0 0 0 0 0 0 0.779999971389771 1.02999997138977 1.23499989509583
1.38999998569489 1.71999990940094 2.01999998092651 2.3199999332428 2.5 2.52999997138977
2.39499998092651 2.33999991416931 2.50999999046326 2.65999984741211 2.65299987792969
2.52699995040894 2.5 2.3899998664856 2.07999992370605 1.20000004768372 0 0 0 0 0 0 0 0 0 0 0 0 0 0 0 0 0 0 0
0 0 0 /<A>
    </Mlc>
  </Cp>
  <Cp>
    <Energy>6x</Energy>
    <Mu>3.83212117955808</Mu>
    <DRate>600</DRate>
    <GantryRtn>90</GantryRtn>
    <CollRtn>180</CollRtn>
    <CouchRtn>180</CouchRtn>
    <Y1>2.5</Y1>
    <Y2>2.4</Y2>
    <X1>2.7</X1>
    <X2>2.7</X2>
  <Mlc>
    <ID>1</ID>
    <B>0 0 0 0 0 0 0 0 0 0 0 0 0 0 0 0 0 0 0 0 0 0 0 0 0 0 0 0 0 0 0 0 1.75999999046326 1.939999993801117 1.99599993228912
```

```

2.04999995231628 2.17999982833862 2.2979998588562 2.37199997901917 2.3600001335144 2.375
2.55999994277954 2.66400003433228 2.59499979019165 2.41000008583069 2.17999982833862
1.49000000953674 0.939999938011169 0.809999942779541 0.5 -0.200000002980232 0 0 0 0 0 0 0 0 0 0
0 0 0 0 0 0 </B>
<A>0 0 0 0 0 0 0 0 0 0 0 0 0 0 0 0 0 0 0 0 0 0 0.779999971389771 1.02999997138977 1.23499989509583
1.38999998569489 1.71999990940094 2.01999998092651 2.3199999332428 2.5 2.52999997138977
2.39499998092651 2.33999991416931 2.50999999046326 2.65999984741211 2.65299987792969
2.52699995040894 2.5 2.3899998664856 2.07999992370605 1.20000004768372 0 0 0 0 0 0 0 0 0 0 0 0 0
0 0 0 </A>
</Mlc>
</Cp>
<Cp>
<Energy>6x</Energy>
<Mu>7.66873393922665</Mu>
<DRate>600</DRate>
<GantryRtn>90</GantryRtn>
<CollRtn>180</CollRtn>
<CouchRtn>181</CouchRtn>
<Y1>2.5</Y1>
<Y2>2.4</Y2>
<X1>2.7</X1>
<X2>2.7</X2>
<Mlc>
<ID>1</ID>
<B>0 0 0 0 0 0 0 0 0 0 0 0 0 0 0 0 0 0 0 0 0 0 0 1.75999999046326 1.93999993801117 1.99699997901917
2.05999994277954 2.20499992370605 2.30599999427795 2.37999987602234 2.3600001335144
2.40000009536743 2.58999991416931 2.66599988937378 2.56500005722046 2.3899998664856
2.1399998664856 1.37000000476837 0.939999938011169 0.809999942779541 0.479999959468842 -
0.439999997615814 0 0 0 0 0 0 0 0 0 0 0 0 0 0 0 0 0 0 0 0 0 </B>
<A>0 0 0 0 0 0 0 0 0 0 0 0 0 0 0 0 0 0 0 0 0 0 0 0.779999971389771 1.02999997138977 1.23499989509583
1.38999998569489 1.71999990940094 2.02999997138977 2.3199999332428 2.5 2.52999997138977
2.39499998092651 2.33999991416931 2.50999999046326 2.65999984741211 2.65299987792969
2.52699995040894 2.5 2.3899998664856 2.07999992370605 1.1599999666214 0 0 0 0 0 0 0 0 0 0 0 0 0 0 0
0 0 </A>
</Mlc>
</Cp>

```

-----continue with the next control points and ends with the last control point as follows----

```

<Cp>
<Energy>6x</Energy>
<Mu>732.574529696145</Mu>
<DRate>600</DRate>
<GantryRtn>270</GantryRtn>
<CollRtn>180</CollRtn>
<CouchRtn>90</CouchRtn>
<Y1>3.8</Y1>
<Y2>3.8</Y2>
<X1>2.8</X1>
<X2>2.7</X2>
<Mlc>
<ID>1</ID>

```

```

<B>0 0 0 0 0 0 0 0 0 0 0 0 0 0 0 0 0 -0.339999973773956 0.389999985694885 0.959999918937683
1.26999998092651 1.51999998092651 1.72999998998642 1.88499999046326 2.03999996185303
2.17499995231628 2.30999994277954 2.42499995231628 2.502999978256226 2.57299995422363
2.66999983787537 2.71199989318848 2.70499992370605 2.69799995422363 2.69000005722046
2.65799999237061 2.59999990463257 2.5 2.375 2.23000001907349 2.07999992370605 1.86999988555908
1.63999998569489 1.37999987602234 1 0.109999999403954 -0.739999949932098 -0.739999949932098 0 0 0
0 0 0 0 0 0 0 0 0 0 </B>
<A>0 0 0 0 0 0 0 0 0 0 0 0 0 0 0 0 1.1800000667572 1.81000006198883 2.11999988555908 2.28999996185303
2.43300008773804 2.48399996757507 2.47399997711182 2.41999983787537 2.26999998092651
2.05999994277954 1.84599995613098 1.8309999704361 1.8199999332428 1.85800004005432
1.90799999237061 1.9559999704361 1.96000003814697 1.96199989318848 2.04499983787537
2.09999990463257 2.20000004768372 2.3600001335144 2.50499987602234 2.5939998626709
2.62599992752075 2.55299997329712 2.44000005722046 2.28500008583069 2.01999998092651
1.1800000667572 1.1800000667572 0 0 0 0 0 0 0 0 0 0 0 0 0 </A>
</Mlc>
</Cp>
</ControlPoints>
</SetBeam>

```

The Figure 6.8 shows the comparison of step and shoot delivery verses the continuous couch motion comparison. Overall, it was an adequate comparison among both dose deliveries. These results validate that the final continuous delivery is exactly the same as step and shoot delivery in terms of dose comparison but much faster and ideal treatment approach for patient on the table.

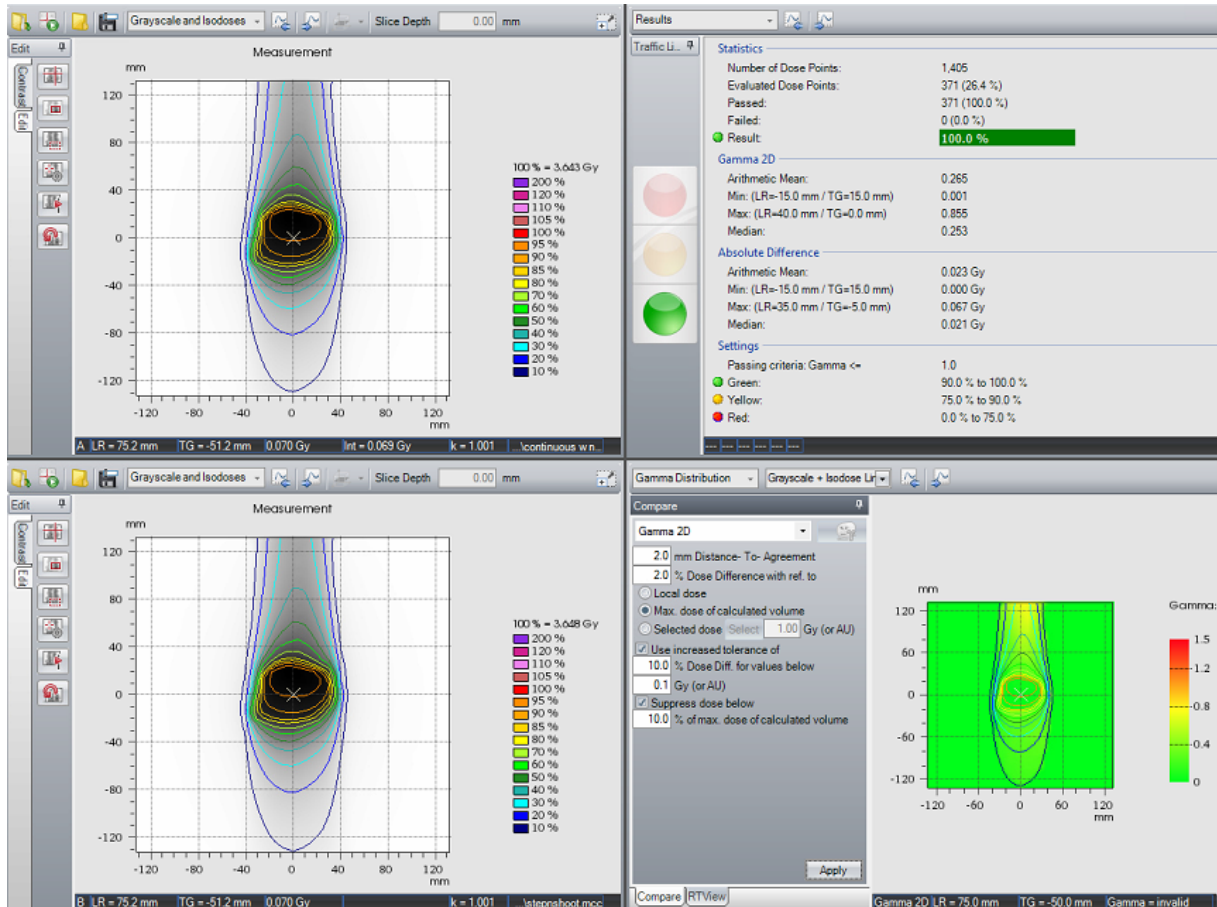


Figure 6. 8. Dose delivery comparison of continuous (upper left) versus the step and shoot (lower left) dose delivery. Both dose distribution satisfies the passing criteria of 2mm/2% with a passing rate of 100%

6.2.2.4.3. Trajectory log file analysis

Due to the dose delivery at dynamic couch motion, it was important to test the couch parameters while beam was ON. Trajectory log files were saved to analyze the couch positions. The accuracy of the gantry angle, collimator angles, X and Y jaws, and MLCs have been very well defined and do not raise any concern. Therefore, our focus was to check the couch parameters since those are the one where dose delivery is mainly dependent upon. From the trajectory log files, we filtered out all the other mechanical parameters but couch. We analyzed the couch positions with respect to gantry, MLCs, and MUs. The analysis also correlated the couch rotation positions from planning system and delivery system with monitor units (MU).

6.2.3. Results

The preliminary step testing the XML scripting verified that all the beam related parameters get correctly translated from planning system to delivery system. The successful conversion was tested for “Varian IEC” scale which is the scaling system used in our institution. The results were shown in Table 6.3.

The comparison of continuous XML plans with treatment plans resulted 2D- γ passing rate of $94\pm 2.3\%$ using 3mm DTA and 3% DD. A good agreement of 2D- γ passing rate of $\geq 99\%$ using 2mm DTA and 2% DD was found between continuous vs step and shot XML script plans.

In comparison to clinical plans, the delivery time was reduced to ~ 2 minutes and accuracy was exactly same as clinical plans.

Trajectory log files showed that the relationship between planned MUs, gantry, and couch positions with delivery was adequate as shown in Figure 6.9. Based on the relationship it is clear how MUs are delivered at each planned gantry and couch positions.

Based on the Figure 6.10., it is clear how the couch positions are represented in discrete lines also describes no beam ON while the couch is in transit. On the right-hand side column, the continuous couch motion is presented which clearly shows that couch was in motion during the beam in ON state. For step and shoot, the couch rotational error was under 0.1 degrees for all five plans. For all continuous plans, the error shown is due to the variable dose rate which causes the couch to move slow at some selected (shown as spikes) positions.

Also, for each leaf position, root mean square error (mm) is shown for step and shoot delivery (left hand side column) and for continuous delivery (right hand side column) as shown in Figure 6.11. For step and shoot delivery, the maximum positioning error was 0.005mm, and 0.006mm for continuous delivery. This error is really small for such beams with no dose modulation.

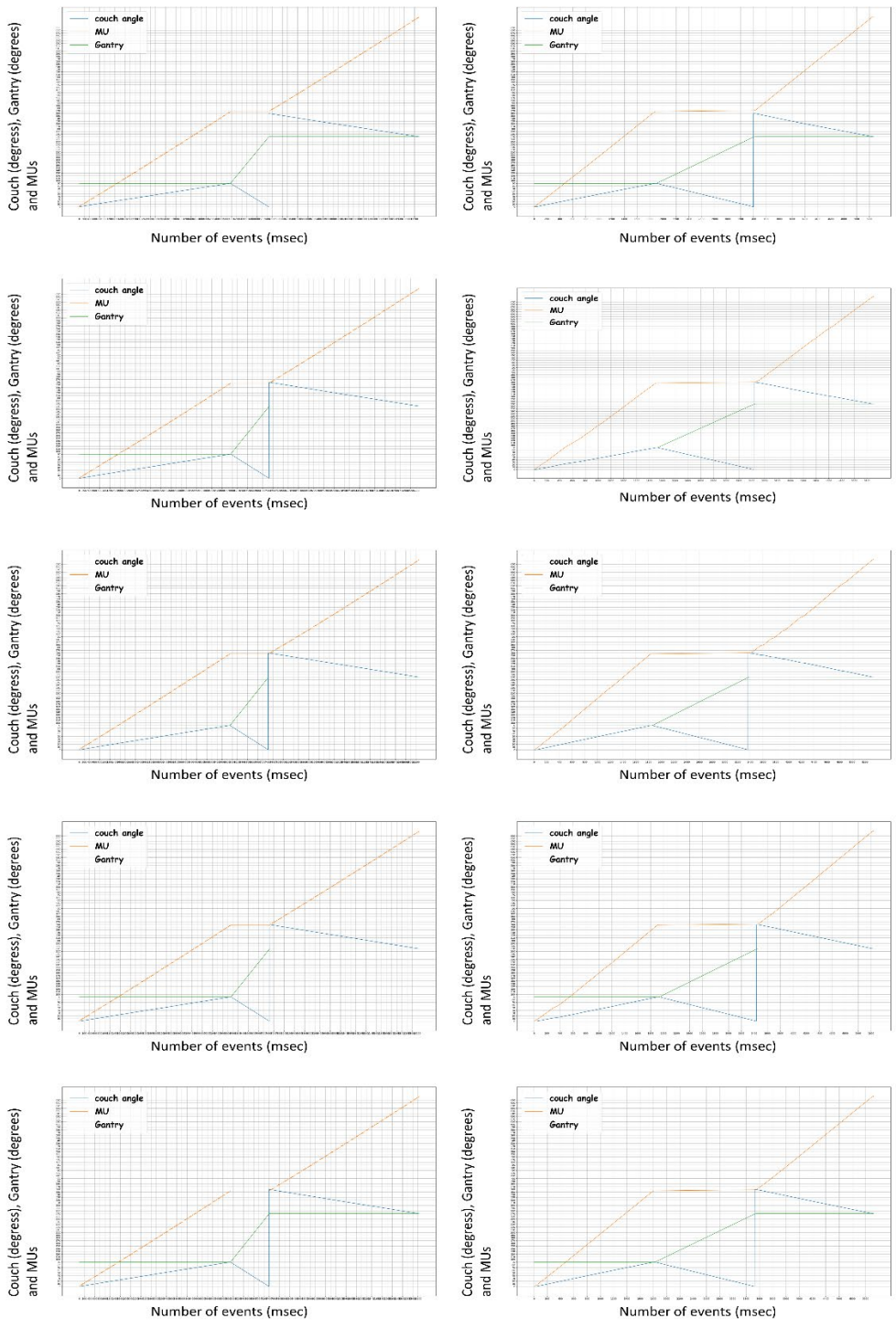


Figure 6. 9. Relationship of couch and gantry position is shown and correlated with the Mus delivered. Based on the graphs for 5 test plans (step and shoot on the left column and continuous delivery on the right-hand side column), it is clear how dose was delivered at each planned gantry and couch positions. On X-axis, number of recorded events are shown which also correlates to total time took to deliver the plan.

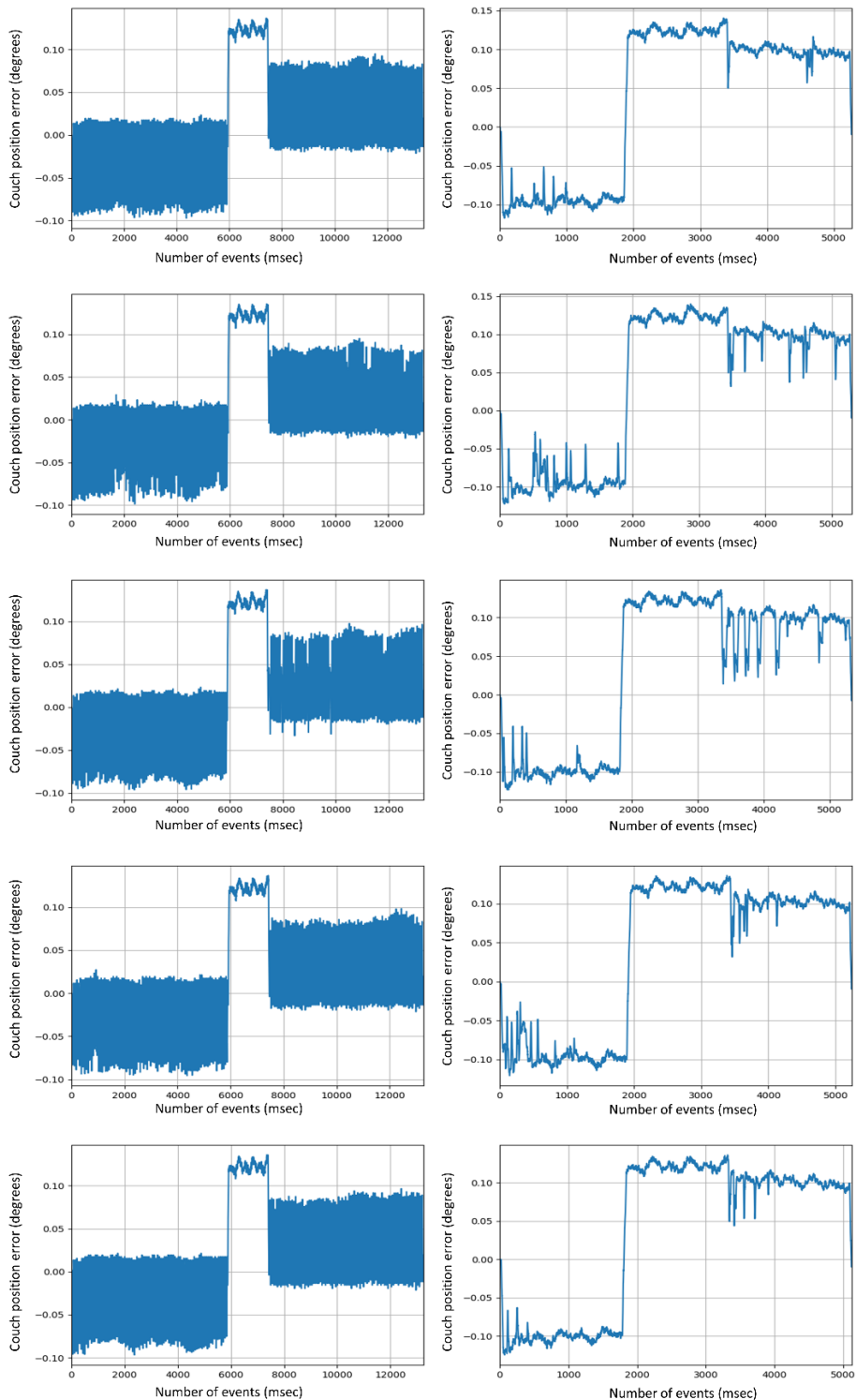


Figure 6. 10. On left hand column, step and shoot delivery is shown. It is clear how the couch positions are represented in discrete lines also describes no beam ON while the couch is in transit. On the right-hand side column, the continues couch motion is presented which clears shows that couch was in motion during the beam in ON state.

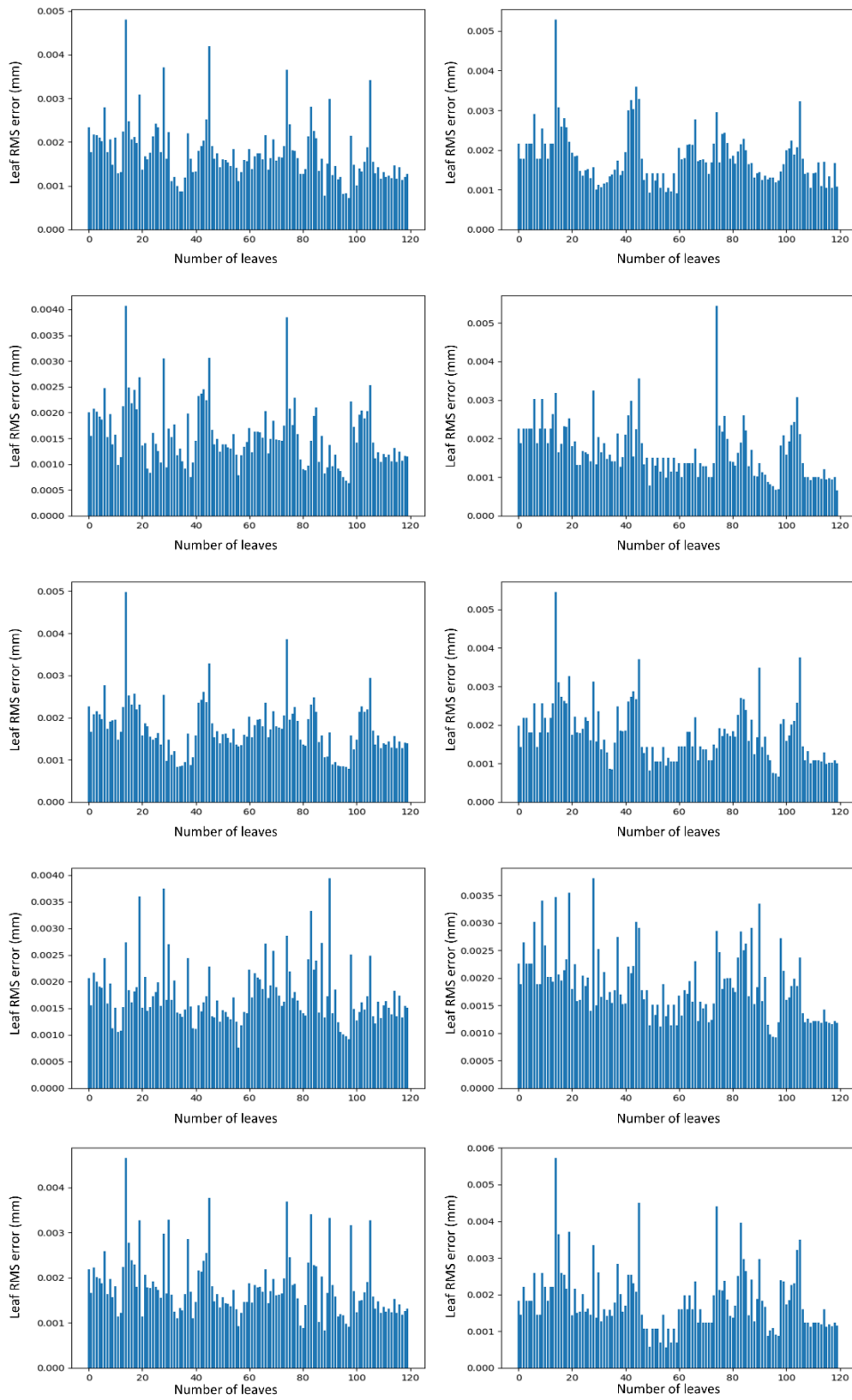


Figure 6. 11. For each individual leaf position, root mean square error (mm) is shown for step and shoot delivery (left hand side column) and for continuous delivery (right hand side column)

6.2.4. Discussion

There have been so many advancements in the treatment planning system since 2000. The user's interaction and ability to learn has fortified the need to develop new radiation dose delivery techniques. Hence, the ability to improve the exiting technology has brought some interest in researchers who always seek for improvement and developing new techniques. The need of improvement, leeway from vendors in terms of providing the open access to their developing tools, have attracted the users more. The interface that is compatible with the planning system for example, C# programming with .NET windows platform has made it easier for users to work on scripting. These scripts can be used to develop some useful programs which help to improve their current methods of checking plans, speeding up the treatment planning process with automation, more robust methods of checking the plan quality in terms of DVH, dose matrices, intelligent way to run optimization, and helping the radiation oncology community to develop new ideas. Our study explored to automate the treatment planning process and motivated us to take advantage of technology which is accessible to us.

Varian offers application programming interface (API) and other developer tools for customers for research purpose to design new dose delivery techniques. Eclipse scripting API (ESAPI) is built into the eclipse treatment planning system which allows developers to create C#.NET scripts, DLLs, and other compatible programs that can read the DICOM (digital imaging and communication in medicine) patient data in the database. Eclipse V15.5 and above allows the users to write scripting and script approval. C# class library is compatible with .NET windows program and fully integrated with Eclipse treatment planning system makes it more suitable for researchers to design custom scripting for their clinical needs. There is so much to offer for developers which require careful monitoring by the site treatment planning administrator (Physicist) and departmental IT.

In this study, the validation of plan quality verified the correct dose delivery at various couch positions in terms of gamma analysis. The accuracy of couch positioning was tested with trajectory log files. We filtered out all the unnecessarily parameters but couch because the accuracy of gantry, collimator, and MLCs have been defined very well and not a question. The couch accuracy was tested by analyzing the log files and RMSE was found under 0.006mm for all kinds of plans.

With all the advanced tools in hand, the need to QA the automated treatment planning still arises which can reduce the potential risks. As discussed by Kisling et.al.⁷², three key factors to include in the QA process in addition to user training on the potential failure modes are (a) independent verification of automated plans, (b) comparison of parameters of automated plans with clinical plans, and (c) comprehensive manual plans checks by physicists and physicians can play an integral role to develop failure mode and effects analysis (FMEA). Our study is one of the many which focused on the development of new treatment planning techniques for radiation therapy. This work focused on creating automated conformal arc types of plans for GsCM

technique. Editing dose fluence and VMAT type dose delivery will remain the focus for future study.

6.2.5. Conclusion

A treatment planning novel approach has been developed in Eclipse to design and automate dynamic couch motion-based treatment plans for cranial site. The results of our study indicated that the automated custom planning including the couch motion is feasible and comparable with clinical planning in terms of dosimetric quality.

Chapter 7: Summary, conclusions, and future work

This dissertation developed a novel radiation treatment technique based on dynamic couch motion radiation dose delivery where couch moves in a continuous fashion while gantry remains stationary. We looked into the inherent deficiencies of current treatment planning systems and worked on designing new methods that can be implemented to take advantage of the capability of delivering the radiation dose in a safer way to avoid the normal structures. Our investigations studied the inclusion of couch during dose calculation, optimization and delivery. Chapter 3 described a feasibility study conducted onto a head and neck anthropomorphic phantom and results of this study formed a baseline of the remaining research in this dissertation. Chapter 4 applied the GsCMO technique in breast tumor patients who were diagnosed with early stage of breast cancer. The GsCMO technique outperformed in comparison with 3D-CRT, WPS and WPD techniques. In addition, we further applied the same approach in partial breast irradiation (PBI) and found out that GsCMO technique can be utilized for APBI treatments. Based on the results we found out that GsCMO provided no exit dose to ipsilateral lung and heart, and a preferred choice for PBI applications. Chapter 5 discussed how integration of couch effects the overall dose delivery. Patient motion during dose delivery is an integral component of any couch motion technique and any additional uncertainty introduced must be accounted for. This chapter focused on determining these uncertainties based on the validation of our GsCMO technique. Further, we evaluated the accuracy of 6DoF couch. Chapter 6 comprised the development of a method to design and test various plans, by introducing simpler planning techniques and evolving with increasing complexity to an automated GsCMO technique. This chapter discussed in detail on the process of simulation, treatment plan design and XML file-based dose delivery. This chapter also focused on how to automate the treatment plan design workflow discussed in the previous chapters, and a robust solution was presented which saves time and effort. The results showed that automated treatment plans were comparable with manually created clinical plans. The knowledge gained from prior chapters allowed interpretation of the results and can guide future utilization of radiation dose delivery in inclusion of the couch motion.

The GsCMO technique addressed a crucial deficiency in the delivery of radiation to many hard to treat tumors. For example, a tumor situated between the optic chiasm and brainstem would typically be at risk of underdosage due to the proximity to the OARs using conventional co-planar techniques. However, implementation of continuous couch motion provided sharp fall-off of dose to target anteriorly and posteriorly while maintaining the dose coverage to the PTV. Further, this approach is not limited to the brain and applied to breast to treat lumpectomy cavity. Introduction of this technique clinically will ultimately result in improved PTV coverage and/or reduced dose to the OARs.

In this dissertation we developed an automated script-based implementation of 3D, step & shoot, sliding window, continuous coronal arc and gantry static couch optimized radiation therapy using Varian Truebeam developer mode. Implementation within the Varian developer mode is crucial as current clinical treatment delivery paradigms do not enable continuous couch motion-based treatment design and dose delivery.

Based on our approach discussed in Chapter 6, automation of treatment planning saves tremendous amount of time and results were same as creating the treatment plans manually which was hours of work. We addressed how motion of treatment couch can impact the overall dose delivery. Treatment couch plays an important role in our technique. The adjustment of couch speed at start and stop positions was critical. Immobilization is must for our technique because of moving couch, and it is also safe to keep the patient steady on the couch throughout the treatment.

Future work will use the methods and results shown in this dissertation to implement the GsCMO technique in clinic in patient treatment. The feasibility approach on anthropomorphic phantom, retrospective study on brain and breast patient lay down the path of its utilization for those patients where our technique can outperform the exiting techniques of radiation treatment planning and dose delivery. Examples of such initiation, its applications in brain and breast, and its validity was thoroughly described by Gill *et al*^{71,73}. Our GsCMO technique push the limits of current treatment planning and we anticipate that its capabilities will be further developed by our group.

References

1. <https://www.cancer.gov>. Accessed.
2. Vogelstein B, Kinzler KW. Cancer genes and the pathways they control. *Nat Med*. 2004;10(8):789-799.
3. Witsch E, Sela M, Yarden Y. Roles for growth factors in cancer progression. *Physiology (Bethesda)*. 2010;25(2):85-101.
4. Waldman T, Zhang Y, Dillehay L, et al. Cell-cycle arrest versus cell death in cancer therapy. *Nat Med*. 1997;3(9):1034-1036.
5. Claessens AKM, Ibragimova KIE, Geurts SME, Bos M, Erdkamp FLG, Tjan-Heijnen VCG. The role of chemotherapy in treatment of advanced breast cancer: an overview for clinical practice. *Crit Rev Oncol Hematol*. 2020;153:102988.
6. Tao S, Zhao Z, Zhang X, et al. The role of macrophages during breast cancer development and response to chemotherapy. *Clin Transl Oncol*. 2020.
7. Hussain SA, Palmer DH, Stevens A, Spooner D, Poole CJ, Rea DW. Role of chemotherapy in breast cancer. *Expert Rev Anticancer Ther*. 2005;5(6):1095-1110.
8. Savas P, Loi S. Expanding the Role for Immunotherapy in Triple-Negative Breast Cancer. *Cancer Cell*. 2020;37(5):623-624.
9. Keenan TE, Tolaney SM. Role of Immunotherapy in Triple-Negative Breast Cancer. *J Natl Compr Canc Netw*. 2020;18(4):479-489.
10. Bertucci F, Goncalves A. Immunotherapy in Breast Cancer: the Emerging Role of PD-1 and PD-L1. *Curr Oncol Rep*. 2017;19(10):64.
11. Israel L. The role of nonspecific immunotherapy in the treatment of breast cancer. *Recent Results Cancer Res*. 1976(57):189-195.
12. Xu W, Huang M, Guo J, et al. The Role of CHK1 Varies with the Status of Oestrogen-receptor and Progesterone-receptor in the Targeted Therapy for Breast Cancer. *Int J Biol Sci*. 2020;16(8):1388-1402.

13. Barinoff J, Schmidt M, Schneeweiss A, et al. Primary metastatic breast cancer in the era of targeted therapy - Prognostic impact and the role of breast tumour surgery. *Eur J Cancer*. 2017;83:116-124.
14. Ibrahim EM, Kazkaz GA, Al-Mansour MM, Al-Foheidi ME. The predictive and prognostic role of phosphatase phosphoinositol-3 (PI3) kinase (PIK3CA) mutation in HER2-positive breast cancer receiving HER2-targeted therapy: a meta-analysis. *Breast Cancer Res Treat*. 2015;152(3):463-476.
15. Lee-Hoeflich ST, Crocker L, Yao E, et al. A central role for HER3 in HER2-amplified breast cancer: implications for targeted therapy. *Cancer Res*. 2008;68(14):5878-5887.
16. Sharifzadeh Y, Slade AN, Weiss E, Sutton AL, Sheppard VB. Attitudes and Perceptions Towards Radiation Therapy in Breast Cancer Patients: The Role of a Multidisciplinary Care Team. *J Cancer Educ*. 2020.
17. Tanguturi S, Warren LEG. The Current and Evolving Role of Radiation Therapy for Central Nervous System Metastases from Breast Cancer. *Curr Oncol Rep*. 2019;21(6):50.
18. Fletcher GH, Montague ED, White EC. Role of radiation therapy in the primary management of breast cancer. *Prog Clin Cancer*. 1970;4:242-256.
19. de Mendoza AH, Cabling M, Dilawari A, et al. Providers' Perspectives on Adherence to Hormonal Therapy in Breast Cancer Survivors. Is there a Role for the Digital Health Feedback System? *Health Technol (Berl)*. 2019;9(2):175-184.
20. Abrial C, Durando X, Mouret-Reynier MA, et al. Role of neo-adjuvant hormonal therapy in the treatment of breast cancer: a review of clinical trials. *Int J Gen Med*. 2009;2:129-140.
21. Noguchi M, Miwa K. The Role of Hormonal Therapy in Breast Cancer. *Breast Cancer*. 1998;5(1):33-46.
22. <https://www.varian.com/oncology/products/treatment-delivery/truebeam-radiotherapy-system>. Accessed.
23. Otto K. Volumetric modulated arc therapy: IMRT in a single gantry arc. *Med Phys*. 2008;35(1):310-317.
24. Yang Y, Zhang P, Happersett L, et al. Choreographing couch and collimator in volumetric modulated arc therapy. *Int J Radiat Oncol Biol Phys*. 2011;80(4):1238-1247.
25. MacDonald RL, Thomas CG. Dynamic trajectory-based couch motion for improvement of radiation therapy trajectories in cranial SRT. *Med Phys*. 2015;42(5):2317-2325.
26. Smyth G, Evans PM, Bamber JC, et al. Non-coplanar trajectories to improve organ at risk sparing in volumetric modulated arc therapy for primary brain tumors. *Radiother Oncol*. 2016;121(1):124-131.

27. Smyth G, Bamber JC, Evans PM, Bedford JL. Trajectory optimization for dynamic couch rotation during volumetric modulated arc radiotherapy. *Phys Med Biol.* 2013;58(22):8163-8177.
28. Dong P, Lee P, Ruan D, et al. 4pi non-coplanar liver SBRT: a novel delivery technique. *Int J Radiat Oncol Biol Phys.* 2013;85(5):1360-1366.
29. Dong P, Lee P, Ruan D, et al. 4pi noncoplanar stereotactic body radiation therapy for centrally located or larger lung tumors. *Int J Radiat Oncol Biol Phys.* 2013;86(3):407-413.
30. Nguyen D, Rwigema JC, Yu VY, et al. Feasibility of extreme dose escalation for glioblastoma multiforme using 4pi radiotherapy. *Radiat Oncol.* 2014;9:239.
31. Rwigema JC, Nguyen D, Heron DE, et al. 4pi noncoplanar stereotactic body radiation therapy for head-and-neck cancer: potential to improve tumor control and late toxicity. *Int J Radiat Oncol Biol Phys.* 2015;91(2):401-409.
32. Hodapp N. [The ICRU Report 83: prescribing, recording and reporting photon-beam intensity-modulated radiation therapy (IMRT)]. *Strahlenther Onkol.* 2012;188(1):97-99.
33. Petrova D, Smickovska S, Lazarevska E. Conformity Index and Homogeneity Index of the Postoperative Whole Breast Radiotherapy. *Open Access Maced J Med Sci.* 2017;5(6):736-739.
34. Paddick I. A simple scoring ratio to index the conformity of radiosurgical treatment plans. Technical note. *J Neurosurg.* 2000;93 Suppl 3:219-222.
35. Papp D, Bortfeld T, Unkelbach J. A modular approach to intensity-modulated arc therapy optimization with noncoplanar trajectories. *Phys Med Biol.* 2015;60(13):5179-5198.
36. Sheng K, Shepard DM, Orton CG. Point/Counterpoint. Noncoplanar beams improve dosimetry quality for extracranial intensity modulated radiotherapy and should be used more extensively. *Med Phys.* 2015;42(2):531-533.
37. Yu VY, Tran A, Nguyen D, et al. The development and verification of a highly accurate collision prediction model for automated noncoplanar plan delivery. *Med Phys.* 2015;42(11):6457-6467.
38. Nguyen D, Dong P, Long T, et al. Integral dose investigation of non-coplanar treatment beam geometries in radiotherapy. *Med Phys.* 2014;41(1):011905.
39. Vicini FA. A Phase III trial of accelerated whole breast irradiation with hypofractionation plus concurrent boost versus standard whole breast irradiation plus sequential boost for early -stge breast cancer. *NRG Oncology.* 2014.
40. Baglan KL, Sharpe MB, Jaffray D, et al. Accelerated partial breast irradiation using 3D conformal radiation therapy (3D-CRT). *Int J Radiat Oncol Biol Phys.* 2003;55(2):302-311.

41. Livi L, Buonamici FB, Simontacchi G, et al. Accelerated partial breast irradiation with IMRT: new technical approach and interim analysis of acute toxicity in a phase III randomized clinical trial. *Int J Radiat Oncol Biol Phys*. 2010;77(2):509-515.
42. Muehler ME. Relationship between irradiated breast volume and late normal tissue complications: a systematic review. *Radiotherapy & Oncology*. 2012;104:1-10.
43. Paliwal B, Tewatia D. Advances in radiation therapy dosimetry. *J Med Phys*. 2009;34(3):108-116.
44. Gregucci F, Fiorentino A, Corradini S, et al. Linac-based radiosurgery or fractionated stereotactic radiotherapy with flattening filter-free volumetric modulated arc therapy in elderly patients : A mono-institutional experience on 110 brain metastases. *Strahlenther Onkol*. 2018.
45. Roa DE, Schiffner DC, Zhang J, et al. The use of RapidArc volumetric-modulated arc therapy to deliver stereotactic radiosurgery and stereotactic body radiotherapy to intracranial and extracranial targets. *Med Dosim*. 2012;37(3):257-264.
46. Timmerman RD. An overview of hypofractionation and introduction to this issue of seminars in radiation oncology. *Semin Radiat Oncol*. 2008;18(4):215-222.
47. Benedict SH, Yenice KM, Followill D, et al. Stereotactic body radiation therapy: the report of AAPM Task Group 101. *Med Phys*. 2010;37(8):4078-4101.
48. Seppala J, Suilamo S, Tenhunen M, et al. Dosimetric Comparison and Evaluation of 4 Stereotactic Body Radiotherapy Techniques for the Treatment of Prostate Cancer. *Technol Cancer Res Treat*. 2017;16(2):238-245.
49. Tran A, Woods K, Nguyen D, et al. Predicting liver SBRT eligibility and plan quality for VMAT and 4pi plans. *Radiat Oncol*. 2017;12(1):70.
50. Woods K, Nguyen D, Tran A, et al. Viability of Non-Coplanar VMAT for Liver SBRT as Compared to Coplanar VMAT and Beam Orientation Optimized 4pi IMRT. *Adv Radiat Oncol*. 2016;1(1):67-75.
51. Naeim A, Keeler EB. Is adjuvant therapy for older patients with node (-) early breast cancer cost-effective? *Crit Rev Oncol Hematol*. 2005;53(1):81-89.
52. Naeim A, Keeler EB. Is adjuvant therapy for older patients with node (+) early breast cancer cost-effective? *Breast Cancer Res Treat*. 2005;94(2):95-103.
53. Siegel RL, Miller KD, Jemal A. Cancer statistics, 2020. *CA Cancer J Clin*. 2020;70(1):7-30.
54. NIH consensus conference. Treatment of early-stage breast cancer. *JAMA*. 1991;265(3):391-395.

55. Veronesi U, Cascinelli N, Mariani L, et al. Twenty-year follow-up of a randomized study comparing breast-conserving surgery with radical mastectomy for early breast cancer. *N Engl J Med*. 2002;347(16):1227-1232.
56. Clarke M, Collins R, Darby S, et al. Effects of radiotherapy and of differences in the extent of surgery for early breast cancer on local recurrence and 15-year survival: an overview of the randomised trials. *Lancet*. 2005;366(9503):2087-2106.
57. Gurtej S, Gill RYJ, Jameson Baker, Terry Button, Jenghwa Chang. Dosimetric advantages of Volumetric Arc Therapy Based Coronal Arc Delivery Technique in Brain Stereotactic Radiosurgery: A Feasibility Study. *International Journal of Medical Physics, Clinical Engineering and Radiation Oncology*. 2019;8(8):80-94.
58. Wolmark Nea. A Randomized Phase III Study of Conventional Whole Breast Irradiation (WBI) Versus Partial Breast Irradiation (PBI) for Women with Stage 0, I, or II Breast Cancer *National Surgical Adjuvant Breast and Bowel Project (NSABP)*. 2011.
59. Popescu CC, Beckham WA, Patenaude VV, Olivotto IA, Vlachaki MT. Simultaneous couch and gantry dynamic arc rotation (CG-Darc) in the treatment of breast cancer with accelerated partial breast irradiation (APBI): a feasibility study. *J Appl Clin Med Phys*. 2013;14(1):4035.
60. Shaitelman SF, Kim LH, Yan D, Martinez AA, Vicini FA, Grills IS. Continuous arc rotation of the couch therapy for the delivery of accelerated partial breast irradiation: a treatment planning analysis. *Int J Radiat Oncol Biol Phys*. 2011;80(3):771-778.
61. Fahimian B, Yu V, Horst K, Xing L, Hristov D. Trajectory modulated prone breast irradiation: a LINAC-based technique combining intensity modulated delivery and motion of the couch. *Radiother Oncol*. 2013;109(3):475-481.
62. *Varian. Eclipse Scripting API Reference guide" (P1021698-003-C). Palo Alto, CA, USA: Varian MEDical Systems.*
63. Covington EL, Chen X, Younge KC, et al. Improving treatment plan evaluation with automation. *Journal of Applied Clinical Medical Physics*. 2016;17(6):16-31.
64. Schreibmann E, Fox T, Curran W, Shu H-K, Crocker I. Automated population-based planning for whole brain radiation therapy. *Journal of Applied Clinical Medical Physics*. 2015;16(5):76-86.
65. Huang X, Quan H, Zhao B, Zhou W, Chen C, Chen Y. A plan template-based automation solution using a commercial treatment planning system. *Journal of Applied Clinical Medical Physics*. n/a(n/a).
66. Wu B, Pang D, Simari P, Taylor R, Sanguineti G, McNutt T. Using overlap volume histogram and IMRT plan data to guide and automate VMAT planning: A head-and-neck case study. *Medical Physics*. 2013;40(2):021714.

67. Guo B, Shah C, Xia P. Automated planning of whole breast irradiation using hybrid IMRT improves efficiency and quality. *Journal of Applied Clinical Medical Physics*. 2019;20(12):87-96.
68. Mitchell RA, Wai P, Colgan R, Kirby AM, Donovan EM. Improving the efficiency of breast radiotherapy treatment planning using a semi-automated approach. *Journal of Applied Clinical Medical Physics*. 2017;18(1):18-24.
69. Kisling K, Zhang L, Shaitelman SF, et al. Automated treatment planning of postmastectomy radiotherapy. *Medical Physics*. 2019;46(9):3767-3775.
70. Amaloo C, Hayes L, Manning M, Liu H, Wiant D. Can automated treatment plans gain traction in the clinic? *Journal of Applied Clinical Medical Physics*. 2019;20(8):29-35.
71. Gill G, Jakubovic, R. , Baker, J. , Button, T. and Chang, J. Dosimetric Advantages of Volumetric Modulated Arc Therapy Based Coronal Arc Delivery Technique in Brain Stereotactic Radiosurgery: A Feasibility Study. *International Journal of Medical Physics, Clinical Engineering and Radiation Oncology*. 2019;8:80-94.
72. Kisling K, Johnson JL, Simonds H, et al. A risk assessment of automated treatment planning and recommendations for clinical deployment. *Medical Physics*. 2019;46(6):2567-2574.
73. Gill GS, Jakubovic RY, Baker J, Button T, Chang J. Dosimetric benefits of gantry-static couch-motion (GsCM) technique for breast boost radiation therapy: Reduced dose to organs-at-risk and improved dosimetric indices. *Journal of Applied Clinical Medical Physics*. n/a(n/a).

Appendix

1.0. C# script to design an automated plan.

The following C# script takes care of the XML conversion step by step. It starts with the system description.

```
using System;
using System.Collections.Generic;
using System.ComponentModel;
using System.Data;
using System.Drawing;
using System.Linq;
using System.Text;
using System.Threading.Tasks;
using System.Windows.Forms;
using VMS.TPS.Common.Model.API;
using VMS.TPS.Common.Model.Types;
using System.Xml;
```

Next, the name of the script was XML1 which runs in Visual Studio application namespace XML1

```
{
    public partial class XML : Form
    {
        public ScriptContext sc;
        public XML(ScriptContext mycontext1)
        {
            InitializeComponent();
            sc = mycontext1;
        }

        public void XML_Load(object sender, EventArgs e)
        {

        }

        public void Button1_Click(object sender, EventArgs e)
        {
            XmlDocument doc = new XmlDocument();
            XmlNode docnode = doc.CreateXmlDeclaration("1.0", "UTF-8", null);
```

```

doc.AppendChild(docnode);
XmlNode beam = doc.CreateElement("SetBeam");
doc.AppendChild(beam);

```

Next, we define the MLC model and XML ID as 1

```

XmlNode id1 = doc.CreateElement("Id");
beam.AppendChild(id1).InnerText="1";
XmlNode mlcmodel = doc.CreateElement("MLCModel");
beam.AppendChild(mlcmodel).InnerText = "NDS120HD";

```

Next, we define the accessories used and control points per field. It also includes the description of MLC bank A, bank B, X jaws, Y jaws, monitor units (Mu), dose rate (DRate), energy, gantry rotation (GantryRtn), collimator rotation (CollRtn), and couch longitudinal (CouchLng), lateral (CouchLat), vertical (CouchVert) and rotation (CouchRtn) positions,

```

XmlNode acc = doc.CreateElement("Accs");
beam.AppendChild(acc);
XmlNode controlpoints = doc.CreateElement("ControlPoints");
beam.AppendChild(controlpoints);
//XmlNode cp = doc.CreateElement("Cp");
//XmlNode mlc = doc.CreateElement("Mlc");
//XmlNode A = doc.CreateElement("A");
//XmlNode B = doc.CreateElement("B");
// XmlNode y1 = doc.CreateElement("Y1");
// XmlNode X1 = doc.CreateElement("X1");
// XmlNode Y2 = doc.CreateElement("Y2");
//XmlNode X2 = doc.CreateElement("X2");
//XmlNode energy = doc.CreateElement("Energy");
//XmlNode mu = doc.CreateElement("Mu");
//XmlNode doserate = doc.CreateElement("DRate");
//XmlNode gantryrotation = doc.CreateElement("GantryRtn");
//XmlNode callrotation = doc.CreateElement("CollRtn");
//XmlNode CouchLng = doc.CreateElement("CouchLng");
//XmlNode CouchRtn = doc.CreateElement("CouchRtn");
//XmlNode CouchLat = doc.CreateElement("CouchLat");
//XmlNode CouchVrt = doc.CreateElement("CouchVrt");

```

```

string w=null;
double jaw = 0;

```

```

var beams = sc.ExternalPlanSetup.Beams;
double MU = 0;
int key = 0;
//string s = null;
int count;
foreach (var b in beams)
{

```



```

count = b.ControlPoints.Count;
//count = count / 2;
for (int j = 0; j < count; j++)
{
XmlNode cp = doc.CreateNode(XmlNodeType.Element, "Cp", null);
controlpoints.AppendChild(cp);

////////////////////////////////next energy////////////////////////////////

XmlNode energy = doc.CreateNode(XmlNodeType.Element, "Energy", null);

cp.AppendChild(energy).InnerText=b.EnergyModeDisplayName.ToString().
ToLower();

////////////////////////////////first mu=0////////////////////////////////

//XmlNode mu = doc.CreateNode(XmlNodeType.Element, "Mu", null);
// cp.AppendChild(mu).InnerText = "0";

////////////////////////////////

//XmlNode cp1 = doc.CreateNode(XmlNodeType.Element, "Cp", null);
//controlpoints.AppendChild(cp1);
XmlNode mu1 = doc.CreateNode(XmlNodeType.Element, "Mu", null);

//s=s+(b.ControlPoints[j].MetersetWeight * b.Meterset.Value).ToString()+"\n";

cp.AppendChild(mu1).InnerText =(MU+ b.ControlPoints[j].MetersetWeight *
b.Meterset.Value).ToString();

////////////////////////////////let's say we have multiple fields////////////////////////////////

cp.AppendChild(mu).InnerText = (b.ControlPoints[j].MetersetWeight *
b.Meterset.Value).ToString();

////////////////////////////////dose rate////////////////////////////////
XmlNode doserate = doc.CreateNode(XmlNodeType.Element, "DRate", null);
cp.AppendChild(doserate).InnerText = b.DoseRate.ToString();

////////////////////////////////Gantry rotation////////////////////////////////

XmlNode gantry = doc.CreateNode(XmlNodeType.Element, "GantryRtn", null);
double gantry_conversion = 0;
gantry_conversion = b.ControlPoints[j].GantryAngle;
if ((gantry_conversion >= 0) && (gantry_conversion <= 180))
{

```

```

        gantry_conversion = 180 - gantry_conversion;
    }
    else
        if ((gantry_conversion <= 359.9) && (gantry_conversion >= 180.1))
        {
            gantry_conversion = 180 + (360 - gantry_conversion);
        }

    cp.AppendChild(gantry).InnerText = gantry_conversion.ToString();

    //////////////////////////////////////////coll rotation////////////////////////////////////////

    XmlNode collimation = doc.CreateNode(XmlNodeType.Element, "CollRtn",
    null);

    double collimation_conversion = 0;
    collimation_conversion = b.ControlPoints[j].CollimatorAngle;
    if ((collimation_conversion >= 0) && (collimation_conversion <= 180))
    {
        collimation_conversion = 180 - collimation_conversion;
    }
    else
        if ((collimation_conversion <= 359.9) && (collimation_conversion >= 180.1))
        {
            collimation_conversion = 180 + (360 - collimation_conversion);
        }

    cp.AppendChild(collimation).InnerText = collimation_conversion.ToString();

    //////////////////////////////////////////couch rotation////////////////////////////////////////

    XmlNode couchrtn = doc.CreateNode(XmlNodeType.Element, "CouchRtn", null);

    double couch_conversion = 0;
    couch_conversion = (360-b.ControlPoints[j].PatientSupportAngle);
    if (couch_conversion == 360)
        couch_conversion = 0;
    // MessageBox.Show(couch_conversion.ToString());

    if ((couch_conversion >= 0) && (couch_conversion <= 180))
    {
        couch_conversion = 180 - couch_conversion;
    }
    else
        if ((couch_conversion <= 359.9) && (couch_conversion >= 180.1))
        {
            couch_conversion = 180 + (360 - couch_conversion);
        }
    couch_conversion = 360 - couch_conversion;

```

```

cp.AppendChild(couchrtn).InnerText = couch_conversion.ToString();

//////////////////////////////////Y1//////////////////////////////////

XmlNode y1 = doc.CreateNode(XmlNodeType.Element, "Y1", null);
jaw = -b.ControlPoints[j].JawPositions.Y1 / 10;
cp.AppendChild(y1).InnerText=jaw.ToString();

//////////////////////////////////Y2//////////////////////////////////

XmlNode y2 = doc.CreateNode(XmlNodeType.Element, "Y2", null);
jaw = b.ControlPoints[j].JawPositions.Y2 / 10;
cp.AppendChild(y2).InnerText = jaw.ToString();

//////////////////////////////////X1//////////////////////////////////

XmlNode x1 = doc.CreateNode(XmlNodeType.Element, "X1", null);
jaw = -b.ControlPoints[j].JawPositions.X1 / 10;
cp.AppendChild(x1).InnerText = jaw.ToString();

//////////////////////////////////X2//////////////////////////////////
XmlNode x2 = doc.CreateNode(XmlNodeType.Element, "X2", null);
jaw = b.ControlPoints[j].JawPositions.X2 / 10;
cp.AppendChild(x2).InnerText = jaw.ToString();

//////////////////////////////////

// XmlNode couchlong = doc.CreateNode(XmlNodeType.Element,
"CouchLng", null);
//controlpoints.AppendChild(couchlong).InnerText =
b.ControlPoints[j].TableTopLongitudinalPosition.ToString();
//XmlNode couchlat = doc.CreateNode(XmlNodeType.Element, "CouchLat",
null);//
controlpoints.AppendChild(couchlat).InnerText =
b.ControlPoints[j].TableTopLateralPosition.ToString();
//XmlNode couchvert = doc.CreateNode(XmlNodeType.Element, "CouchVrt",
null);
//controlpoints.AppendChild(couchvert).InnerText =
b.ControlPoints[j].TableTopVerticalPosition.ToString();
//controlpoints.AppendChild(cp);
XmlNode mlc = doc.CreateNode(XmlNodeType.Element, "Mlc", null);
cp.AppendChild(mlc);
XmlNode id = doc.CreateElement("ID");
mlc.AppendChild(id).InnerText = "1";
for (int p = 0; p <60; p++)
{
    w=w+ (-b.ControlPoints[j].LeafPositions[0, p])/10).ToString()+" ";
}
}

```

```

XmlNode B = doc.CreateNode(XmlNodeType.Element, "B", null);
mlc.AppendChild(B).InnerText = w;
w = null;
for (int p = 0; p < 60; p++)
{
    w = w + ((b.ControlPoints[j].LeafPositions[1,p])/10).ToString() + " ";
}
XmlNode A = doc.CreateNode(XmlNodeType.Element, "A", null);
mlc.AppendChild(A).InnerText = w;
w = null;
/* XmlNode cp1 = doc.CreateNode(XmlNodeType.Element, "Cp", null);
controlpoints.AppendChild(cp1);
XmlNode mu1 = doc.CreateNode(XmlNodeType.Element, "Mu", null);
if (key == 0)
{
    MU = b.ControlPoints[j].MetersetWeight * b.Meterset.Value;
    key = 1;
}
else
if (key == 1)
{
    MU = MU + b.ControlPoints[j].MetersetWeight * b.Meterset.Value;
    key = 0;
}
cp1.AppendChild(mu1).InnerText = MU.ToString(); */
}

key = count-1;
MU = MU+b.ControlPoints[key].MetersetWeight * b.Meterset.Value;
}

//MessageBox.Show(s);
saveFileDialog1.Filter = "XML files(.xml)|*.xml|all Files (*.*)|*.*";
saveFileDialog1.ShowDialog();
doc.Save(saveFileDialog1.FileName);
}
}
}

```

2.0. MATLAB code to convert IMRT step & shoot fields into XML. All fields were combined to create a single deliverable arc

```
close all
clc
clear all

%% Eclipse portion

%% Reading in DICOM info

A = dicominfo('TB3 test plans\04B IMRT Step & Shoot approach w 5 control points each
field TB3\RP.A171047.04bimrtSSTB3x.dcm');
NumberofBeams = zeros(1,A.FractionGroupSequence.Item_1.NumberOfBeams);
GantryAngle = zeros(1,A.FractionGroupSequence.Item_1.NumberOfBeams);
CouchAngle = zeros(1,A.FractionGroupSequence.Item_1.NumberOfBeams);
CollimatorAngle = zeros(1,A.FractionGroupSequence.Item_1.NumberOfBeams);

MU = zeros(1,A.FractionGroupSequence.Item_1.NumberOfBeams);
MU_SUM = 0;

for i = 1:length(NumberofBeams)
    GantryAngle(:,i) =
eval(strcat('A.BeamSequence.Item_',num2str(i),'.ControlPointSequence.Item_1.GantryAngle'))
;
    CouchAngle(:,i) =
eval(strcat('A.BeamSequence.Item_',num2str(i),'.ControlPointSequence.Item_1.PatientSupport
Angle')) - 180;

%% Convert Couch angle
    if CouchAngle(:,i) > 0 && CouchAngle(:,i) < 180
        CouchAngle(:,i) = 360 - CouchAngle(:,i);
    else
        CouchAngle(:,i) = abs(CouchAngle(:,i));
    end

    NumControlPts =
eval(strcat('A.BeamSequence.Item_',num2str(i),'.NumberOfControlPoints'));
    MU(i) =
eval(strcat('A.FractionGroupSequence.Item_1.ReferencedBeamSequence.Item_',num2str(i),'.B
eamMeterset'));

    for j = 1
        if
isempty(strcat('A.BeamSequence.Item_',num2str(i),'.ControlPointSequence.Item_1.BeamLimit
ingDevicePositionSequence.Item_1.LeafJawPositions'))==0
            X =
eval(strcat('A.BeamSequence.Item_',num2str(i),'.ControlPointSequence.Item_1.BeamLimiting
DevicePositionSequence.Item_1.LeafJawPositions'))/10;
```

```

Y =
eval(strcat('A.BeamSequence.Item_',num2str(i),'ControlPointSequence.Item_1.BeamLimiting
DevicePositionSequence.Item_2.LeafJawPositions'))/10;

X1(:,i,j) = (abs(X(1)));
X2(:,i,j) = (abs(X(2)));

Y1(:,i,j) = (abs(Y(1)));
Y2(:,i) = (abs(Y(2)));
end

MLC = eval(strcat('A.BeamSequence.Item_',num2str(i),'ControlPointSequence.Item_',
num2str(j),'BeamLimitingDevicePositionSequence.Item_3.LeafJawPositions'));
MLC_A(:,i,j) = MLC(61:120)/10;
MLC_B(:,i,j) = -MLC(1:60)/10;
end

for j = 2:NumControlPts
MLC = eval(strcat('A.BeamSequence.Item_',num2str(i),'ControlPointSequence.Item_',
num2str(j),'BeamLimitingDevicePositionSequence.Item_1.LeafJawPositions'));
MLC_A(:,i,j) = MLC(61:120)/10;
MLC_B(:,i,j) = -MLC(1:60)/10;
end

end

for i = 1
NumControlPts =
eval(strcat('A.BeamSequence.Item_',num2str(i),'NumberOfControlPoints'));

for j = 1
MU_CP(i,j) = 0;
end

for j = 2:2:NumControlPts+1
MU_CP(i,j) =
MU(i)*eval(strcat('A.BeamSequence.Item_',num2str(i),'ControlPointSequence.Item_',num2str
(j),'CumulativeMetersetWeight'));
end
for j = 3:2:NumControlPts
MU_CP(i,j) = MU_CP(i,j-1);
end
end

for i = 2:length(MU)
NumControlPts =
eval(strcat('A.BeamSequence.Item_',num2str(i),'NumberOfControlPoints'));

MU_SUM = MU_SUM + MU(i-1);

```

```

for j = 1
    MU_CP(i,j) = MU_SUM;
end

for j = 2:2:NumControlPts
    MU_CP(i,j) = MU_SUM +
MU(i)*eval(strcat('A.BeamSequence.Item_',num2str(i),'.ControlPointSequence.Item_',num2str
(j),'.CumulativeMetersetWeight'));

end

for j = 3:2:NumControlPts
    MU_CP(i,j) = MU_CP(i,j-1);
end
end

%% XML PORTION
%%Read in XML template file

file_name = 'C:\Users\Raphael\Desktop\XML\4. Raphy Test\MU update test_1cp';
xDoc = xmlread([file_name '.xml']);
xRoot = xDoc.getDocumentElement;

SetBeam_node = xDoc.createElement('SetBeam');

Id_node = xDoc.createElement('Id');
Id_text = xDoc.createTextNode('1');
Id_node.appendChild(Id_text);
SetBeam_node.appendChild(Id_node);

MLCModel_node = xDoc.createElement('MLCModel');
MLCModel_text = xDoc.createTextNode('NDS120HD');
MLCModel_node.appendChild(MLCModel_text);
SetBeam_node.appendChild(MLCModel_node);

Accs_node = xDoc.createElement('Accs');
SetBeam_node.appendChild(Accs_node);

ControlPoints_node = xDoc.createElement('ControlPoints');
SetBeam_node.appendChild(ControlPoints_node);

for i = 1

    NumControlPts =
eval(strcat('A.BeamSequence.Item_',num2str(i),'.NumberOfControlPoints'));

    for j = 1:1:NumControlPts
        Cp_node = xDoc.createElement('Cp');
        ControlPoints_node.appendChild(Cp_node);
    end
end

```

```

% SubBeam_node = xDoc.createElement('SubBeam');
% Cp_node.appendChild(SubBeam_node);

% Seq_node = xDoc.createElement('Seq');
% Seq_text = xDoc.createTextNode(num2str(j));
% Seq_node.appendChild(Seq_text);
% SubBeam_node.appendChild(Seq_node);

% Name_node = xDoc.createElement('Name');
% Name_text = xDoc.createTextNode('Beam ON!');
% Name_node.appendChild(Name_text);
% SubBeam_node.appendChild(Name_node);

Energy_node = xDoc.createElement('Energy');
Energy_text = xDoc.createTextNode('6xFFF');
Energy_node.appendChild(Energy_text);
Cp_node.appendChild(Energy_node);

MU_node = xDoc.createElement('Mu');
MU_text = xDoc.createTextNode(num2str(MU_CP(i,j)));
MU_node.appendChild(MU_text);
Cp_node.appendChild(MU_node);

DRate_node = xDoc.createElement('DRate');
DRate_text = xDoc.createTextNode('1400');
DRate_node.appendChild(DRate_text);
Cp_node.appendChild(DRate_node);

GantryRtn_node = xDoc.createElement('GantryRtn');
GantryRtn_text = xDoc.createTextNode(num2str(GantryAngle(i)));
GantryRtn_node.appendChild(GantryRtn_text);
Cp_node.appendChild(GantryRtn_node);

CollRtn_node = xDoc.createElement('CollRtn');
CollRtn_text = xDoc.createTextNode('180');
CollRtn_node.appendChild(CollRtn_text);
Cp_node.appendChild(CollRtn_node);

CouchRtn_node = xDoc.createElement('CouchRtn');
CouchRtn_text = xDoc.createTextNode(num2str(CouchAngle(i)));
CouchRtn_node.appendChild(CouchRtn_text);
Cp_node.appendChild(CouchRtn_node);

Y1_node = xDoc.createElement('Y1');
Y1_text = xDoc.createTextNode(mat2str(abs(Y1(i))));
Y1_node.appendChild(Y1_text);
Cp_node.appendChild(Y1_node);

Y2_node = xDoc.createElement('Y2');
Y2_text = xDoc.createTextNode(mat2str(abs(Y2(i))));

```



```

Y2_node.appendChild(Y2_text);
Cp_node.appendChild(Y2_node);

X1_node = xDoc.createElement('X1');
X1_text = xDoc.createTextNode(mat2str(abs(X1(i))));
X1_node.appendChild(X1_text);
Cp_node.appendChild(X1_node);

X2_node = xDoc.createElement('X2');
X2_text = xDoc.createTextNode(mat2str(abs(X2(i))));
X2_node.appendChild(X2_text);
Cp_node.appendChild(X2_node);

Mlc_node = xDoc.createElement('Mlc');
Cp_node.appendChild(Mlc_node);

Cp_node.appendChild(Mlc_node);
ID_MLC_node = xDoc.createElement('ID');
Mlc_node.appendChild(ID_MLC_node);

ID_MLC_text = xDoc.createTextNode(num2str(i));
ID_MLC_node.appendChild(ID_MLC_text);

ID_MLC_node_B = xDoc.createElement('B');
MLC_BB = mat2str((MLC_B(:,i,j)));
ID_MLC_text_B = xDoc.createTextNode(MLC_BB(2:end-1));
ID_MLC_node_B.appendChild(ID_MLC_text_B);
Mlc_node.appendChild(ID_MLC_node_B);

ID_MLC_node_A = xDoc.createElement('A');
MLC_AA = mat2str((MLC_A(:,i,j)));
ID_MLC_text_A = xDoc.createTextNode(MLC_AA(2:end-1));
ID_MLC_node_A.appendChild(ID_MLC_text_A);
Mlc_node.appendChild(ID_MLC_node_A);
xDoc.getDocumentElement.appendChild(SetBeam_node);
end
end
for i = 2:length(CouchAngle)

    NumControlPts =
eval(strcat('A.BeamSequence.Item_',num2str(i),'NumberOfControlPoints'));
    for j = 1:NumControlPts
        Cp_node = xDoc.createElement('Cp');
        ControlPoints_node.appendChild(Cp_node);

        %SubBeam_node = xDoc.createElement('SubBeam');
        %Cp_node.appendChild(SubBeam_node);

        %Seq_node = xDoc.createElement('Seq');
        %Seq_text = xDoc.createTextNode(num2str(j));

```

```

%Seq_node.appendChild(Seq_text);
%SubBeam_node.appendChild(Seq_node);

MU_node = xDoc.createElement('Mu');
MU_text = xDoc.createTextNode(num2str(MU_CP(i,j)));
MU_node.appendChild(MU_text);
Cp_node.appendChild(MU_node);

GantryRtn_node = xDoc.createElement('GantryRtn');
GantryRtn_text = xDoc.createTextNode(num2str(GantryAngle(i)));
GantryRtn_node.appendChild(GantryRtn_text);
Cp_node.appendChild(GantryRtn_node);

CollRtn_node = xDoc.createElement('CollRtn');
CollRtn_text = xDoc.createTextNode('180');
CollRtn_node.appendChild(CollRtn_text);
Cp_node.appendChild(CollRtn_node);

CouchRtn_node = xDoc.createElement('CouchRtn');
CouchRtn_text = xDoc.createTextNode(num2str(CouchAngle(i)));
CouchRtn_node.appendChild(CouchRtn_text);
Cp_node.appendChild(CouchRtn_node);

Y1_node = xDoc.createElement('Y1');
Y1_text = xDoc.createTextNode(mat2str(abs(Y1(i))));
Y1_node.appendChild(Y1_text);
Cp_node.appendChild(Y1_node);

Y2_node = xDoc.createElement('Y2');
Y2_text = xDoc.createTextNode(mat2str(abs(Y2(i))));
Y2_node.appendChild(Y2_text);
Cp_node.appendChild(Y2_node);

X1_node = xDoc.createElement('X1');
X1_text = xDoc.createTextNode(mat2str(abs(X1(i))));
X1_node.appendChild(X1_text);
Cp_node.appendChild(X1_node);

X2_node = xDoc.createElement('X2');
X2_text = xDoc.createTextNode(mat2str(abs(X2(i))));
X2_node.appendChild(X2_text);
Cp_node.appendChild(X2_node);

Mlc_node = xDoc.createElement('Mlc');
Cp_node.appendChild(Mlc_node);

Cp_node.appendChild(Mlc_node);
ID_MLC_node = xDoc.createElement('ID');
Mlc_node.appendChild(ID_MLC_node);

```

```

ID_MLC_text = xDoc.createTextNode(num2str(i));
ID_MLC_node.appendChild(ID_MLC_text);

ID_MLC_node_B = xDoc.createElement('B');
MLC_BB = mat2str((MLC_B(:,i,j)));
ID_MLC_text_B = xDoc.createTextNode(MLC_BB(2:end-1));
ID_MLC_node_B.appendChild(ID_MLC_text_B);
Mlc_node.appendChild(ID_MLC_node_B);

ID_MLC_node_A = xDoc.createElement('A');
MLC_AA = mat2str((MLC_A(:,i,j)));
ID_MLC_text_A = xDoc.createTextNode(MLC_AA(2:end-1));
ID_MLC_node_A.appendChild(ID_MLC_text_A);
Mlc_node.appendChild(ID_MLC_node_A);

% if mod(i,2) == 0
% GantryRtn_node = xDoc.createElement('GantryRtn');
% GantryRtn_text = xDoc.createTextNode(num2str(GantryAngle_repeat(2,i,j)));
% GantryRtn_node.appendChild(GantryRtn_text);
% Cp_node.appendChild(GantryRtn_node);
%
% CouchRtn_node = xDoc.createElement('CouchRtn');
% CouchRtn_text = xDoc.createTextNode(num2str(CouchAngle_repeat(2,i,j)));
% CouchRtn_node.appendChild(CouchRtn_text);
% Cp_node.appendChild(CouchRtn_node);
%
% Y1_node = xDoc.createElement('Y1');
% Y1_text = xDoc.createTextNode(mat2str(abs(Y1_repeat(i))));
% Y1_node.appendChild(Y1_text);
% Cp_node.appendChild(Y1_node);
%
% Y2_node = xDoc.createElement('Y2');
% Y2_text = xDoc.createTextNode(mat2str(abs(Y2_repeat(i))));
% Y2_node.appendChild(Y2_text);
% Cp_node.appendChild(Y2_node);
%
% X1_node = xDoc.createElement('X1');
% X1_text = xDoc.createTextNode(mat2str(abs(X1_repeat(i))));
% X1_node.appendChild(X1_text);
% Cp_node.appendChild(X1_node);
%
% X2_node = xDoc.createElement('X2');
% X2_text = xDoc.createTextNode(mat2str(abs(X2_repeat(i))));
% X2_node.appendChild(X2_text);
% Cp_node.appendChild(X2_node);
%
% Mlc_node = xDoc.createElement('Mlc');
% Cp_node.appendChild(Mlc_node);
%
% Cp_node.appendChild(Mlc_node);

```

```

% ID_MLC_node = xDoc.createElement('ID');
% Mlc_node.appendChild(ID_MLC_node);
%
% ID_MLC_text = xDoc.createTextNode(num2str(i/2));
% ID_MLC_node.appendChild(ID_MLC_text);
%
% ID_MLC_node_B = xDoc.createElement('B');
% MLC_BB = mat2str((MLC_B_repeat(i,:)));
%
% ID_MLC_text_B = xDoc.createTextNode(MLC_BB(2:end-1));
% ID_MLC_node_B.appendChild(ID_MLC_text_B);
% Mlc_node.appendChild(ID_MLC_node_B);
%
% ID_MLC_node_A = xDoc.createElement('A');
% MLC_AA = mat2str((MLC_A_repeat(i,:)));
% ID_MLC_text_A = xDoc.createTextNode(MLC_AA(2:end-1));
% ID_MLC_node_A.appendChild(ID_MLC_text_A);
% Mlc_node.appendChild(ID_MLC_node_A);
%
end
end
xDoc.getDocumentElement.appendChild(SetBeam_node);

%% ADDING FINAL MU DELIVERY
for i = size(MU,2)
    MU(i) = MU(i-1) +
eval(strcat('A.FractionGroupSequence.Item_1.ReferencedBeamSequence.Item_',num2str(i-
1),'.BeamMeterset'));

    Cp_node = xDoc.createElement('Cp');
    ControlPoints_node.appendChild(Cp_node);

    MU_node = xDoc.createElement('Mu');
    MU_text = xDoc.createTextNode(num2str(MU(i)));
    MU_node.appendChild(MU_text);
    Cp_node.appendChild(MU_node);
end

xmlwrite(['Stepshoot_output.xml'],xDoc);

```

3.0. MATLAB code to convert gantry arc into couch arc.

```
close all
clc
clear all

%% SCRIPT DETAILS
...THIS SCRIPT AUTOMATES ARC DELIVERY WITH OR WITHOUT
GANTRY/COUCH/COLLIMATOR MOTION. TO ENABLE OR DISABLE
GANTRY/COUCH/COLLIMATOR MOTION...
... see options in XML portion of script
%% Eclipse portion
%% Reading in DICOM info
A = dicominfo('TB3 test plans\05RandoUshape\RP.A171047.05RandoUshape.dcm');
NumberOfBeams = zeros(1,A.FractionGroupSequence.Item_1.NumberOfBeams);
DoseRt = zeros(1,A.FractionGroupSequence.Item_1.NumberOfBeams);
Energy = zeros(1,A.FractionGroupSequence.Item_1.NumberOfBeams);
GantryAngle = zeros(1,A.FractionGroupSequence.Item_1.NumberOfBeams);
CouchAngle = zeros(1,A.FractionGroupSequence.Item_1.NumberOfBeams);
CollimatorAngle = zeros(1,A.FractionGroupSequence.Item_1.NumberOfBeams);
MU = zeros(1,A.FractionGroupSequence.Item_1.NumberOfBeams);
MU_SUM = 0;

%% Read in XML template file
file_name = 'template_input';
xDoc = xmlread([file_name '.xml']);
xRoot = xDoc.getDocumentElement;

for i = 1:ndims(A.BeamSequence)

    %Use for a single arc
    %for i = 1
    NumControlPts =
eval(strcat('A.BeamSequence.Item_',num2str(i),'.NumberOfControlPoints'));

    for j = 1

        Energy(i,j) =
eval(strcat('A.BeamSequence.Item_',num2str(i),'.ControlPointSequence.Item_',num2str(j),'.NominalBeamEnergy'));
        DoseRt(i,j) =
eval(strcat('A.BeamSequence.Item_',num2str(i),'.ControlPointSequence.Item_',num2str(j),'.DoseRateSet'));

        if
eval(strcat('A.BeamSequence.Item_',num2str(i),'.ControlPointSequence.Item_',num2str(j),'.GantryAngle')) > 180
            GantryAngle(i,j) = 360 -
eval(strcat('A.BeamSequence.Item_',num2str(i),'.ControlPointSequence.Item_',num2str(j),'.GantryAngle'))+180;
```

```

else
    GantryAngle(i,j) = 180 -
eval(strcat('A.BeamSequence.Item_',num2str(i),'ControlPointSequence.Item_',num2str(j),'GantryAngle'));
end
CollimatorAngle(i,j) =
eval(strcat('A.BeamSequence.Item_',num2str(i),'ControlPointSequence.Item_',num2str(j),'BeamLimitingDeviceAngle'));

CouchAngle(i,j) = 180 -
eval(strcat('A.BeamSequence.Item_',num2str(i),'ControlPointSequence.Item_',num2str(j),'PatientSupportAngle'));

% if CouchAngle(i,j) > 0 && CouchAngle(i,j) < 180
% CouchAngle(i,j) = 360 - CouchAngle(i,j);
%else
% CouchAngle(i,j) = 180 - abs(CouchAngle(i,j));
%end

if
isempty(strcat('A.BeamSequence.Item_',num2str(i),'ControlPointSequence.Item_1.BeamLimitingDevicePositionSequence.Item_1.LeafJawPositions'))==0
    X =
eval(strcat('A.BeamSequence.Item_',num2str(i),'ControlPointSequence.Item_1.BeamLimitingDevicePositionSequence.Item_1.LeafJawPositions'))/10;
    Y =
eval(strcat('A.BeamSequence.Item_',num2str(i),'ControlPointSequence.Item_1.BeamLimitingDevicePositionSequence.Item_2.LeafJawPositions'))/10;

    X1(:,i,j) = (abs(X(1)));
    X2(:,i,j) = (abs(X(2)));

    Y1(:,i,j) = (abs(Y(1)));
    Y2(:,i,j) = (abs(Y(2)));
end

MLC = eval(strcat('A.BeamSequence.Item_',num2str(i),'ControlPointSequence.Item_',num2str(j),'BeamLimitingDevicePositionSequence.Item_3.LeafJawPositions'));
MLC_A(:,i,j) = MLC(61:120)/10;
MLC_B(:,i,j) = -MLC(1:60)/10;

MU(i) =
eval(strcat('A.FractionGroupSequence.Item_1.ReferencedBeamSequence.Item_',num2str(i),'BeamMeterset'));

if i == 1
    MU_CP(i,j) = 0;
else
    MU_CP(i,j) = MU(i-1);
end

```

```

end

for j = 2:1:NumControlPts
    if
eval(strcat('A.BeamSequence.Item_',num2str(i),'ControlPointSequence.Item_',num2str(j),'GantryAngle')) > 180
        GantryAngle(i,j) = 360 -
eval(strcat('A.BeamSequence.Item_',num2str(i),'ControlPointSequence.Item_',num2str(j),'GantryAngle'))+180;
    else
        GantryAngle(i,j) = 180 -
eval(strcat('A.BeamSequence.Item_',num2str(i),'ControlPointSequence.Item_',num2str(j),'GantryAngle'));
    end

    %CouchAngle(i,j) =
eval(strcat('A.BeamSequence.Item_',num2str(i),'ControlPointSequence.Item_',num2str(j),'PatientSupportAngle'));
    %if CouchAngle(:,i,j) > 0 && CouchAngle(:,i,j) < 180
    % CouchAngle(:,i,j) = 360 - CouchAngle(:,i,j);
    %else
    % CouchAngle(:,i,j) = abs(CouchAngle(:,i,j));
    %end

    if
isempty(strcat('A.BeamSequence.Item_',num2str(i),'ControlPointSequence.Item_1.BeamLimitingDevicePositionSequence.Item_1.LeafJawPositions'))==0
        X =
eval(strcat('A.BeamSequence.Item_',num2str(i),'ControlPointSequence.Item_1.BeamLimitingDevicePositionSequence.Item_1.LeafJawPositions'))/10;
        Y =
eval(strcat('A.BeamSequence.Item_',num2str(i),'ControlPointSequence.Item_1.BeamLimitingDevicePositionSequence.Item_2.LeafJawPositions'))/10;

        X1(:,i,j) = (abs(X(1)));
        X2(:,i,j) = (abs(X(2)));

        Y1(:,i,j) = (abs(Y(1)));
        Y2(:,i,j) = (abs(Y(2)));
    end

    MLC = eval(strcat('A.BeamSequence.Item_',num2str(i),'ControlPointSequence.Item_',num2str(j),'BeamLimitingDevicePositionSequence.Item_3.LeafJawPositions'));
    MLC_A(:,i,j) = MLC(61:120)/10;
    MLC_B(:,i,j) = -MLC(1:60)/10;

    if i == 1
        MU_CP(i,j) =
MU(i)*eval(strcat('A.BeamSequence.Item_',num2str(i),'ControlPointSequence.Item_',num2str(j),'CumulativeMetersetWeight'));
    end
end

```

```

else
    MU_CP(i,j) = MU(i-1) +
MU(i)*eval(strcat('A.BeamSequence.Item_',num2str(i),'.ControlPointSequence.Item_',num2str
(j),'.CumulativeMetersetWeight'));
end
end
end

%% XML PORTION

SetBeam_node = xDoc.createElement('SetBeam');

Id_node = xDoc.createElement('Id');
Id_text = xDoc.createTextNode('1');
Id_node.appendChild(Id_text);
SetBeam_node.appendChild(Id_node);

% SELECT MLC MODEL
MLCModel_node = xDoc.createElement('MLCModel');
MLCModel_text = xDoc.createTextNode('NDS120HD');
MLCModel_node.appendChild(MLCModel_text);
SetBeam_node.appendChild(MLCModel_node);

Accs_node = xDoc.createElement('Accs');
SetBeam_node.appendChild(Accs_node);

ControlPoints_node = xDoc.createElement('ControlPoints');
SetBeam_node.appendChild(ControlPoints_node);

for i = 1:ndims(A.BeamSequence)

    NumControlPts =
eval(strcat('A.BeamSequence.Item_',num2str(i),'.NumberOfControlPoints'));
%Initial control point
    for j = 1
        Cp_node = xDoc.createElement('Cp');
        ControlPoints_node.appendChild(Cp_node);

        Energy_node = xDoc.createElement('Energy');
        Energy_text = xDoc.createTextNode(num2str(Energy(i)));
        Energy_node.appendChild(Energy_text);
        Cp_node.appendChild(Energy_node);

        MU_node = xDoc.createElement('Mu');
        MU_text = xDoc.createTextNode(num2str(MU_CP(i,j)));
        MU_node.appendChild(MU_text);
        Cp_node.appendChild(MU_node);

        Drate_node = xDoc.createElement('DRate');
        Drate_text = xDoc.createTextNode(num2str(DoseRt(i)));

```



```

Drate_node.appendChild(Drate_text);
Cp_node.appendChild(Drate_node);

GantryRtn_node = xDoc.createElement('GantryRtn');
GantryRtn_text = xDoc.createTextNode(num2str(GantryAngle(i,j)));
GantryRtn_node.appendChild(GantryRtn_text);
Cp_node.appendChild(GantryRtn_node);

CollRtn_node = xDoc.createElement('CollRtn');
CollRtn_text = xDoc.createTextNode(num2str(CollimatorAngle(i,j)));
CollRtn_node.appendChild(CollRtn_text);
Cp_node.appendChild(CollRtn_node);

CouchRtn_node = xDoc.createElement('CouchRtn');
CouchRtn_text = xDoc.createTextNode(num2str(CouchAngle(i,j)));
CouchRtn_node.appendChild(CouchRtn_text);
Cp_node.appendChild(CouchRtn_node);

Y1_node = xDoc.createElement('Y1');
Y1_text = xDoc.createTextNode(num2str(abs(Y1(:,i,j))));
Y1_node.appendChild(Y1_text);
Cp_node.appendChild(Y1_node);

Y2_node = xDoc.createElement('Y2');
Y2_text = xDoc.createTextNode(num2str(abs(Y2(:,i,j))));
Y2_node.appendChild(Y2_text);
Cp_node.appendChild(Y2_node);

X1_node = xDoc.createElement('X1');
X1_text = xDoc.createTextNode(num2str(abs(X1(:,i,j))));
X1_node.appendChild(X1_text);
Cp_node.appendChild(X1_node);

X2_node = xDoc.createElement('X2');
X2_text = xDoc.createTextNode(num2str(abs(X2(:,i,j))));
X2_node.appendChild(X2_text);
Cp_node.appendChild(X2_node);

Mlc_node = xDoc.createElement('Mlc');
Cp_node.appendChild(Mlc_node);

Cp_node.appendChild(Mlc_node);
ID_MLC_node = xDoc.createElement('ID');
Mlc_node.appendChild(ID_MLC_node);

ID_MLC_text = xDoc.createTextNode(num2str(i,j));
ID_MLC_node.appendChild(ID_MLC_text);

ID_MLC_node_B = xDoc.createElement('B');
MLC_BB = mat2str((MLC_B(:,i,j)));

```

```

ID_MLC_text_B = xDoc.createTextNode(MLC_BB(2:end-1));
ID_MLC_node_B.appendChild(ID_MLC_text_B);
Mlc_node.appendChild(ID_MLC_node_B);

ID_MLC_node_A = xDoc.createElement('A');
MLC_AA = mat2str((MLC_A(:,i,j)));
ID_MLC_text_A = xDoc.createTextNode(MLC_AA(2:end-1));
ID_MLC_node_A.appendChild(ID_MLC_text_A);
Mlc_node.appendChild(ID_MLC_node_A);

xDoc.getDocumentElement.appendChild(SetBeam_node);

end

%Subsequent control points
for j = 2:1:NumControlPts
    Cp_node = xDoc.createElement('Cp');
    ControlPoints_node.appendChild(Cp_node);

    MU_node = xDoc.createElement('Mu');
    MU_text = xDoc.createTextNode(num2str(MU_CP(i,j)));
    MU_node.appendChild(MU_text);
    Cp_node.appendChild(MU_node);

    GantryRtn_node = xDoc.createElement('GantryRtn');
    GantryRtn_text = xDoc.createTextNode(num2str(GantryAngle(i,j)));
    GantryRtn_node.appendChild(GantryRtn_text);
    Cp_node.appendChild(GantryRtn_node);

%% UNCOMMENT IF PLAN INCLUDES COLLIMATOR ROTATION DURING
TREATMENT
    % CollRtn_node = xDoc.createElement('CollRtn');
    % CollRtn_text = xDoc.createTextNode(num2str(CollimatorAngle(i,j)));
    % CollRtn_node.appendChild(CollRtn_text);
    % Cp_node.appendChild(CollRtn_node);
%% UNCOMMENT IF PLAN INCLUDES COLLIMATOR ROTATION DURING
TREATMENT
    % CouchRtn_node = xDoc.createElement('CouchRtn');
    % CouchRtn_text = xDoc.createTextNode(num2str(CouchAngle(i,j)));
    % CouchRtn_node.appendChild(CouchRtn_text);
    % Cp_node.appendChild(CouchRtn_node);

    Y1_node = xDoc.createElement('Y1');
    Y1_text = xDoc.createTextNode(num2str(abs(Y1(:,i,j))));
    Y1_node.appendChild(Y1_text);
    Cp_node.appendChild(Y1_node);

    Y2_node = xDoc.createElement('Y2');
    Y2_text = xDoc.createTextNode(num2str(abs(Y2(:,i,j))));
    Y2_node.appendChild(Y2_text);

```

```

Cp_node.appendChild(Y2_node);

X1_node = xDoc.createElement('X1');
X1_text = xDoc.createTextNode(num2str(abs(X1(:,i,j))));
X1_node.appendChild(X1_text);
Cp_node.appendChild(X1_node);

X2_node = xDoc.createElement('X2');
X2_text = xDoc.createTextNode(num2str(abs(X2(:,i,j))));
X2_node.appendChild(X2_text);
Cp_node.appendChild(X2_node);

Mlc_node = xDoc.createElement('Mlc');
Cp_node.appendChild(Mlc_node);

Cp_node.appendChild(Mlc_node);
ID_MLC_node = xDoc.createElement('ID');
Mlc_node.appendChild(ID_MLC_node);

ID_MLC_text = xDoc.createTextNode(num2str(i,j));
ID_MLC_node.appendChild(ID_MLC_text);

ID_MLC_node_B = xDoc.createElement('B');
MLC_BB = mat2str((MLC_B(:,i,j)));
ID_MLC_text_B = xDoc.createTextNode(MLC_BB(2:end-1));
ID_MLC_node_B.appendChild(ID_MLC_text_B);
Mlc_node.appendChild(ID_MLC_node_B);

ID_MLC_node_A = xDoc.createElement('A');
MLC_AA = mat2str((MLC_A(:,i,j)));
ID_MLC_text_A = xDoc.createTextNode(MLC_AA(2:end-1));
ID_MLC_node_A.appendChild(ID_MLC_text_A);
Mlc_node.appendChild(ID_MLC_node_A);

xDoc.getDocumentElement.appendChild(SetBeam_node);
end
end

xDoc.getDocumentElement.appendChild(SetBeam_node);
xmlwrite(['Arc_output.xml'],xDoc);

```

4.0. Final script used for designing the GsCM plan. It describes step by step process from inserting a plan, adding a field as a starting point, choosing the target, adding margin around the PTV, dose calculation, and creating an XML.

```
using System;
using System.Collections.Generic;
using System.ComponentModel;
using System.Data;
using System.Drawing;
using System.Linq;
using System.Text;
using System.Threading.Tasks;
using System.Windows.Forms;
using VMS.TPS.Common.Model.API;
using VMS.TPS.Common.Model.Types;
using System.Xml;
using System.IO;
namespace XML1
{
    public partial class XML : Form
    {
        public ScriptContext sc;
        public string my_target= " ";
        public XML(ScriptContext mycontext1)
        {
            InitializeComponent();
            sc = mycontext1;
        }

        public void XML_Load(object sender, EventArgs e)
        {
            var mystruc_list = sc.ExternalPlanSetup.StructureSet.Structures;
            //mystruc = sc.ExternalPlanSetup.StructureSet.Structures.Where(s =>
            s.Id.Contains("ptv1") || s.Id.Contains("PTV1") || s.Id.Contains("Ptv1"));
            foreach(var s in mystruc_list)
            {
                //richTextBox1.AppendText("\r\n"+s.Name.ToString());
                comboBox1.Items.Add(s.Id.ToString());
            }
        }

        public void Button1_Click(object sender, EventArgs e)
        {
            XmlDocument doc = new XmlDocument();
            XmlNode docnode = doc.CreateXmlDeclaration("1.0", "UTF-8", null);
            doc.AppendChild(docnode);
            XmlNode beam = doc.CreateElement("SetBeam");
            doc.AppendChild(beam);
        }
    }
}
```

```

XmlNode id1 = doc.CreateElement("Id");
beam.AppendChild(id1).InnerText="1";
XmlNode mlcmodel = doc.CreateElement("MLCModel");
beam.AppendChild(mlcmodel).InnerText = "NDS120HD";
XmlNode acc = doc.CreateElement("Accs");
beam.AppendChild(acc);
XmlNode controlpoints = doc.CreateElement("ControlPoints");
beam.AppendChild(controlpoints);
//XmlNode cp = doc.CreateElement("Cp");
//XmlNode mlc = doc.CreateElement("Mlc");
//XmlNode A = doc.CreateElement("A");
//XmlNode B = doc.CreateElement("B");
// XmlNode y1 = doc.CreateElement("Y1");
// XmlNode X1 = doc.CreateElement("X1");
// XmlNode Y2 = doc.CreateElement("Y2");
//XmlNode X2 = doc.CreateElement("X2");
//XmlNode energy = doc.CreateElement("Energy");
//XmlNode mu = doc.CreateElement("Mu");
//XmlNode doserate = doc.CreateElement("DRate");
//XmlNode gantryrotation = doc.CreateElement("GantryRtn");
//XmlNode callrotation = doc.CreateElement("CollRtn");
//XmlNode CouchLng = doc.CreateElement("CouchLng");
//XmlNode CouchRtn = doc.CreateElement("CouchRtn");
//XmlNode CouchLat = doc.CreateElement("CouchLat");
//XmlNode CouchVrt = doc.CreateElement("CouchVrt");
string w=null;
double jaw = 0;
int initialization = 0;
var beams = sc.ExternalPlanSetup.Beams;
double MU = 0;
int key = 0;
//string s = null;
int count;
foreach (var b in beams)
{

    count = b.ControlPoints.Count;
    //count = count / 2;
    for (int j = 0; j < count; j++)
    {
        if (((b.ControlPoints[j].MetersetWeight * b.Meterset.Value) > 0) || (initialization
        == 0))
        {
            ///
            initialization = 1;
            XmlNode cp = doc.CreateNode(XmlNodeType.Element, "Cp", null);
            controlpoints.AppendChild(cp);
            //////////////////////////////////////next energy////////////////////////////////////
            XmlNode energy = doc.CreateNode(XmlNodeType.Element, "Energy", null);
            cp.AppendChild(energy).InnerText =

```

```

b.EnergyModeDisplayName.ToString().ToLower();
////////////////////////////////first mu=0////////////////////////////////
//XmlNode mu = doc.CreateNode(XmlNodeType.Element, "Mu", null);
// cp.AppendChild(mu).InnerText = "0";
////////////////////////////////////////////////////////////////
//XmlNode cp1 = doc.CreateNode(XmlNodeType.Element, "Cp", null);
//controlpoints.AppendChild(cp1);
XmlNode mu1 = doc.CreateNode(XmlNodeType.Element, "Mu", null);

//s=s+(b.ControlPoints[j].MetersetWeight * b.Meterset.Value).ToString()+"\n";

cp.AppendChild(mu1).InnerText = (MU + b.ControlPoints[j].MetersetWeight *
b.Meterset.Value).ToString();
/////////////////////////////////let's say we have multiple
  fields////////////////////////////////
////////////////////////////////////////////////////////////////
// cp.AppendChild(mu).InnerText = (b.ControlPoints[j].MetersetWeight *
b.Meterset.Value).ToString();
////////////////////////////////dose rate
////////////////////////////////
XmlNode doserate = doc.CreateNode(XmlNodeType.Element, "DRate", null);
cp.AppendChild(doserate).InnerText = b.DoseRate.ToString();
////////////////////////////////Gantry rotation////////////////////////////////
XmlNode gantry = doc.CreateNode(XmlNodeType.Element, "GantryRtn",
null);
double gantry_conversion = 0;
gantry_conversion = b.ControlPoints[j].GantryAngle;
if ((gantry_conversion >= 0) && (gantry_conversion <= 180))
{
  gantry_conversion = 180 - gantry_conversion;
}
else
  if ((gantry_conversion <= 359.9) && (gantry_conversion >= 180.1))
  {
    gantry_conversion = 180 + (360 - gantry_conversion);
  }

cp.AppendChild(gantry).InnerText = gantry_conversion.ToString();
////////////////////////////////coll
rotation////////////////////////////////
XmlNode collimation = doc.CreateNode(XmlNodeType.Element, "CollRtn",
null);

double collimation_conversion = 0;
collimation_conversion = b.ControlPoints[j].CollimatorAngle;
if ((collimation_conversion >= 0) && (collimation_conversion <= 180))
{
  collimation_conversion = 180 - collimation_conversion;
}
else

```

```

if ((collimation_conversion <= 359.9) && (collimation_conversion >=
180.1))
{
    collimation_conversion = 180 + (360 - collimation_conversion);
}

cp.AppendChild(collimation).InnerText = collimation_conversion.ToString();
////////////////////////////////////////couch rotation////////////////////////////////////////
XmlNode couchrtn = doc.CreateNode(XmlNodeType.Element, "CouchRtn",
null);

double couch_conversion = 0;
couch_conversion = (360 - b.ControlPoints[j].PatientSupportAngle);
if (couch_conversion == 360)
    couch_conversion = 0;
// MessageBox.Show(couch_conversion.ToString());

if ((couch_conversion >= 0) && (couch_conversion <= 180))
{
    couch_conversion = 180 - couch_conversion;
}
else
    if ((couch_conversion <= 359.9) && (couch_conversion >= 180.1))
    {
        couch_conversion = 180 + (360 - couch_conversion);
    }
couch_conversion = 360 - couch_conversion;
cp.AppendChild(couchrtn).InnerText = couch_conversion.ToString();
////////////////////////////////////////Y1////////////////////////////////////////
XmlNode y1 = doc.CreateNode(XmlNodeType.Element, "Y1", null);
jaw = -b.ControlPoints[j].JawPositions.Y1 / 10;
cp.AppendChild(y1).InnerText = jaw.ToString();
////////////////////////////////////////Y2////////////////////////////////////////
XmlNode y2 = doc.CreateNode(XmlNodeType.Element, "Y2", null);
jaw = b.ControlPoints[j].JawPositions.Y2 / 10;
cp.AppendChild(y2).InnerText = jaw.ToString();
////////////////////////////////////////x1////////////////////////////////////////
XmlNode x1 = doc.CreateNode(XmlNodeType.Element, "X1", null);
jaw = -b.ControlPoints[j].JawPositions.X1 / 10;
cp.AppendChild(x1).InnerText = jaw.ToString();
////////////////////////////////////////x2////////////////////////////////////////
XmlNode x2 = doc.CreateNode(XmlNodeType.Element, "X2", null);
jaw = b.ControlPoints[j].JawPositions.X2 / 10;
cp.AppendChild(x2).InnerText = jaw.ToString();
////////////////////////////////////////
// XmlNode couchlong = doc.CreateNode(XmlNodeType.Element,
"CouchLng", null);
//controlpoints.AppendChild(couchlong).InnerText =
b.ControlPoints[j].TableTopLongitudinalPosition.ToString();
//XmlNode couchlat = doc.CreateNode(XmlNodeType.Element, "CouchLat",

```

```

null);
// controlpoints.AppendChild(couchlat).InnerText =
b.ControlPoints[j].TableTopLateralPosition.ToString();
//XmlNode couchvert = doc.CreateNode(XmlNodeType.Element, "CouchVrt",
null);
//controlpoints.AppendChild(couchvert).InnerText =
b.ControlPoints[j].TableTopVerticalPosition.ToString();
//controlpoints.AppendChild(cp);
XmlNode mlc = doc.CreateNode(XmlNodeType.Element, "Mlc", null);
cp.AppendChild(mlc);
XmlNode id = doc.CreateElement("ID");
mlc.AppendChild(id).InnerText = "1";

for (int p = 0; p < 60; p++)
{
    double mymlc = (b.ControlPoints[j].LeafPositions[0, p]) / 10;

    // if (Math.Abs(mymlc) < .1)
    // mymlc = 0;
    //lets close MLCs at 0 //////////////////////////////////////
    if (b.ControlPoints[j].LeafPositions[1, p]-b.ControlPoints[j].LeafPositions[0,
p] == 0)
    {
        //MessageBox.Show(" zeroooo");
        mymlc = 0;

    }
    //////////////////////////////////////end of closing MLC at 0////////////////////////////////////
    //double mymlc = (b.ControlPoints[j].LeafPositions[0, p]) / 10;
    w = w + (-mymlc).ToString() + " ";

}
XmlNode B = doc.CreateNode(XmlNodeType.Element, "B", null);
mlc.AppendChild(B).InnerText = w;
w = null;
for (int p = 0; p < 60; p++)
{
    double mymlc1 = (b.ControlPoints[j].LeafPositions[1, p]) / 10;
    //if (Math.Abs(mymlc1) < .1)
    //mymlc1 = 0;
    //lets close MLCs at 0 //////////////////////////////////////
    if (b.ControlPoints[j].LeafPositions[1, p] -
b.ControlPoints[j].LeafPositions[0,
p] == 0)
    {
        //MessageBox.Show(" zeroooo");
        mymlc1 = 0;

    }
    //////////////////////////////////////end of closing MLC at 0////////////////////////////////////

```



```

        w = w + (mymlc1).ToString() + " ";
    }
    XmlNode A = doc.CreateNode(XmlNodeType.Element, "A", null);
    mlc.AppendChild(A).InnerText = w;
    w = null;
    /* XmlNode cp1 = doc.CreateNode(XmlNodeType.Element, "Cp", null);
    controlpoints.AppendChild(cp1);
    XmlNode mu1 = doc.CreateNode(XmlNodeType.Element, "Mu", null);
    if (key == 0)
    {
        MU = b.ControlPoints[j].MetersetWeight * b.Meterset.Value;
        key = 1;
    }
    else
        if (key == 1)
        {
            MU = MU + b.ControlPoints[j].MetersetWeight * b.Meterset.Value;
            key = 0;
        }
    cp1.AppendChild(mu1).InnerText = MU.ToString(); */

    }
}
key = count - 1;
MU = MU + b.ControlPoints[key].MetersetWeight * b.Meterset.Value;

}

//MessageBox.Show(s);
saveFileDialog1.Filter = "XML files(.xml)|*.xml|all Files(*.*)|*.*";
saveFileDialog1.ShowDialog();
doc.Save(saveFileDialog1.FileName);

}

public void Button2_Click(object sender, EventArgs e)
{
    // Patient p = sc.Patient;
    // p.BeginModifications();
    var beams = sc.ExternalPlanSetup.Beams;
    // sc.ExternalPlanSetup.AddMLCBeam(beams(0).)
    var mystruc = sc.ExternalPlanSetup.StructureSet.Structures;
    mystruc = sc.ExternalPlanSetup.StructureSet.Structures.Where(s =>
    s.Id.Contains(my_target));
    var beam1 = beams.Single(s => s.Id == "1");
    //var beamarray = new object[90];

    int key = 1;
    double couchangle = (beam1.ControlPoints[0].PatientSupportAngle);

```

```

double couchkey = 0;
ExternalBeamMachineParameters beamparameters = new
ExternalBeamMachineParameters(beam1.TreatmentUnit.Id.ToString(),
beam1.EnergyModeDisplayName.ToString(), beam1.DoseRate,
beam1.Technique.Id.ToString(), null);
//////////checking gantry angle//////////
// if (beam1.ControlPoints[0].Gantry Angle == 90)
////////// now we have to make the first field we created in eclipse to 90 gantry
angles so doesn't matter what user put initially , so the field angles start with 90////////
///
beam1.GantryAngleToUser(90.00);
{
for (int j = 1; j <= 90; j++)
{
couchkey++;
couchangle = (360 - couchkey);

key++;
sc.ExternalPlanSetup.AddMLCBeam(beamparameters,
beam1.ControlPoints[0].LeafPositions, beam1.ControlPoints[0].JawPositions,
beam1.ControlPoints[0].CollimatorAngle, 90, couchangle,
beam1.IsocenterPosition);
//label2.Text = "Field progress for 90-degree gantry..." + key.ToString();
}
}
//else
couchkey = 0;
// if (beam1.ControlPoints[0].GantryAngle == 270)
{
for (int j = 1; j <= 90; j++)
{
couchkey++;
couchangle = (couchkey);

key++;
sc.ExternalPlanSetup.AddMLCBeam(beamparameters,
beam1.ControlPoints[0].LeafPositions, beam1.ControlPoints[0].JawPositions,
beam1.ControlPoints[0].CollimatorAngle, 270, couchangle,
beam1.IsocenterPosition);
label2.Text = "Field progress completed..." + key.ToString();

}
}

//////////end of gantry angle check //////////
var newbeams = sc.ExternalPlanSetup.Beams;
//////////fit to structure
parameters//////////
///
double margin = System.Convert.ToDouble(textBox1.Text);

```

```

FitToStructureMargins mymargins = new FitToStructureMargins(margin);
JawFitting myjawfit = new JawFitting();
OpenLeavesMeetingPoint openmyleaves = new OpenLeavesMeetingPoint();
ClosedLeavesMeetingPoint closemyleave = new ClosedLeavesMeetingPoint();
closemyleave = ClosedLeavesMeetingPoint.ClosedLeavesMeetingPoint_Center;
////////////////////////////////////
foreach (var b in newbeams)
{
    // couchangle = couchangle + 1;
    //b.PatientSupportAngleToUser(couchangle);
    //b.PatientSupportAngleToUser(30);

    foreach (var s in mystruc)
    {
        b.FitCollimatorToStructure(mymargins, s, true, true, false);
        b.FitMLCToStructure(mymargins, s, false, myjawfit, openmyleaves,
        closemyleave);
        ////////////////////////////////////for testing now////////////////////////////////////
    }
}
}

private void Label1_Click(object sender, EventArgs e)
{
}

private void button3_Click(object sender, EventArgs e)
{
    ExternalPlanSetup myplan = sc.ExternalPlanSetup;

    myplan.CalculateDose();
    label2.Text = " ";
    label4.Text = "Calculation Completed!";
}

private void button4_Click(object sender, EventArgs e)
{
    // Patient p = sc.Patient;
    // p.BeginModifications();
    var beams = sc.ExternalPlanSetup.Beams;
    // sc.ExternalPlanSetup.AddMLCBeam(beams(0).)
    var mystruc = sc.ExternalPlanSetup.StructureSet.Structures;
    mystruc = sc.ExternalPlanSetup.StructureSet.Structures.Where(s =>
    s.Id.Contains("ptv1") || s.Id.Contains("PTV1") || s.Id.Contains("Ptv1"));
    var beam1 = beams.Single(s => s.Id == "1");
    //var beamarray = new object[90];
    int key = 1;
}

```

```

double couchangle = (beam1.ControlPoints[0].PatientSupportAngle);
double couchkey = 0;
ExternalBeamMachineParameters beamparameters = new
ExternalBeamMachineParameters(beam1.TreatmentUnit.Id.ToString(),
beam1.EnergyModeDisplayName.ToString(), beam1.DoseRate,
beam1.Technique.Id.ToString(), null);
////////////////////////////////////for gantry 90 degree////////////////////////////////////
// if (beam1.ControlPoints[0].GantryAngle == 90)
{
    for (int j = 1; j <= 90; j++)
    {
        couchkey++;
        couchangle = (360 - couchkey);
        key++;
        sc.ExternalPlanSetup.AddStaticBeam(beamparameters,
        beam1.ControlPoints[0].JawPositions, beam1.ControlPoints[0].CollimatorAngle,
        90, couchangle, beam1.IsocenterPosition);
        //label2.Text = "Field progress..." + key.ToString();

    }
}
////////////////////////////////////for gantry 270 degree////////////////////////////////////
///
//else
couchkey = 0;
//if (beam1.ControlPoints[0].GantryAngle == 270)
{
    for (int j = 1; j <=90; j++)
    {
        couchkey++;
        couchangle = (couchkey);

        key++;
        sc.ExternalPlanSetup.AddStaticBeam(beamparameters,
        beam1.ControlPoints[0].JawPositions, beam1.ControlPoints[0].CollimatorAngle,
        270, couchangle, beam1.IsocenterPosition);
        label2.Text = "Field progress completed..." + key.ToString();
    }
}

////////////////////////////////////end of checking gantry angles////////////////////////////////////
var newbeams = sc.ExternalPlanSetup.Beams;
////////////////////////////////////fit to structure
parameters////////////////////////////////////
///
//double margin = System.Convert.ToDouble(textBox1.Text);
// FitToStructureMargins mymargins = new FitToStructureMargins(margin);
//JawFitting myjawfit = new JawFitting();
// OpenLeavesMeetingPoint openmyleaves = new OpenLeavesMeetingPoint();
// ClosedLeavesMeetingPoint closemyleave = new ClosedLeavesMeetingPoint();

```

```

////////////////////////////////////
foreach (var b in newbeams)
{
    // couchangle = couchangle + 1;
    //b.PatientSupportAngleToUser(couchangle);
    //b.PatientSupportAngleToUser(30);
    foreach (var s in mystruc)
    {
        //b.FitCollimatorToStructure(mymargins, s, true, true, true);
        //b.FitMLCToStructure(mymargins, s, false, myjawfit, openmyleaves,
        closemyleave);
        //////////////////////////////////for testing now////////////////////////////////
    }
}

}

private void richTextBox1_TextChanged(object sender, EventArgs e)
{
}

private void richTextBox1_SelectionChanged(object sender, EventArgs e)
{
    //my_target = richTextBox1.SelectedText.ToString();
}

private void comboBox1_SelectedIndexChanged(object sender, EventArgs e)
{
    my_target = comboBox1.SelectedItem.ToString();
}

private void button5_Click(object sender, EventArgs e)
{
    Dose dose1 = null;

    var beams1 = sc.ExternalPlanSetup.Beams;
    // Fluence myfluence=new Fluence(null,null,null,null);
    //Fluence newf= new Fluence() has some parameters to import new fluence after
    optiomization
    int key=0;
    int X=0, Y=0;
    float[,] pixels=null;
    foreach (var b in beams1)
    {
        if (key == 0)
        {
            Fluence myfluence = b.GetOptimalFluence();

```

```

        dose1 = b.Dose;
        int x = myfluence.XSizePixel;
        int y = myfluence.YSizePixel;
        pixels = new float[x,y];
        X = x; Y = y;
        pixels = myfluence.GetPixels();
    }
    key++;
}

////////////////////////////////////let's play with dose now////////////////////////////////////

System.IO.StreamWriter streamWriter = new System.IO.StreamWriter("c:\\pixels.txt");
////////////////////////////////////writing pixels to file////////////////////////////////////
string output = "";
for (int i = 0; i < X; i++)
{
    for (int j = 0; j < Y; j++)
    {
        output += pixels[i, j].ToString();
    }
    streamWriter.WriteLine(output);
    output = "";
}
streamWriter.Close();
}
}
}
}
}

```